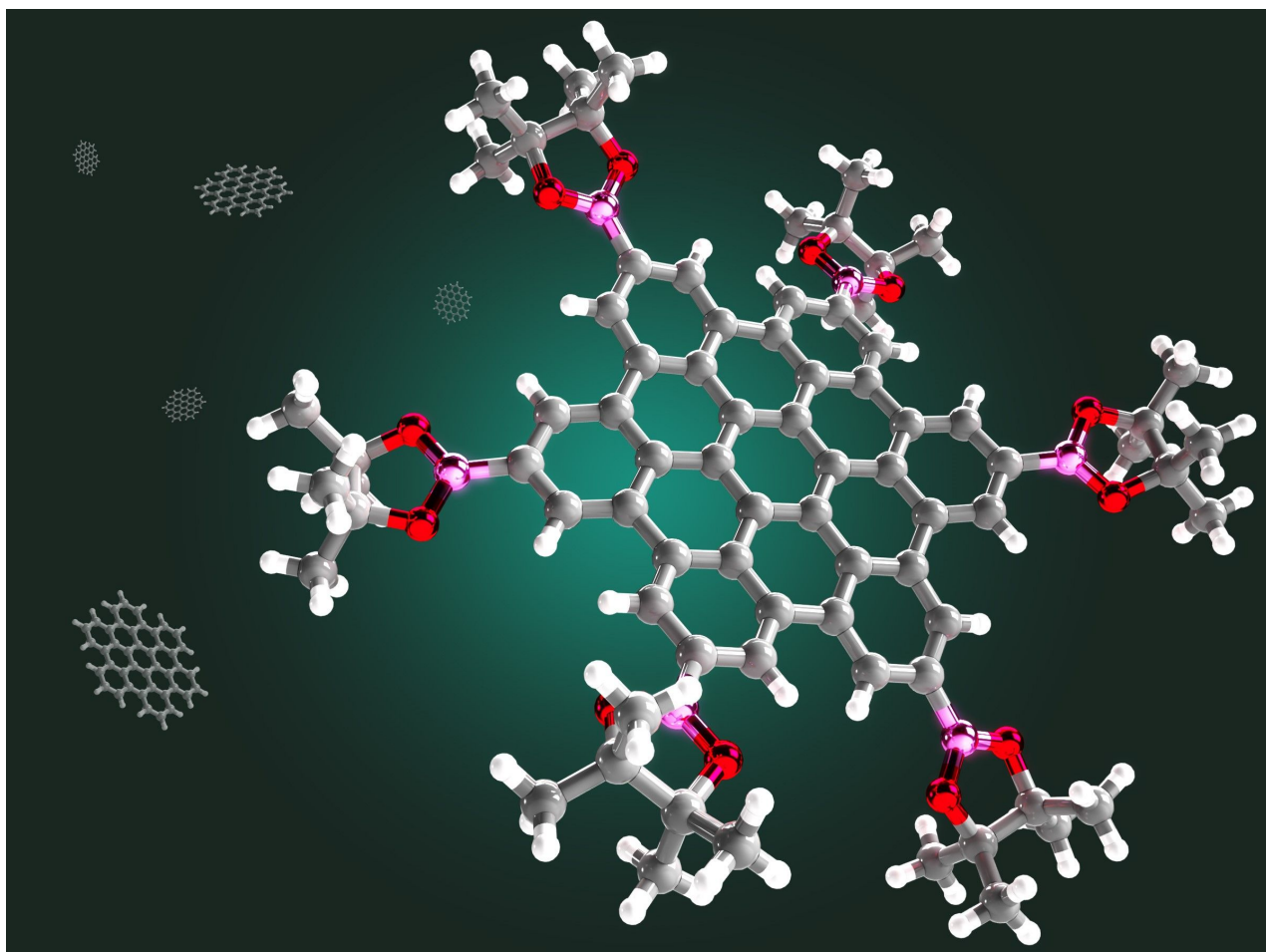




C–H functionalization for materials science

Edited by Kenichiro Itami



Imprint

Beilstein Journal of Organic Chemistry
www.bjoc.org
ISSN 1860-5397
Email: journals-support@beilstein-institut.de

The *Beilstein Journal of Organic Chemistry* is published by the Beilstein-Institut zur Förderung der Chemischen Wissenschaften.

Beilstein-Institut zur Förderung der
Chemischen Wissenschaften
Trakehner Straße 7–9
60487 Frankfurt am Main
Germany
www.beilstein-institut.de

The copyright to this document as a whole, which is published in the *Beilstein Journal of Organic Chemistry*, is held by the Beilstein-Institut zur Förderung der Chemischen Wissenschaften. The copyright to the individual articles in this document is held by the respective authors, subject to a Creative Commons Attribution license.

The cover image is copyright 2020 Kenichiro Itami under the terms of the Creative Commons Attribution License (<https://creativecommons.org/licenses/by/4.0>); licensee Beilstein-Institut.



Formal preparation of regioregular and alternating thiophene–thiophene copolymers bearing different substituents

Atsunori Mori^{*1,2}, Keisuke Fujita¹, Chihiro Kubota¹, Toyoko Suzuki¹, Kentaro Okano¹, Takuya Matsumoto¹, Takashi Nishino¹ and Masaki Horie³

Full Research Paper

[Open Access](#)

Address:

¹Department of Chemical Science and Engineering, Kobe University, 1-1 Rokkodai, Nada, Kobe 657-8501, Japan, ²Research Center for Membrane and Film Technology, Kobe University, 1-1 Rokkodai, Nada, Kobe 657-8501, Japan and ³Department of Chemical Engineering, National Tsing Hua University, 101, Sec. 2, Kuang-Fu Road, Hsinchu 30013, Taiwan

Email:

Atsunori Mori^{*} - amori@kobe-u.ac.jp

^{*} Corresponding author

Keywords:

alternating copolymer; nickel(II) catalyst; oligosiloxane; regioregular polythiophene; solubility

Beilstein J. Org. Chem. **2020**, *16*, 317–324.

doi:10.3762/bjoc.16.31

Received: 27 December 2019

Accepted: 26 February 2020

Published: 05 March 2020

This article is part of the thematic issue "C–H functionalization for materials science".

Guest Editor: K. Itami

© 2020 Mori et al.; licensee Beilstein-Institut.

License and terms: see end of document.

Abstract

Differently substituted thiophene–thiophene-alternating copolymers were formally synthesized employing a halo-bithiophene as a monomer. Nickel-catalyzed polymerization of bithiophene with substituents at the 3-position, including alkyl-, fluoroalkyl-, or oligosiloxane-containing groups, afforded the corresponding copolymers in good to excellent yield. The solubility test in organic solvents was performed to reveal that several copolymers showed a superior solubility. X-ray diffraction analysis of the thin film of the alternating copolymers composed of methyl and branched oligosiloxane substituents was also performed, and the results suggested the formation of a dual-layered film structure.

Introduction

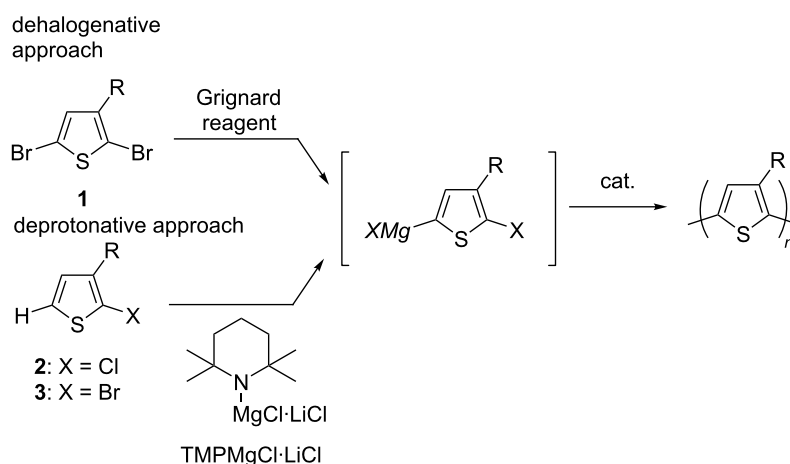
Polythiophenes attract much attention in materials science because of their extended π -conjugation, which is applied for a wide range of electronic materials. In particular, the regioregular polymers with a head-to-tail (HT) orientation with respect to the substituent at the 3-position are extensively studied to

date since they generally show superior performances as materials [1–6]. Cross-coupling polymerization catalyzed by a transition metal complex has been recognized as an effective tool to afford the regioregular polythiophene in which 2,5-dihalo-3-substituted thiophene **1** is employed as a monomer precursor,

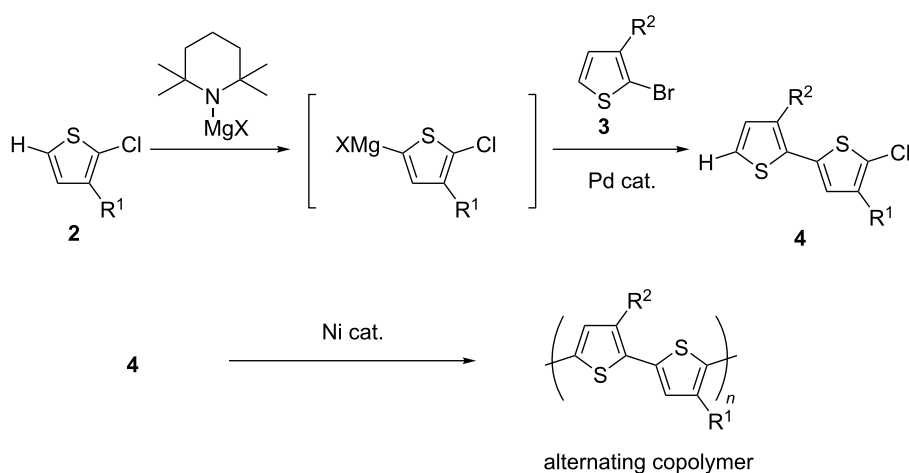
converting to the corresponding organometallic monomer by a halogen–magnesium exchange reaction with a Grignard reagent. The employment of **1** leading to polythiophene has been shown to proceed in a dehalogenative manner [3]. We have recently shown that the generation of the organometallic monomer species can alternatively also be achieved by deprotonation, using 2-halo-3-substituted thiophene **2** or **3** with a bulky magnesium amide Knochel–Hauser base (TMPMgCl·LiCl) [7], followed by polymerization catalyzed by a nickel complex, leading to the regioregular HT polythiophene (Scheme 1) [8,9]. An additional feature of the deprotonative protocol for polythiophene is the possibility to use chlorothiophene **3**, in which the use of a nickel N-heterocyclic carbene (NHC) complex was found to be effective [10,11]. We have also engaged in the design of the side chain of polythiophenes, and several functionalities have been successfully introduced

[12–14]. We further focused on the copolymerization of thiophene, employing differently substituted thiophene monomers, with which several copolymerizations are plausible, giving thiophene–thiophene copolymers of random (statistical) [15], gradient [16,17], block [18,19], alternating [20–23], etc. [24,25] makeup. We are thus interested in the preparation of alternating polythiophenes bearing two kinds of different substituents. We envisaged that such an alternating copolymer in perfect regularity can be achieved by deprotonative polymerization employing a bithiophene with different substituents at the 3- and 3'-position.

We have recently shown that the coupling of 2-chloro-3-substituted thiophene **2** with 2-bromo-3-substituted thiophene **3** efficiently gave chlorobithiophene **4** in a facile manner (Scheme 2) [25]. The use of a palladium catalyst efficiently suppressed the



Scheme 1: Cross-coupling polymerization of thiophene.



Scheme 2: Polymerization of bithiophene.

undesired polymerization to afford the HT halobithiophene with different substituents [26]. Compared to an alternative pathway to **4**, in which initial coupling is followed by chlorination, this protocol exploits the improved deprotonation efficiency of **2** toward 3'-unsubstituted 3-substituted bithiophene, and this method enabled the synthesis of **4** (where $R^1 = H$) regioselectively. Polymerization of **4** (where $R^1 = n$ -hexyl and $R^2 = (CH_2)_4Si(Me)_2OSiMe_3$) was also examined preliminarily, and it was confirmed that the alternating copolymer was obtained with extremely high regularity. Herein, we wished to study the polymerization of bithiophene **4** possessing several kinds of substituents and a variety of functionalities. Since the homopolymer is considered rather insoluble in most organic solvents, the presumed improved solubility of the related alternating copolymers was also part of this study.

Results and Discussion

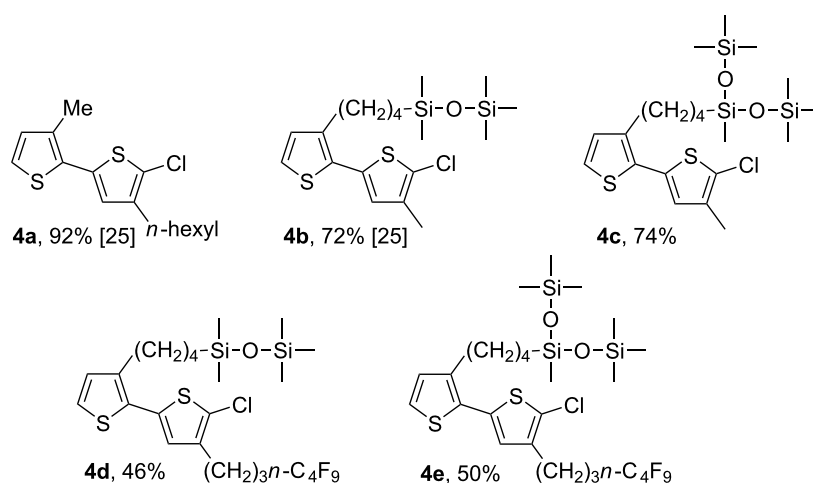
The synthesis of chlorobithiophenes with different substituents at the 3- and 3'-position was carried out in a manner that we have described previously [25]. We chose five chlorobithiophenes as monomer precursors for the alternating copolymers, as summarized in Scheme 3. The cross-couplings, as shown in Scheme 2, proceeded smoothly to afford the bithiophenes **4** in 46–92% yield.

The synthesis of the alternating copolymers was carried out with monomer precursors **4** by deprotonation with Knochel–Hauser base followed by the addition of the nickel catalyst $NiCl_2(PPh_3)IPr$ to initiate the polymerization of bithiophene.

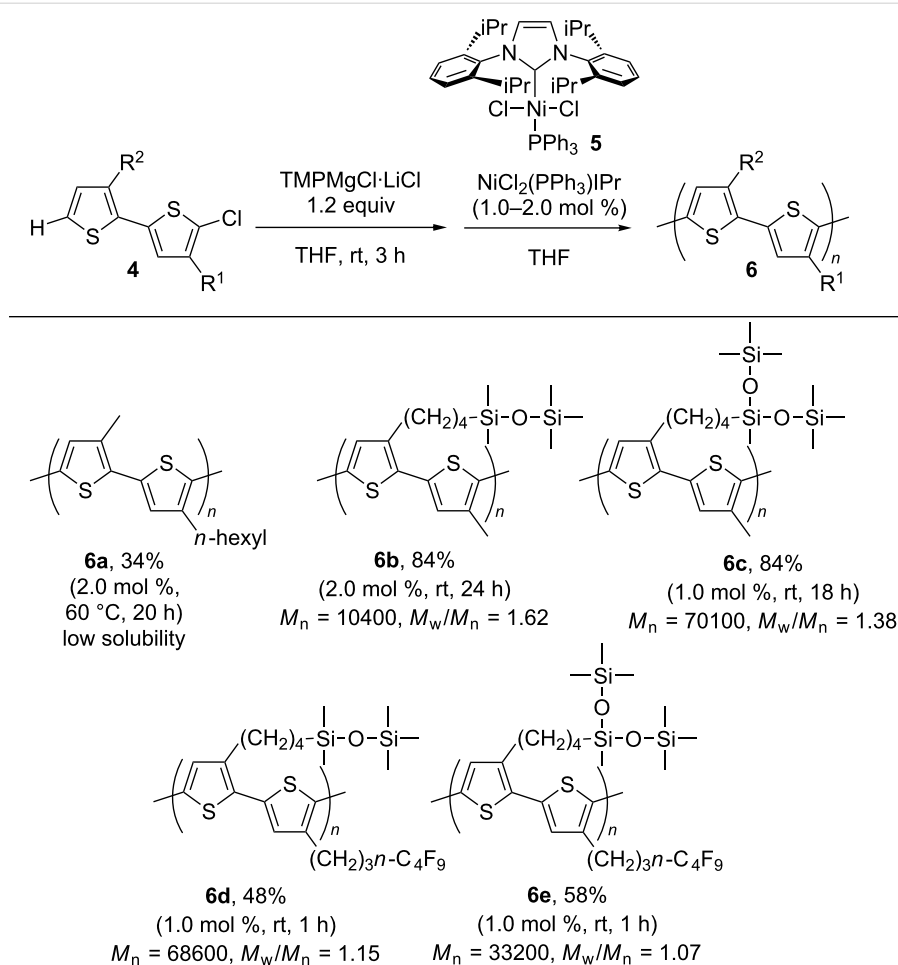
We first carried out the polymerization of chlorobithiophene **4a**, bearing hexyl and methyl substituents at the 3- and 3'-position,

respectively. Although the polymerization took place in moderate yield (34%), the formation of hardly soluble precipitates was observed during the reaction, and the thus obtained solid was found to fail to dissolve in any organic solvent. As previously reported for the regioregular polythiophene synthesis, poly(3-hexylthiophene) (P3HT) can smoothly be dissolved in several organic solvents. In contrast, there have been few reports on the preparation of regioregular polythiophene bearing a methyl group at the 3-position [27]. Accordingly, the incorporation of the alternating methyl substituent would result in much inferior solubility as compared to the alternating copolymer. Several chlorobithiophenes **4** were then similarly subjected to the polymerization. The results of the alternating copolymerizations are summarized in Scheme 4. The deprotonation by the Knochel–Hauser base was carried out at room temperature for 3 h. The addition of the nickel catalyst **5** and further stirring at room temperature followed. The reactions proceeded smoothly to afford the corresponding formally alternating copolymers in 48–84% yields [28]. The molecular weight of the products was found to be controllable based on the ratio of monomer/catalyst feed, and the molecular weight distributions were relatively narrow.

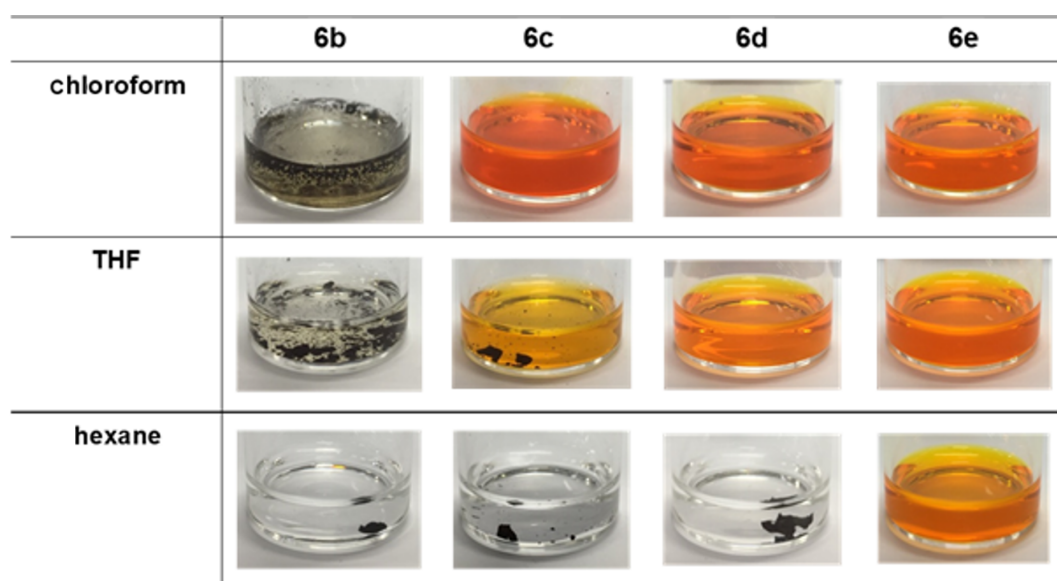
Solubility tests of the obtained polymers were performed as summarized in Figure 1. Although the alternating copolymer **6b**, substituted with methyl and C-4 alkyl groups as well as terminal pentamethyldisiloxane groups, was obtained with a slightly low molecular weight, suggesting improved solubility compared to **6a** ($R^2 = Me$ and $R^1 = n$ -hexyl), the attempted dissolution of the obtained polythiophene **6b** in chloroform was unsuccessful. Switching the oligosiloxane moiety to a branched derivative ($R^2 = (CH_2)_4Si(Me)(OSiMe_3)_2$) in **6c** remarkably improved the solubility, and the copolymer **6c** was soluble



Scheme 3: Preparation of chlorobithiophenes.



Scheme 4: Polymerization of chlorobithiophenes.

Figure 1: Solubility tests of alternating copolymer **6** (1 mg of material dissolved in 1 mL of the solvent).

in chloroform, whereas the dissolution in hexane was unsuccessful. Copolymers bearing a fluoroalkyl substituent ($(\text{CH}_2)_3n\text{-C}_4\text{F}_9$), with a corresponding homopolymer solubility that was lower than that of the long-chained alkyl derivatives, were then examined. The alternating copolymer **6d**, bearing fluoroalkyl and non-branched disiloxane substituents was readily soluble in chloroform, while the attempted dissolution of **6d** in hexanes was unsuccessful. However, a remarkable solubility of the copolymer **6e** bearing a fluoroalkyl group and a branched oligosiloxane unit in hexanes was noted.

XRD analysis of the copolymer **6c**, bearing branched oligosiloxane and methyl groups, was carried out. Two remarkable peaks were observed at $2\theta = 3.94^\circ$ and 12.18° , respectively, as shown in Figure 2a. The result suggested that the thin film of the alternating copolymer **6c** had a bilayer lamellar structure with 7.3 Å and 22.4 Å distances, respectively (Figure 2b) [13,29,30]. Molecular modeling of the alternating copolymer **6c** suggested chain lengths of 11.6 Å and 2.2 Å, respectively. The values of the observed layer distances of copolymer **6c** closely corresponded to twice the values, 11.6×2 and 2.2×2 (Figure 2c), in which the conformation of the carbon–carbon single bond between the thiophene rings was *anti*. The proposed layer distance of regiorandom poly(3-methylthiophene) of 7.7 Å reported by Yan and co-workers was close to our result from the XRD analysis (7.3 Å) corresponding to the aggregation of the alternating methyl substituent [27].

Conclusion

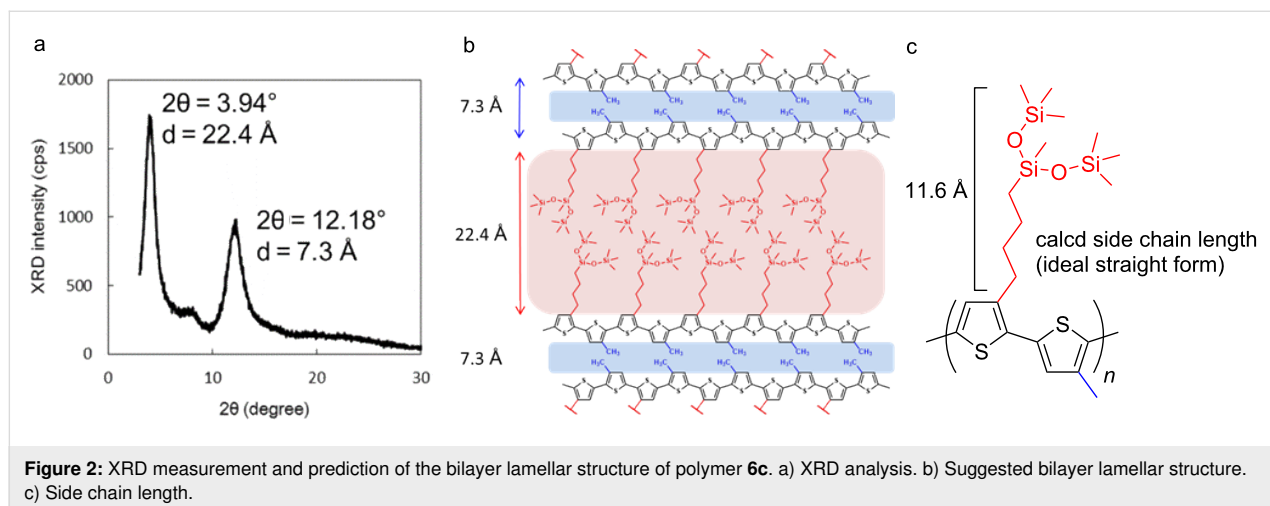
In summary, we showed that formally alternating thiophene–thiophene copolymers could be synthesized by employing differently substituted halobithiophenes as monomers in nickel-catalyzed deprotonative polymerizations. The introduction of oligosiloxanes as side chains improved the solubility in organic solvents, and copolymer components involving less

soluble functional groups, such as short alkyl chains or fluoroalkyl groups, could be incorporated into the alternating copolymers. X-ray diffraction measurements revealed that the alternating copolymers bearing different side chain lengths had dual-layer structures in the thin-film state.

Experimental

General

Polymerization was carried out with the standard Schlenk technique under a nitrogen or argon atmosphere. ^1H NMR (400 MHz), ^{19}F NMR (376 MHz), and $^{13}\text{C}\{^1\text{H}\}$ NMR (100 MHz) spectra were measured on a JEOL ECZ400 spectrometer as a CDCl_3 solution, unless otherwise noted. The chemical shifts were expressed in ppm with CHCl_3 (7.26 ppm for ^1H), C_6F_6 (−164.9 ppm for ^{19}F), or CDCl_3 (77.16 ppm for ^{13}C) as internal standards. IR spectra were recorded on Bruker Alpha spectrometer with an ATR attachment (Ge). High-resolution mass spectra (HRMS) were measured using a JEOL JMS-T100LP AccuTOF LC-Plus apparatus (ESI) with a JEOL MS-5414DART attachment. For thin-layer chromatography (TLC) analyses throughout this work, Merck precoated TLC plates (silica gel 60 F₂₅₄) were used. Purification by HPLC with preparative SEC columns (JAI-GEL-1H and JAI-GEL-2H) was performed by a JAI LC-9201 system. SEC analyses were carried out with a standard HPLC system equipped with a UV detector at 40 °C using CHCl_3 as an eluent with Shodex KF-402HQ and KF-404HQ. Molecular weights and molecular weight distributions were estimated on the basis of the calibration curve obtained by 6 standard polystyrenes. UV–vis absorption spectra of the polymer films were measured with a Shimadzu UV-3150 spectrometer. XRD analysis was carried out with a Rigaku RINT-2000($\text{CuK}\alpha$) device. Concerning the solvent of the nickel- and palladium-catalyzed reactions, THF (anhydrous grade) was purchased from Kanto Chemical Co. Ltd. and passed through alumina and copper columns (Nikko



Hansen & Co. Ltd.) or distilled from a sodium dispersion in mineral oil/benzophenone ketyl [31] prior to use. The Knochel–Hauser base (TMPMgCl–LiCl) was purchased from Sigma–Aldrich Co. Ltd. as a 1 M THF solution. NiCl₂(PPh₃)IPr (**5**) was purchased from TCI Co. Ltd. All other chemicals were purchased and used without further purification. The preparation of the chlorobithiophenes **4a** and **4b** was performed in a manner reported previously [25].

The synthesis of the chlorobithiophenes **4** was carried out in a manner shown in our previous report [25]. The spectroscopic properties and analytical data for **4** are summarized below.

2-Chloro-3-hexyl-5-(3-methylthiophen-2-yl)thiophene (4a) [25]: 92% yield as a light yellow oil. ¹H NMR (500 MHz, CDCl₃) δ 0.92 (t, *J* = 7.5 Hz, 3H), 1.31–1.43 (m, 6H), 1.58–1.67 (m, 2H), 2.37 (s, 3H), 2.59 (t, *J* = 7.5 Hz, 2H), 6.83 (s, 1H), 6.87 (d, *J* = 5.0 Hz, 1H), 7.14 (d, *J* = 5.0 Hz, 1H); ¹³C{¹H} NMR (100 MHz, CDCl₃) δ 14.2, 15.3, 22.8, 28.2, 29.1, 29.7, 31.8, 123.5, 124.0, 126.2, 130.6, 131.4, 133.1, 134.2, 139.8; IR (ATR): 2954, 2926, 2856, 1463, 1199, 1042, 830, 705, 617 cm^{−1}; HRMS (DART-ESI⁺) *m/z*: calcd for C₁₅H₂₀³⁵ClS₂, 299.0695; found, 299.0687.

2-Chloro-3-methyl-5-(3-(4-(1,1,3,3,3-pentamethyldisiloxy)butan-1-yl)thiophen-2-yl)thiophene (4b) [25]: 72% yield as a light yellow oil. ¹H NMR (400 MHz, CDCl₃) δ 0.0 (s, 6H), 0.05 (s, 9H), 0.50–0.57 (m, 2H), 1.33–1.44 (m, 2H), 1.58–1.68 (m, 2H), 2.19 (s, 3H), 2.67–2.74 (m, 2H), 6.77 (s, 1H), 6.90 (d, *J* = 5.0 Hz, 1H), 7.15 (d, *J* = 5.0 Hz, 1H); ¹³C{¹H} NMR (100 MHz, CDCl₃) δ 0.5, 2.2, 13.7, 18.4, 23.3, 29.0, 34.5, 124.0, 124.6, 127.6, 128.4, 130.0, 132.7, 134.7, 140.0; IR (ATR): 2955, 2924, 2858, 1567, 1411, 1252, 1194, 1051, 840, 807, 783, 753, 687, 651, 625 cm^{−1}; HRMS (DART-ESI⁺) *m/z*: calcd for C₁₈H₃₀³⁵ClS₂Si₂, 417.0951; found, 417.0979.

2-Chloro-3-methyl-5-(3-(4-(bis(trimethylsiloxy)-(methyl)silyl)butan-1-yl)thiophen-2-yl)thiophene (4c): 74% yield as a light yellow oil. ¹H NMR (400 MHz, CDCl₃) δ 0.0 (s, 3H), 0.07 (s, 18H), 0.44–0.51 (m, 2H), 1.33–1.42 (m, 2H), 1.58–1.67 (m, 2H), 2.19 (s, 3H), 2.67–2.73 (m, 2H), 6.77 (s, 1H), 6.90 (d, *J* = 5.0 Hz, 1H), 7.15 (d, *J* = 5.0 Hz, 1H); ¹³C{¹H} NMR (100 MHz, CDCl₃) δ −0.1, 2.0, 13.7, 17.6, 23.1, 28.9, 34.4, 124.1, 124.5, 127.6, 130.0, 130.1, 132.6, 134.7, 140.0; IR (ATR): 2957, 1411, 1256, 1045, 840, 799, 783, 754, 688, 651 cm^{−1}; HRMS (DART-ESI⁺) *m/z*: calcd for C₂₀H₃₅³⁵ClO₂S₂Si₃, 491.1153; found, 491.1177.

2-Chloro-3-(4,4,5,5,6,6,7,7,7-nonafluoroheptyl)-5-(3-(4-(1,1,3,3,3-pentamethyldisiloxy)butan-1-yl)thiophen-2-

yl)thiophene (4d): 46% yield as a light yellow oil. ¹H NMR (400 MHz, CDCl₃) δ 0.0 (s, 6H), 0.05 (s, 9H), 0.50–0.57 (m, 2H), 1.33–1.43 (m, 2H), 1.58–1.69 (m, 2H), 1.89–1.99 (m, 2H), 2.05–2.21 (m, 2H), 2.69 (t, *J* = 7.3 Hz, 2H), 2.71 (t, *J* = 7.3 Hz, 2H), 6.79 (s, 1H), 6.91 (d, *J* = 5.0 Hz, 1H), 7.17 (d, *J* = 5.0 Hz, 1H); ¹³C{¹H} NMR (100 MHz, CDCl₃) δ 0.4, 2.1, 18.3, 20.5 (br), 23.4, 27.4, 29.0, 30.4 (t, *J* = 22 Hz), 34.5, 124.3, 125.1, 126.0, 129.7, 130.2, 133.6, 137.6, 140.3; ¹⁹F NMR (376 MHz, C₆F₆) δ −129.2, −127.6, −117.6, −84.2; IR (ATR): 2957, 1252, 1232, 1167, 1133, 1101, 1057, 1013, 879, 842, 807, 784, 752, 736, 719, 689, 651 cm^{−1}; HRMS (DART-ESI⁺) *m/z*: calcd for C₂₄H₃₃³⁵ClF₉OS₂Si₂, 663.1056; found, 663.1050.

2-Chloro-3-(4,4,5,5,6,6,7,7,7-nonafluoroheptyl)-5-(3-(4-(bis(trimethylsiloxy)(methyl)silyl)butan-1-yl)thiophen-2-yl)thiophene (4e): 50% yield as a light yellow oil. ¹H NMR (400 MHz, CDCl₃) δ 0.0 (s, 3H), 0.07 (s, 18H), 0.44–0.52 (m, 2H), 1.32–1.43 (m, 2H), 1.58–1.68 (m, 2H), 1.89–1.99 (m, 2H), 2.04–2.21 (m, 2H), 2.68 (t, *J* = 7.8 Hz, 2H), 2.70 (t, *J* = 7.8 Hz, 2H), 6.79 (s, 1H), 6.91 (d, *J* = 5.0 Hz, 1H), 7.17 (d, *J* = 5.0 Hz, 1H); ¹³C{¹H} NMR (100 MHz, CDCl₃) δ −0.2, 2.0, 17.6, 20.5 (br), 23.1, 27.4, 29.0, 30.4 (t, *J* = 22 Hz), 34.3, 124.3, 125.1, 126.0, 129.7, 130.2, 133.6, 137.6, 140.2; ¹⁹F NMR (376 MHz, C₆F₆) δ −129.2, −127.6, −117.6, −84.2; IR (ATR): 2958, 1252, 1233, 1167, 1134, 1046, 870, 841, 800, 783, 754, 719, 689, 651 cm^{−1}; HRMS (DART-ESI⁺) *m/z*: calcd for C₂₇H₄₃³⁵ClF₉OS₂Si₃, 737.1608; found, 737.1611.

General procedure for the polymerization of chlorobithiophene representatives: the reaction of 4b leading to poly(3-(4-(1,1,3,3,3-pentamethyldisiloxy)butan-3-yl)thiophen-2,5-diyl)-alt-poly(3-methylthiophen-2,5-diyl) (6b): To a 20 mL Schlenk tube equipped with a magnetic stirring bar were added **4b** (104 mg, 0.25 mmol) and a 1 M THF solution of TMPMgCl–LiCl (0.3 mL, 0.3 mmol) was added at room temperature. After stirring at room temperature for 3 h, THF (2.5 mL) and NiCl₂(PPh₃)IPr (**5**, 3.9 mg, 6.0 μmol) were added to initiate the polymerization. The color of the solution changed to light orange and then to dark purple with the formation of slightly insoluble material. After stirring at room temperature for 24 h, the reaction mixture was poured into a mixture of hydrochloric acid (1.0 M, 2 mL) and methanol (10 mL) to form a precipitate, which was filtered off to leave a dark purple solid. After washing with methanol and hexanes repeatedly, the solid was dried under reduced pressure to afford 79.6 mg of **6b** (84% isolated yield). The HT regioregularity was confirmed by ¹H NMR analysis, and the molecular weight (*M_n*) and the molecular weight distribution (*M_w*/*M_n*) were estimated by SEC analysis. HT = 98%, *M_n* = 10400, *M_w* = 16900, *M_w*/*M_n* = 1.62; ¹H NMR (400 MHz, CDCl₃) δ 0.02–0.08 (br, 15H), 0.50–0.63 (m, 2H), 1.41–1.52 (m, 2H), 1.64–1.78 (m, 2H), 2.44 (s, 3H),

2.75–2.85 (m, 2H), 6.95 (s, 1H), 6.99 (s, 1H); IR (ATR): 2956, 2925, 2855, 1728, 1445, 1252, 1057, 841, 806, 782, 753 cm⁻¹.

The other polymers **6c–e** were synthesized similarly. The polymerization was continued for 18–24 h or terminated after 1 h when **4** bearing a fluoroalkyl substituent was employed, due to faster polymerization, which brought about an uncontrollable molecular weight. The properties and spectroscopic data are summarized below.

Poly(3-(4-(bis(trimethylsiloxy)(methyl)silyl)butan-1-yl)thiophen-2,5-diyl)-alt-poly(3-methylthiophen-2,5-diyl) (6c): 84% yield. $M_n = 70100$, $M_w/M_n = 1.38$; ¹H NMR (400 MHz, CDCl₃) δ 0.03 (s, 3H), 0.09 (s, 18H), 0.43–0.65 (m, 2H), 1.35–1.55 (m, 2H), 1.63–1.85 (m, 2H), 2.44 (s, 3H), 2.71–2.92 (m, 2H), 6.95 (s, 1H), 7.00 (s, 1H); ¹³C{¹H} NMR (100 MHz, CDCl₃) δ -0.1, 2.1, 15.9, 17.7, 23.3, 29.4, 34.2, 128.3, 130.0, 130.4, 131.0, 133.5, 134.3, 134.4, 140.0; IR (ATR): 2957, 2926, 2858, 1511, 1449, 1256, 1046, 841, 802, 782, 754, 668 cm⁻¹.

Poly(3-(4-(1,1,3,3,3-pentamethyldisiloxy)butan-3-yl)thiophen-2,5-diyl)-alt-poly(3-(4,4,5,5,6,6,7,7,7-nonafluoroheptyl)thiophen-2,5-diyl) (6d): 48% yield. $M_n = 68600$, $M_w/M_n = 1.15$; ¹H NMR (400 MHz, CDCl₃) δ 0.06 (s, 15H), 0.55–0.66 (m, 2H), 1.41–1.55 (m, 2H), 1.67–1.83 (m, 2H), 1.97–2.12 (m, 2H), 2.12–2.30 (m, 2H), 2.73–2.88 (m, 2H), 2.88–3.01 (m, 2H), 7.00 (br, 2H); ¹³C{¹H} NMR (100 MHz, CDCl₃) δ 0.5, 2.1, 18.4, 21.3 (br), 23.5, 28.7, 29.4, 30.6 (t, $J = 22$ Hz), 34.4, 128.2, 129.3, 130.7, 131.6, 133.3, 134.4, 137.8, 140.4; IR (ATR): 2957, 2925, 1452, 1356, 1252, 1232, 1169, 1134, 1059, 879, 842, 807, 783, 752, 720, 701 cm⁻¹.

Poly(3-(4-(bis(trimethylsiloxy)(methyl)silyl)butan-1-yl)thiophen-2,5-diyl)-alt-poly(3-(4,4,5,5,6,6,7,7,7-nonafluoroheptyl)thiophen-2,5-diyl) (6e): 58% yield. SEC analysis showed $M_n = 33200$, $M_w/M_n = 1.07$; ¹H NMR (400 MHz, CDCl₃) δ 0.03 (s, 3H), 0.09 (s, 18H), 0.44–0.66 (m, 2H), 1.37–1.60 (m, 2H), 1.60–1.86 (m, 2H), 1.94–2.33 (m, 4H), 2.63–3.11 (m, 4H), 7.00 (br, 2H); ¹³C{¹H} NMR (100 MHz, CDCl₃) δ -0.2, 2.0, 17.7, 21.3, 23.3, 28.7, 29.4, 30.6 (t, $J = 22$ Hz), 34.2, 128.2, 129.3, 130.7, 131.6, 133.3, 134.5, 137.8, 140.4; IR (ATR): 2957, 1455, 1356, 1251, 1233, 1134, 1052, 840, 801, 773, 754, 720, 700 cm⁻¹.

Funding

This work was partially supported by JSPS Kakenhi B Grant Number JP19182273, Cooperative Research Program of “Network Joint Research Center for Materials and Devices”, and Kobe University for the promotion of international collaboration researches.

ORCID® iDs

Atsunori Mori - <https://orcid.org/0000-0002-1163-264X>

Masaki Horie - <https://orcid.org/0000-0002-7734-5694>

Preprint

A non-peer-reviewed version of this article has been previously published as a preprint doi:10.3762/bxiv.2019.160.v1

References

- Sirringhaus, H.; Tessler, N.; Friend, R. H. *Science* **1998**, *280*, 1741–1744. doi:10.1126/science.280.5370.1741
- Li, G.; Shrotriya, V.; Huang, J.; Yao, Y.; Moriarty, T.; Emery, K.; Yang, Y. *Nat. Mater.* **2005**, *4*, 864–868. doi:10.1038/nmat1500
- Osaka, I.; McCullough, R. D. *Acc. Chem. Res.* **2008**, *41*, 1202–1214. doi:10.1021/ar800130s
- Bao, Z.; Dodabalapur, A.; Lovinger, A. J. *Appl. Phys. Lett.* **1996**, *69*, 4108–4110. doi:10.1063/1.117834
- Yokozawa, T.; Ohta, Y. *Chem. Rev.* **2016**, *116*, 1950–1968. doi:10.1021/acs.chemrev.5b00393
- Okamoto, K.; Luscombe, C. K. *Polym. Chem.* **2011**, *2*, 2424–2434. doi:10.1039/c1py00171j
- Krasovskiy, A.; Krasovskaya, V.; Knochel, P. *Angew. Chem., Int. Ed.* **2006**, *45*, 2958–2961. doi:10.1002/anie.200504024
- Tamba, S.; Shono, K.; Sugie, A.; Mori, A. *J. Am. Chem. Soc.* **2011**, *133*, 9700–9703. doi:10.1021/ja2033525
- Tamba, S.; Tanaka, S.; Okubo, Y.; Meguro, H.; Okamoto, S.; Mori, A. *Chem. Lett.* **2011**, *40*, 398–399. doi:10.1246/cl.2011.398
- Matsubara, K.; Ueno, K.; Shibata, Y. *Organometallics* **2006**, *25*, 3422–3427. doi:10.1021/om0602658
- Herrmann, W. A. *Angew. Chem., Int. Ed.* **2002**, *41*, 1290–1309. doi:10.1002/1521-3773(20020415)41:8<1290::aid-anie1290>3.0.co;2-y
- Fujita, K.; Sumino, Y.; Ide, K.; Tamba, S.; Shono, K.; Shen, J.; Nishino, T.; Mori, A.; Yasuda, T. *Macromolecules* **2016**, *49*, 1259–1269. doi:10.1021/acs.macromol.5b02524
- Mori, A.; Ide, K.; Tamba, S.; Tsuji, S.; Toyomori, Y.; Yasuda, T. *Chem. Lett.* **2014**, *43*, 640–642. doi:10.1246/cl.131222
- Ogura, T.; Kubota, C.; Suzuki, T.; Okano, K.; Tanaka, N.; Matsumoto, T.; Nishino, T.; Mori, A.; Okita, T.; Funahashi, M. *Chem. Lett.* **2019**, *48*, 611–614. doi:10.1246/cl.190139
- Noh, S.; Gobalasingham, N. S.; Thompson, B. C. *Macromolecules* **2016**, *49*, 6835–6845. doi:10.1021/acs.macromol.6b01178
- Locke, J. R.; McNeil, A. J. *Macromolecules* **2010**, *43*, 8709–8710. doi:10.1021/ma102218y
- Palermo, E. F.; Darling, S. B.; McNeil, A. J. *J. Mater. Chem. C* **2014**, *2*, 3401–3406. doi:10.1039/c3tc32512a
- Lee, E.; Hammer, B.; Kim, J.-K.; Page, Z.; Emrick, T.; Hayward, R. C. *J. Am. Chem. Soc.* **2011**, *133*, 10390–10393. doi:10.1021/ja2038547
- Ouhib, F.; Desbief, S.; Lazzaroni, R.; De Winter, J.; Gerbaux, P.; Jérôme, C.; Detrembleur, C. *Macromolecules* **2012**, *45*, 6796–6806. doi:10.1021/ma3009405
- Hong, X. M.; Tyson, J. C.; Collard, D. M. *Macromolecules* **2000**, *33*, 3502–3504. doi:10.1021/ma991997x
- Björnholm, T.; Greve, D. R.; Reitzel, N.; Hassenkam, T.; Kjaer, K.; Howes, P. B.; Larsen, N. B.; Bøgelund, J.; Jayaraman, M.; Ewbank, P. C.; McCullough, R. D. *J. Am. Chem. Soc.* **1998**, *120*, 7643–7644. doi:10.1021/ja981077e

22. Reitzel, N.; Greve, D. R.; Kjaer, K.; Howes, P. B.; Jayaraman, M.; Savoy, S.; McCullough, R. D.; McDevitt, J. T.; Bjørnholm, T. *J. Am. Chem. Soc.* **2000**, *122*, 5788–5800. doi:10.1021/ja9924501
23. Smith, Z. C.; Meyer, D. M.; Simon, M. G.; Staii, C.; Shukla, D.; Thomas, S. W., III. *Macromolecules* **2015**, *48*, 959–966. doi:10.1021/ma502289n
24. Nakamura, K.; Tamba, S.; Sugie, A.; Mori, A. *Chem. Lett.* **2013**, *42*, 1200–1202. doi:10.1246/cl.130523
25. Fujita, K.; Nakagawa, N.; Sunahara, K.; Ogura, T.; Okano, K.; Mori, A. *Synthesis* **2017**, *49*, 1285–1294. doi:10.1055/s-0036-1588094
26. Kantchev, E. A. B.; O'Brien, C. J.; Organ, M. G. *Angew. Chem., Int. Ed.* **2007**, *46*, 2768–2813. doi:10.1002/anie.200601663
27. Sun, D.; Li, Y.; Ren, Z.; Bryce, M. R.; Li, H.; Yan, S. *Chem. Sci.* **2014**, *5*, 3240–3245. doi:10.1039/c4sc01068j
28. Nakagawa, N.; Ogura, T.; Fujita, K.; Sumino, Y.; Hashimoto, T.; Okano, K.; Mori, A. *Chem. Lett.* **2017**, *46*, 453–455. doi:10.1246/cl.161180
29. Shen, J.; Fujita, K.; Matsumoto, T.; Hongo, C.; Misaki, M.; Ishida, K.; Mori, A.; Nishino, T. *Macromol. Chem. Phys.* **2017**, *218*, No. 1700197. doi:10.1002/macp.201700197
30. Matsumoto, T.; Nishi, K.; Tamba, S.; Kotera, M.; Hongo, C.; Mori, A.; Nishino, T. *Polymer* **2017**, *119*, 76–82. doi:10.1016/j.polymer.2017.05.027
31. Inoue, R.; Yamaguchi, M.; Murakami, Y.; Okano, K.; Mori, A. *ACS Omega* **2018**, *3*, 12703–12706. doi:10.1021/acsomega.8b01707

License and Terms

This is an Open Access article under the terms of the Creative Commons Attribution License (<https://creativecommons.org/licenses/by/4.0>). Please note that the reuse, redistribution and reproduction in particular requires that the authors and source are credited.

The license is subject to the *Beilstein Journal of Organic Chemistry* terms and conditions: (<https://www.beilstein-journals.org/bjoc>)

The definitive version of this article is the electronic one which can be found at:
doi:10.3762/bjoc.16.31



Synthesis and circularly polarized luminescence properties of BINOL-derived bisbenzofuro[2,3-*b*:3',2'-*e*]pyridines (BBZFPys)

Ryo Takishima¹, Yuji Nishii^{*2}, Tomoaki Hinoue¹, Yoshitane Imai³ and Masahiro Miura^{*1}

Full Research Paper

[Open Access](#)

Address:

¹Department of Applied Chemistry, Graduate School of Engineering, Osaka University, Suita, Osaka 565-0871, Japan, ²Frontier Research Base for Global Young Researchers, Graduate School of Engineering, Osaka University, Suita, Osaka 565-0871, Japan and ³Department of Applied Chemistry, Faculty of Science and Engineering, Kindai University, Higashi-Osaka, Osaka 577-8502, Japan

Email:

Yuji Nishii^{*} - y_nishii@chem.eng.osaka-u.ac.jp; Masahiro Miura^{*} - miura@chem.eng.osaka-u.ac.jp

^{*} Corresponding author

Keywords:

BINOL; C–H activation; circularly polarized luminescence; palladium

Beilstein J. Org. Chem. **2020**, *16*, 325–336.

doi:10.3762/bjoc.16.32

Received: 07 January 2020

Accepted: 21 February 2020

Published: 06 March 2020

This article is part of the thematic issue "C–H functionalization for materials science".

Guest Editor: K. Itami

© 2020 Takishima et al.; licensee Beilstein-Institut.

License and terms: see end of document.

Abstract

A series of optically active bisbenzofuro[2,3-*b*:3',2'-*e*]pyridine (BBZFPy) derivatives was synthesized starting with the readily available (*S*)- and (*R*)-1,1'-bi-2-naphthols through a palladium-catalyzed multiple intramolecular C–H/C–H coupling as the key ring-closure step. The effect of terminal *tert*-butyl substituents on the BBZFPy skeleton was systematically investigated to uncover a unique aggregation-induced enhancement of CPL characteristics in the solid state. The crystal structures of the coupling products were also evaluated by single crystal X-ray analysis and the well-ordered intermolecular stacking arrangements appeared to be responsible for the enhanced CPL.

Introduction

Densely-fused (hetero)aromatic compounds have been a key motif in a wide range of manufactured functional molecules, as they exhibit fundamentally useful electrochemical and photo-physical properties. Considerable effort has therefore taken into the development of efficient methods for the construction of such polycyclic scaffolds, and the last decade has witnessed a remarkable improvement in the palladium-catalyzed C–H/C–H oxidative coupling as one of the potential synthetic strategies

[1]. This method is straightforward and highly step-economical, enabling us to produce condensed (hetero)acenes from rather simple polyarenes, in which several aromatic units are connected with each other through appropriate linker units [2–11]. Recently, we reported the synthesis and optical properties of a series of furan-fused aromatics via the formal dehydrogenative coupling adopting oxygen atom as the linker [12–17]. In particular, bisbenzofuro[2,3-*b*:3',2'-*e*]pyridines (BBZFPys)

were found to exhibit intense photoluminescence with relatively high quantum efficiency (Φ_{flu} up to 0.70), indicating that the BBFZPy scaffold may serve as a key fluorophore unit in certain light-emitting functional materials (Scheme 1) [14].

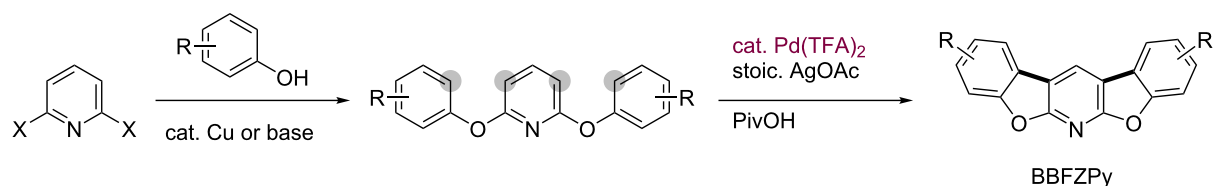
Meanwhile, organic optoelectronic materials with circularly polarized luminescence (CPL) characteristics have attracted significant research interests in recent years [18–21] for their potential applications in three-dimensional displays [22], information storage systems [23], molecular photoswitches [24], etc. Among a series of chiral scaffolds for CPL emitting molecules, axially chiral 1,1'-bi-2-naphthol (BINOL) has been frequently adopted for the core structure owing to the availability of both enantiomers as well as the ease of site-selective functionalization. Up to date, many BINOL-based CPL active compounds have been established by installing aromatic subunits on the periphery of the binaphthyl skeleton or on the hydroxy groups [25–32], extending the π -system [33], and linearly connecting the naphthyl rings [34–36]. In these compounds, the hydroxy groups are remained untouched or protected as the corresponding ethers or esters. We envisioned that the assembly of the binaphthyl-fused furan motif embedding the BINOL hydroxy groups into the polyaromatic scaffolds would lead to the development of new chiroptical materials. Such molecules, however, have hardly been investigated to date probably because of the synthetic difficulty to obtain them as pure enantiomers. There

have been only a few reports for the binaphthyl-fused furan-ring construction from the C3-alkynylated BINOL derivatives [37–39]. In this context, we herein describe the synthesis of axially chiral BINOL-derived BBFZPys through the palladium-catalyzed oxidative coupling reaction. The optical properties of the synthesized polyaromatic compounds were systematically studied, and some of them displayed an interesting aggregation-induced enhancement of CPL in the solid state with considerably higher dissymmetry factors compared to those in solution.

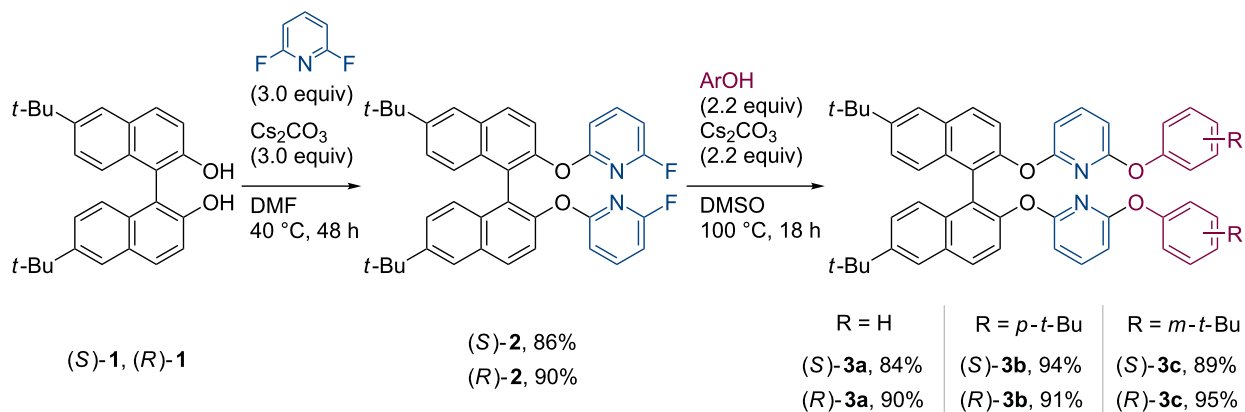
Results and Discussion

Synthesis of BINOL-derived BBFPys

The study was initiated with the synthesis of 2,6-diaryloxy-pyridines **3** bearing a 1,1'-binaphthyl backbone as precursors for the dehydrogenative coupling reaction (Scheme 2). In general, functionalization of the BINOL hydroxy groups should be performed at temperatures below 80 °C to prevent racemization [40,41]. 6,6'-Di-*tert*-butyl-1,1'-bi-2-naphthol (**1**) was treated with 2,6-difluoropyridine using cesium carbonate as base in DMF at 40 °C [42], giving both the enantiomers of **2** in optically pure forms. The remaining fluorine substituents were subsequently replaced by a series of phenols including unsubstituted phenol, *p*-*tert*-butylphenol, and *m*-*tert*-butylphenol to produce the corresponding unsymmetrically substituted pyridines **3a–c** in high yields. We then examined the oxidative cyclization of these compounds under the standard conditions



Scheme 1: Synthesis of BBFZPys through the Pd-catalyzed C–H/C–H coupling.



Scheme 2: Synthesis of **3a–c**.

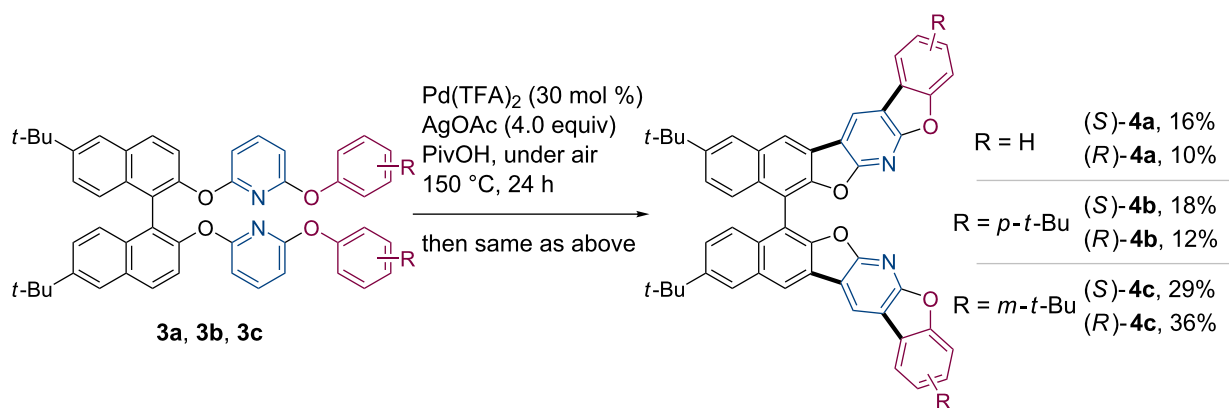
adopting $\text{Pd}(\text{TFA})_2$ (30 mol %), TFA = trifluoroacetate) and AgOAc (3.0 equiv) as catalyst and oxidant, respectively, in pivalic acid as solvent (Scheme 3). Since the desired four-fold coupling products **4** were obtained only in small quantities after the reactions, the crude mixtures containing incompletely cyclized compounds were again subjected to the same catalytic conditions. To our delight, all the target molecules **4a–c** were successfully isolated as pure enantiomers in 10–36% yields. The higher yield of **4c** was probably due to its better solubility.

In order to systematically evaluate the optical properties of these coupling products, a simple benzofuran-fused 1,1'-binaphthyl **6** was also synthesized as a benchmark (Scheme 4). The parent ether **5** was obtained through the arylation of **1** utilizing Ph_2IOTf as arylating reagent [43,44]. Some copper-mediated arylation protocols using bromobenzene or iodobenzene [45,46] were also applicable to the preparation of **5**, but significant loss of optical purity was inevitable. After the Pd-catalyzed cyclization under the standard conditions, the desired compounds (*S*)- and (*R*)-**6** were obtained as pure enantiomers in 18% yield.

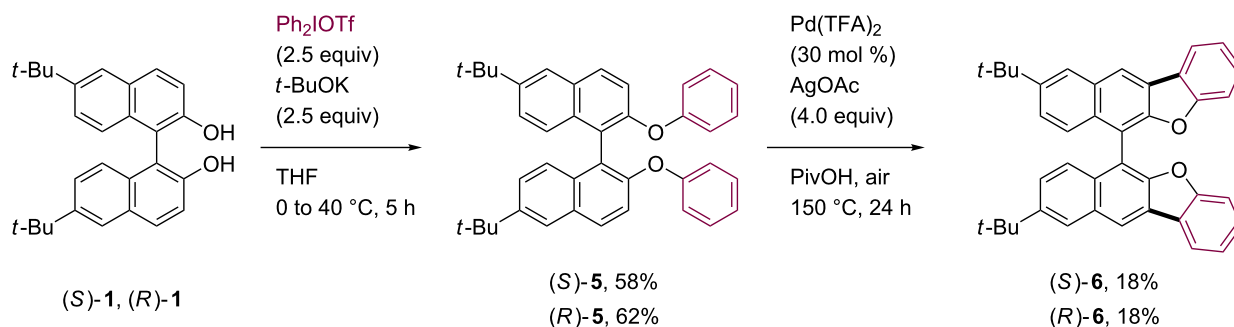
Optical properties

We next investigated the optical properties of the coupling products (Figure 1 and Table 1). The parent compounds **3a–c** emitted fluorescence at around 360 nm both in sufficiently diluted CHCl_3 solutions (1.0×10^{-5} M) and in the solid states. The quantum yields of these molecules were around 0.15 in solution, which is typical for binaphthyl compounds [47]. In contrast, **4a–c** as well as **6** exhibited fluorescence at around 390 nm in solution, with relatively higher quantum yields of 0.37–0.40. The emission bands of **4a–c** in their solid state were considerably red-shifted as compared to that of **6**, suggesting that these compounds displayed the appreciable effect of molecular aggregation. Interestingly, **4b** and **4c**, bearing the additional terminal *tert*-butyl substituents, were more red-shifted than **4a** despite such a sterically demanding group usually disturbs intermolecular stacking interactions.

Subsequently, the chiroptical properties of the synthesized compounds were evaluated (Figure 2 and Figure 3, Table 2). The circular dichroism (CD) spectra in CHCl_3 solutions showed apparent Cotton signals characteristic to axially chiral mole-



Scheme 3: Synthesis of **4a–c** through oxidative coupling reaction.



Scheme 4: Synthesis of **6**.

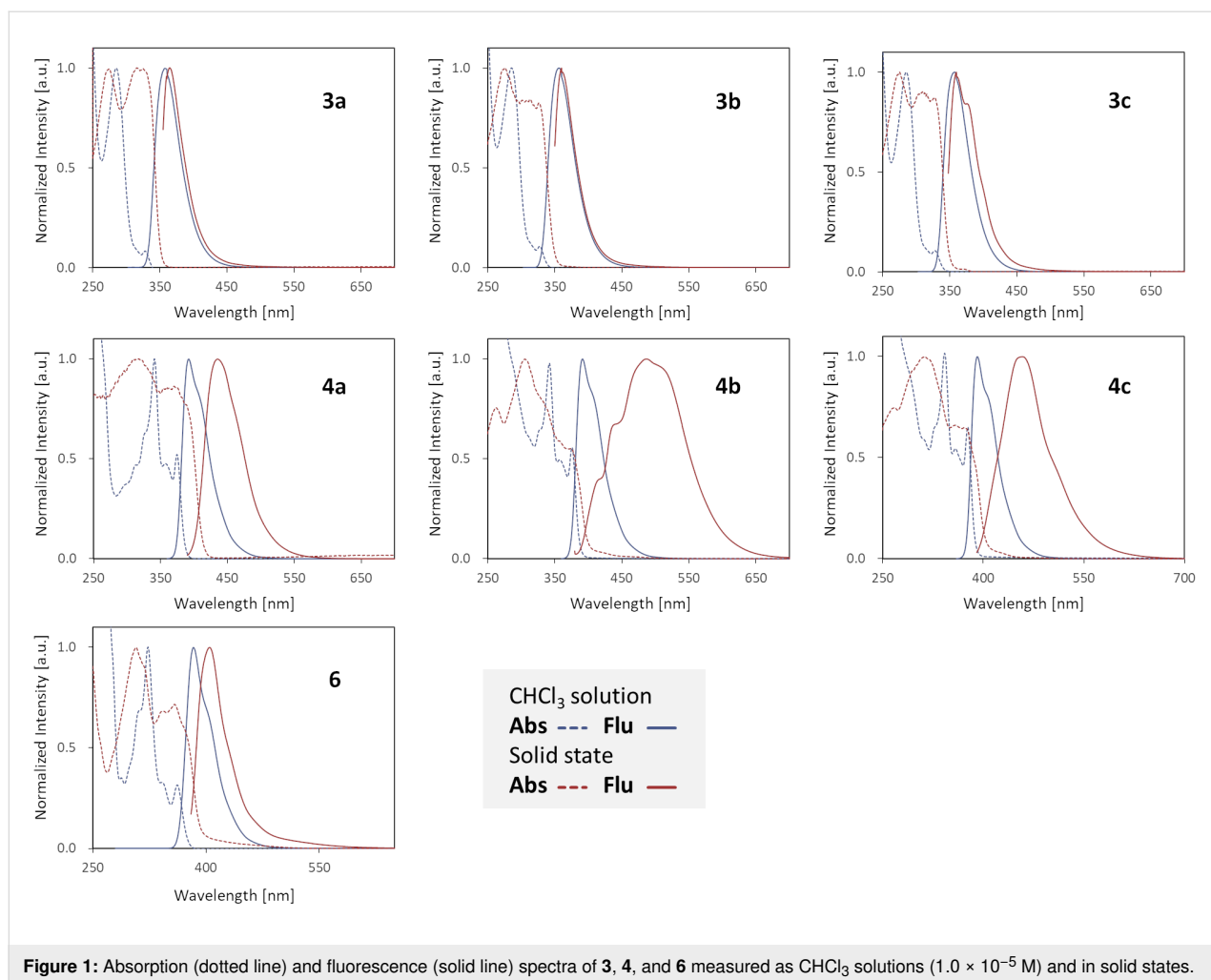


Figure 1: Absorption (dotted line) and fluorescence (solid line) spectra of **3**, **4**, and **6** measured as CHCl_3 solutions (1.0×10^{-5} M) and in solid states.

Table 1: Fluorescence properties.^a

Compd.	solution λ_{max} (λ_{ex})	solid λ_{max} (λ_{ex})	Φ (solution)	Φ (solid)
3a	358 nm (282 nm)	360 nm (341 nm)	0.13	0.30
3b	357 nm (283 nm)	360 nm (338 nm)	0.14	0.21
3c	357 nm (283 nm)	360 nm (338 nm)	0.16	0.19
4a	392 nm (341 nm)	436 nm (369 nm)	0.39	0.17
4b	391 nm (342 nm)	488 nm (369 nm)	0.38	0.08
4c	391 nm (342 nm)	457 nm (370 nm)	0.40	0.07
6	384 nm (263 nm)	405 nm (380 nm)	0.37	0.13

^aMeasured at room temperature as solution in CHCl_3 (1.0×10^{-5} M) and in the solid states.

cules. In all cases, the (*S*)- and (*R*)-enantiomers were evidently mirror images of each other while the anisotropy factors g_{abs} are relatively small and in the range of 10^{-4} to 10^{-7} . The spec-

tral shapes of **3a–c** and **4a–c** were respectively comparable, indicating that the posted positions of the terminal *tert*-butyl groups exerted minimal influence on the Cotton effect in the

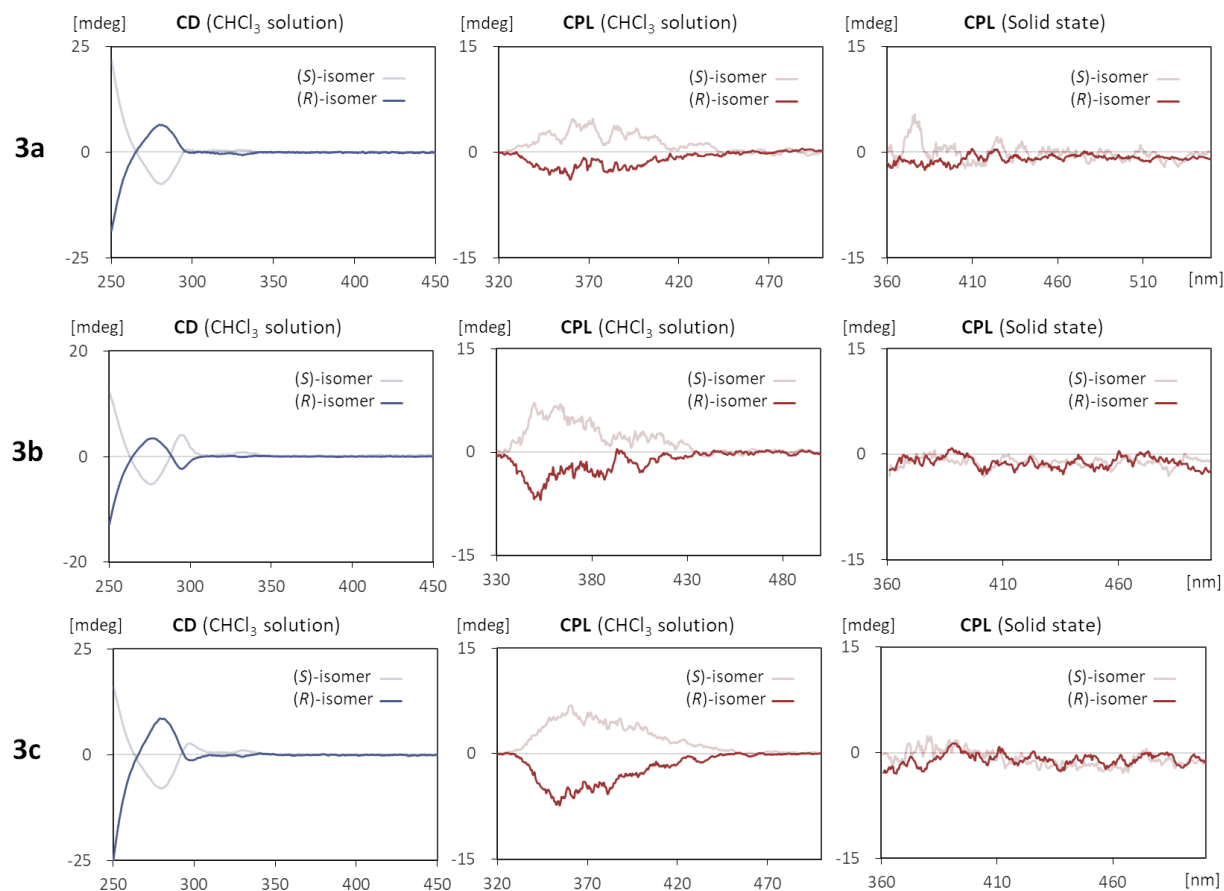


Figure 2: CD and CPL spectra of **3** measured as CHCl_3 solutions (1.0×10^{-5} M) and in the solid states (dispersed in Fomblin®).

Table 2: Calculated dimensionless dissymmetry factors.^a

Compd.	g_{abs} (solution)	g_{lum} (solution)	g_{lum} (solid)
3a	8.72×10^{-7} (285 nm)	4.37×10^{-4} (358 nm)	n.d. ^b
3b	3.18×10^{-7} (285 nm)	6.72×10^{-4} (357 nm)	n.d. ^b
3c	1.06×10^{-6} (285 nm)	6.90×10^{-4} (357 nm)	n.d. ^b
4a	5.60×10^{-6} (341 nm)	5.57×10^{-4} (392 nm)	5.40×10^{-4} (436 nm)
4b	9.96×10^{-5} (342 nm)	4.60×10^{-4} (391 nm)	6.68×10^{-3} (488 nm)
4c	8.72×10^{-5} (342 nm)	6.40×10^{-4} (391 nm)	6.06×10^{-3} (457 nm)
6	1.00×10^{-4} (256 nm)	3.80×10^{-4} (384 nm)	1.40×10^{-4} (405 nm)

^aMeasured at room temperature as solution in CHCl_3 (1.0×10^{-5} M) and in solid states (dispersed in Fomblin®). ^bNot determined.

solution state. A similar trend was observed for the CPL spectra. The (*S*)-isomers displayed left-handed CPL characteristics throughout the wavelengths of their corresponding fluorescence emission bands, whereas the (*R*)-isomers emitted right-

handed CPL to produce the mirror images. The calculated luminescence dissymmetry factors [48] g_{lum} for the solutions were all within the range of 3.80×10^{-4} to 6.90×10^{-4} . On the other hand, in the dispersed solid state in Fomblin® PFPE (perfluoro-

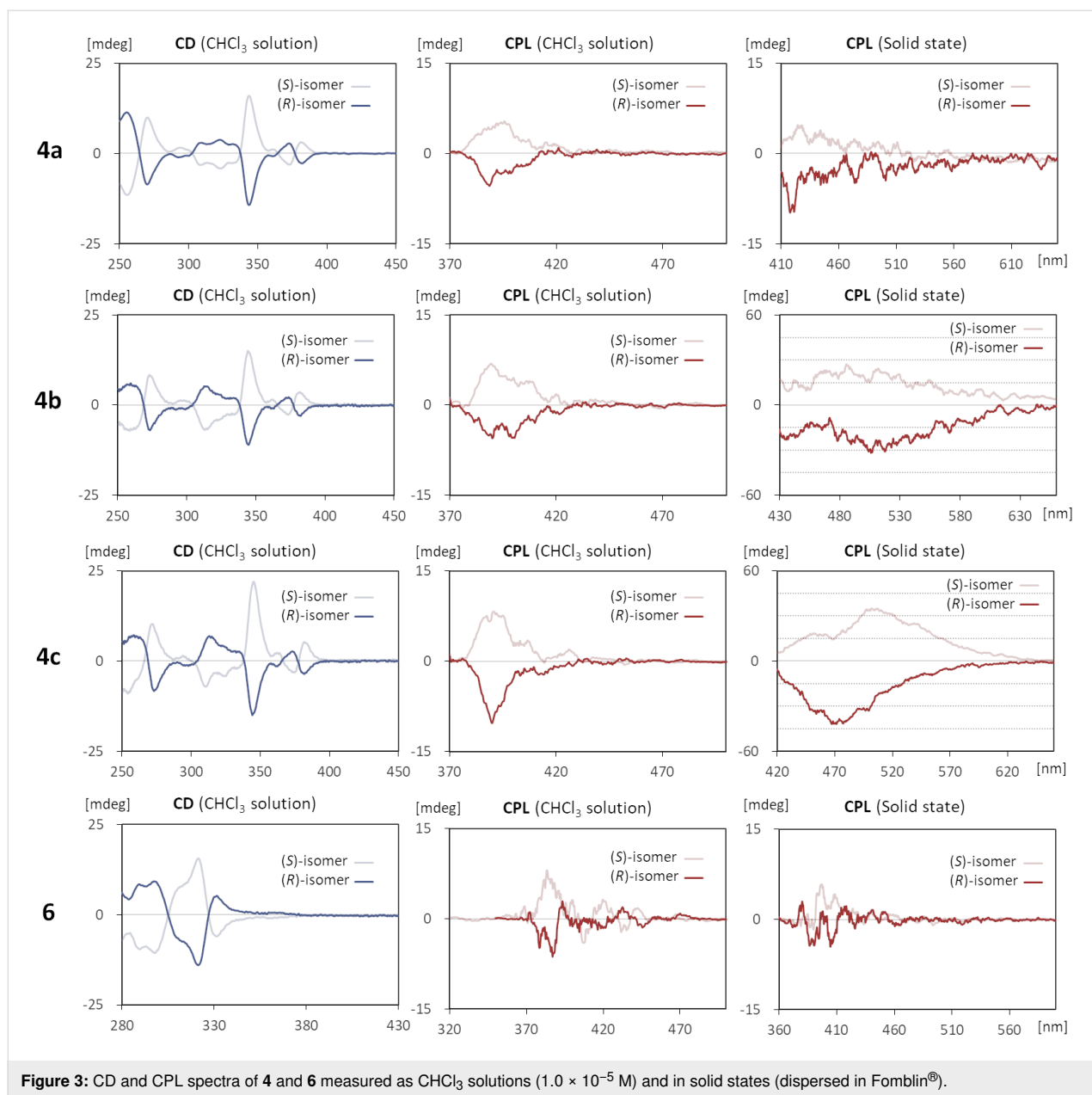
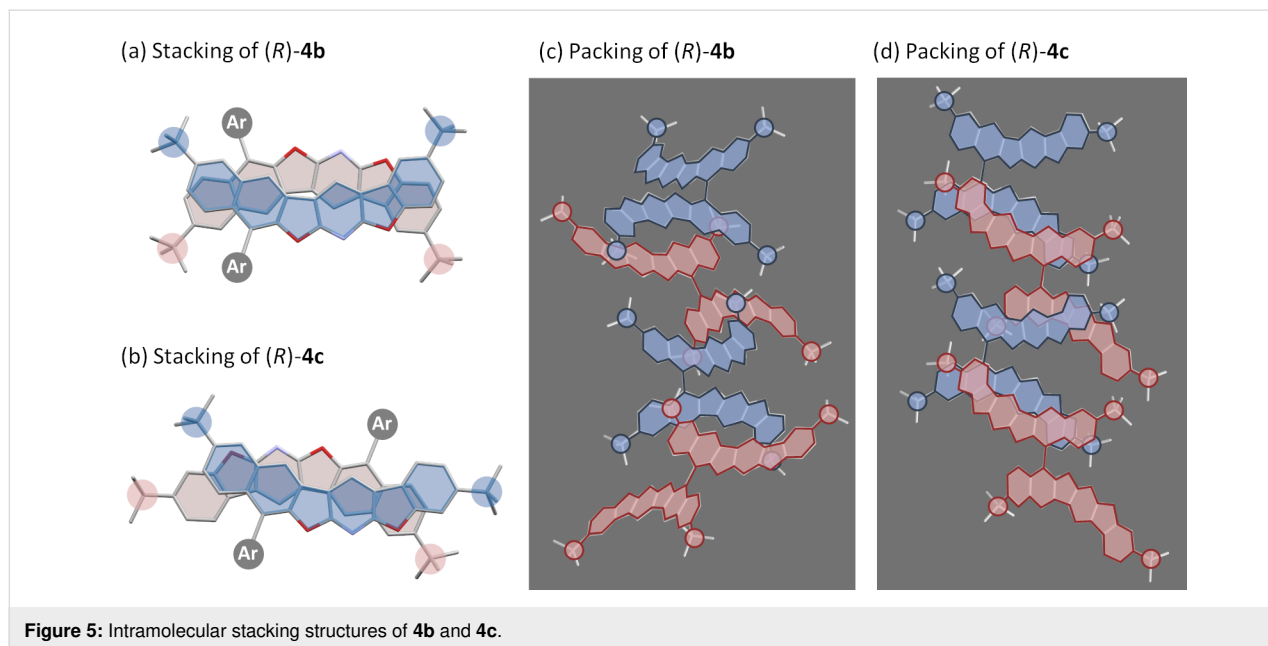
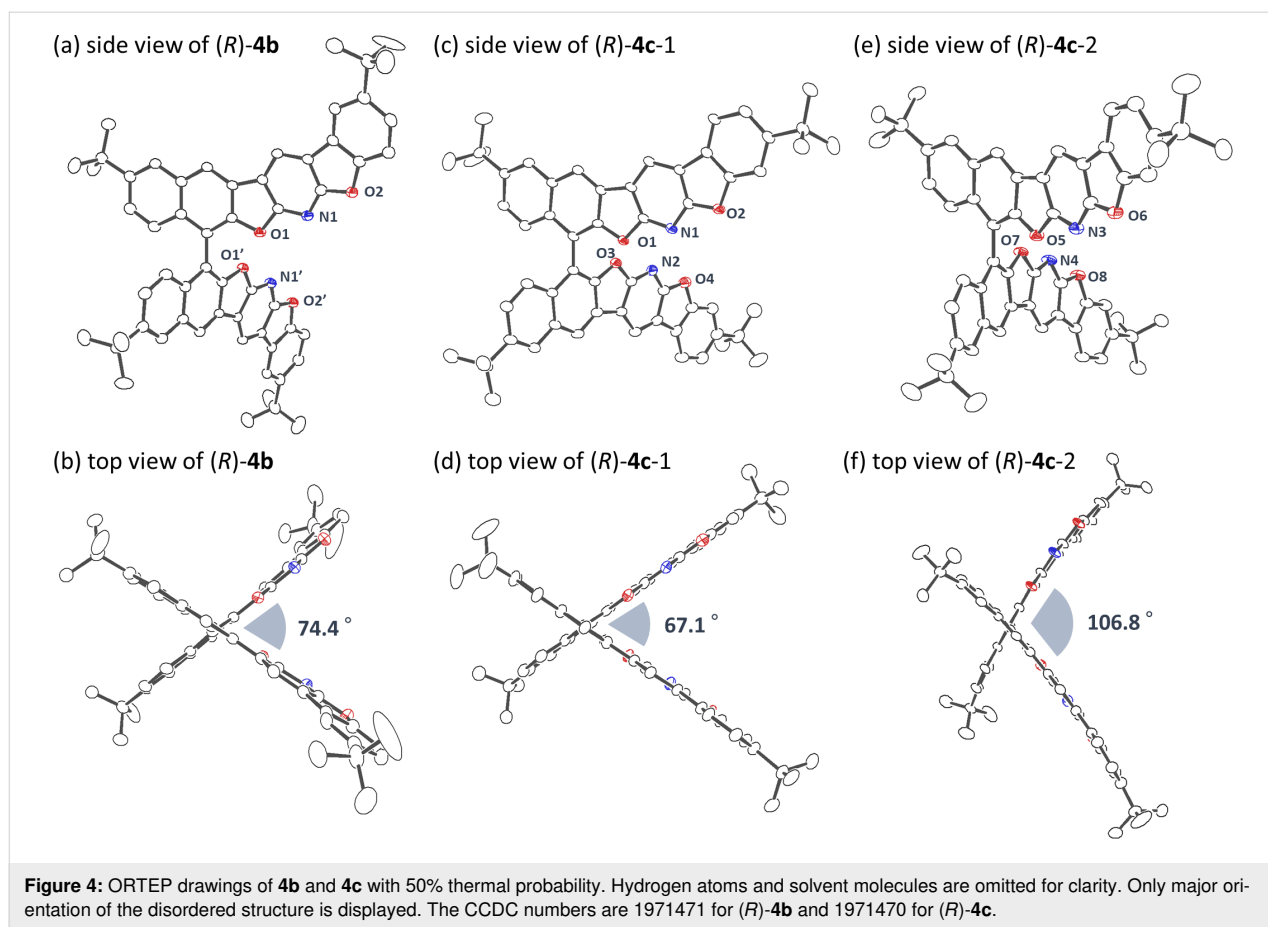


Figure 3: CD and CPL spectra of **4** and **6** measured as CHCl_3 solutions (1.0×10^{-5} M) and in solid states (dispersed in Fomblin®).

ropolyether) fluid (each sample was not soluble in the fluid and gave the expected solid-state luminescence), the signal intensity drastically changed depending on the molecular structures. In particular, **4b** and **4c** exhibited enhanced CPL characteristics with considerably high g_{lum} values of 6.68×10^{-3} and 6.06×10^{-3} , respectively, which were approximately ten times larger than those of the CHCl_3 solutions [49]. The parent compounds **3a–c**, however, did not give clear mirror images in the CPL measurements. Since such a phenomenon was not observed for **4a** and **6**, the terminal *tert*-butyl substituents in **4b** and **4c** were likely to assist the formation of well-ordered aggregates, being consistent with the observation of the red-shifted luminescence discussed above.

Crystal structures of **4b** and **4c**

The molecular structures of **4b** and **4c** were unambiguously determined by single crystal X-ray diffraction analysis. The crystal of **4b** is classified into a space group $P4_322$ (tetragonal) with a biaryl torsion angle of 74.4° (Figure 4b). A considerable intermolecular π – π stacking interaction was observed in between its polyaromatic fragments whose distance is approximately 3.44 \AA . The polycyclic subunits overlap each other, being line-symmetrically aligned (Figure 5a). Meanwhile, the isomer **4c** has two independent molecules in the unit cell, and the torsion angles are 67.1° and 106.8° , respectively (Figure 4d and 4f). As displayed in Figure 4b, the aromatic fragments are point-symmetrically overlapped with the π – π stacking distance



of around 3.45 Å. It is noteworthy that both **4b** and **4c** pile up while minimizing the steric repulsion between the *tert*-butyl groups which occupy “staggered” orientations in their crystal

structures (Figure 5c and 5d). Unfortunately, the crystal structure of **4a** was not determined after numerous attempts for obtaining crystals suitable for the X-ray analysis. Based on these

observations, it is reasonable to conclude that the *tert*-butyl substituents effectively restricted the stacking structure to the specific conformations, thereby facilitating the assembly of well-ordered aggregates in the solid state [50–54].

Conclusion

In summary, we have achieved the synthesis of a series of CPL-active polyheteroaromatic compounds from readily available chiral BINOLs via the *O*-arylation and subsequent palladium-catalyzed C–H/C–H coupling reaction. The substitution pattern on the BBZFPy skeleton had much effect on the solid-state optical properties. Particularly, the compounds **4b** and **4c** bearing terminal *tert*-butyl groups exhibited solid-state fluorescence with the enhanced CPL characteristics ($g_{lum} = 6.68 \times 10^{-3}$ and 6.06×10^{-3}), as compared to those in solution. Their solid-state structures were investigated by X-ray diffraction analysis to find well-ordered intermolecular stacking structures within the crystals.

Experimental

General

All manipulations were performed under N₂ using standard Schlenk techniques unless otherwise noted. DMF was dried and deoxygenated by a Glass Counter Solvent Dispensing System (Nikko Hansen & Co., Ltd.). DMSO was distilled from CaH₂ and stored over molecular sieves 4 Å. Silica gel column chromatography was performed using Wakosil® C-200 (64–210 µm). Nuclear magnetic resonance spectra were measured at 400 MHz (¹H NMR) and at 100 MHz (¹³C NMR) in 5 mm NMR tubes. ¹H NMR chemical shifts were reported in ppm relative to the resonance of TMS (δ 0.00) or the residual solvent signals at δ 7.26 for CDCl₃. ¹³C NMR chemical shifts were reported in ppm relative to the residual solvent signals at δ 77.2 for CDCl₃. Melting points were measured using a Mettler Toledo MP90. High-resolution mass spectra (HRMS) were recorded by APCI-TOF or EI. Preparative gel permeation chromatography (GPC) was conducted with a YMC GPC-T2000 column eluting with CHCl₃. Absorption spectra were recorded with JASCO V-750 spectrometer. Photoluminescence spectra were recorded with JASCO FP-8500 spectrometer. Quantum yield was determined using an integration sphere system. CD and CPL spectra were recorded with JASCO J-820AC and JASCO CPL-300 spectrometers. HPLC analysis was carried out with JASCO EXTREMA (PU4180/MD4015/CO4065) equipped with YMC CHIRAL ART Amylose-SA and YMC CHIRAL ART Cellulose-SB columns.

Preparation of 6,6'-di-*tert*-butyl-BINOL (**1**)

Compound **1** was prepared according to a literature procedure [55]. ¹H NMR (400 MHz, CDCl₃) δ 1.38 (s, 18H), 4.96 (s, 2H), 7.13 (d, *J* = 8.9 Hz, 2H), 7.36 (d, *J* = 8.9 Hz, 2H), 7.41 (dd, *J* =

2.0, 8.9 Hz, 2H), 7.82 (d, *J* = 2.0 Hz, 2H), 7.94 (d, *J* = 8.9 Hz, 2H); ¹³C NMR (100 MHz, CDCl₃) δ 31.25, 34.61, 110.62, 117.54, 123.49, 124.01, 126.36, 129.35, 131.34, 131.42, 146.69, 152.29; HRMS–APCI (*m/z*): [M + H]⁺ calcd for C₂₈H₃₁O₂, 399.2330; found, 399.2319. The enantiomeric purity was confirmed by HPLC analysis: CHIRAL ART Amylose-SA column, *n*-hexane/2-propanol 90:10, 1.0 mL/min, 40 °C; (*S*)-**1**: *t*_R = 17.9 min, (*R*)-**1**: *t*_R = 6.83 min, UV detection at 250.0 nm.

Preparation of **2**

To a 20 mL two-necked round-bottomed flask were added **1** (796 mg, 2.0 mmol) and Cs₂CO₃ (978 mg, 6.0 mmol). 2,6-Difluoropyridine (0.55 mL, 6.0 mmol) and DMF (10 mL) were added via syringe. The mixture was stirred at 40 °C for 48 h under N₂. The resulting mixture was extracted with EtOAc. The organic layer was washed with water, dried over Na₂SO₄, and evaporated in vacuo. The residue was purified by silica gel column chromatography (eluent: hexane/EtOAc 2:1) and GPC to give the title compound as white solid; (*S*)-**2** (1.01 g, 86% yield), (*R*)-**2** (1.06 g, 90% yield). Mp 212–214 °C; ¹H NMR (400 MHz, CDCl₃) δ 1.37 (s, 18H), 6.28 (dd, *J* = 2.6, 7.8 Hz, 2H), 6.37 (dd, *J* = 1.2, 8.0 Hz, 2H), 7.20 (d, *J* = 0.8 Hz, 2H), 7.33 (d, *J* = 8.8 Hz, 2H), 7.34 (d, *J* = 8.8 Hz, 2H), 7.39 (dd, *J* = 2.0, 8.4 Hz, 2H), 7.77 (d, *J* = 2.0 Hz, 2H), 7.89 (d, *J* = 8.8 Hz, 2H); ¹³C NMR (100 MHz, CDCl₃) δ 31.18, 34.68, 101.52, 101.87, 121.38, 122.81, 123.20, 125.29, 126.12, 129.51, 131.09, 131.96, 142.60 (d, *J*_{C–F} = 7.8 Hz), 147.89, 148.95, 161.61 (d, *J*_{C–F} = 14.0 Hz), 162.28 (d, *J*_{C–F} = 240 Hz); ¹⁹F NMR (376 MHz, CDCl₃) δ 69.06; HRMS–APCI (*m/z*): [M + H]⁺ calcd for C₃₈H₃₅F₂N₂O₂, 589.2644; found, 589.2661. The enantiomeric purity was confirmed by HPLC analysis: CHIRAL ART Cellulose-SB column, *n*-hexane/chloroform 95:5, 1.0 mL/min, 40 °C; (*S*)-**2**: *t*_R = 9.86 min, (*R*)-**2**: *t*_R = 21.29 min, UV detection at 250.0 nm.

Preparation of **3a–c**

Compound 3a: To a 10 mL Schlenk flask were added **2** (294 mg, 0.5 mmol), phenol (103 mg, 1.1 mmol), and Cs₂CO₃ (358 mg, 1.1 mmol). DMSO (3.5 mL) was added via the syringe. The mixture was stirred at 100 °C for 18 h under N₂. The resulting mixture was extracted with EtOAc. The organic layer was washed with water, dried over Na₂SO₄, and evaporated in vacuo. The residue was purified by silica gel column chromatography (eluent: hexane/EtOAc 6:1) and GPC to give the title compound as white solid; (*S*)-**3a** (309 mg, 84% yield), (*R*)-**3a** (332 mg, 90%). Mp 110–112 °C; ¹H NMR (400 MHz, CDCl₃) δ 1.29 (s, 18H), 6.10 (d, *J* = 7.9 Hz, 2H), 6.16 (d, *J* = 7.9 Hz, 2H), 6.91 (dd, *J* = 0.92, 8.5 Hz, 4H), 6.99–7.03 (m, 4H), 7.14–7.17 (m, 8H), 7.22 (d, *J* = 8.8 Hz, 2H), 7.68 (d, *J* = 2.0 Hz, 2H), 7.73 (d, *J* = 8.8 Hz, 2H); ¹³C NMR (100 MHz, CDCl₃) δ 31.23, 34.63, 103.72, 104.83, 121.03, 121.55, 122.67, 123.15,

124.27, 125.03, 126.13, 129.10, 129.30, 130.90, 132.04, 141.35, 147.49, 149.54, 154.00, 161.86, 162.48; HRMS–APCI (m/z): $[M + H]^+$ calcd for $C_{50}H_{45}N_2O_4$, 737.3367; found, 737.3374. The enantiomeric purity was confirmed by HPLC analysis: CHIRAL ART Amylose-SA column, *n*-hexane/chloroform 95:5, 1.0 mL/min, 40 °C; (*S*)-**3a**: t_R = 7.25 min, (*R*)-**3a**: t_R = 14.12 min, UV detection at 250.0 nm.

Compound 3b: Synthesized similarly to **3a** using 4-*tert*-butylphenol. Purified by silica gel column chromatography (eluent: hexane/EtOAc 4:1) and GPC to give the title compound as white solid; (*S*)-**3b** (399 mg, 94% yield), (*R*)-**3b** (386 mg, 91% yield). Mp 113–115 °C; 1H NMR (400 MHz, $CDCl_3$) δ 1.16 (s, 18H), 1.35 (s, 18H), 6.20 (d, J = 8.0 Hz, 2H), 6.28 (d, J = 7.6 Hz, 2H), 6.77 (d, J = 8.9 Hz, 2H), 6.88 (dd, J = 2.1, 6.7 Hz, 4H), 7.09 (dd, J = 2.0, 8.0 Hz, 2H), 7.12 (dd, J = 2.1, 7.0 Hz, 4H), 7.23 (d, J = 8.8 Hz, 2H), 7.29 (t, J = 8.0 Hz, 2H), 7.72 (d, J = 2.0 Hz, 2H), 7.78 (d, J = 8.8 Hz, 2H); ^{13}C NMR (100 MHz, $CDCl_3$) δ 31.23, 31.95, 34.22, 34.58, 103.43, 104.29, 120.83, 121.94, 122.40, 123.40, 125.01, 125.73, 126.23, 128.83, 130.79, 132.05, 141.29, 146.89, 147.26, 149.60, 151.15, 161.82, 162.41; HRMS–APCI (m/z): $[M + H]^+$ calcd for $C_{58}H_{61}N_2O_4$, 849.4603; found, 849.4626. The enantiomeric purity was confirmed by HPLC analysis: CHIRAL ART Amylose-SA column, *n*-hexane/chloroform 95:5, 1.0 mL/min, 40 °C; (*S*)-**3b**: t_R = 8.36 min, (*R*)-**3b**: t_R = 10.05 min, UV detection at 250.0 nm.

Compound 3c: Synthesized similarly to **3a** using 3-*tert*-butylphenol. Purified by silica gel column chromatography (eluent: hexane/EtOAc 6:1) and GPC to give the title compound as white solid; (*S*)-**3c** (377 mg, 89% yield), (*R*)-**3c** (403 mg, 95% yield). Mp 88–90 °C; 1H NMR (400 MHz, $CDCl_3$) δ 1.17 (s, 18H), 1.36 (s, 18H), 6.14 (d, J = 8.0 Hz, 2H), 6.23 (d, J = 7.6 Hz, 2H), 6.79 (ddd, J = 1.0, 2.2, 7.3 Hz, 2H), 7.02 (t, J = 2.0 Hz, 2H), 7.09–7.13 (m, 4H), 7.16–7.28 (m, 8H), 7.73 (d, J = 1.6 Hz, 2H), 7.76 (d, J = 8.8 Hz, 2H); ^{13}C NMR (100 MHz, $CDCl_3$) δ 31.16, 31.22, 34.61, 34.63, 103.53, 104.62, 117.99, 118.29, 121.39, 121.53, 122.67, 123.11, 124.94, 126.13, 128.82, 129.06, 130.86, 132.03, 141.26, 147.42, 149.48, 153.01, 153.87, 162.23, 162.50; HRMS–APCI (m/z): $[M + H]^+$ calcd for $C_{58}H_{61}N_2O_4$, 849.4599; found, 849.4626. The enantiomeric purity was confirmed by HPLC analysis: CHIRAL ART Amylose-SA column, *n*-hexane/chloroform 95:5, 1.0 mL/min, 40 °C; (*S*)-**3c**: t_R = 9.00 min, (*R*)-**3c**: t_R = 8.61 min, UV detection at 250.0 nm.

Preparation of 4a–c

Compound 4a: To a 10 mL Schlenk flask were added **3a** (184 mg, 0.25 mmol), $Pd(TFA)_2$ (24.9 mg, 0.075 mmol), $AgOAc$ (167 mg, 1.0 mmol), and $PivOH$ (2.0 mL). The mix-

ture was heated at 150 °C for 24 h under air. After cooling to room temperature, the resulting mixture was diluted with water and filtered through a pad of Celite eluting with dichloromethane. The filtrate was washed with water, dried over Na_2SO_4 , and concentrated in vacuo. The obtained crude material was again subjected to the catalytic conditions described above. The residue was purified by silica gel column chromatography (eluent: hexane/dichloromethane 4:1) and GPC to give the title compound as pale yellow solid; (*S*)-**4a** (28.2 mg, 16% yield), (*R*)-**4a** (18.1 mg, 10% yield). Mp >300 °C; 1H NMR (400 MHz, $CDCl_3$) δ 1.46 (s, 18H), 7.44–7.52 (m, 8H), 7.62 (d, J = 8.0 Hz, 2H), 8.07 (dd, J = 0.8, 7.6 Hz, 2H), 8.12 (d, J = 2.0 Hz, 2H), 8.67 (s, 2H), 8.96 (s, 2H); ^{13}C NMR (100 MHz, $CDCl_3$) δ 31.25, 34.82, 112.20, 112.62, 113.07, 113.65, 120.13, 120.59, 122.80, 122.93, 123.21, 123.61, 123.62, 125.68, 125.81, 127.39, 130.67, 130.90, 147.553, 151.62, 154.63, 161.90, 163.10; HRMS–APCI (m/z): $[M + H]^+$ calcd for $C_{50}H_{37}N_2O_4$, 729.2723; found, 729.2748. The enantiomeric purity was determined by HPLC analysis: CHIRAL ART Amylose-SA column, *n*-hexane/chloroform 60:40, 1.0 mL/min, 40 °C; (*S*)-**4a**: t_R = 4.39 min, (*R*)-**4a**: t_R = 6.73 min, UV detection at 250.0 nm.

Compound 4b: Synthesized similarly to **4b** from **3b** (254 mg, 0.30 mmol). Purified by silica gel column chromatography (eluent: hexane/EtOAc 4:1) and GPC to give the title compound as pale yellow solid; (*S*)-**4b** (45.4 mg, 18% yield), (*R*)-**4b** (30.2 mg, 12% yield). Single crystals suitable for the X-ray analysis were obtained by slow evaporation from EtOAc solution. Mp >300 °C; 1H NMR (400 MHz, $CDCl_3$) δ 1.46 (s, 18H), 1.48 (s, 18H), 7.47–7.71 (m, 8H), 8.07 (d, J = 0.8 Hz, 2H), 8.11 (d, J = 1.6 Hz, 2H), 8.65 (s, 2H), 8.98 (s, 2H); ^{13}C NMR (100 MHz, $CDCl_3$) δ 31.26, 31.87, 34.82, 34.98, 111.49, 112.62, 113.40, 113.47, 116.98, 119.97, 122.31, 122.75, 122.35, 123.57, 125.13, 125.69, 125.73, 130.64, 130.87, 146.82, 147.48, 151.62, 152.78, 162.25, 162.94; HRMS–EI (m/z): $[M]^+$ calcd for $C_{58}H_{52}N_2O_4$, 840.3927; found, 840.3932; $[\alpha]_D^{20}$ = +31.8 (*S*-isomer), –32.4 (*R*-isomer) as $CHCl_3$ solution. The enantiomeric purity was determined by HPLC analysis: CHIRAL ART Amylose-SA column, *n*-hexane/2-propanol 90:10, 1.0 mL/min, 40 °C; (*S*)-**4b**: t_R = 15.95 min, (*R*)-**4b**: t_R = 24.38 min, UV detection at 250.0 nm.

Compound 4c: Synthesized similarly to **4c** from **3c** (254 mg, 0.3 mmol). Purified by silica gel column chromatography (eluent: hexane/EtOAc 4:1) and GPC to give the title compound as pale yellow solid; (*S*)-**4c** (74.1 mg, 29% yield), (*R*)-**4c** (90.0 mg, 36% yield). Single crystals suitable for the X-ray analysis were obtained by hexane vapor diffusion into $CHCl_3$ solution. Mp >300 °C; 1H NMR (400 MHz, $CDCl_3$) δ 1.41 (s, 18H), 1.45 (s, 18H), 7.47–7.64 (m, 6H), 7.637 (d, J = 0.8 Hz, 2H), 7.97 (d, J = 8.4 Hz, 2H), 8.10 (d, J = 0.8 Hz, 2H), 8.65 (s,

2H), 8.91 (s, 2H); ^{13}C NMR (100 MHz, CDCl_3) δ 31.26, 31.57, 34.81, 3.38, 109.04, 112.62, 113.23, 113.39, 119.98, 119.99, 120.05, 121.20, 122.53, 123.35, 123.58, 125.69, 125.70, 130.63, 130.88, 147.46, 151.62, 151.76, 155.05, 162.12, 162.77; HRMS–APCI (m/z): $[\text{M} + \text{H}]^+$ calcd for $\text{C}_{58}\text{H}_{53}\text{N}_2\text{O}_4$, 841.3970; found, 841.4000. The enantiomeric purity was determined by HPLC analysis: CHIRAL ART Amylose-SA column, *n*-hexane/chloroform 70:30, 1.0 mL/min, 40 °C; (*S*)-**4c**: t_R = 4.48 min, (*R*)-**4c**: t_R = 6.66 min, UV detection at 250.0 nm.

Preparation of 5

In a 200 mL three-necked round-bottomed flask, **1** (1.99 g, 5.0 mmol) was added to a suspension of *t*-BuOK (1.40 g, 12.5 mmol) in THF (80 mL) at 0 °C. After stirring for 2 h, Ph_2IOTf (5.38 g, 12.5 mmol) was added in one portion. The mixture was allowed to warm to 40 °C, and stirred at this temperature until the complete consumption **1** was confirmed by TLC. The resulting suspension was poured into ice water and extracted with Et_2O . The combined organic layer was dried over Na_2SO_4 and concentrated in vacuo. The residue was purified by silica gel column chromatography (eluent: hexane/EtOAc 20:1) and GPC (CHCl_3) to give the title compound as white solid; (*S*)-**5** (1.59 g, 58% yield), (*R*)-**5** (1.71 g, 62% yield). Mp 167.0–169.0 °C; ^1H NMR (400 MHz, CDCl_3) δ 1.39 (s, 18H), 6.79 (d, J = 7.6 Hz, 4H), 6.92 (t, J = 7.6 Hz, 2H), 7.10 (t, J = 7.6 Hz, 4H), 7.17 (d, J = 8.9 Hz, 2H), 7.27 (d, J = 9.2 Hz, 2H), 7.39 (dd, J = 2.0, 8.9 Hz, 2H), 7.79 (d, J = 1.7 Hz, 2H), 7.83 (d, J = 8.9 Hz, 2H); ^{13}C NMR (100 MHz, CDCl_3) δ 31.25, 34.65, 118.84, 119.29, 122.06, 122.43, 123.04, 125.46, 125.63, 129.19, 129.46, 130.30, 132.44, 147.18, 152.08, 157.74; HRMS–APCI [m/z]: $[\text{M} + \text{H}]^+$ calcd for $\text{C}_{40}\text{H}_{39}\text{O}_2$, 551.2959; found, 551.2945. The enantiomeric purity was confirmed by HPLC analysis: CHIRAL ART Amylose-SA column, *n*-hexane/chloroform 98:2, 1.0 mL/min, 40 °C; (*S*)-**5**: t_R = 4.91 min, (*R*)-**5**: t_R = 5.32 min, UV detection at 250.0 nm.

Preparation of 6

To a 10 mL Schlenk flask were added **5** (165 mg, 0.3 mmol), $\text{Pd}(\text{TFA})_2$ (29.9 mg, 0.09 mmol), AgOAc (198 mg, 1.2 mmol), and PivOH (3.0 mL). The mixture was heated at 150 °C for 24 h under air. After cooling to room temperature, the resulting mixture was diluted with water and filtered through a pad of Celite eluting with dichloromethane. The filtrate was washed with water, dried over Na_2SO_4 , and concentrated in vacuo. The residue was purified by silica gel column chromatography (eluent: hexane/EtOAc 2:1) and GPC to give the title compound as pale yellow solid; (*S*)-**6** (30.1 mg, 18% yield), (*R*)-**6** (30.3 mg, 18% yield). Mp 212–214 °C; ^1H NMR (400 MHz, CDCl_3) δ 1.41 (s, 18H), 7.31 (dd, J = 0.8, 7.6 Hz, 2H), 7.35 (dd, J = 1.2, 7.6 Hz, 2H), 7.38–7.43 (m, 6H), 8.09 (s, 2H), 8.13–8.16 (m, 2H), 8.61 (s, 2H); ^{13}C NMR (100 MHz, CDCl_3) δ 31.26,

34.74, 111.88, 112.25, 119.71, 121.16, 122.62, 123.61, 124.35, 125.08, 125.26, 125.55, 128.08, 130.54, 130.75, 146.80, 153.36, 157.70; HRMS–APCI (m/z): $[\text{M} + \text{H}]^+$ calcd for $\text{C}_{40}\text{H}_{35}\text{O}_2$, 547.2622; found, 547.2632. The enantiomeric purity was confirmed by HPLC analysis: CHIRAL ART Amylose-SA column, *n*-hexane/EtOAc 95:5, 1.0 mL/min, 40 °C; (*S*)-**6**: t_R = 6.47 min, (*R*)-**6**: t_R = 6.24 min, UV detection at 250.0 nm.

Supporting Information

Supporting Information File 1

Summary of X-ray crystallography data, copy of NMR spectra, and copy of HPLC charts.

[<https://www.beilstein-journals.org/bjoc/content/supplementary/1860-5397-16-32-S1.pdf>]

Funding

This work was supported by JSPS KAKENHI Grant No. JP 19K15586 (Grant-in-Aid for Young Scientists) to Y.N. and JP 17H06092 (Grant-in-Aid for Specially Promoted Research) to M.M.

ORCID® iDs

Yuji Nishii - <https://orcid.org/0000-0002-6824-0639>

Masahiro Miura - <https://orcid.org/0000-0001-8288-6439>

References

- Yang, Y.; Lan, J.; You, J. *Chem. Rev.* **2017**, *117*, 8787–8863. doi:10.1021/acs.chemrev.6b00567
See for a recent review on the oxidative coupling.
- Yoshimoto, H.; Itatani, H. *Bull. Chem. Soc. Jpn.* **1973**, *46*, 2490–2492. doi:10.1246/bcsj.46.2490
- Shiotani, A.; Itatani, H. *Angew. Chem., Int. Ed. Engl.* **1974**, *13*, 471–472. doi:10.1002/anie.197404711
- Åkermark, B.; Eberson, L.; Jonsson, E.; Pettersson, E. *J. Org. Chem.* **1975**, *40*, 1365–1367. doi:10.1021/jo00897a048
- Knölker, H.-J.; O'Sullivan, N. *Tetrahedron* **1994**, *50*, 10893–10908. doi:10.1016/s0040-4020(01)85701-x
- Åkermark, B.; Oslob, J. D.; Heuschert, U. *Tetrahedron Lett.* **1995**, *36*, 1325–1326. doi:10.1016/0040-4039(94)02467-p
- Hagelin, H.; Oslob, J. D.; Åkermark, B. *Chem. – Eur. J.* **1999**, *5*, 2413–2416. doi:10.1002/(sici)1521-3765(19990802)5:8<2413::aid-chem2413>3.0.co;2-3
- Knölker, H.-J.; Fröhner, W.; Reddy, K. R. *Synthesis* **2002**, 557–564. doi:10.1055/s-2002-20953
- Matsubara, S.; Asano, K.; Kajita, Y.; Yamamoto, M. *Synthesis* **2007**, 2055–2059. doi:10.1055/s-2007-983738
- Watanabe, T.; Ueda, S.; Inuki, S.; Oishi, S.; Fujii, N.; Ohno, H. *Chem. Commun.* **2007**, 4516–4518. doi:10.1039/b707899d
- Liegault, B.; Lee, D.; Huestis, M. P.; Stuart, D. R.; Fagnou, K. *J. Org. Chem.* **2008**, *73*, 5022–5028. doi:10.1021/jo800596m
- Kaida, H.; Satoh, T.; Hirano, K.; Miura, M. *Chem. Lett.* **2015**, *44*, 1125–1127. doi:10.1246/cl.150408

13. Kaida, H.; Satoh, T.; Nishii, Y.; Hirano, K.; Miura, M. *Chem. Lett.* **2016**, *45*, 1069–1071. doi:10.1246/cl.160496
14. Kaida, H.; Goya, T.; Nishii, Y.; Hirano, K.; Satoh, T.; Miura, M. *Org. Lett.* **2017**, *19*, 1236–1239. doi:10.1021/acs.orglett.7b00323
15. Itai, Y.; Nishii, Y.; Stachelek, P.; Data, P.; Takeda, Y.; Minakata, S.; Miura, M. *J. Org. Chem.* **2018**, *83*, 10289–10302. doi:10.1021/acs.joc.8b01451
16. Nakamura, S.; Tohnai, N.; Nishii, Y.; Hinoue, T.; Miura, M. *ChemPhotoChem* **2019**, *3*, 46–53. doi:10.1002/cptc.201800189
17. Nakamura, S.; Okamoto, M.; Tohnai, N.; Nakayama, K.-i.; Nishii, Y.; Miura, M. *Bull. Chem. Soc. Jpn.* **2020**, *93*, 99–108. doi:10.1246/bcsj.20190269
18. Sánchez-Carnerero, E. M.; Agarrabeitia, A. R.; Moreno, F.; Maroto, B. L.; Muller, G.; Ortiz, M. J.; de la Moya, S. *Chem. – Eur. J.* **2015**, *21*, 13488–13500. doi:10.1002/chem.201501178
19. Tanaka, H.; Inoue, Y.; Mori, T. *ChemPhotoChem* **2018**, *2*, 386–402. doi:10.1002/cptc.201800015
20. Chen, N.; Yan, B. *Molecules* **2018**, *23*, 3376. doi:10.3390/molecules23123376
21. Ma, J.-L.; Peng, Q.; Zhao, C.-H. *Chem. – Eur. J.* **2019**, *25*, 15441–15454. doi:10.1002/chem.201903252
22. Schadt, M. *Annu. Rev. Mater. Sci.* **1997**, *27*, 305–379. doi:10.1146/annurev.matsci.27.1.305
23. Sherson, J. F.; Krauter, H.; Olsson, R. K.; Julsgaard, B.; Hammerer, K.; Cirac, I.; Polzik, E. S. *Nature* **2006**, *443*, 557–560. doi:10.1038/nature05136
24. Feringa, B. L. *Acc. Chem. Res.* **2001**, *34*, 504–513. doi:10.1021/ar0001721
25. Kawai, T.; Kawamura, K.; Tsumatori, H.; Ishikawa, M.; Naito, M.; Fujiki, M.; Nakashima, T. *ChemPhysChem* **2007**, *8*, 1465–1468. doi:10.1002/cphc.200600747
26. Amako, T.; Kimoto, T.; Tajima, N.; Fujiki, M.; Imai, Y. *Tetrahedron* **2013**, *69*, 2753–2757. doi:10.1016/j.tet.2013.01.084
27. Nakabayashi, K.; Amako, T.; Tajima, N.; Fujiki, M.; Imai, Y. *Chem. Commun.* **2014**, *50*, 13228–13230. doi:10.1039/c4cc02946a
28. Feuillastre, S.; Pauton, M.; Gao, L.; Desmarchelier, A.; Riives, A. J.; Prim, D.; Tondelier, D.; Geoffroy, B.; Muller, G.; Clavier, G.; Pieters, G. *J. Am. Chem. Soc.* **2016**, *138*, 3990–3993. doi:10.1021/jacs.6b00850
29. Kitatobe, T.; Mimura, Y.; Tsujimoto, S.; Tajima, N.; Fujiki, M.; Imai, Y. *Tetrahedron* **2017**, *73*, 6856–6862. doi:10.1016/j.tet.2017.10.036
30. Zhang, X.; Zhang, Y.; Li, Y.; Quan, Y.; Cheng, Y.; Li, Y. *Chem. Commun.* **2019**, *55*, 9845–9848. doi:10.1039/c9cc04289j
31. Zhang, X.; Zhang, Y.; Zhang, H.; Quan, Y.; Li, Y.; Cheng, Y.; Ye, S. *Org. Lett.* **2019**, *21*, 439–443. doi:10.1021/acs.orglett.8b03620
32. Wu, Z.-G.; Han, H.-B.; Yan, Z.-P.; Luo, X.-F.; Wang, Y.; Zheng, Y.-X.; Zuo, J.-L.; Pan, Y. *Adv. Mater. (Weinheim, Ger.)* **2019**, *31*, 1900524. doi:10.1002/adma.201900524
33. Hassan, K.; Yamashita, K.-i.; Hirabayashi, K.; Shimizu, T.; Nakabayashi, K.; Imai, Y.; Matsumoto, T.; Yamano, A.; Sugiura, K.-i. *Chem. Lett.* **2015**, *44*, 1607–1609. doi:10.1246/cl.150704
34. Takaishi, K.; Yamamoto, T.; Hinoide, S.; Ema, T. *Chem. – Eur. J.* **2017**, *23*, 9249–9252. doi:10.1002/chem.201702143
35. Takaishi, K.; Takehana, R.; Ema, T. *Chem. Commun.* **2018**, *54*, 1449–1452. doi:10.1039/c7cc09187g
36. Takaishi, K.; Iwachido, K.; Takehana, R.; Uchiyama, M.; Ema, T. *J. Am. Chem. Soc.* **2019**, *141*, 6185–6190. doi:10.1021/jacs.9b02582
37. Droz, A. S.; Neidlein, U.; Anderson, S.; Seiler, P.; Diederich, F. *Helv. Chim. Acta* **2001**, *84*, 2243–2289. doi:10.1002/1522-2675(20010815)84:8<2243::aid-hlca2243>3.0.co;2-g
38. Ye, P.; Li, Q.; Bai, Z.; Dong, K.; Liu, Q. *Heterocycles* **2015**, *91*, 1986–1995. doi:10.3987/com-15-13302
39. Octa-Smolín, F.; van der Vicht, F.; Yadav, R.; Bhangu, J.; Soloviova, K.; Wölper, C.; Daniliuc, C. G.; Strassert, C. A.; Somnitz, H.; Jansen, G.; Niemeyer, J. *J. Org. Chem.* **2018**, *83*, 14568–14587. doi:10.1021/acs.joc.8b02353
40. Meca, L.; Řeha, D.; Havlas, Z. *J. Org. Chem.* **2003**, *68*, 5677–5680. doi:10.1021/jo034344u
41. Moustafa, G. A. I.; Oki, Y.; Akai, S. *Angew. Chem., Int. Ed.* **2018**, *57*, 10278–10282. doi:10.1002/anie.201804161
42. Paul, A.; Kumar, A.; Nanjunda, R.; Farahat, A. A.; Boykin, D. W.; Wilson, W. D. *Org. Biomol. Chem.* **2017**, *15*, 827–835. doi:10.1039/c6ob02390h
43. Jalalian, N.; Ishikawa, E. E.; Silva, L. F., Jr.; Olofsson, B. *Org. Lett.* **2011**, *13*, 1552–1555. doi:10.1021/ol200265t
44. Jalalian, N.; Petersen, T. B.; Olofsson, B. *Chem. – Eur. J.* **2012**, *18*, 14140–14149. doi:10.1002/chem.201201645
45. Sperotto, E.; de Vries, J. G.; van Klink, G. P. M.; van Koten, G. *Tetrahedron Lett.* **2007**, *48*, 7366–7370. doi:10.1016/j.tetlet.2007.08.026
46. Liu, X.; Zhang, S. *Synlett* **2011**, 268–272. doi:10.1055/s-0030-1259291
47. Kimoto, T.; Tajima, N.; Fujiki, M.; Imai, Y. *Chem. – Asian J.* **2012**, *7*, 2836–2841. doi:10.1002/asia.201200725
48. Emeis, C. A.; Oosterhoff, L. J. *J. Chem. Phys.* **1971**, *54*, 4809–4819. doi:10.1063/1.1674756
49. Tsumatori, H.; Nakashima, T.; Kawai, T. *Org. Lett.* **2010**, *12*, 2362–2365. doi:10.1021/ol100701w
50. Schweicher, G.; Lemaire, V.; Niebel, C.; Ruzié, C.; Diao, Y.; Goto, O.; Lee, W.-Y.; Kim, Y.; Arlin, J.-B.; Karpinska, J.; Kennedy, A. R.; Parkin, S. R.; Olivier, Y.; Mannsfeld, S. C. B.; Cornil, J.; Geerts, Y. H.; Bao, Z. *Adv. Mater. (Weinheim, Ger.)* **2015**, *27*, 3066–3072. doi:10.1002/adma.201500322
51. Sugino, H.; Takimiya, K. *Chem. Lett.* **2017**, *46*, 345–347. doi:10.1246/cl.161020
52. Kohl, B.; Bohnwagner, M. V.; Rominger, F.; Wadepohl, H.; Dreuw, A.; Mastalerz, M. *Chem. – Eur. J.* **2016**, *22*, 646–655. doi:10.1002/chem.201503863
53. Wu, T.-L.; Kuo, C.-H.; Lin, B.-C.; Tao, Y.-T.; Hsu, C.-P.; Liu, R.-S. *J. Mater. Chem. C* **2015**, *3*, 7583–7588. doi:10.1039/c5tc01455g
54. Mallory, F. B.; Mallory, C. W.; Regan, C. K.; Aspden, R. J.; Ricks, A. B.; Racowski, J. M.; Nash, A. I.; Gibbons, A. V.; Carroll, P. J.; Bohlen, J. M. *J. Org. Chem.* **2013**, *78*, 2040–2045. doi:10.1021/jo3020819
55. Balaraman, E.; Kumara Swamy, K. C. *Tetrahedron: Asymmetry* **2007**, *18*, 2037–2048. doi:10.1016/j.tetasy.2007.06.028

License and Terms

This is an Open Access article under the terms of the Creative Commons Attribution License (<https://creativecommons.org/licenses/by/4.0>). Please note that the reuse, redistribution and reproduction in particular requires that the authors and source are credited.

The license is subject to the *Beilstein Journal of Organic Chemistry* terms and conditions: (<https://www.beilstein-journals.org/bjoc>)

The definitive version of this article is the electronic one which can be found at:
[doi:10.3762/bjoc.16.32](https://doi.org/10.3762/bjoc.16.32)



Room-temperature Pd/Ag direct arylation enabled by a radical pathway

Amy L. Mayhugh¹ and Christine K. Luscombe^{*2}

Full Research Paper

Open Access

Address:

¹Department of Chemistry, University of Washington, Seattle, WA 98195, USA and ²Department of Materials Science & Engineering, University of Washington, Seattle, WA 98195, USA

Email:

Christine K. Luscombe^{*} - luscombe@uw.edu

^{*} Corresponding author

Keywords:

direct arylation; indole; palladium radical; visible light

Beilstein J. Org. Chem. **2020**, *16*, 384–390.

doi:10.3762/bjoc.16.36

Received: 25 January 2020

Accepted: 05 March 2020

Published: 13 March 2020

This article is part of the thematic issue "C–H functionalization for materials science".

Guest Editor: K. Itami

© 2020 Mayhugh and Luscombe; licensee Beilstein-Institut.

License and terms: see end of document.

Abstract

Direct arylation is an appealing method for preparing π -conjugated materials, avoiding the prefunctionalization required for traditional cross-coupling methods. A major effort in organic electronic materials development is improving the environmental and economic impact of production; direct arylation polymerization (DArP) is an effective method to achieve these goals. Room-temperature polymerization would further improve the cost and energy efficiencies required to prepare these materials. Reported herein is new mechanistic work studying the underlying mechanism of room temperature direct arylation between iodobenzene and indole. Results indicate that room-temperature, Pd/Ag-catalyzed direct arylation systems are radical-mediated. This is in contrast to the commonly proposed two-electron mechanisms for direct arylation and appears to extend to other substrates such as benzo[*b*]thiophene and pentafluorobenzene.

Introduction

π -Conjugated polymers are of significant interest as they have the potential to combine the mechanical flexibility and affordability of synthetic polymers with the optical and electronic properties of semiconductors. One of the limitations to this field's continued growth are the expensive, toxic, and energy-intensive methods in which these materials are typically prepared [1]. Direct arylation is one solution to these problems, which allows improved atom and step economy in polymer syn-

thesis. Traditional coupling methods form a new C–C bond using a reactive C–M bond (M = SnR₃, B(OH)₂, etc.) and a C–X (X = I, Br, OTs) coupling partner. In contrast, direct arylation couples C–H and C–X bonds directly without the need to prepare the C–M substrate. As a polymerization method, direct arylation polymerization (DArP) is of great interest due to its potential to reduce waste and toxicity by removing the need for stoichiometric amounts of toxic organometallics [2].

While significant progress has been made in DArP, C–H bonds are more challenging to functionalize than their C–M counterparts. Known DArP conditions have limited monomers that can produce polymers with both high molecular weight and regioregularity, and elevated reaction temperatures are typically required [3]. Mild conditions for C–H functionalization is of growing interest within the broader synthetic community as an opportunity to improve functional group tolerance, and environmental impact [4,5]. While many direct arylation systems occur under neutral conditions and without the need for strong oxidants or reductants, only few proceed at ambient temperatures [3,6]. To our knowledge, only one example of room-temperature DArP exists, namely polymerizing poly-3-hexylthiophene to an acceptably high number average molecular weight of 14 kg/mol, although in 9% yield [7]. Room-temperature DArP would improve the simplicity of conjugated polymer synthesis, and reduce the energy requirements.

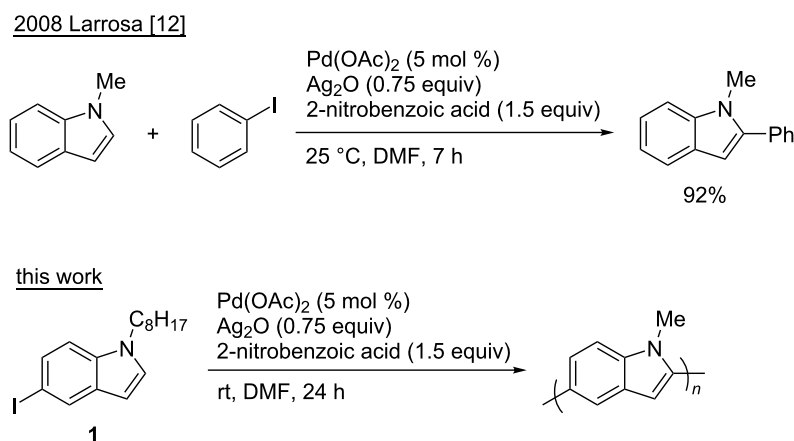
Small molecule reactions can help predict a method's utility in polymerizations, as DArP proceeds through a step-growth polymerization mechanism. Generically, a small molecule reaction is a candidate for adaptation to a polymerization when it is highly regioselective, and high yielding. Under step-growth conditions a high yielding reaction is essential for producing a high molecular weight material [8], which directly influences the quality and electronic performance of the material [7,9]. More specific to this work, the direct arylation method should be catalytic, directing-group free and at room temperature; a handful of such methods have been reported [10–14]. One such method, an indole/iodoarene direct arylation method reported by Larrosa is notable: proceeding in high yields, at room temperature, and with no reported regioselectivity issues (Scheme 1) [12]. This system is hypothesized to proceed under mild conditions due to a highly electrophilic Pd catalyst gener-

ated in situ. In this paper, we investigated the mechanism of room-temperature direct arylation and DArP by extending the method reported by Larrosa to synthesize a conjugated polymer, polyindole (PIn). Small molecule mechanistic studies were undertaken that will help future development of mild, efficient DArP conditions.

Results and Discussion

Initial attempts to polymerize iodoindole monomer **1** using the reported conditions (Scheme 1) produced oligomers with an unanticipated coupling pattern in good yield (87%, Figure 1, Supporting Information File 1, Figure S3). The ^1H NMR signals from the C2-H, C3-H on the pyrrole ring and the N-CH₂-R on the alkyl chain indicate the product is highly branched [15]. Comparing the monomer's spectrum to the polymer's shows large peaks from unfunctionalized pyrrole rings at the chain ends with a ratio of interior to end groups of 1:0.57. While low molecular weight also contributes to the large signals from the chain ends, there are a few factors that indicate branching is occurring: firstly, the large variety in C3-H signals; secondly, the relative integration of the C2-H/C3-H signals to the N-CH₂-R signals show that for every indole unit, there is less than one H on the pyrrole ring. Finally, branching is evidenced by the discrepancy in molecular weight as calculated for a linear polymer by ^1H NMR compared with that indicated by MALDI-TOF MS (Figure 2). Due to the high regioselectivity in small molecule couplings, defects to this extent were unexpected.

MALDI-TOF MS was collected for PIn to further clarify the nature of the coupling pattern (Figure 2, Supporting Information File 1, Figure S2). The repeat unit corresponds to C/H–C/I coupling ($m/z = 227$) as expected for direct arylation. In contrast to the expected I/H end groups, the mass spectrum indicates



Scheme 1: A high yielding, highly selective room-temperature direct arylation reaction between indole and iodobenzene reported in ref. [12] and adapted in this work to study room-temperature DArP.

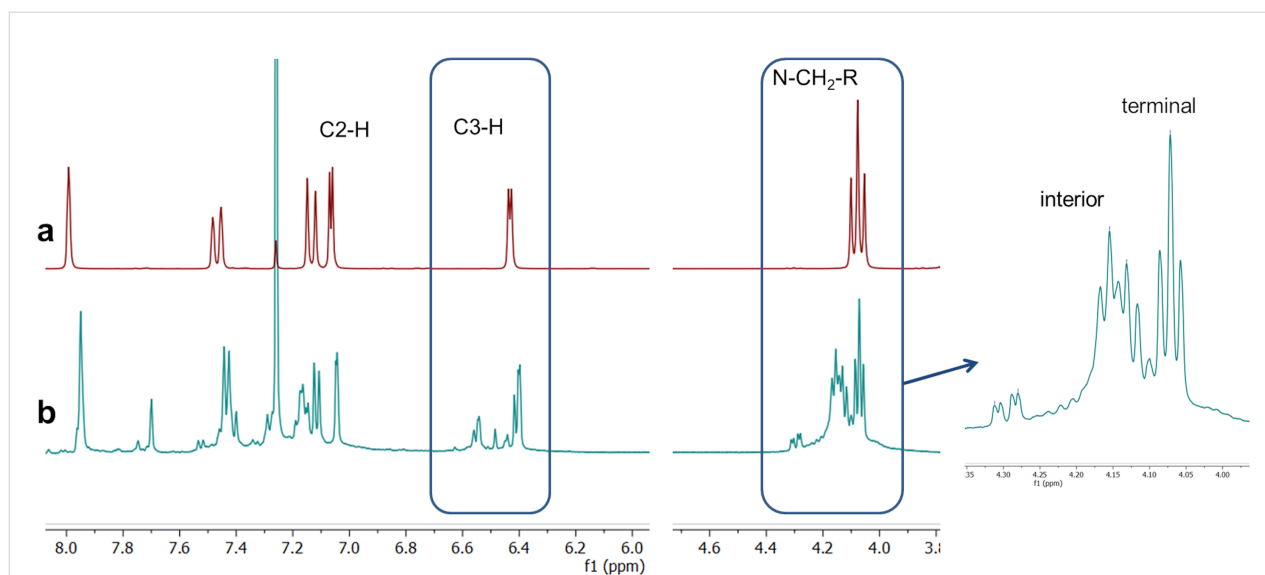


Figure 1: ^1H NMR (500 MHz, CDCl_3) of (a) 5-iodo-1-octylindole monomer (b) PIn prepared according to conditions in Scheme 1. The region from 4–4.5 ppm indicates the interior indole repeat units compared with the terminal indole units.

various incorporations of nitrobenzene into the polymer chains. The 2-nitrobenzoic acid used to form a silver carboxylate in the reaction system is the origin of the nitrophenyl group. Three different types of chains are represented, corresponding to incorporation of I/nitrophenyl, H/nitrophenyl, and two nitrophenyl end groups.

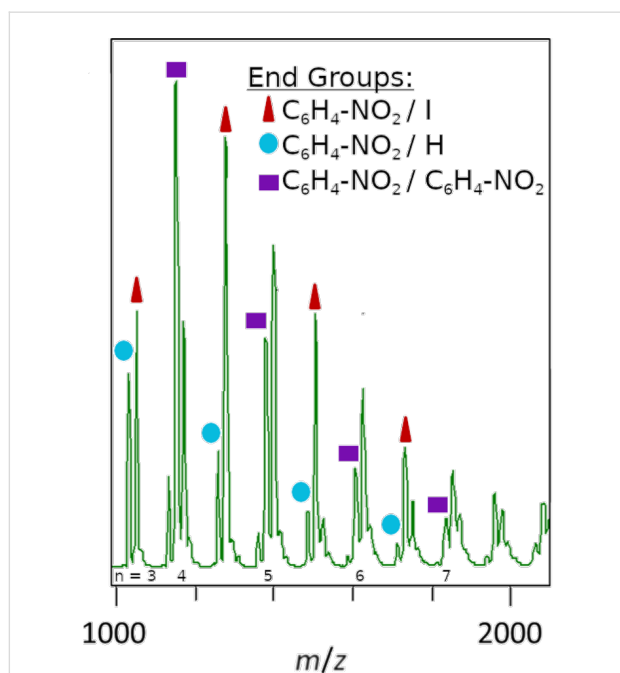


Figure 2: MALDI–TOF MS of PIn, indicating octylindole repeat units with three different types of end groups. These include 2-nitrophenyl, iodine, and hydrogen.

2-Substituted benzoic acids in general, and 2-nitrobenzoic acid in particular, are reactive substrates in decarboxylative coupling reactions [16,17]. However, more forceful conditions are typically required than used in the room-temperature system. Indeed, a very similar Pd/Ag system has been reported for decarboxylative coupling between indole and 2-nitrobenzoic acids at 110 °C [18]. Under such conditions, silver carboxylates decompose to produce carbonyl and phenyl radicals, which could explain the origin of nitrobenzene incorporation [19,20]. When the radical trapping agent BHT was added to the polymerization conditions, no polymerization occurred (Table 1). Additionally, the reaction was completely inhibited when run in the dark. These results indicate that visible light may be responsible for radical generation in the polymerization.

Table 1: Polymerization control experiments.

Variation	Yield (%)	
1	+ BHT ^{a,b}	0
2	dark	0
3	no Pd(OAc) ₂	0

^a(2,6-Di-*tert*-butyl-4-methylphenol); ^b1 equiv was used; conditions: Pd(OAc)₂ (5 mol %), Ag₂O (0.75 equiv), 2-nitrobenzoic acid (1.5 equiv), DMF, rt.

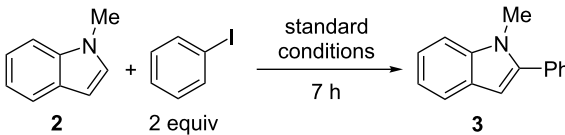
To further investigate the possibility of a radical-mediated reaction, additional radical capture experiments were performed for the small molecule reaction using 1-methylindole and iodobenzene (Table 2). Similar results were observed for 1-octylindole and iodobenzene (Supporting Information File 1, Table S2). In all cases, coupling was completely suppressed by the addition of TEMPO and BHT. Moreover, Ph-BHT was observed by GC–MS when BHT was added. Similar to the polymerization trials, coupling was inhibited when the standard conditions were run in the dark. Both the Ph-BHT adduct and continued

poor reactivity in the dark provides growing evidence for a radical mechanism. Moreover, the observed behavior appears to be common between the iodoindole monomer and iodobenzene/indole system, rather than a phenomenon unique to an electron-rich iodoindole.

The growing evidence for a phenyl radical in the catalytic cycle is in contrast to the typically proposed mechanisms for direct arylation (Scheme 2). Amongst these mechanisms, the most widely accepted is the concerted metalation–deprotonation (CMD) pathway [21]. Within the indole direct-arylation literature, however, there remains much discussion of an electrophilic metalation mechanism, with the majority of experimental evidence supporting this pathway [22–26]. In this case, C2 selectivity is often observed, theoretically from a C3/C2 Pd migration. A third possible mechanism that has had little experimental evidence but cannot be ruled out, is a Heck-type carbopalladation. This mechanism has been recently supported by ^{13}C and ^2H KIE experiments for the arylation of benzo[*b*]thiophene, although at C3 [13]. In contrast to these pathways, the radical trap and dark experiments reported above indicate a hybrid Pd(I) radical species induced by visible light is involved in the catalytic cycle. This type of mechanism has been previously proposed for aryl and alkene alkylations [27,28], but not for direct arylation systems.

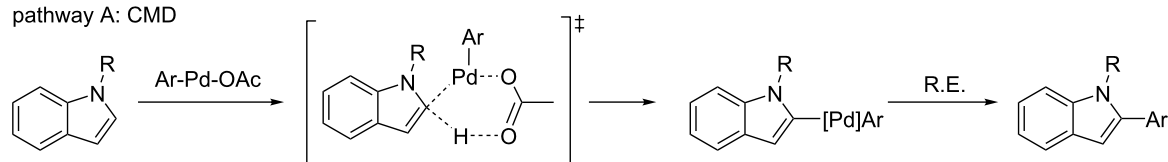
A possible mechanism is outlined in Scheme 3, informed by the previous reports [27–30]. The aryl iodide **4** undergoes SET with

Table 2: Small molecule control experiments.

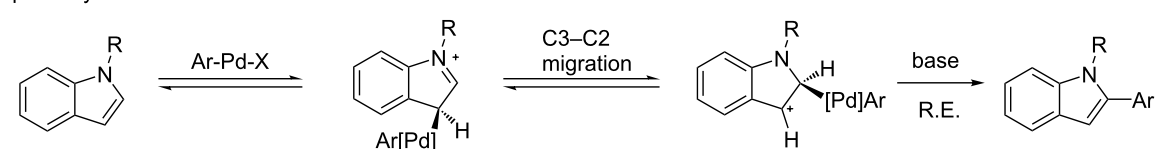
		
	Variation	Yield (%) ^a
1	none	85 ^b
2	+ BHT ^{c,d}	0
3	+ TEMPO ^{c,e}	0
4	dark	20

^aDetermined by ^1H NMR using ethylene carbonate as an internal standard; ^bisolated yield; ^c2 equiv was used; ^dPh-BHT adduct observed by GC–MS; ^e((2,2,6,6-tetramethylpiperidin-1-yl)oxyl); conditions: $\text{Pd}(\text{OAc})_2$ (5 mol %), Ag_2O (0.75 equiv), 2-nitrobenzoic acid (1.5 equiv), DMF, rt.

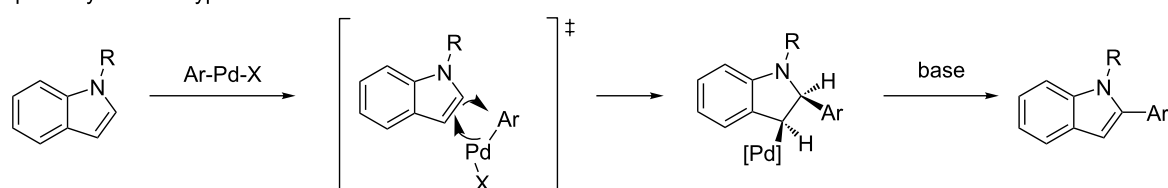
pathway A: CMD



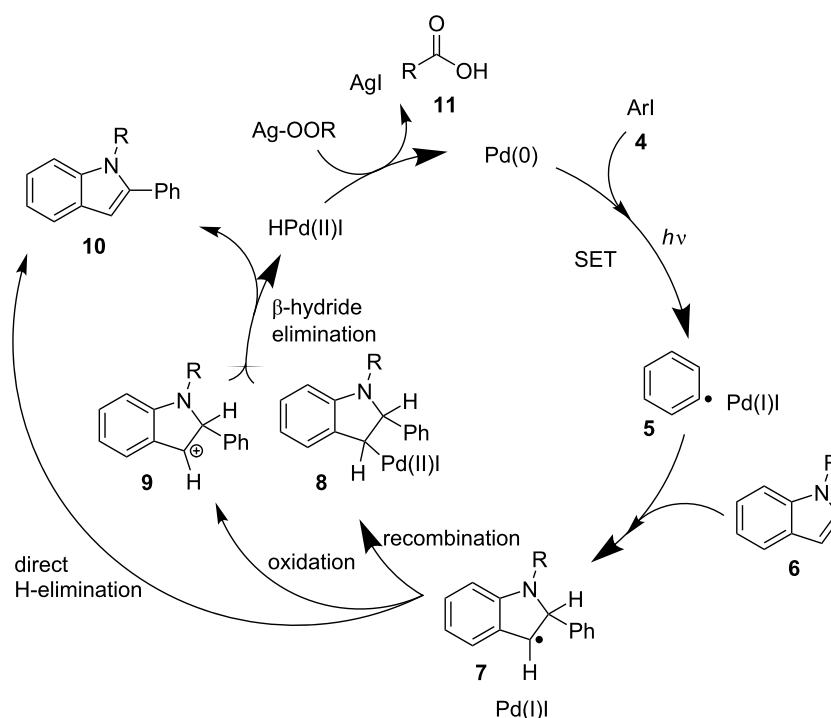
pathway B: SEAr



pathway C: Heck-type



Scheme 2: Commonly discussed mechanisms for C2 selective direct arylation, none containing radical intermediates.



Scheme 3: Proposed mechanism for palladium radical involved reaction between indole and iodobenzene.

an excited palladium(0) species to form hybrid palladium-radical intermediate **5**. This carbon-centered radical can then add to the indole. From here, three different pathways to rearomatize **7** are possible, eventually affording the arylated product **10**. Pd(0) can be regenerated by a base; in this case, the silver carboxylate. This accounts for the formation of a carboxylate radical **11**, explaining the presence of 2-nitrophenyl incorporation into the polymer chain. Additionally, this explains the formation of a phenyl radical at room temperature, and the poor control in which the nitrophenyl groups are incorporated into the chain.

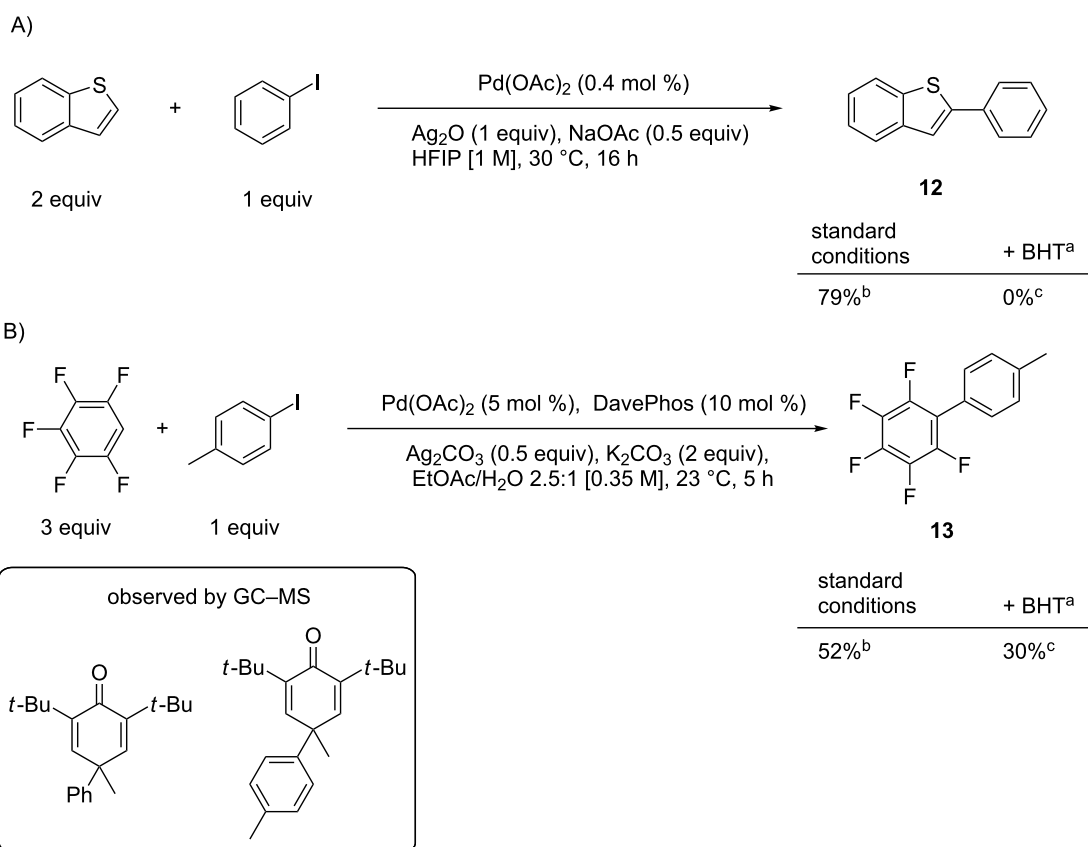
There are limited examples across the aryl C–H functionalization literature indicating a transition metal-catalyzed radical process, limited largely to cobalt catalysis [31,32]. While there are several reports of palladium-catalyzed systems for room-temperature direct arylation (i.e., no directing group, transition-metal catalyzed), a radical mechanism has not been previously discussed. Some of these reports indicate a marked difference in selectivity between elevated and ambient temperatures, which we found may be due to a change in mechanism (Supporting Information File 1, Table S1, Figure S1) [11].

We hypothesized that other known palladium-catalyzed room-temperature direct arylation methods could proceed using a single electron process. Two such Pd/Ag methods were investi-

gated: a method for benzothiophene arylation [11], and a method for fluoroarene coupling [10] (Scheme 4). First the published results were replicated, then radical traps were introduced. In these cases, BHT completely eliminated the formation of product **12** and partially inhibited the conversion to product **13**. In both cases the arene–BHT adduct was observed by GC–MS as shown in the inset of Scheme 4. While more extensive studies are needed to conclusively indicate a radical mechanism, the trap experiments and room-temperature reactivity indicate that a radical-mediated mechanism similar to the indole direct arylation may be governing the observed reactivity.

Conclusion

In conclusion, in the midst of investigating room-temperature DArP, we have discovered room-temperature palladium-catalyzed direct arylation may often be governed by radical processes. Based on the use of radical scavengers and experiments in the dark, it has become evident that a light-mediated SET is likely involved in the reported coupling of indole with iodobenzene. Moreover, other substrates such as benzo[*b*]thiophene and pentafluorobenzene appear to undergo a radical-mediated Pd/Ag room-temperature direct arylation. This is a useful insight for advancing the direct arylation knowledge base, and serves as inspiration for designing new polymerization systems that proceed under mild conditions, improving energy require-



Scheme 4: Radical trap effects on literature methods for the direct arylation at room temperature. A) From ref. [11]; B) from ref. [10]; ^a1.1 equiv BHT added to the reported conditions; ^bisolated yield; ^cdetermined by ¹H NMR against an internal standard.

ments and scalability. Work is ongoing to leverage this insight into new direct arylation methods utilizing palladium-involved radicals.

Supporting Information

Supporting Information File 1

Additional condition screenings, experimental procedures, and compound characterization including ¹H and ¹³C NMR spectra.

[<https://www.beilstein-journals.org/bjoc/content/supplementary/1860-5397-16-36-S1.pdf>]

Funding

Financial support was provided by NSF under the CCI Center for Selective C–H Functionalization (CHE-1700982).

ORCID® iDs

Amy L. Mayhugh - <https://orcid.org/0000-0002-1238-6874>

Christine K. Luscombe - <https://orcid.org/0000-0001-7456-1343>

References

- Po, R.; Bianchi, G.; Carbonera, C.; Pellegrino, A. *Macromolecules* **2015**, *48*, 453–461. doi:10.1021/ma501894w
- Huang, Y.; Luscombe, C. K. *Chem. Rec.* **2019**, *19*, 1039–1049. doi:10.1002/tcr.201800145
- Pouliot, J.-R.; Grenier, F.; Blaskovits, J. T.; Beaupré, S.; Leclerc, M. *Chem. Rev.* **2016**, *116*, 14225–14274. doi:10.1021/acs.chemrev.6b00498
- Wencel-Delord, J.; Dröge, T.; Liu, F.; Glorius, F. *Chem. Soc. Rev.* **2011**, *40*, 4740. doi:10.1039/c1cs15083a
- Gensch, T.; Hopkinson, M. N.; Glorius, F.; Wencel-Delord, J. *Chem. Soc. Rev.* **2016**, *45*, 2900–2936. doi:10.1039/c6cs00075d
- Gobalasingham, N. S.; Thompson, B. C. *Prog. Polym. Sci.* **2018**, *83*, 135–201. doi:10.1016/j.progpolymsci.2018.06.002
- Rudenko, A. E.; Thompson, B. C. *J. Polym. Sci., Part A: Polym. Chem.* **2015**, *53*, 135–147. doi:10.1002/pola.27279
- Cowie, J. M. G.; Arrighi, V. *Polymers: Chemistry and Physics of Modern Materials*, 3rd ed.; CRC Press: Boca Raton, FL, USA, 2007; pp 31–32.
- Zhou, C.; Liang, Y.; Liu, F.; Sun, C.; Huang, X.; Xie, Z.; Huang, F.; Roncali, J.; Russell, T. P.; Cao, Y. *Adv. Funct. Mater.* **2014**, *24*, 7538–7547. doi:10.1002/adfm.201401945
- René, O.; Fagnou, K. *Org. Lett.* **2010**, *12*, 2116–2119. doi:10.1021/ol1006136

11. Colletto, C.; Panigrahi, A.; Fernández-Casado, J.; Larrosa, I. *J. Am. Chem. Soc.* **2018**, *140*, 9638–9643. doi:10.1021/jacs.8b05361
12. Lebrasseur, N.; Larrosa, I. *J. Am. Chem. Soc.* **2008**, *130*, 2926–2927. doi:10.1021/ja710731a
13. Colletto, C.; Islam, S.; Juliá-Hernández, F.; Larrosa, I. *J. Am. Chem. Soc.* **2016**, *138*, 1677–1683. doi:10.1021/jacs.5b12242
14. Islam, S.; Larrosa, I. *Chem. – Eur. J.* **2013**, *19*, 15093–15096. doi:10.1002/chem.201302838
15. Okamoto, K.; Housekeeper, J. B.; Michael, F. E.; Luscombe, C. K. *Polym. Chem.* **2013**, *4*, 3499–3506. doi:10.1039/c3py00412k
16. Gooßen, L. J.; Deng, G.; Levy, L. M. *Science* **2006**, *313*, 662–664. doi:10.1126/science.1128684
17. Cornella, J.; Lahlali, H.; Larrosa, I. *Chem. Commun.* **2010**, *46*, 8276–8278. doi:10.1039/c0cc01943g
18. Cornella, J.; Lu, P.; Larrosa, I. *Org. Lett.* **2009**, *11*, 5506–5509. doi:10.1021/ol902304n
19. Stateman, L. M.; Nakafuku, K. M.; Nagib, D. A. *Synthesis* **2018**, *50*, 1569–1586. doi:10.1055/s-0036-1591930
20. Renaud, P.; Sibi, M. P., Eds. *Radicals in organic synthesis*; Wiley-VCH: Weinheim, Germany, 2001. doi:10.1002/9783527618293
21. Lapointe, D.; Fagnou, K. *Chem. Lett.* **2010**, *39*, 1118–1126. doi:10.1246/cl.2010.1118
22. Lebrasseur, N.; Larrosa, I. *Adv. Heterocycl. Chem.* **2012**, *105*, 309–351. doi:10.1016/b978-0-12-396530-1.00004-8
23. Seregin, I. V.; Gevorgyan, V. *Chem. Soc. Rev.* **2007**, *36*, 1173–1193. doi:10.1039/b606984n
24. Lane, B. S.; Brown, M. A.; Sames, D. *J. Am. Chem. Soc.* **2005**, *127*, 8050–8057. doi:10.1021/ja043273t
25. Deprez, N. R.; Kalyani, D.; Krause, A.; Sanford, M. S. *J. Am. Chem. Soc.* **2006**, *128*, 4972–4973. doi:10.1021/ja060809x
26. Kurokhtina, A. A.; Larina, E. V.; Yarosh, E. V.; Lagoda, N. A.; Schmidt, A. F. *Organometallics* **2018**, *37*, 2054–2063. doi:10.1021/acs.organomet.8b00216
27. Zhou, W.-J.; Cao, G.-M.; Shen, G.; Zhu, X.-Y.; Gui, Y.-Y.; Ye, J.-H.; Sun, L.; Liao, L.-L.; Li, J.; Yu, D.-G. *Angew. Chem., Int. Ed.* **2017**, *56*, 15683–15687. doi:10.1002/anie.201704513
28. Kurandina, D.; Parasram, M.; Gevorgyan, V. *Angew. Chem., Int. Ed.* **2017**, *56*, 14212–14216. doi:10.1002/anie.201706554
29. Parasram, M.; Chuentragool, P.; Sarkar, D.; Gevorgyan, V. *J. Am. Chem. Soc.* **2016**, *138*, 6340–6343. doi:10.1021/jacs.6b01628
30. Liu, Q.; Dong, X.; Li, J.; Xiao, J.; Dong, Y.; Liu, H. *ACS Catal.* **2015**, *5*, 6111–6137. doi:10.1021/acscatal.5b01469
31. Punji, B.; Song, W.; Shevchenko, G. A.; Ackermann, L. *Chem. – Eur. J.* **2013**, *19*, 10605–10610. doi:10.1002/chem.201301409
32. Guo, X.-K.; Zhang, L.-B.; Wei, D.; Niu, J.-L. *Chem. Sci.* **2015**, *6*, 7059–7071. doi:10.1039/c5sc01807b

License and Terms

This is an Open Access article under the terms of the Creative Commons Attribution License (<https://creativecommons.org/licenses/by/4.0>). Please note that the reuse, redistribution and reproduction in particular requires that the authors and source are credited.

The license is subject to the *Beilstein Journal of Organic Chemistry* terms and conditions: (<https://www.beilstein-journals.org/bjoc>)

The definitive version of this article is the electronic one which can be found at:
doi:10.3762/bjoc.16.36



Six-fold C–H borylation of hexa-*peri*-hexabenzocoronene

Mai Nagase¹, Kenta Kato¹, Akiko Yagi¹, Yasutomo Segawa^{*1,2} and Kenichiro Itami^{*1,2,3}

Full Research Paper

Open Access

Address:

¹Graduate School of Science, Nagoya University, Chikusa, Nagoya, 464-8602, Japan, ²JST-ERATO, Itami Molecular Nanocarbon Project, Nagoya, 464-8602, Japan and ³Institute of Transformative Bio-Molecules (WPI-ITbM), Nagoya University, Chikusa, Nagoya, 464-8602, Japan

Email:

Yasutomo Segawa* - ysegawa@nagoya-u.jp; Kenichiro Itami* - itami@chem.nagoya-u.ac.jp

* Corresponding author

Keywords:

C–H borylation; hexa-*peri*-hexabenzocoronene; iridium catalyst; X-ray crystallography

Beilstein J. Org. Chem. **2020**, *16*, 391–397.

doi:10.3762/bjoc.16.37

Received: 01 February 2020

Accepted: 05 March 2020

Published: 13 March 2020

This article is part of the thematic issue "C–H functionalization for materials science".

Associate Editor: L. Ackermann

© 2020 Nagase et al.; licensee Beilstein-Institut.

License and terms: see end of document.

Abstract

Hexa-*peri*-hexabenzocoronene (HBC) is known to be a poorly soluble polycyclic aromatic hydrocarbon for which direct functionalization methods have been very limited. Herein, the synthesis of hexaborylated HBC from unsubstituted HBC is described. Iridium-catalyzed six-fold C–H borylation of HBC was successfully achieved by screening solvents. The crystal structure of hexaborylated HBC was confirmed via X-ray crystallography. Optoelectronic properties of the thus-obtained hexaborylated HBC were analyzed with the support of density functional theory calculations. The spectra revealed a bathochromic shift of absorption bands compared with unsubstituted HBC under the effect of the σ -donation of boryl groups.

Introduction

Polycyclic aromatic hydrocarbons (PAHs) are beneficial chemical compounds as semiconductors and luminescent materials [1–3]. Direct functionalizations of PAHs are extensively studied because physical and electronic properties can be tuned by their peripheral substituents [4–6]. For instance, the introduction of electron-donating or -withdrawing groups alters electronic properties, as well as the solubility of PAHs increases by introducing long alkyl chains or bulky substituents.

In general, it is indispensable to directly functionalize large molecular weight PAHs [7]. As the molecular weight of planar

PAHs increases, solubility in common organic solvents greatly decreases due to the π – π interactions. Hexa-*peri*-hexabenzocoronene (HBC) is a notable compound investigated in the fields from synthetic chemistry to astrophysics among PAHs [4,8–10], and also known as a poorly soluble PAH [11]. Against the context of difficulty in functionalizing poorly soluble compounds, functionalized HBC is typically synthesized by dehydrogenative cyclization, which is called Scholl reaction, of precursors having solubilizing substituents [12,13]. However, the Scholl reaction sometimes causes unexpected rearrangement such as 1,2-aryl shift, and produces undesired cyclic com-

pounds [14]. To design and synthesize a variety of HBC derivatives, methods for regioselective functionalization of HBC are in strong demand.

As for functional groups on the HBC core, the introduction of halogen and boryl groups is an effective way to enable further functionalization [15]. Perchlorination was reported to functionalize HBC directly (Figure 1a) [16], and perchlorinated HBC was utilized for the formation of multiply functionalized HBC derivatives [17,18]. Other than perchlorination, hexaiodinated HBC was employed in subsequent reactions to introduce substituents [19]. However, there is no report on the hexaborylation of unfunctionalized HBC, although Shinokubo and co-workers reported the di- and triborylation of HBCs substituted by 2,4,6-trimethylphenyl (Mes) groups as solubilizing groups (Figure 1b) [20]. Since boryl groups can be converted into various functional groups [15], hexaborylated HBC is expected to be a platform for the synthesis of diverse functionalized HBCs.

Herein, we report the six-fold C–H borylation of unfunctionalized HBC (Figure 1c). By screening solvents, we have established suitable reaction conditions for the synthesis of hexaborylated HBC **1**. The structure of thus-obtained **1** was confirmed by X-ray crystallography, and the electronic effects of the boryl

groups were investigated through optoelectronic measurements and density functional theory (DFT) calculations.

Results and Discussion

We have examined the conditions for C–H borylation of unsubstituted HBC. HBC was pulverized by a ball mill prior to use. First, we attempted the iridium catalyst and reagents that we have reported as the suitable C–H borylation conditions for warped nanographene: [Ir(OMe)cod]₂, 3,4,7,8-tetramethyl-1,10-phenanthroline (tmphen), HBpin (Bpin: 4,4,5,5-tetramethyl-1,3,2-dioxaborolan-2-yl) and cyclopentyl methyl ether (CPME) [21]. With these conditions at 80 °C for 2 days, **1** was afforded in 27% isolated yield (Figure 2a, entry 1), albeit the solubility of HBC in CPME was quite low. As a common solvent for C–H borylation, THF was used at 80 °C in a sealed tube to give 5.0% yield (Figure 2a, entry 2). When applying the same conditions in *N*-methylpyrrolidone (NMP) aiming to improve the solubility of HBC [11], **1** was obtained in 13% yield (Figure 2a, entry 3). The obtained hexaborylated HBC **1** can be dissolved in various solvents such as THF, ethyl acetate, diethyl ether, ethanol, CH₂Cl₂ and CHCl₃.

To compare the efficiency of the current method, the stepwise synthesis of **1** was also examined. The synthesis of hexaiodinated HBC **3** was conducted through Scholl reaction ac-

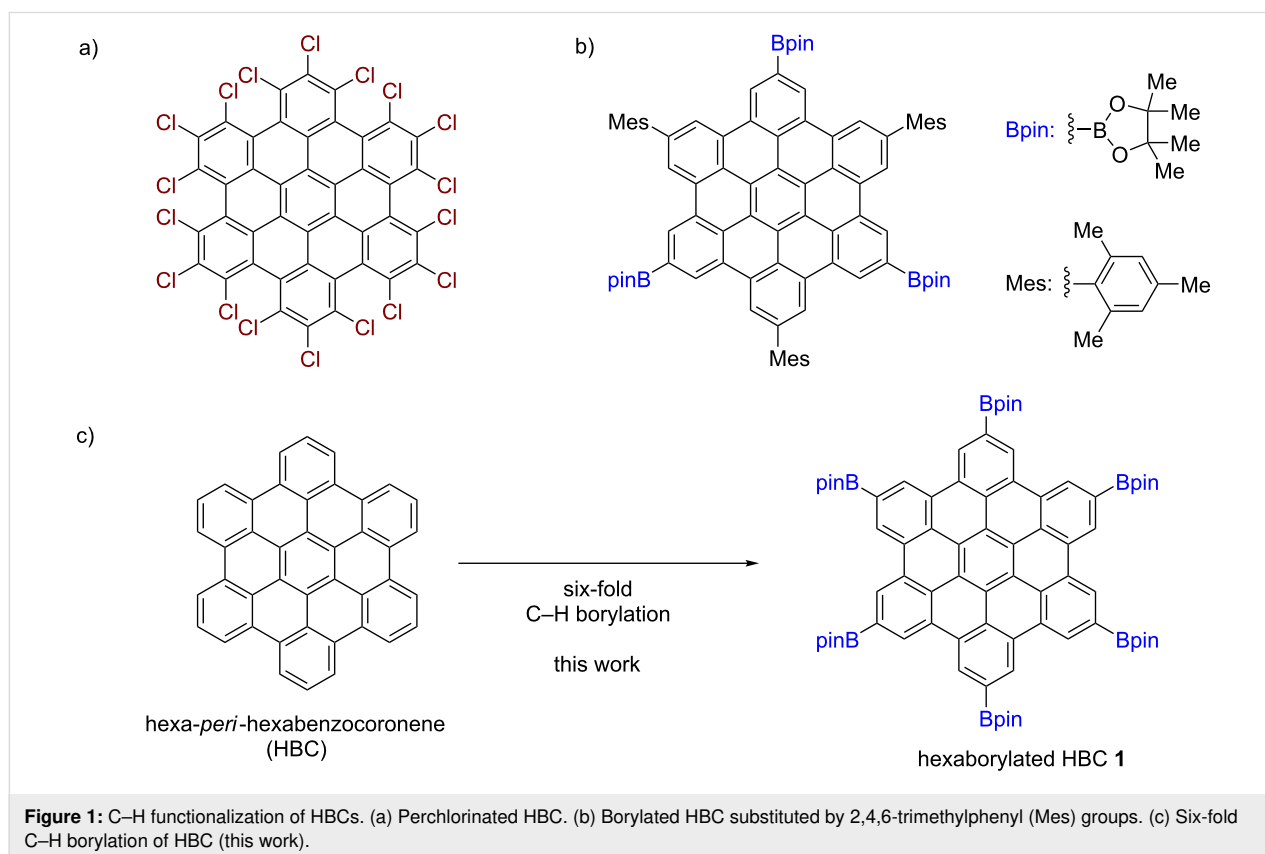


Figure 1: C–H functionalization of HBCs. (a) Perchlorinated HBC. (b) Borylated HBC substituted by 2,4,6-trimethylphenyl (Mes) groups. (c) Six-fold C–H borylation of HBC (this work).

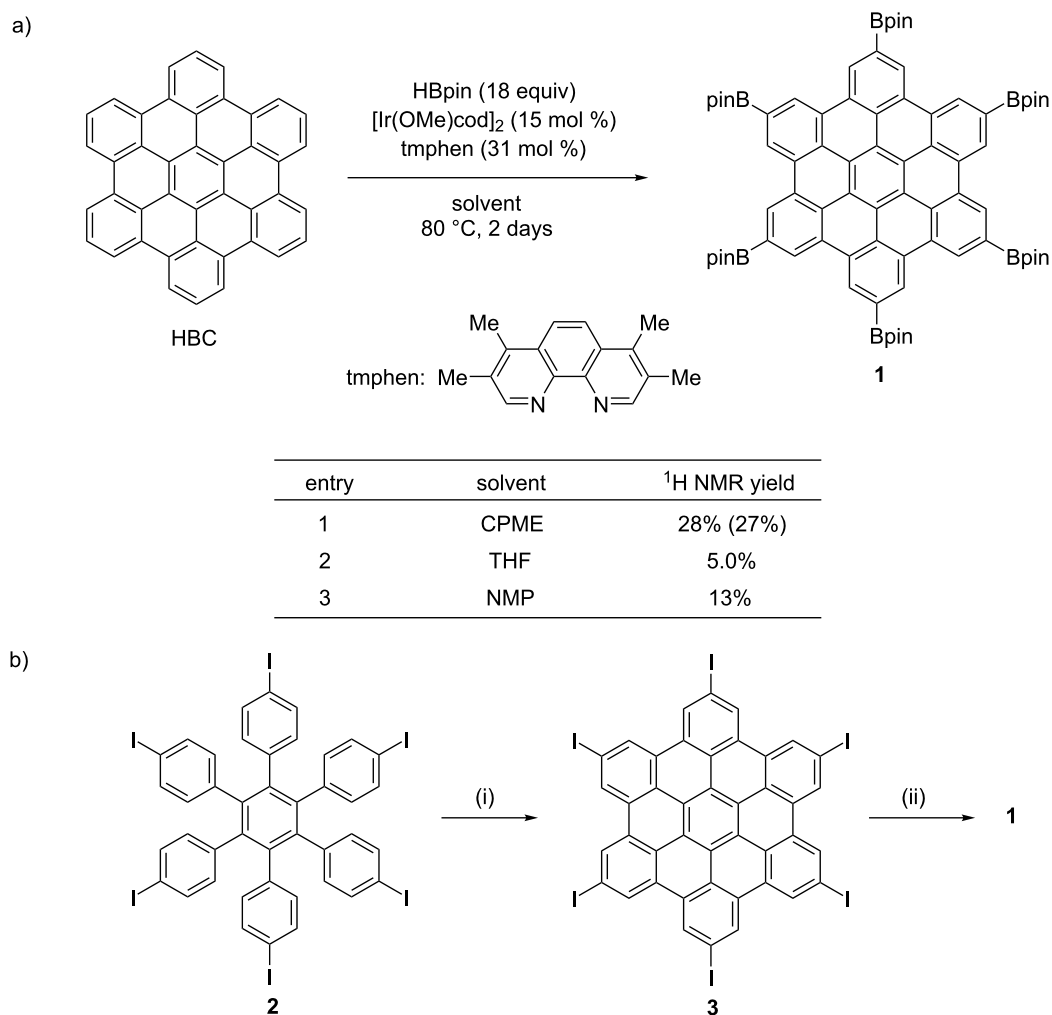


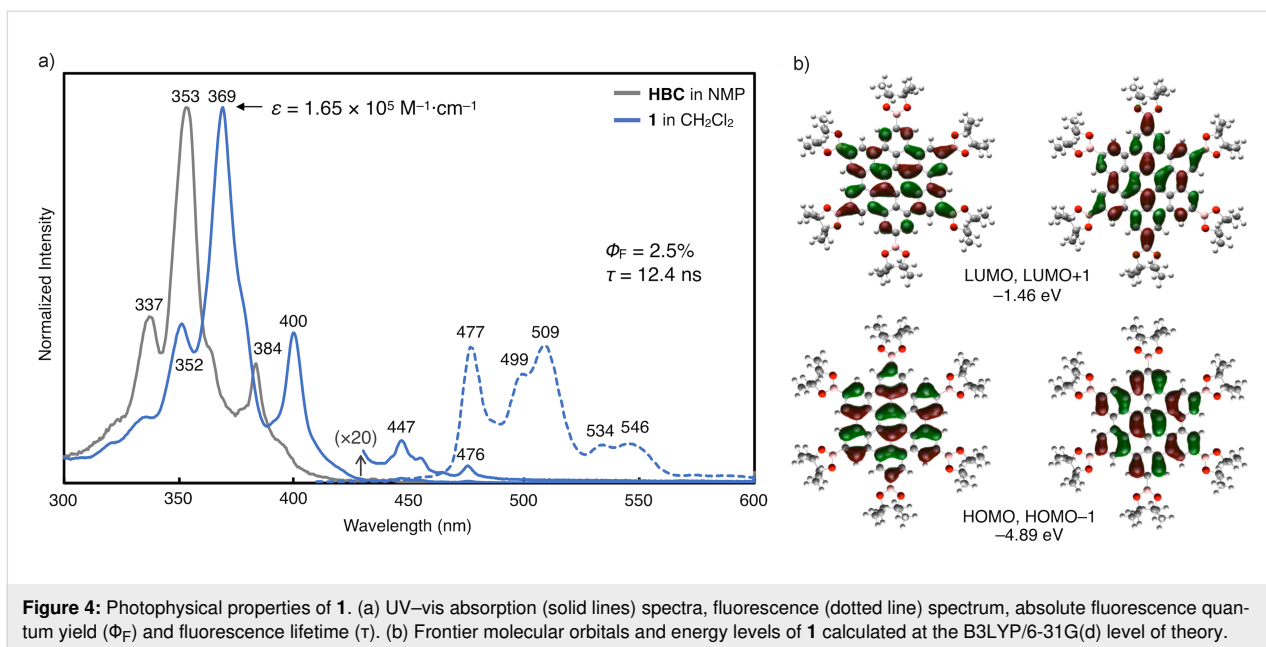
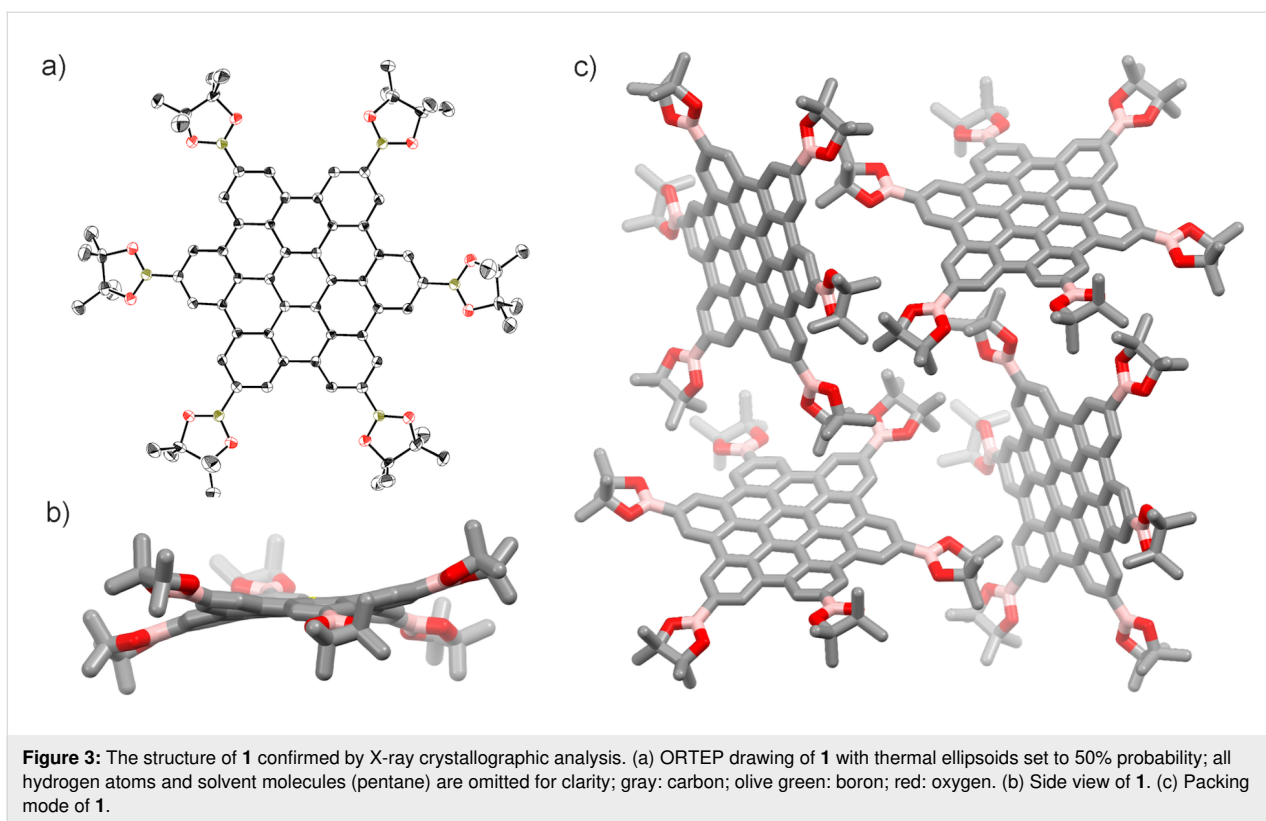
Figure 2: Synthesis of hexaborylated HBC **1**. (a) Solvent screening of six-fold C–H borylation of unsubstituted HBC. 2,3,4-Trimethoxybenzaldehyde was used as an internal standard to estimate the yield of **1**. The yield in parentheses is the isolated yield of **1**. (b) Stepwise synthesis of **1** via Miyaura–Ishiyama borylation. Reaction conditions: (i) FeCl₃ (32 equiv), CH₃NO₂/CH₂Cl₂, rt, 21 h; (ii) B₂pin₂ (10 equiv), Pd(dppf)Cl₂ (50 mol %), KOAc (6.2 equiv), toluene/DMF (1:1), 80 °C, 18 h.

cording to a literature procedure [19]. The subsequent Miyaura–Ishiyama borylation [22] was carried out with B₂pin₂ in the presence of Pd(dppf)Cl₂ (50 mol %) and KOAc (6.2 equiv) in toluene/DMF (1:1) at 80 °C for 18 h to afford **1** in 0.8% yield based on **2** (Figure 2b). This result suggests the usefulness of the direct borylation of unsubstituted HBC although the yield of the Miyaura–Ishiyama borylation step is possibly increased by further conditions screening. The thus-obtained **1** was identical to the product from the C–H borylation of HBC according to ¹H NMR spectroscopy, and the ¹³C NMR and HRMS by MALDI–TOF MS results also supported the identification.

The hexaborylated HBC **1** was subjected to X-ray crystallographic analysis. Orange single crystals were formed by the

diffusion of pentane vapor to a 1,1,1-trichloroethane solution of **1** synthesized by the C–H borylation method. The crystal structure confirmed that the C–H borylation proceeded regioselectively at the least hindered C–H bonds of HBC (Figure 3a). An equivalent amount of pentane for **1** was co-crystallized. As illustrated in Figure 3b and 3c, **1** is slightly distorted to have S₆ symmetry, and no π–π interaction is observed in the packing mode reflecting the steric hindrance of boryl groups. This result corresponds with the high solubility of **1**.

In order to analyze the optoelectronic properties of **1**, the UV–vis absorption spectra, fluorescence spectrum, absolute fluorescence quantum yield and fluorescence lifetime were measured (Figure 4a and Figure S1, Supporting Information File 1). In comparison with the absorption spectra of pristine



HBC, the characteristic three peaks of the HBC core were red-shifted about 15 nm for **1**. The molar absorption coefficient (ϵ) at the maximum absorption wavelength of **1** (369 nm) was $1.65 \times 10^5 \text{ M}^{-1}\text{cm}^{-1}$. The maximum absorption peak and the minimum fluorescence peak were nearly overlapped, which indicated that these peaks can be assigned to 0–0 transitions. The

absolute fluorescence quantum yield (Φ_F) and fluorescence lifetime (τ) were 2.5% and 12.4 ns, respectively. According to the equations $\Phi_F = k_r \times \tau$ and $k_r + k_{nr} = \tau^{-1}$, the radiative (k_r) and nonradiative (k_{nr}) decay rate constants from the singlet excited state were determined ($k_r = 2.0 \times 10^6 \text{ s}^{-1}$; $k_{nr} = 7.9 \times 10^7 \text{ s}^{-1}$). The frontier molecular orbitals of **1** calculated by DFT calcula-

tions at the B3LYP/6-31G(d) level of theory are shown in Figure 4b. Owing to the highly symmetrical structure of **1**, both its HOMO and HOMO–1 as well as its LUMO and LUMO+1 are degenerate. The HOMO and LUMO energies of **1** increase under the influence of the σ -donation of the boryl groups, resulting in a decrease of the HOMO–LUMO energy gap. This is in line with the bathochromic shift observed in the absorption spectrum of **1** from that of HBC.

Conclusion

In summary, the six-fold C–H borylation of unsubstituted HBC has been achieved. The optimal conditions were discovered through the screening of solvents, and **1** was obtained in 27% yield. The isolated yield of 0.8% in a stepwise method via a Miyaura–Ishiyama borylation indicates the advantage of the present method. The analyzed structure from X-ray crystallography confirmed the regioselective C–H borylations at the least sterically hindered C–H bonds of HBC. Optoelectronic measurements of **1** revealed bathochromic shifts of the absorption bands compared with unsubstituted HBC. DFT calculations also showed that the boryl groups increased the energies of frontier molecular orbitals and decreased the HOMO–LUMO energy gap. Compound **1** will contribute to a step-economical synthesis of various HBC derivatives as a platform, and furthermore, the currently developed borylation method gives insight into the functionalization of a variety of large and poorly soluble PAHs.

Experimental

General

Unless otherwise noted, all materials including dry solvent were obtained from commercial suppliers and used without further purification. Work-up and purification procedures were carried out with reagent-grade solvents under air. HBC (sublimated) was purchased from FUJIFILM Wako Pure Chemical Corporation (Catalog No. W01N40HZ370). Compound **2** was synthesized according to a reported procedure [23]. Flash column chromatography was performed with KANTO Silica Gel 60N (spherical, neutral, 40–100 μ m). Preparative recycling gel permeation chromatography (GPC) was performed with a JAI LaboACE LC-5060 instrument equipped with JAIGEL-2H columns using chloroform as an eluent. Retsch MM400, zirconia milling jars and zirconia balls were used for pulverizing at 30 Hz and 60 min. The high-resolution mass spectrum (HRMS) was obtained from a JEOL JMS-S3000 SpiralTOF (MALDI–TOF MS). Nuclear magnetic resonance (NMR) spectra were recorded on a JEOL ECS-600 (^1H 600 MHz, ^{13}C 150 MHz) spectrometer or a JEOL ECA 600II spectrometer with UltraCoolTM probe (^1H 600 MHz, ^{13}C 150 MHz). Chemical shifts for ^1H NMR are expressed in parts per million (ppm) relative to CHCl_3 (δ 7.26 ppm). Chemical shifts for ^{13}C NMR are expressed in ppm relative to CDCl_3 (δ 77.0 ppm). Data are

reported as follows: chemical shift, multiplicity (s = singlet) and integration.

General procedure of the C–H borylation of HBC

To a 20-mL J-Young[®] Schlenk tube equipped with a magnetic stirring bar was added HBC (10.0 mg, 19.1 μ mol, 1.0 equiv). The flask was put in an argon-filled glove box, and a solution of $[\text{Ir}(\text{OMe})\text{cod}]_2$ (1.9 mg, 2.9 μ mol, 15 mol %) and 3,4,7,8-tetramethyl-1,10-phenanthroline (tmphen; 1.4 mg, 5.9 μ mol, 31 mol %) in a dry solvent (300 μ L) was added to the flask. Then 4,4,5,5-tetramethyl-1,3,2-dioxaborolane (HBpin; 44.1 mg, 344 μ mol, 18 equiv) was added to the mixture and the Schlenk tube was sealed with a J-Young[®] screw tap. The resultant mixture was stirred at 80 $^\circ\text{C}$ for 2 days. After cooling the mixture to room temperature, the reaction mixture was passed through short-path silica gel with chloroform. The solvent was removed under reduced pressure. ^1H NMR yields were determined by using 2,3,4-trimethoxybenzaldehyde as an internal standard in CDCl_3 . The crude material obtained from the reaction with CPME was purified by GPC (eluent: chloroform) to afford **1** (6.7 mg, 27%). ^1H NMR (600 MHz, CDCl_3) δ 9.78 (s, 1H), 1.61 (s, 6H).

Stepwise synthesis of **1** from **3**

The Scholl reaction of **2** was performed according to a literature procedure [19]. To a 1 L two-necked round bottom flask containing a magnetic stirring bar were added dichloromethane (400 mL) and compound **2** (998 mg, 773 μ mol) under nitrogen atmosphere. Then a solution of anhydrous FeCl_3 (4.02 g, 24.8 mmol, 32 equiv) in nitromethane (10 mL) was added via syringe. The mixture was stirred at room temperature for 21 h. After quenched by methanol, the precipitate was collected and washed by dichloromethane, methanol and acetone. The reaction mixture containing **3** was obtained as a brown solid, which was used for the next reaction without further purifications.

A 15 mL Schlenk tube containing a magnetic stirring bar and KOAc (48.0 mg, 0.489 mmol, 6.2 equiv) was dried by a heat gun, cooled to room temperature and then refilled with nitrogen. To this vessel were added **3** (100 mg, 78.3 μ mol, 1.0 equiv), $\text{Pd}(\text{dppf})\text{Cl}_2$ (28.6 mg, 39.1 μ mol, 0.5 equiv), bis(pinacolato)diboron (B_2pin_2 ; 199 mg, 783 μ mol, 10 equiv), toluene (0.36 mL) and *N,N*-dimethylformamide (DMF; 0.36 mL). The mixture was stirred at 80 $^\circ\text{C}$ for 18 h. After cooling the mixture to room temperature, the reaction mixture was passed through short-path silica gel with chloroform. The solvent was removed under reduced pressure. The crude material was purified by GPC (eluent: chloroform) and recrystallized with 1,1,1-trichloroethane and pentane to furnish **1** (1.1 mg,

0.8% yield based on **2**) as an orange solid. ^1H NMR (600 MHz, CDCl_3) δ 9.78 (s, 1H), 1.61 (s, 6H); ^{13}C NMR (150 MHz, CDCl_3) δ 25.6, 84.4, 122.4, 127.0, 127.3, 128.8, 129.9; HRMS (MALDI-TOF MS) m/z : $[\text{M}]^+$ calcd for $\text{C}_{78}\text{H}_{84}\text{B}_6\text{O}_{12}$, 1278.6571; found, 1278.6582.

X-ray crystallography

Details of the crystal data and a summary of the intensity data collection parameters for **1** are listed below. A suitable crystal was mounted with mineral oil on a MiTeGen MicroMounts and transferred to the goniometer of the kappa goniometer of a RIGAKU XtaLAB Synergy-S system with 1.2 kW MicroMax-007HF microfocus rotating anode (Graphite-monochromated Mo K α radiation ($\lambda = 0.71073 \text{ \AA}$)) and PILATUS200K hybrid photon-counting detector. Cell parameters were determined and refined, and raw frame data were integrated using CrysAlis^{Pro} (Agilent Technologies, 2010). The structures were solved by direct methods with (SHELXT) [24] and refined by full-matrix least-squares techniques against F^2 (SHELXL-2018/3) [25] by using Olex2 software package [26]. The intensities were corrected for Lorentz and polarization effects. Non-hydrogen atoms were refined anisotropically, and hydrogen atoms were placed using AFIX instructions.

Crystal Data for **1**: CCDC 1981141. $\text{C}_{88}\text{H}_{108}\text{B}_6\text{O}_{12}$ ($\text{C}_{78}\text{H}_{84}\text{B}_6\text{O}_{12} \cdot 2\text{C}_5\text{H}_{12}$) ($M = 1422.60 \text{ g}\cdot\text{mol}^{-1}$), crystal size: $0.2 \times 0.2 \times 0.2 \text{ mm}$, cubic, space group $Pa\bar{3}$ (no. 205), $a = 19.9143(8) \text{ \AA}$, $V = 7897.6(10) \text{ \AA}^3$, $Z = 4$, $T = 123(2) \text{ K}$, $\mu(\text{Mo K}\alpha) = 0.076 \text{ mm}^{-1}$, $D_{\text{calc}} = 1.196 \text{ g}\cdot\text{cm}^{-3}$, 8158 reflections measured ($4.09^\circ \leq 2\theta \leq 55.862^\circ$), 2594 unique ($R_{\text{int}} = 0.0529$). Goodness-of-fit on F^2 : 1.093. $R_1 = 0.0733$, $wR_2 = 0.2041$ ($I > 2\sigma(I)$) and $R_1 = 0.1252$, $wR_2 = 0.2378$ (all data).

Photophysical measurements

UV–vis absorption spectra were recorded on a Shimadzu UV-3510 spectrometer with a resolution of 0.5 nm. The emission spectrum was measured on a Shimadzu RF-6000 spectrometer with a resolution of 0.5 nm. Absolute fluorescence quantum yield (Φ_F) was determined on a Shimadzu RF-6000 spectrometer using a calibrated integrating sphere system upon excitation at 340 nm. For FL lifetime measurement, a Hamamatsu Photonics QuantaTaurus-Tau[®] fluorescence lifetime spectrometer C11367-21 with LED as a light source was used (excitation: 365 nm, emission: 510 nm, frequency: 1 MHz). Dilute solutions in NMP or spectral grade dichloromethane in a 1 cm square quartz cell were used for measurements.

Computational study

The Gaussian 16 program [27] running on a NEC LX 110Rh system was used for optimization (B3LYP/6-31G(d)) [28,29]. Structures were optimized without any symmetry assumptions.

Supporting Information

Supporting information features copies of ^1H and ^{13}C NMR spectra and UV-vis absorption spectra of compound **1** and Cartesian coordinates of the optimized structure of **1**.

Supporting Information File 1

UV–vis spectra, NMR spectra and Cartesian coordinates. [<https://www.beilstein-journals.org/bjoc/content/supplementary/1860-5397-16-37-S1.pdf>]

Supporting Information File 2

Crystallographic information file of compound **1**. [<https://www.beilstein-journals.org/bjoc/content/supplementary/1860-5397-16-37-S2.cif>]

Acknowledgements

We thank Prof. Tsuyohiko Fujigaya (Kyushu University) for fruitful advice. Calculations were performed using resources of the Research Center for Computational Science, Okazaki, Japan.

Funding

This work was supported by the ERATO program from JST (JPMJER1302 to K.I.), the Funding Program for KAKENHI from MEXT (JP1905463 to K.I., JP16K05771, JP19H02701, JP19K22183 to Y.S., JP19K15537 to A.Y.), the Grant-in-aid for Scientific Research on Innovative Areas "π-Figuration" (JP17H05149 to Y.S.) and CREST program from JST (JPMJCR19R1 to A.Y.). M.N. acknowledges "Graduate Program of Transformative Chem-Bio Research" in Nagoya University supported by MEXT (WISE Program). K.K. acknowledges the JSPS fellowship for young scientists. ITbM is supported by the World Premier International Research Center Initiative (WPI), Japan.

ORCID[®] iDs

Kenta Kato - <https://orcid.org/0000-0003-0095-4296>
Akiko Yagi - <https://orcid.org/0000-0003-2941-4357>
Yasutomo Segawa - <https://orcid.org/0000-0001-6439-8546>
Kenichiro Itami - <https://orcid.org/0000-0001-5227-7894>

References

- Harvey, R. G. *Polycyclic aromatic hydrocarbons*; Wiley-VCH: New York, NY, USA, 1997.
- Narita, A.; Wang, X.-Y.; Feng, X.; Müllen, K. *Chem. Soc. Rev.* **2015**, *44*, 6616–6643. doi:10.1039/c5cs00183h
- Wang, X.-Y.; Yao, X.; Müllen, K. *Sci. China: Chem.* **2019**, *62*, 1099–1144. doi:10.1007/s11426-019-9491-2

4. Wu, J.; Pisula, W.; Müllen, K. *Chem. Rev.* **2007**, *107*, 718–747. doi:10.1021/cr068010r
5. Seyler, H.; Purushothaman, B.; Jones, D. J.; Holmes, A. B.; Wong, W. W. H. *Pure Appl. Chem.* **2012**, *84*, 1047–1067. doi:10.1351/pac-con-11-09-24
6. Segawa, Y.; Maekawa, T.; Itami, K. *Angew. Chem., Int. Ed.* **2015**, *54*, 66–81. doi:10.1002/anie.201403729
7. Fetzer, J. C. *Large (> 24) Polycyclic Aromatic Hydrocarbons - Chemistry and Analysis*; Wiley Interscience: New York, NY, USA, 2000.
8. Krieg, E.; Bastings, M. M. C.; Besenius, P.; Rybtchinski, B. *Chem. Rev.* **2016**, *116*, 2414–2477. doi:10.1021/acs.chemrev.5b00369
9. Kokkin, D. L.; Troy, T. P.; Nakajima, M.; Nauta, K.; Varberg, T. D.; Metha, G. F.; Lucas, N. T.; Schmidt, T. W. *Astrophys. J.* **2008**, *681*, L49–L51. doi:10.1086/590207
10. Steglich, M.; Bouwman, J.; Huisken, F.; Henning, T. *Astrophys. J.* **2011**, *742*, 2. doi:10.1088/0004-637x/742/1/2
11. Hughes, J. M.; Hernandez, Y.; Aherne, D.; Doessel, L.; Müllen, K.; Moreton, B.; White, T. W.; Partridge, C.; Costantini, G.; Shmeliov, A.; Shannon, M.; Nicolosi, V.; Coleman, J. N. *J. Am. Chem. Soc.* **2012**, *134*, 12168–12179. doi:10.1021/ja303683v
12. Grzybowski, M.; Skonieczny, K.; Butenschön, H.; Gryko, D. T. *Angew. Chem., Int. Ed.* **2013**, *52*, 9900–9930. doi:10.1002/anie.201210238
13. Grzybowski, M.; Sadowski, B.; Butenschön, H.; Gryko, D. T. *Angew. Chem., Int. Ed.* **2020**, *59*, 2998–3027. doi:10.1002/anie.201904934
14. Dou, X.; Yang, X.; Bodwell, G. J.; Wagner, M.; Enkelmann, V.; Müllen, K. *Org. Lett.* **2007**, *9*, 2485–2488. doi:10.1021/ol0708018
15. Hartwig, J. F. *Acc. Chem. Res.* **2012**, *45*, 864–873. doi:10.1021/ar200206a
16. Tan, Y.-Z.; Yang, B.; Parvez, K.; Narita, A.; Osella, S.; Beljonne, D.; Feng, X.; Müllen, K. *Nat. Commun.* **2013**, *4*, 2646. doi:10.1038/ncomms3646
17. Cao, J.; Liu, Y.-M.; Jing, X.; Yin, J.; Li, J.; Xu, B.; Tan, Y.-Z.; Zheng, N. *J. Am. Chem. Soc.* **2015**, *137*, 10914–10917. doi:10.1021/jacs.5b06493
18. Liu, Y.-M.; Hou, H.; Zhou, Y.-Z.; Zhao, X.-J.; Tang, C.; Tan, Y.-Z.; Müllen, K. *Nat. Commun.* **2018**, *9*, 1901. doi:10.1038/s41467-018-04321-6
19. Wu, J.; Fechtenkötter, A.; Gauss, J.; Watson, M. D.; Kastler, M.; Fechtenkötter, C.; Wagner, M.; Müllen, K. *J. Am. Chem. Soc.* **2004**, *126*, 11311–11321. doi:10.1021/ja047577r
20. Yamaguchi, R.; Hiroto, S.; Shinokubo, H. *Org. Lett.* **2012**, *14*, 2472–2475. doi:10.1021/ol300743f
21. Kato, K.; Lin, H.-A.; Kuwayama, M.; Nagase, M.; Segawa, Y.; Scott, L. T.; Itami, K. *Chem. Sci.* **2019**, *10*, 9038–9041. doi:10.1039/c9sc03061a
22. Ishiyama, T.; Murata, M.; Miyaura, N. *J. Org. Chem.* **1995**, *60*, 7508–7510. doi:10.1021/jo00128a024
23. Kobayashi, K.; Kobayashi, N.; Ikuta, M.; Therrien, B.; Sakamoto, S.; Yamaguchi, K. *J. Org. Chem.* **2005**, *70*, 749–752. doi:10.1021/jo048521i
24. Sheldrick, G. M. *Acta Crystallogr., Sect. A: Found. Adv.* **2015**, *71*, 3–8. doi:10.1107/s2053273314026370
25. Sheldrick, G. M. *Acta Crystallogr., Sect. C: Struct. Chem.* **2015**, *71*, 3–8. doi:10.1107/s2053229614024218
26. Dolomanov, O. V.; Bourhis, L. J.; Gildea, R. J.; Howard, J. A. K.; Puschmann, H. *J. Appl. Crystallogr.* **2009**, *42*, 339–341. doi:10.1107/s0021889808042726
27. *Gaussian 16*, Revision B.01; Gaussian, Inc.: Wallingford, CT, 2016.
28. Becke, A. D. *J. Chem. Phys.* **1993**, *98*, 5648–5652. doi:10.1063/1.464913
29. Lee, C.; Yang, W.; Parr, R. G. *Phys. Rev. B: Condens. Matter Mater. Phys.* **1988**, *37*, 785–789. doi:10.1103/physrevb.37.785

License and Terms

This is an Open Access article under the terms of the Creative Commons Attribution License (<https://creativecommons.org/licenses/by/4.0>). Please note that the reuse, redistribution and reproduction in particular requires that the authors and source are credited.

The license is subject to the *Beilstein Journal of Organic Chemistry* terms and conditions: (<https://www.beilstein-journals.org/bjoc>)

The definitive version of this article is the electronic one which can be found at: doi:10.3762/bjoc.16.37



Synthesis of six-membered silacycles by borane-catalyzed double sila-Friedel–Crafts reaction

Yafang Dong¹, Masahiko Sakai¹, Kazuto Fuji¹, Kohei Sekine^{1,2} and Yoichiro Kuninobu^{*1,2}

Letter

Open Access

Address:

¹Interdisciplinary Graduate School of Engineering Sciences, Kyushu University, 6-1 Kasugakoen, Kasuga-shi, Fukuoka 816-8580, Japan and ²Institute for Materials Chemistry and Engineering, Kyushu University, 6-1 Kasugakoen, Kasuga-shi, Fukuoka 816-8580, Japan

Email:

Yoichiro Kuninobu* - kuninobu@cm.kyushu-u.ac.jp

* Corresponding author

Keywords:

borane; cyclic compound; organosilane; sila-Friedel–Crafts; silylation

Beilstein J. Org. Chem. **2020**, *16*, 409–414.

doi:10.3762/bjoc.16.39

Received: 01 February 2020

Accepted: 11 March 2020

Published: 17 March 2020

This article is part of the thematic issue "C–H functionalization for materials science".

Guest Editor: K. Itami

© 2020 Dong et al.; licensee Beilstein-Institut.

License and terms: see end of document.

Abstract

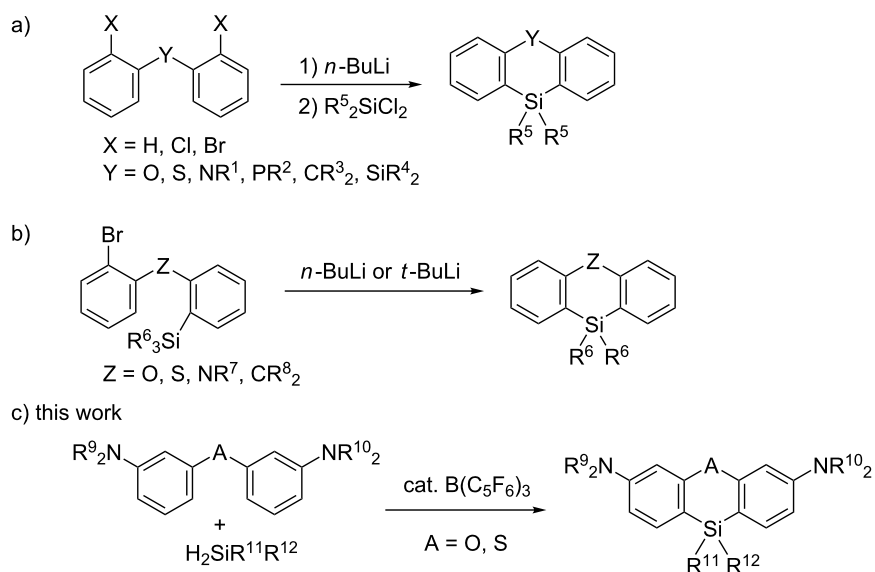
We have developed a catalytic synthetic method to prepare phenoxasilins. A borane-catalyzed double sila-Friedel–Crafts reaction between amino group-containing diaryl ethers and dihydrosilanes can be used to prepare a variety of phenoxasilin derivatives in good to excellent yields. The optimized reaction conditions were also applicable for diaryl thioethers to afford their corresponding six-membered silacyclic products. The gram-scale synthesis of a representative bis(dimethylamino)phenoxasilin and the transformation of its amino groups have also been demonstrated.

Introduction

Six-membered silacyclic compounds, such as phenoxasilin and phenothiasilin derivatives, are attractive compounds for applications as organic electronic materials [1–4], ligands [5–10], and reagents [11–14]. Therefore, the development of new methods to construct silacyclic skeletons is highly desirable. These compounds are commonly synthesized upon the reaction of heteroatom-bridged dilithiated diaryl compounds, such as dilithiated diaryl ethers and dilithiated diaryl thioethers with a range of dichlorosilane derivatives (Scheme 1a) [15–24]. An intramolecular silylation via Si–C bond cleavage can also be used to prepare a variety of six-membered silacyclic derivatives (Scheme 1b) [25]. However, some problems still remain in terms of the functional group tolerance and versatility of these

previously reported synthetic methods due to the use of a stoichiometric amount of the organolithium reagents. In addition, despite these contributions, catalytic reaction systems have not been developed as much [26,27].

The sila-Friedel–Crafts reaction is emerging as a powerful tool for C–H silylation [28,29]. In addition, intra- and intermolecular sila-Friedel–Crafts reactions have been recently developed [30–39], which have great potential as efficient synthetic strategies to construct silacycles. For example, the intramolecular C–H silylation of biphenylhydrosilanes can be used to prepare various silafluorene derivatives [30–34] and the ruthenium-catalyzed intermolecular Friedel–Crafts-type reaction of



Scheme 1: Synthetic methods of six-membered silacyclic compounds.

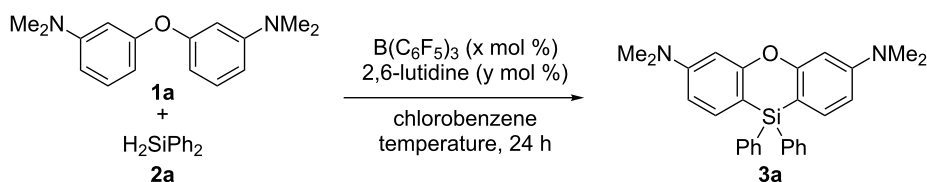
2-phenylindole with a variety of dihydrosilanes affords indole-fused benzosiloles [39]. We have also contributed to the synthesis of silafluorenes from biphenyls and dihydrosilanes using a borane-catalyzed double sila-Friedel–Crafts reaction [40,41]. Subsequently, we envisaged that the catalytic reaction between diaryl ethers and dihydrosilanes may be a useful protocol to prepare phenoxasilin derivatives (Scheme 1c). Herein, we report a borane-catalyzed double sila-Friedel–Crafts reaction used for the synthesis of six-membered silacyclic compounds, such as phenoxasilin and phenothiasilin derivatives.

Results and Discussion

A double sila-Friedel–Crafts reaction was initially investigated using diaryl ether **1a** and dihydrodiphenylsilane (**2a**) as model

substrates (Table 1). Under the optimized reaction conditions used for the synthesis of silafluorenes in our previous report [40] ($\text{B}(\text{C}_6\text{F}_5)_3$ (5.0 mol %) and 2,6-lutidine (7.5 mol %) in chlorobenzene at 100 °C), the desired reaction between **1a** with **2a** proceeded to give phenoxasilin **3a** in 60% yield (Table 1, entry 1). The structure of phenoxasilin **3a** was confirmed using single-crystal X-ray crystallography (see Supporting Information File 1 for details) [42]. Upon increasing the reaction temperature to 140 °C, the yield of **3a** was improved to 88% (Table 1, entry 2). Although the reaction in the presence of 3.0 mol % of the catalyst also proceeded efficiently (Table 1, entry 3, conditions A), the yield of **3a** decreased when compared to that obtained using 1.5 mol % of the catalyst (Table 1, entry 4). The best result was obtained in the absence of 2,6-luti-

Table 1: Optimization of the reaction conditions for the synthesis of phenoxalin **3a**.



entry ^a	x (mol%)	y (mol %)	temp (°C)	yield (%)
1	5.0	7.5	100	60
2	5.0	7.5	140	88
3	3.0	7.5	140	97
4	1.5	7.5	140	87
5	3.0	0	140	99

^a**1a** (0.250 mmol), **2a** (0.750 mmol), chlorobenzene (0.4 mL).

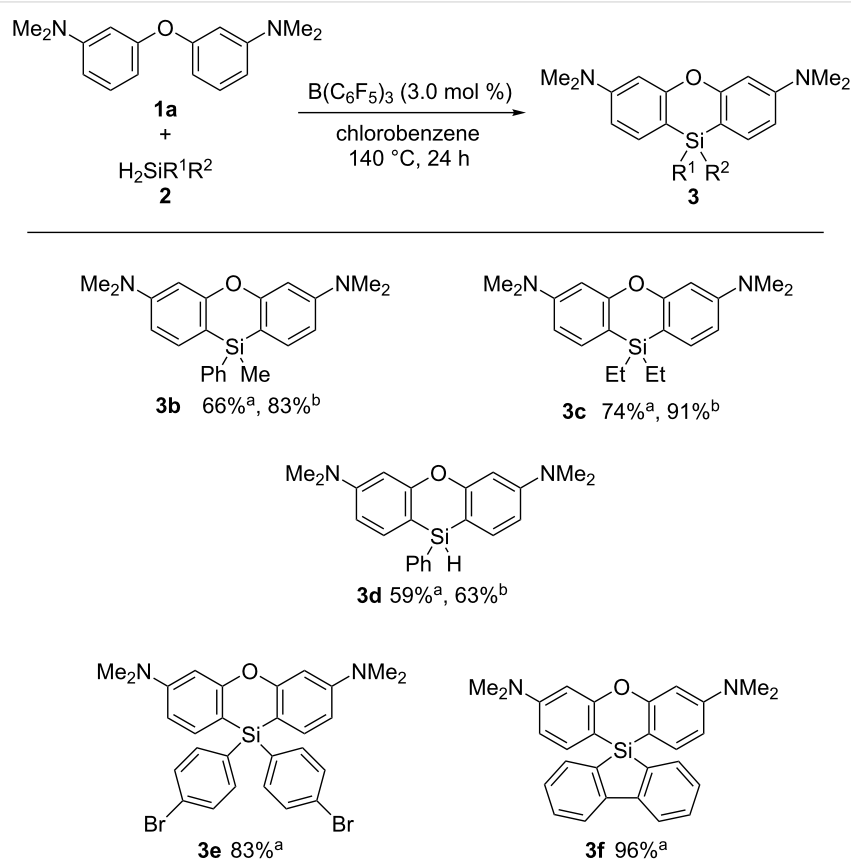
dine by which phenoxasilin **3a** formed in 99% yield (Table 1, entry 5, conditions B).

Next, the scope of the dihydrosilane starting materials used in the reaction was investigated (Scheme 2). The reactions of phenylmethylsilane (**2b**) and diethyldihydrosilane (**2c**) afforded their corresponding phenoxasilin derivatives **3b** and **3c** in 66 and 74% yield, respectively. The yields of **3b** and **3c** were improved to 83 and 91% in the presence of a catalytic amount of 2,6-lutidine, probably due to the acceleration of the deprotonation step by 2,6-lutidine [33]. In the case of phenylsilane (**2d**), the phenoxasilin product **3d** was formed in 59% yield using conditions B and in 63% yield under conditions A. Di(4-bromophenyl)dihydrosilane (**2e**) was transformed successfully into phenoxasilin **3e** in 83% yield without loss of the bromine substituent. The reaction system was also applicable for 9,9-dihydro-5-silafluorene (**2f**), which gave the spiro-type phenoxasilin **3f** in 96% yield.

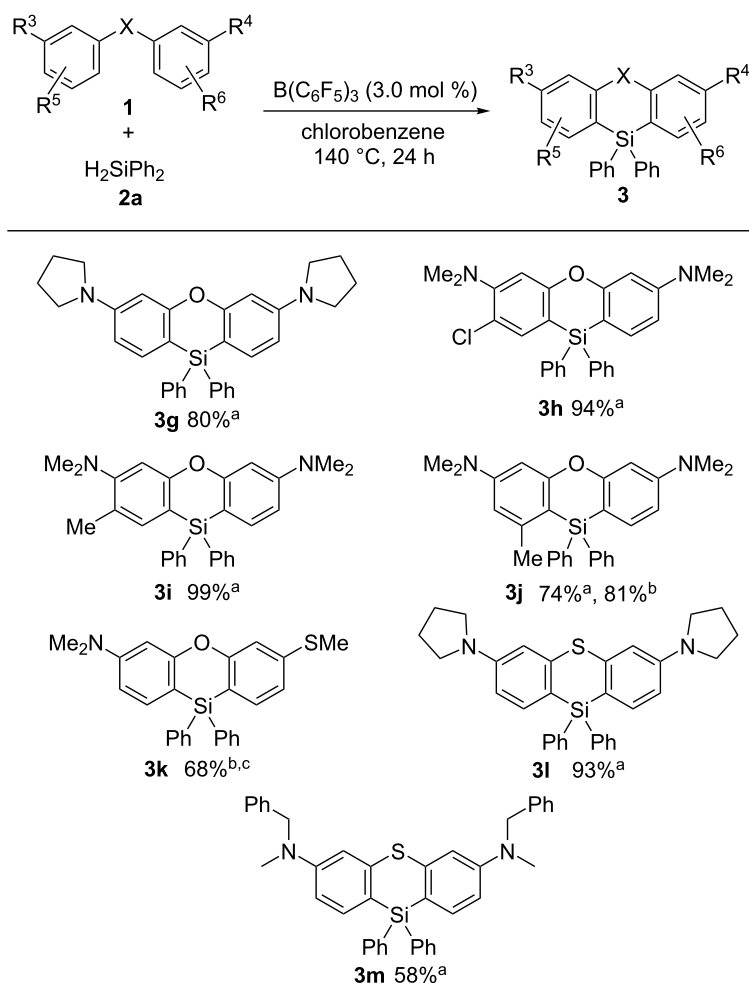
We then investigated the scope of the starting biaryl ethers used in the reaction as well as related derivatives thereof using dihydrodiphenylsilane (**2a**, Scheme 3). Pyrrolidine-substituted diaryl ether **1b** was transformed into phenoxasilin **3g** in 80% yield.

Also, the chloro-substituted diaryl ether gave its corresponding phenoxasilin **3h** in 94% yield without affecting the chlorine substituent. The methyl-substituted phenoxasilin derivatives **3i** and **3j** were formed in good yield despite of the steric hindrance of the methyl group in **3j**. When one of the NMe₂ groups was replaced with a SMe group, a mixture of the corresponding phenoxasilin product (**3k**) and the hydrosilane compound (**3k'**) was obtained via a single sila-Friedel–Crafts reaction in 35% yield in the presence of 2,6-lutidine (**3k:3k'** = 63:37). This result was probably due to the weaker electron-donating ability of the SMe group compared to that of NMe₂. The double C–H silylation reaction proceeds efficiently upon increasing the temperature to 180 °C that afforded the mixture (**3k:3k'** = 92:8) in 68% yield. The reaction system can also be applied to the synthesis of phenothiasilin **3l** that was obtained in 93% yield starting from diaryl thioether **1g**. *N*-(Benzyl)methylamine-substituted diaryl thioether **1h** was also transformed into phenothiasilin **3m** in 58% yield. The corresponding six-membered silacycles were not formed using *N*-aryl-bridged biaryls as substrates.

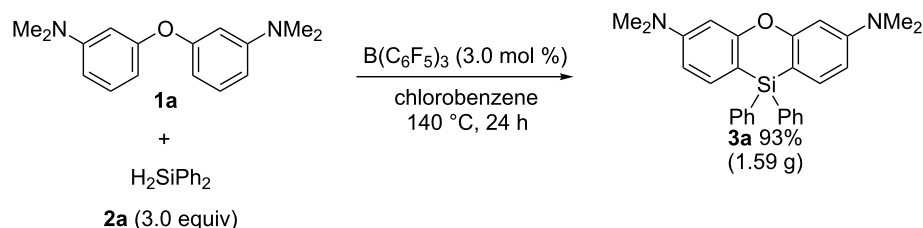
To test the applicability of the method, a gram-scale synthesis of phenoxasilin **3a** was carried out (Scheme 4). The reaction of



Scheme 2: Scope of dihydrosilanes. Conditions: a: conditions B (Table 1, entry 5); b: conditions A (Table 1, entry 3).



Scheme 3: Scope of diaryl ether and diaryl thioether derivatives. Conditions: a: conditions B (Table 1, entry 5); b: conditions A (Table 1, entry 3). c: temperature 180°C .



Scheme 4: Gram-scale Synthesis of **3a**.

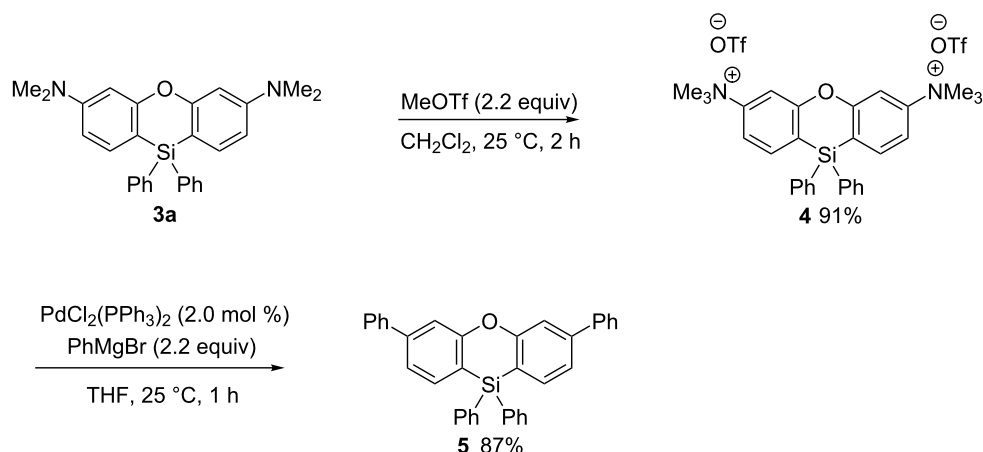
diaryl ether **1a** (1.00 g) with dihydrosilane (**2a**, 2.16 g) in the presence of a catalytic amount of $\text{B}(\text{C}_6\text{F}_5)_3$ afforded phenoxasilin **3a** in 93% yield (1.59 g).

Finally, the transformation of the amino groups in phenoxasilin **3a** into phenyl groups was carried out (Scheme 5). First, the ammonium salt **4** was prepared by treating **3a** with MeOTf fol-

lowed by a palladium-catalyzed cross-coupling reaction with the Grignard reagent (PhMgBr) that afforded the desired diphenylated phenoxasilin **5** in 87% yield [43].

Conclusion

In summary, we have developed a new catalytic synthetic method to prepare six-membered silacyclic compounds, such as



Scheme 5: Transformation of the amino groups in **3a**.

phenoxasilin and phenothiasilin derivatives, using a double sila-Friedel–Crafts reaction. The reaction system is applicable to diaryl ethers with halogen substituents or sterical hindrance. A gram-scale synthesis of phenoxasilins and transformation of the amino groups in the phenoxasilin product were also achieved. We hope that the developed protocol will prove to be a useful and efficient method to synthesize six-membered silacyclic compounds.

Supporting Information

Supporting Information File 1

Experimental procedures, compounds characterization data, and copies of ^1H and ^{13}C NMR spectra.

[<https://www.beilstein-journals.org/bjoc/content/supplementary/1860-5397-16-39-S1.pdf>]

Supporting Information File 2

CIF file for **3a**.

[<https://www.beilstein-journals.org/bjoc/content/supplementary/1860-5397-16-39-S2.cif>]

Funding

This work was supported in part by JSPS KAKENHI Grant Numbers JP 17H03016 and 18H04656, The Sumitomo Foundation, and A-STEP (VP30218088652) from JST. Y.D. is grateful to the CSC (China Scholarship Council) for the PhD fellowship.

ORCID® iDs

Kohei Sekine - <https://orcid.org/0000-0001-7588-3176>

Yoichiro Kuninobu - <https://orcid.org/0000-0002-8679-9487>

References

- Li, J.; Ding, D.; Wei, Y.; Zhang, J.; Xu, H. *Adv. Opt. Mater.* **2016**, *4*, 522–528. doi:10.1002/adom.201500673
- Hayashi, H.; Nakao, H.; Miyabayashi, T.; Murase, M. *Jpn. J. Appl. Phys.* **2013**, *52*, 05DA13. doi:10.7567/jjap.52.05da13
- Sun, J. W.; Baek, J. Y.; Kim, K.-H.; Moon, C.-K.; Lee, J.-H.; Kwon, S.-K.; Kim, Y.-H.; Kim, J.-J. *Chem. Mater.* **2015**, *27*, 6675–6681. doi:10.1021/acs.chemmater.5b02515
- Matsuo, K.; Yasuda, T. *Chem. Sci.* **2019**, *10*, 10687–10697. doi:10.1039/c9sc04492b
- Kranenburg, M.; van der Burgt, Y. E. M.; Kamer, P. C. J.; van Leeuwen, P. W. N. M.; Goubitz, K.; Fraanje, J. *Organometallics* **1995**, *14*, 3081–3089. doi:10.1021/om00006a057
- Kranenburg, M.; Kamer, P. C. J.; van Leeuwen, P. W. N. M. *Eur. J. Inorg. Chem.* **1998**, 25–27. doi:10.1002/(sici)1099-0682(199801)1998:1<25::aid-ejic25>3.0.co;2-k
- van der Veen, L. A.; Keeven, P. H.; Schoemaker, G. C.; Reek, J. N. H.; Kamer, P. C. J.; van Leeuwen, P. W. N. M.; Lutz, M.; Spek, A. L. *Organometallics* **2000**, *19*, 872–883. doi:10.1021/om990734o
- Bronger, R. P. J.; Kamer, P. C. J.; van Leeuwen, P. W. N. M. *Organometallics* **2003**, *22*, 5358–5369. doi:10.1021/om034012f
- Clayden, J.; Fletcher, S. P.; Senior, J.; Worrall, C. P. *Tetrahedron: Asymmetry* **2010**, *21*, 1355–1360. doi:10.1016/j.tetasy.2010.06.017
- Rajesh, K.; Dudle, B.; Blacque, O.; Berke, H. *Adv. Synth. Catal.* **2011**, *353*, 1479–1484. doi:10.1002/adsc.201000867
- Corey, J. Y.; Corey, E. R.; Chang, V. H. T.; Hauser, M. A.; Leiber, M. A.; Reinsel, T. E.; Riva, M. E. *Organometallics* **1984**, *3*, 1051–1060. doi:10.1021/om00085a015
- Betson, M. S.; Clayden, J.; Worrall, C. P.; Peace, S. *Angew. Chem., Int. Ed.* **2006**, *45*, 5803–5807. doi:10.1002/anie.200601866
- Betson, M. S.; Clayden, J. *Synlett* **2006**, 745–746. doi:10.1055/s-2006-933111
- Braddock-Wilking, J.; Corey, J. Y.; French, L. M.; Choi, E.; Speedie, V. J.; Rutherford, M. F.; Yao, S.; Xu, H.; Rath, N. P. *Organometallics* **2006**, *25*, 3974–3988. doi:10.1021/om060391b
- Oita, K.; Gilman, H. J. *Am. Chem. Soc.* **1957**, *79*, 339–342. doi:10.1021/ja01559a026

16. Hitchcock, C. H. S.; Mann, F. G.; Vanterpool, A. *J. Chem. Soc.* **1957**, 4537–4546. doi:10.1039/jr9570004537
17. Gilman, H.; Miles, D. *J. Org. Chem.* **1958**, *23*, 1363–1365. doi:10.1021/jo01103a036
18. Gilman, H.; Trepka, W. *J. Org. Chem.* **1961**, *26*, 5202–5203. doi:10.1021/jo01070a512
19. Gilman, H.; Trepka, W. *J. Org. Chem.* **1962**, *27*, 1418–1422. doi:10.1021/jo01051a071
20. Belsky, V. K.; Saratov, I. E.; Reikhsfeld, V. O.; Simonenko, A. A. *J. Organomet. Chem.* **1983**, *258*, 283–289. doi:10.1016/s0022-328x(00)99273-8
21. Corey, J. Y.; Trankler, K. A.; Braddock-Wilking, J.; Rath, N. P. *Organometallics* **2010**, *29*, 5708–5713. doi:10.1021/om100544f
22. Wittenberg, D.; McNinch, H. A.; Gilman, H. *J. Am. Chem. Soc.* **1958**, *80*, 5418–5422. doi:10.1021/ja01553a025
23. McCarthy, W. Z.; Corey, J. Y.; Corey, E. R. *Organometallics* **1984**, *3*, 255–263. doi:10.1021/om00080a016
24. van der Boon, L. J. P.; Hendriks, J. H.; Roolvink, D.; O’Kennedy, S. J.; Lutz, M.; Slootweg, J. C.; Ehlers, A. W.; Lammertsma, K. *Eur. J. Inorg. Chem.* **2019**, 3318–3328. doi:10.1002/ejic.201900641
25. Onoe, M.; Morioka, T.; Tobisu, M.; Chatani, N. *Chem. Lett.* **2013**, *42*, 238–240. doi:10.1246/cl.2013.238
26. Li, H.; Wang, Y.; Yuan, K.; Tao, Y.; Chen, R.; Zheng, C.; Zhou, X.; Li, J.; Huang, W. *Chem. Commun.* **2014**, *50*, 15760–15763. doi:10.1039/c4cc06636g
27. Sato, Y.; Takagi, C.; Shintani, R.; Nozaki, K. *Angew. Chem., Int. Ed.* **2017**, *56*, 9211–9216. doi:10.1002/anie.201705500
28. Bhr, S.; Oestreich, M. *Angew. Chem., Int. Ed.* **2017**, *56*, 52–59. doi:10.1002/anie.201608470
29. Richter, S. C.; Oestreich, M. *Trends Chem.* **2020**, *2*, 13–27. doi:10.1016/j.trechm.2019.07.003
30. Furukawa, S.; Kobayashi, J.; Kawashima, T. *J. Am. Chem. Soc.* **2009**, *131*, 14192–14193. doi:10.1021/ja906566r
31. Furukawa, S.; Kobayashi, J.; Kawashima, T. *Dalton Trans.* **2010**, *39*, 9329–9336. doi:10.1039/c0dt00136h
32. Aii, H.; Nakabayashi, K.; Mochida, K.; Kawashima, T. *Molecules* **2016**, *21*, 999. doi:10.3390/molecules21080999
33. Curless, L. D.; Ingleson, M. J. *Organometallics* **2014**, *33*, 7241–7246. doi:10.1021/om501033p
34. Omann, L.; Oestreich, M. *Angew. Chem., Int. Ed.* **2015**, *54*, 10276–10279. doi:10.1002/anie.201504066
35. Chen, Q.-A.; Klare, H. F. T.; Oestreich, M. *J. Am. Chem. Soc.* **2016**, *138*, 7868–7871. doi:10.1021/jacs.6b04878
36. Yin, Q.; Klare, H. F. T.; Oestreich, M. *Angew. Chem., Int. Ed.* **2016**, *55*, 3204–3207. doi:10.1002/anie.201510469
37. Ma, Y.; Wang, B.; Zhang, L.; Hou, Z. *J. Am. Chem. Soc.* **2016**, *138*, 3663–3666. doi:10.1021/jacs.6b01349
38. Han, Y.; Zhang, S.; He, J.; Zhang, Y. *J. Am. Chem. Soc.* **2017**, *139*, 7399–7407. doi:10.1021/jacs.7b03534
39. Omann, L.; Oestreich, M. *Organometallics* **2017**, *36*, 767–776. doi:10.1021/acs.organomet.6b00801
40. Dong, Y.; Takata, Y.; Yoshigoe, Y.; Sekine, K.; Kuninobu, Y. *Chem. Commun.* **2019**, *55*, 13303–13306. doi:10.1039/c9cc07692a
41. Ureshino, T.; Yoshida, T.; Kuninobu, Y.; Takai, K. *J. Am. Chem. Soc.* **2010**, *132*, 14324–14326. doi:10.1021/ja107698p
See for Rhodium-catalyzed intramolecular C–H silylation for the synthesis of silafluorenes.
42. CCDC 1979913 (**3a**) contains the supplementary crystallographic data for this paper. The data can be obtained free of charge from The Cambridge Crystallographic Data Centre via <https://www.ccdc.cam.ac.uk/structures/>.
43. Reeves, J. T.; Fandrick, D. R.; Tan, Z.; Song, J. J.; Lee, H.; Yee, N. K.; Senanayake, C. H. *Org. Lett.* **2010**, *12*, 4388–4391. doi:10.1021/ol1018739

License and Terms

This is an Open Access article under the terms of the Creative Commons Attribution License (<http://creativecommons.org/licenses/by/4.0>). Please note that the reuse, redistribution and reproduction in particular requires that the authors and source are credited.

The license is subject to the *Beilstein Journal of Organic Chemistry* terms and conditions: (<https://www.beilstein-journals.org/bjoc>)

The definitive version of this article is the electronic one which can be found at:
[doi:10.3762/bjoc.16.39](https://doi.org/10.3762/bjoc.16.39)



Synthesis of triphenylene-fused phosphole oxides via C–H functionalizations

Md. Shafiqur Rahman and Naohiko Yoshikai*

Letter

Open Access

Address:

Division of Chemistry and Biological Chemistry, School of Physical and Mathematical Sciences, Nanyang Technological University, Singapore 637371, Singapore

Email:

Naohiko Yoshikai* - nyoshikai@ntu.edu.sg

* Corresponding author

Keywords:

C–H functionalization; fluorescence; phosphole; polycyclic aromatic hydrocarbons; triphenylene

Beilstein J. Org. Chem. **2020**, *16*, 524–529.

doi:10.3762/bjoc.16.48

Received: 17 February 2020

Accepted: 20 March 2020

Published: 27 March 2020

This article is part of the thematic issue "C–H functionalization for materials science".

Guest Editor: K. Itami

© 2020 Rahman and Yoshikai; licensee Beilstein-Institut.

License and terms: see end of document.

Abstract

The synthesis of triphenylene-fused phosphole oxides has been achieved through two distinct C–H functionalization reactions as key steps. The phosphole ring was constructed by a three-component coupling of 3-(methoxymethoxy)phenylzinc chloride, an alkyne, and dichlorophenylphosphine, involving the regioselective C–H activation of the C2 position of the arylzinc intermediate via 1,4-cobalt migration. The resulting 7-hydroxybenzo[*b*]phosphole derivative was used for further π -extension through Suzuki–Miyaura couplings and a Scholl reaction, the latter closing the triphenylene ring. The absorption and emission spectra of the thus-synthesized compounds illustrated their nature as hybrids of triphenylene and benzo[*b*]phosphole.

Introduction

The phosphorus-containing five-membered ring, phosphole, has attracted significant attention as a structural motif in π -conjugated functional molecules [1–9]. Its inherently unique electronic structure, along with opportunities to modify the phosphorus center and the periphery by substitution or ring fusion, have stimulated chemists to explore a structurally diverse range of phosphole derivatives with extended π -system. These included, in particular, those fused with polycyclic aromatic hydrocarbons (PAHs) for possible applications in organic electronics, bioimaging and sensing, and asymmetric catalysis (Figure 1). To name a few examples, Yamaguchi et al. described synthetic routes to novel phosphorus-containing ladder

molecules and their application as fluorescence probes for biological imaging [10,11]. Marinetti extensively studied the synthesis of phosphahelicenes with linear fusion of the phosphole and the carbohelicene units [12], and their applications in asymmetric catalysis [13] and organic light-emitting diodes [14]. Recently, Saito et al. reported the synthesis of phosphorus-bridged triphenylenes, that is, triphosphasumanene trisulfides, and demonstrated their capability as a junction for single-molecule conductors [15].

The synthesis of PAH-fused phospholes typically requires efficient methods for the construction of the phosphole ring as well

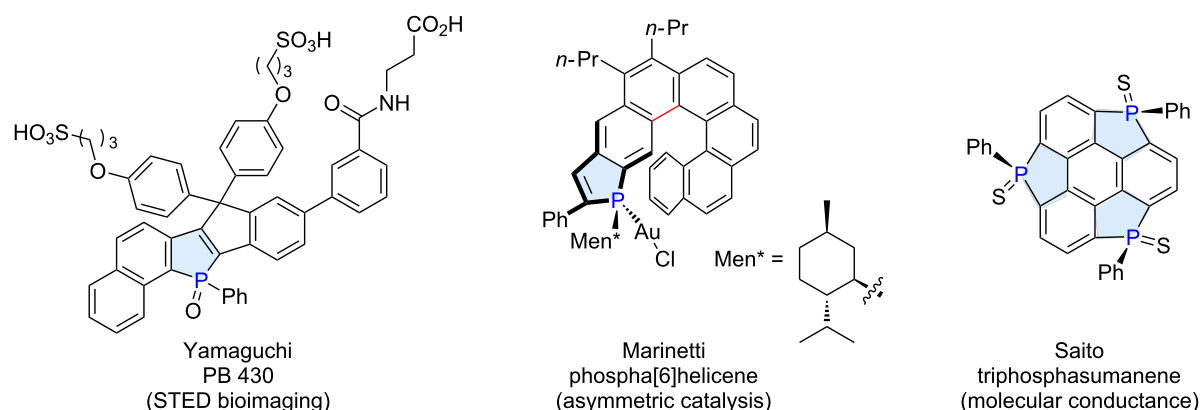


Figure 1: Examples of functional molecules based on π -extended phospholes.

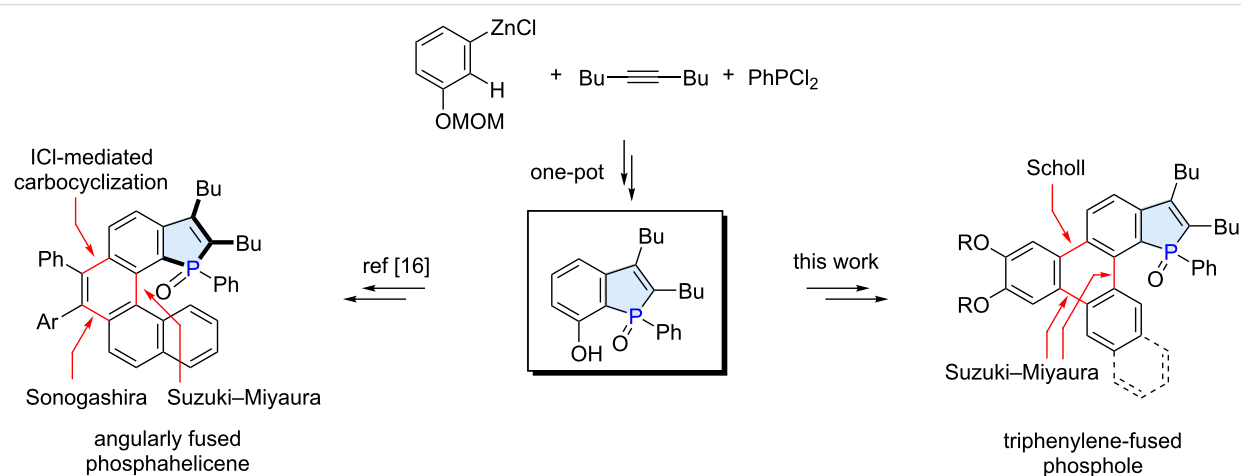
as for the π -extension/fusion of the PAH moiety, which should be smoothly implemented into the overall synthetic planning. In this context, we have recently reported the synthesis of novel phosphahelicenes that featured angular fusion of the phosphole and the carbohelicene moieties (Scheme 1) [16]. The approach focused on the regioselective one-pot synthesis of a 7-hydroxybenzo[*b*]phosphole derivative from an 3-alkoxyphenylzinc reagent, an alkyne, and dichlorophenylphosphine [17]. The hydroxy group of this key intermediate served as a handle for the π -extension through a Suzuki–Miyaura coupling, Sonogashira coupling, and electrophilic alkyne carbocyclization [18].

Given the successful synthesis of the angularly fused phosphahelicenes, we became interested in the further exploitation of 7-hydroxybenzo[*b*]phosphole as an intermediate for the synthesis of π -extended phospholes. In this respect, our attention focused on the fusion of phosphole with triphenylene, which

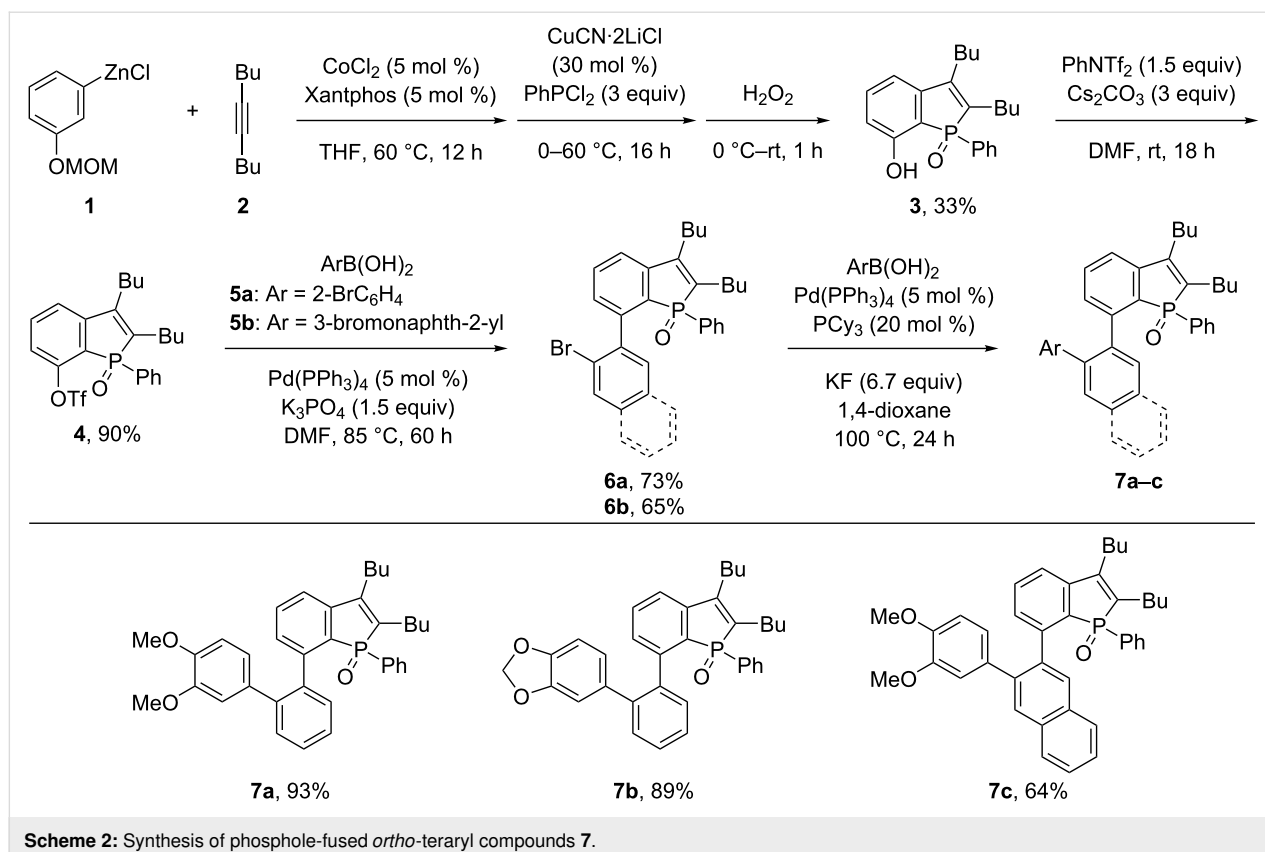
represents one of the most common disc-like PAH motifs in organic materials chemistry [19–25]. Herein, we report on the synthesis of triphenylene-fused phosphole oxides, which are distinct from Saito's compounds [15] as well as from other reported examples [26–28] in terms of the mode of fusion of the phosphole and triphenylene units. The present phosphole/triphenylene hybrid molecules displayed absorption and emission profiles that reflected the characteristics of both triphenylene and benzo[*b*]phosphole.

Results and Discussion

The present synthetic study commenced with the recently reported preparation of 7-hydroxybenzo[*b*]phosphole derivative **3** from 3-(methoxymethoxy)phenylzinc (**1**), 5-decyne (**2**), and PhPCl_2 in the presence of a cobalt–diphosphine catalyst (Scheme 2). This one-pot construction of the benzo[*b*]phosphole core ensured the preferential phosphole ring closure in proximity of the alkoxy group of the arylzinc reagent **1** (regio-



Scheme 1: Syntheses of PAH-fused phospholes featuring a 7-hydroxybenzo[*b*]phosphole as a key intermediate.



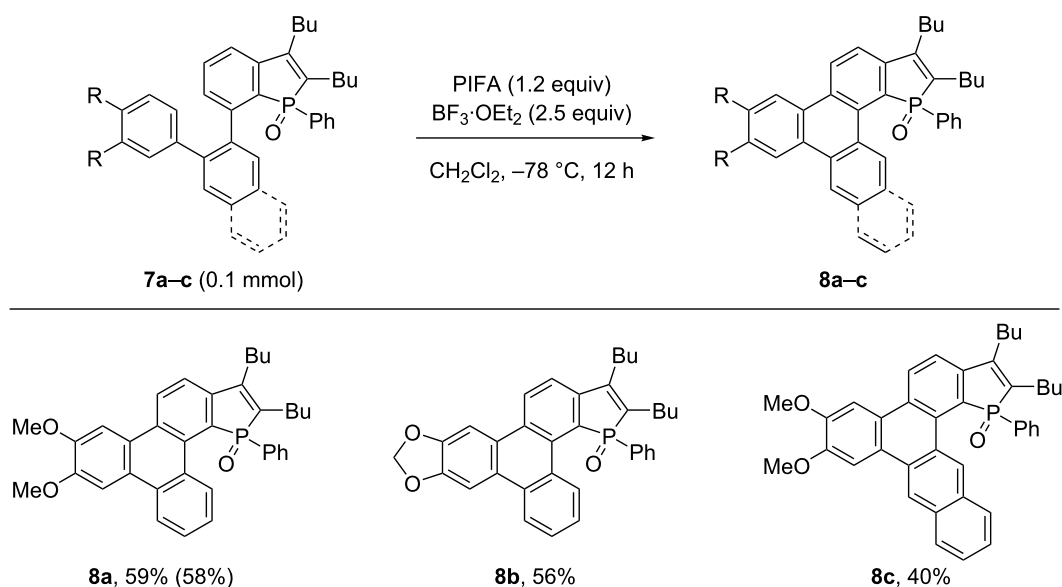
selectivity of $\approx 3:1$), presumably due to a secondary interaction between the MOM group and the cobalt catalyst during the key C–H activation step, i.e., 1,4-cobalt migration in the alkenyl-cobalt intermediate [29]. The oxidation of the benzo[*b*]phosphole phosphorous atom and cleavage of the MOM group took place simultaneously, and thus afforded compound **3** in 33% yield on a 5 mmol scale [16]. Compound **3** was then converted to the triflate, and subjected to Suzuki–Miyaura couplings with 2-bromophenylboronic acid (**5a**) or 3-bromonaphth-2-ylboronic acid (**5b**) to afford the phosphole-fused biaryls **6a** and **6b**, respectively, in decent yields. Subsequent Suzuki–Miyaura couplings of **6a** or **6b** with 3,4-dialkoxyarylboronic acids furnished the phosphole-fused *ortho*-teraryl products **7a–c** in moderate to high yields.

With the phosphole-fused *ortho*-teraryl compounds **7** in hand, we next examined their cyclization into triphenylene derivatives by the Scholl reaction (Scheme 3) [30]. The reaction of **7a** (0.1 mmol) in the presence of [bis(trifluoroacetoxy)iodo]benzene] (PIFA) and $\text{BF}_3 \cdot \text{OEt}_2$ in dichloromethane at -78°C afforded, after 12 h, the desired cyclized product **8a** in 59% yield. The reaction could be performed on a 0.5 mmol scale in a similar yield of 58%. Note that other typical reagents used for the Scholl reaction, such as $\text{DDQ}/\text{CF}_3\text{CO}_2\text{H}$, FeCl_3 , $\text{Cu}(\text{OTf})_2$, and AlCl_3 failed to promote the cyclization of **7a** to

8a. The PIFA/ $\text{BF}_3 \cdot \text{OEt}_2$ system also promoted the Scholl reaction of terphenyl **7b** bearing a methylenedioxy moiety with a comparable efficiency to afford **8b** in 56% yield. Compound **8c**, a naphthylene-linked analogue of **8a**, also underwent cyclization under the same conditions to give the corresponding product **8c** albeit in a somewhat lower yield of 40%.

The triphenylene-fused phosphole oxide **8a** was recrystallized from CH_2Cl_2 , and the molecular structure was unambiguously confirmed by single crystal X-ray analysis (Figure 2) [31]. As can be seen from the side view, the triphenylene moiety slightly deviated from planarity, because the fusion with the phosphole ring caused a subtle steric repulsion between the phosphorus substituents and the triphenylene edge within the phospha[4]helicene moiety. Unlike many triphenylene derivatives, the crystal packing of **8a** did not involve columnar π – π stacking of the PAH moiety (Figure S1, Supporting Information File 1). This is likely due to the fact that such π – π stacking is inhibited by the steric bulk of the phosphole substituents (i.e., the butyl groups, the phenyl group, and the oxygen atom).

Upon the successful synthesis of the triphenylene-fused phosphole oxides **8**, we studied the absorption and emission properties of these compounds in CH_2Cl_2 solution. Figure 3 shows the absorption and emission spectra of compounds **8a–c**, and



Scheme 3: Oxidative cyclization of phosphole-fused *ortho*-teraryl compounds **7** into triphenylene-fused phosphole oxides **8**. The yields in parentheses were obtained in a 0.5 mmol-scale reaction.

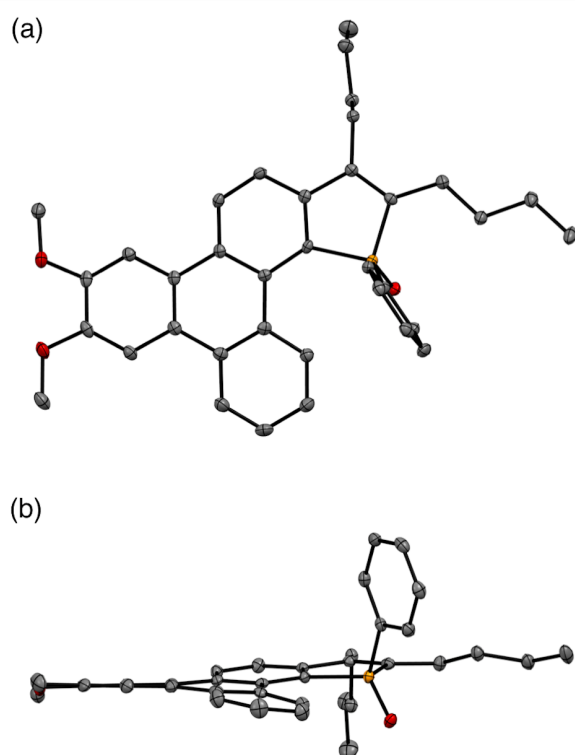


Figure 2: ORTEP drawings of compound **8a** (thermal ellipsoids set at 50% probability). a) top view; b) side view.

Table 1 provides a summary of these spectra and reported spectral data of structurally related benzo[*b*]phosphole and triphenylene derivatives. The optical data illustrate the nature of compounds **8a–c** as hybrids of triphenylene and benzo[*b*]phos-

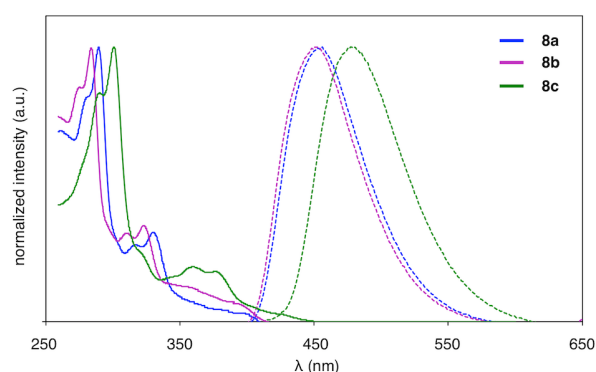


Figure 3: UV-vis absorption (solid lines) and fluorescence (dashed lines) spectra of compounds **8a–c**.

phole oxide. Regarding the absorption, **8a** and **8b** displayed multiple absorption bands from 250–400 nm (Table 1, entries 1 and 2), which reflected the characteristics of PAHs including triphenylene derivatives (Table 1, entries 5 and 6) [32–34], rather than the 2,3-dialkylbenzo[*b*]phosphole core (Table 1, entry 4). As expected, the absorption of **8c** showed a bathochromic shift compared to **8a** and **8b** as a result of π -extension (Table 1, entry 3). Like many 2,3-dialkylbenzo[*b*]phospholes [17,35], **8a–c** showed strong fluorescence in solution ($\Phi_F = 0.67$ and 0.34 for **8a** and **8b**, respectively). In contrast to the highly resolved bands in the absorption spectra, the fluorescence spectra were rather simple, with distinct emission peaks at 452 nm (**8a**), 450 nm (**8b**), and 477 nm (**8c**). Such a behavior was distinct from the fluorescence of the parent triphenylene and 2,3-dialkoxytriphenylene, which have been re-

Table 1: Summary of the absorption and emission spectra.^a

entry	compound	λ_{abs} (nm) ^b	$\log \epsilon_{\text{max}}$ ^c	λ_{em} (nm)	Φ_{F} ^d
1	8a	289, 330, 393 (sh)	4.16	452	0.67
2	8b	284, 324, 387 (sh)	4.27	450	0.34
3	8c	301, 361, 420 (sh)	4.41	477	—
4 ^e	BP	320	3.27	387	0.11
5 ^f	TP	260, 285, 320 (sh)	4.23	355, 364, 371	0.02
6 ^g	TP(OC ₁₂ H ₂₅) ₂	277, 298, 356	—	364, 382	—

^aMeasured in CH₂Cl₂ at 5×10^{-6} M. ^bRepresentative absorption maxima (sh stands for a shoulder peak). ^cMolar absorption coefficient for the longest-wavelength absorption maximum (except the shoulder). ^dDetermined using quinine sulfate as the standard (54% in 0.1 M H₂SO₄). ^eBP = 1-phenyl-2,3-dibutylbenzo[*b*]phosphole oxide. Data taken from [17]. ^fTP = triphenylene. Data taken from [32] (λ_{abs} and $\log \epsilon$) and [33] (λ_{em} and Φ_{F}). ^gTP(OC₁₂H₂₅)₂ = 2,3-di(*n*-dodecyloxy)triphenylene. Data taken from [34].

ported to show multiple emission peaks (Table 1, entries 5 and 6).

Conclusion

In summary, we synthesized novel triphenylene-fused phosphole oxides through C–H functionalization and cross-coupling reactions. The phosphole ring was constructed in the early stage of the synthesis by a three-component assembly method featuring a 1,4-cobalt migration as the key step. Unlike other C–H activation/alkyne annulation approaches to benzo[*b*]phospholes [36–40], this three-component method guarantees a good regioselectivity for the formation of the desired 7-hydroxy-benzo[*b*]phosphole derivatives. The triphenylene moiety was completed in the last step through a Scholl reaction. The synthesized triphenylene-fused phosphole oxides showed strong blue fluorescence in solution. The absorption and emission profiles of the π -extended phosphole oxide revealed their characteristics as hybrids of 2,3-dialkoxytriphenylene and 1-phenyl-2,3-dialkylbenzo[*b*]phosphole. We anticipate that the key intermediate of the present synthesis, **3**, and related benzo[*b*]phospholes accessible by the three-component assembly hold promise for further explorations in novel π -extended phosphole derivatives.

Supporting Information

Supporting Information File 1

Experimental details and characterization data of new compounds.

[<https://www.beilstein-journals.org/bjoc/content/supplementary/1860-5397-16-48-S1.pdf>]

Supporting Information File 2

Crystallographic data for compound **8a**.

[<https://www.beilstein-journals.org/bjoc/content/supplementary/1860-5397-16-48-S2.cif>]

Acknowledgements

We thank Dr. Yongxin Li (Nanyang Technological University) for his assistance with the X-ray crystallographic analysis.

Funding

This work was supported by Ministry of Education (Singapore) and Nanyang Technological University (MOE2016-T2-2-043 and RG114/18).

ORCID® iDs

Naohiko Yoshikai - <https://orcid.org/0000-0002-8997-3268>

References

- Baumgartner, T.; Réau, R. *Chem. Rev.* **2006**, *106*, 4681–4727. doi:10.1021/cr040179m
- Crassous, J.; Réau, R. *Dalton Trans.* **2008**, 6865–6876. doi:10.1039/b810976a
- Matano, Y.; Imahori, H. *Org. Biomol. Chem.* **2009**, *7*, 1258–1271. doi:10.1039/b819255n
- Ren, Y.; Baumgartner, T. *Dalton Trans.* **2012**, *41*, 7792–7800. doi:10.1039/c2dt00024e
- Baumgartner, T. *Acc. Chem. Res.* **2014**, *47*, 1613–1622. doi:10.1021/ar500084b
- Stolar, M.; Baumgartner, T. *Chem. – Asian J.* **2014**, *9*, 1212–1225. doi:10.1002/asia.201301670
- Duffy, M. P.; Delaunay, W.; Bouit, P.-A.; Hissler, M. *Chem. Soc. Rev.* **2016**, *45*, 5296–5310. doi:10.1039/c6cs00257a
- Shameem, M. A.; Orthaber, A. *Chem. – Eur. J.* **2016**, *22*, 10718–10735. doi:10.1002/chem.201600005
- Hibner-Kulicka, P.; Joule, J. A.; Skalik, J.; Balczewski, P. *RSC Adv.* **2017**, *7*, 9194–9236. doi:10.1039/c6ra26333j
- Wang, C.; Fukazawa, A.; Taki, M.; Sato, Y.; Higashiyama, T.; Yamaguchi, S. *Angew. Chem., Int. Ed.* **2015**, *54*, 15213–15217. doi:10.1002/anie.201507939
- Wang, C.; Taki, M.; Sato, Y.; Fukazawa, A.; Higashiyama, T.; Yamaguchi, S. *J. Am. Chem. Soc.* **2017**, *139*, 10374–10381. doi:10.1021/jacs.7b04418
- Yavari, K.; Moussa, S.; Ben Hassine, B.; Retailleau, P.; Voituriez, A.; Marinetti, A. *Angew. Chem., Int. Ed.* **2012**, *51*, 6748–6752. doi:10.1002/anie.201202024

13. Yavari, K.; Aillard, P.; Zhang, Y.; Nuter, F.; Retailleau, P.; Voituriez, A.; Marinetti, A. *Angew. Chem., Int. Ed.* **2014**, *53*, 861–865. doi:10.1002/anie.201308377
14. Yavari, K.; Delaunay, W.; De Rycke, N.; Reynaldo, T.; Aillard, P.; Srebro-Hooper, M.; Chang, V. Y.; Muller, G.; Tondelier, D.; Geffroy, B.; Voituriez, A.; Marinetti, A.; Hissler, M.; Crassous, J. *Chem. – Eur. J.* **2019**, *25*, 5303–5310. doi:10.1002/chem.201806140
15. Furukawa, S.; Suda, Y.; Kobayashi, J.; Kawashima, T.; Tada, T.; Fujii, S.; Kiguchi, M.; Saito, M. *J. Am. Chem. Soc.* **2017**, *139*, 5787–5792. doi:10.1021/jacs.6b12119
16. Rahman, M. S.; Yoshikai, N. *Org. Lett.* **2019**, *21*, 3232–3236. doi:10.1021/acs.orglett.9b00955
17. Wu, B.; Santra, M.; Yoshikai, N. *Angew. Chem., Int. Ed.* **2014**, *53*, 7543–7546. doi:10.1002/anie.201404019
18. Wakatsuki, A.; Yukimoto, M.; Minoura, M.; Fujii, K.; Kimura, Y.; Matano, Y. *Dalton Trans.* **2018**, *47*, 7123–7127. doi:10.1039/c8dt01503a
19. Watson, M. D.; Fechtenkötter, A.; Müllen, K. *Chem. Rev.* **2001**, *101*, 1267–1300. doi:10.1021/cr990322p
20. Pérez, D.; Gutiérrez, E. *Chem. Soc. Rev.* **2004**, *33*, 274–283. doi:10.1039/b305549n
21. Kumar, S. *Chem. Soc. Rev.* **2006**, *35*, 83–109. doi:10.1039/b506619k
22. Sergeyev, S.; Pisula, W.; Geerts, Y. H. *Chem. Soc. Rev.* **2007**, *36*, 1902–1929. doi:10.1039/b417320c
23. Alam, M. A.; Motoyanagi, J.; Yamamoto, Y.; Fukushima, T.; Kim, J.; Kato, K.; Takata, M.; Saeki, A.; Seki, S.; Tagawa, S.; Aida, T. *J. Am. Chem. Soc.* **2009**, *131*, 17722–17723. doi:10.1021/ja905373d
24. Percec, V.; Imam, M. R.; Peterca, M.; Wilson, D. A.; Graf, R.; Spiess, H. W.; Balagurusamy, V. S. K.; Heiney, P. A. *J. Am. Chem. Soc.* **2009**, *131*, 7662–7677. doi:10.1021/ja8094944
25. Badjic, J. D.; Ronconi, C. M.; Stoddart, J. F.; Balzani, V.; Silvi, S.; Credi, A. *J. Am. Chem. Soc.* **2006**, *128*, 1489–1499. doi:10.1021/ja0543954
26. Wang, S.; Yan, C.; Shang, J.; Wang, W.; Yuan, C.; Zhang, H.-L.; Shao, X. *Angew. Chem., Int. Ed.* **2019**, *58*, 3819–3823. doi:10.1002/anie.201813070
27. Wu, B.; Chopra, R.; Yoshikai, N. *Org. Lett.* **2015**, *17*, 5666–5669. doi:10.1021/acs.orglett.5b02950
28. Aillard, P.; Gicquel, M.; Yavari, K.; Retailleau, P.; Voituriez, A.; Marinetti, A. *Eur. J. Org. Chem.* **2018**, 5853–5860. doi:10.1002/ejoc.201800438
29. Tan, B.-H.; Dong, J.; Yoshikai, N. *Angew. Chem., Int. Ed.* **2012**, *51*, 9610–9614. doi:10.1002/anie.201204388
30. Grzybowski, M.; Skonieczny, K.; Butenschön, H.; Gryko, D. T. *Angew. Chem., Int. Ed.* **2013**, *52*, 9900–9930. doi:10.1002/anie.201210238
31. CCDC 1984209 (**8a**) contains crystallographic data for this paper. These data can be obtained free of charge from The Cambridge Crystallographic Data Centre.
32. Rieger, R.; Müllen, K. *J. Phys. Org. Chem.* **2010**, *23*, 315–325. doi:10.1002/poc.1644
33. Verbitskiy, E. V.; Eltsov, O. S.; Zhilina, E. F.; Pakhomov, I. M.; Rusinov, G. L.; Chupakhin, O. N.; Charushin, V. N. *Tetrahedron* **2019**, *75*, 2687–2696. doi:10.1016/j.tet.2019.03.044
34. Schwab, M. G.; Qin, T.; Pisula, W.; Mavrinskiy, A.; Feng, X.; Baumgarten, M.; Kim, H.; Laquai, F.; Schuh, S.; Trattig, R.; List, E. J. W.; Müllen, K. *Chem. – Asian J.* **2011**, *6*, 3001–3010. doi:10.1002/asia.201100258
35. Yoshikai, N.; Santra, M.; Wu, B. *Organometallics* **2017**, *36*, 2637–2645. doi:10.1021/acs.organomet.7b00244
36. Wu, B.; Yoshikai, N. *Org. Biomol. Chem.* **2016**, *14*, 5402–5416. doi:10.1039/c6ob00219f
37. Chen, Y.-R.; Duan, W.-L. *J. Am. Chem. Soc.* **2013**, *135*, 16754–16757. doi:10.1021/ja407373g
38. Unoh, Y.; Hirano, K.; Satoh, T.; Miura, M. *Angew. Chem., Int. Ed.* **2013**, *52*, 12975–12979. doi:10.1002/anie.201307211
39. Quint, V.; Morlet-Savary, F.; Lohier, J.-F.; Lalevée, J.; Gaumont, A.-C.; Lakhdar, S. *J. Am. Chem. Soc.* **2016**, *138*, 7436–7441. doi:10.1021/jacs.6b04069
40. Liu, W.-Q.; Lei, T.; Zhou, S.; Yang, X.-L.; Li, J.; Chen, B.; Sivaguru, J.; Tung, C.-H.; Wu, L.-Z. *J. Am. Chem. Soc.* **2019**, *141*, 13941–13947. doi:10.1021/jacs.9b06920

License and Terms

This is an Open Access article under the terms of the Creative Commons Attribution License (<http://creativecommons.org/licenses/by/4.0>). Please note that the reuse, redistribution and reproduction in particular requires that the authors and source are credited.

The license is subject to the *Beilstein Journal of Organic Chemistry* terms and conditions: (<https://www.beilstein-journals.org/bjoc>)

The definitive version of this article is the electronic one which can be found at: doi:10.3762/bjoc.16.48



Copper-catalyzed remote C–H arylation of polycyclic aromatic hydrocarbons (PAHs)

Anping Luo, Min Zhang, Zhangyi Fu, Jingbo Lan*, Di Wu and Jingsong You*

Full Research Paper

Open Access

Address:

Key Laboratory of Green Chemistry and Technology of Ministry of Education, College of Chemistry, Sichuan University, 29 Wangjiang Road, Chengdu 610064, P.R. China

Email:

Jingbo Lan* - jingbolan@scu.edu.cn; Jingsong You* - jsyou@scu.edu.cn

* Corresponding author

Keywords:

C–H arylation; nonprecious metal catalyst; copper catalysis; polycyclic aromatic hydrocarbons (PAHs); regioselectivity

Beilstein J. Org. Chem. **2020**, *16*, 530–536.

doi:10.3762/bjoc.16.49

Received: 18 January 2020

Accepted: 06 March 2020

Published: 30 March 2020

This article is part of the thematic issue "C–H functionalization for materials science".

Guest Editor: K. Itami

© 2020 Luo et al.; licensee Beilstein-Institut.

License and terms: see end of document.

Abstract

The regioselective C–H arylation of substituted polycyclic aromatic hydrocarbons (PAHs) is a desired but challenging task. A copper-catalyzed C7–H arylation of 1-naphthamides has been developed by using arylodonium salts as arylating reagents. This protocol does not need to use precious metal catalysts and tolerates wide variety of functional groups. Under standard conditions, the remote C–H arylation of other PAHs including phenanthrene-9-carboxamide, pyrene-1-carboxamide and fluoranthene-3-carboxamide has also accomplished, which provides an opportunity for the development of diverse organic optoelectronic materials.

Introduction

Polycyclic aromatic hydrocarbons (PAHs) with rigid planar structure, such as naphthalene, phenanthrene, pyrene and their derivatives, can usually emit relatively strong fluorescence, and have been widely applied in many scientific areas including chemistry, biomedicine and materials science [1–6]. The arylation reaction of PAHs is an important strategy to further extend the π -conjugation length, which can effectively adjust the photophysical properties of molecules, thus having drawn much attention. Transition metal-catalyzed C–X/C–M cross-coupling reactions such as Suzuki and Stille couplings are the main approaches to achieve the arylation of PAHs [7–11]. How-

ever, the selective arylation of the C7-position of 1-naphthoic acid derivatives remains a challenging task due to the inaccessibility of the corresponding 7-halonaphthalene substrates [12].

Recently, transition metal-catalyzed C–H bond functionalization has emerged as a powerful tool to construct various biaryl skeletons [13–17]. The direct C7–H arylation of 1-naphthoic acid derivatives is undoubtedly a more effective route for the synthesis of 7-arylnaphthalene derivatives. Although the transition metal-catalyzed C2–H and C8–H arylations of 1-naphthoic acid derivatives have been widely reported, the studies on

their C7–H arylation remain rare [18–25]. Our group has recently reported F^+ reagent-promoted Pd-catalyzed C7–H arylation of 1-naphthamides, but this method still suffers from a few disadvantages (Scheme 1) [26]. First, the precious metal palladium is employed as a catalyst. Moreover, stoichiometric F^+ reagent is needed to oxidize Pd(II) species to more electrophilic high-valent cationic Pd(IV). In addition, this protocol is not compatible with other PAHs except naphthalene, such as phenanthrene, pyrene and fluoranthene, and cannot tolerate some special functional groups, such as alkenyl and alkynyl groups.

As a component part of our ongoing research on direct C–H bond functionalization [20,27–29], we herein represent a copper-catalyzed remote C–H arylation of PAHs with arylidonium salts as arylating reagents (Scheme 1). This protocol is compatible with different PAH substrates including 1-naphthamides, phenanthrene-9-carboxamide, pyrene-1-carboxamide and fluoranthene-3-carboxamide, which provides an opportunity for the development of diverse organic photoelectrical materials.

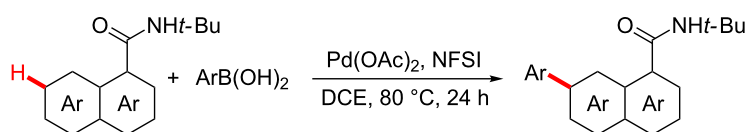
Results and Discussion

Our investigation commenced with the reaction between *N*-(*tert*-butyl)-1-naphthamide (**1a**) and mesityl(phenyl)iodonium triflate (**2a**, for detailed optimization, see Table S1, Supporting Information File 1). Initially, the reaction was performed in 1,2-dichloroethane (DCE, 1 mL) at 80 °C for 24 h in the presence of $Cu(OTf)_2$ (10 mol %) as a catalyst. The direct

C7–H arylation product *N*-(*tert*-butyl)-7-phenyl-1-naphthamide (**3a**) was obtained in 79% yield (Table 1, entry 1). Gratifyingly, when the reaction temperature was reduced to 70 °C, **3a** was obtained in 92% yield (Table 1, entry 2). The C7–H arylation could also occur with active copper powder as a catalyst (Table 1, entry 5). Other copper sources including CuO, CuCl and $Cu(OAc)_2$ were also found to be effective catalysts in this reaction, albeit with slightly lower yields (Table 1, entries 6–8). The control experiment confirmed that this transformation did not occur in the absence of Cu catalyst (Table 1, entry 9). The screening of other solvents, such as dichloromethane (DCM), *ortho*-dichlorobenzene (ODCB), $CHCl_3$ and $PhCF_3$, indicated that DCE was still the best effective (Table 1, entries 10–13). Finally, the optimal reaction system was established, which composed of $Cu(OTf)_2$ (10 mol %) in DCE (1.0 mL) at 70 °C under a nitrogen atmosphere for 24 hours.

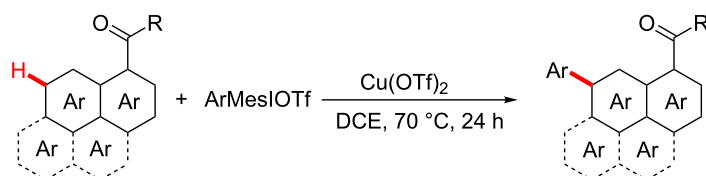
With the optimal conditions in hand, we first examined the scope of arylidonium salts. We were very pleased to find that a range of arylidonium salts could be employed as arylating reagents, affording 7-arylated 1-naphthamides (**3a–q**) in moderate to excellent yields (Scheme 2). This protocol tolerated a wide variety of functional groups, including electron-donating methyl and methoxy groups, as well as electron-withdrawing ester, trifluoromethyl, fluoro, chloro, bromo, iodo and formyl groups. The arylating reactivity of arylidonium salts with various substituents varied greatly due to the different electronic effects and steric hindrances. Arylating reagents with *ortho*-substituents led to slightly reduced yields (Scheme 2, **3f**

our recent work: Pd-catalyzed C7–H arylation of 1-naphthamides



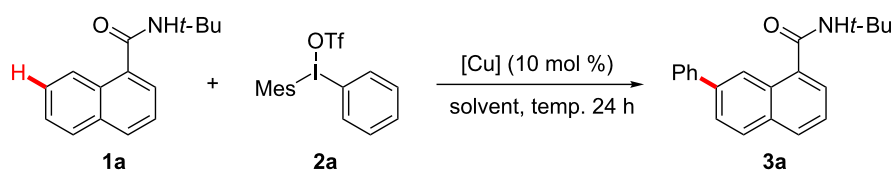
- precious metal catalyst
- stoichiometric F^+ reagent
- moderate functional group tolerance
- no tolerance for other PAHs

this work: Cu-catalyzed remote C–H arylation of PAHs



- nonprecious metal catalyst
- simple reaction system
- mild reaction conditions
- excellent functional group tolerance
- tolerance for different PAHs

Scheme 1: Direct C–H arylation of PAHs.

Table 1: Optimization of reaction conditions.^a

Entry	Solvent	[Cu]	T (°C)	Yield (%)
1	DCE	Cu(OTf) ₂	80	79
2	DCE	Cu(OTf) ₂	70	92
3	DCE	Cu(OTf) ₂	90	53
4	DCE	Cu(OTf) ₂	60	41
5	DCE	Cu	70	54
6	DCE	CuO	70	81
7	DCE	CuCl	70	84
8	DCE	Cu(OAc) ₂	70	80
9	DCE	–	70	nd
10	DCM	Cu(OTf) ₂	70	38
11	ODCB	Cu(OTf) ₂	70	77
12	CHCl ₃	Cu(OTf) ₂	70	trace
13	PhCF ₃	Cu(OTf) ₂	70	trace

^aReaction conditions: **1a** (0.2 mmol, 1.0 equiv), **2a** (0.3 mmol, 1.5 equiv), [Cu] (10 mol %) and solvent (1 mL) under N₂ for 24 h. Isolated yield. DCE = 1,2-dichloroethane. DCM = dichloromethane. ODCB = *ortho*-dichlorobenzene. nd: not detected.

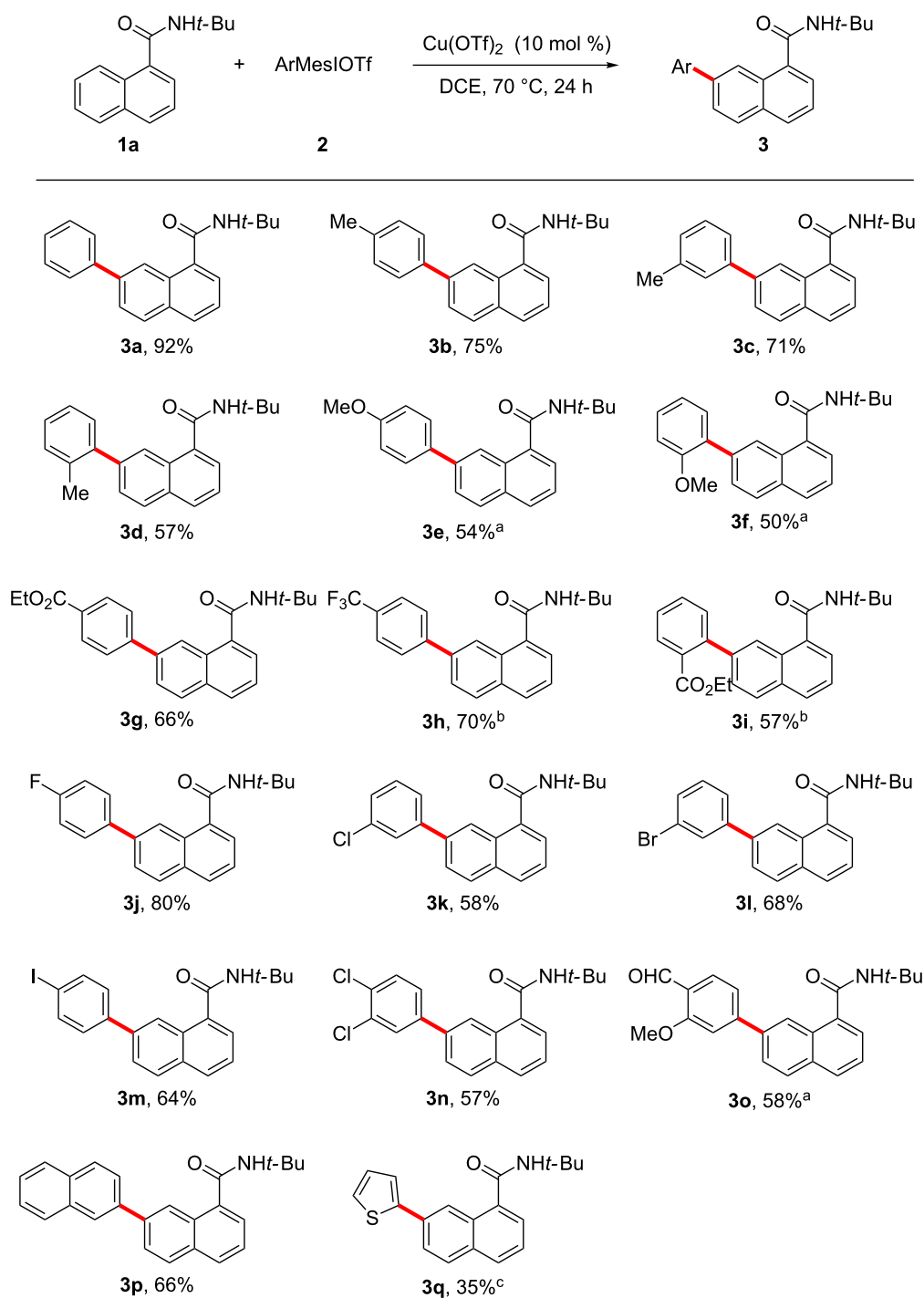
and **3i**). Aryliodonium salts containing halogen substituents, especially bromo and iodo atoms, could afford the desired products in moderate to good yields (Scheme 2, **3j–n**), making it possible to introduce useful functional groups into the products through the further transformation of corresponding aryl halides. 2-Naphthylidonium salt could react smoothly with **1a** to provide **3p** in 66% yield (Scheme 2, **3p**). Moreover, thiophen-2-ylidonium salt could be tolerated, albeit with a lower yield (Scheme 2, **3q**).

We next examined the scope of various naphthalene substrates (Scheme 3, **4a–l**). The electronic effect of C4-substituents on *N*-(*tert*-butyl)-1-naphthamide was not obvious. The 4-substituted 1-naphthamide substrates, whether with electron-donating methyl and methoxy groups, or with electron-withdrawing phenyl, ester, fluoro and bromo groups, gave the corresponding products in good to excellent yields (Scheme 3, **4a–f**). Substrates with C2-substituents also exhibited excellent reactivity, providing the desired products **4h** and **4i** in 85% and 80% yields, respectively (Scheme 3, **4h** and **4i**). Notably, 1-naphthamides with alkenyl (**1l**) and alkynyl (**1m**) groups were also suitable substrates for this direct C7–H arylation, affording **4k** and **4l** in good yields (Scheme 3, **4k** and **4l**). Furthermore, this Cu-catalyzed direct C–H arylation could tolerate other PAH substrates. The regioselective arylation of PAHs is challenging,

and so far, there are no examples on the selective remote C–H arylation of phenanthrene-9-carboxamide, pyrene-1-carboxamide and fluoranthene-3-carboxamide. Gratifyingly, the remote C–H arylation of these PAH substrates occurred smoothly, giving the corresponding arylation products in moderate to good yields (Scheme 3, **4m–o**).

This catalytic system was also compatible with substrates bearing other directing groups except *tert*-butylaminocarbonyl (Scheme 3, **4p–s**). When employing methylaminocarbonyl and cyclohexylaminocarbonyl as directing groups, the 7-arylation products of naphthalene rings were obtained in good yields (Scheme 3, **4p** and **4q**). A keto carbonyl group was also proved to be a suitable directing group, affording the corresponding arylation products in moderate yields (Scheme 3, **4r** and **4s**).

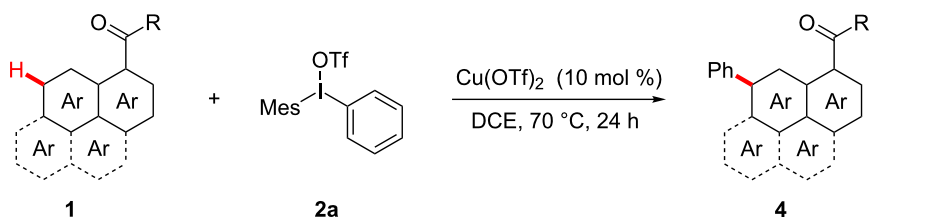
Considering that Cu(0), Cu(I) and Cu(II) all could catalyze this C–H arylation reaction and referring to previous research results [30–32], a Cu(I)/Cu(III) catalytic cycle was proposed (Scheme 4). First, Cu(I) is formed by the reduction or disproportionation of Cu(II). Then, arylidonium salt oxidizes Cu(I) to highly electrophilic Cu(III)–aryl intermediate **I**. The coordination of the carbonyl oxygen to **I** gives intermediate **II**, which undergoes an aryl-transfer reaction via a Heck-like four-membered-ring transition state **III** to form the intermediate **IV** with



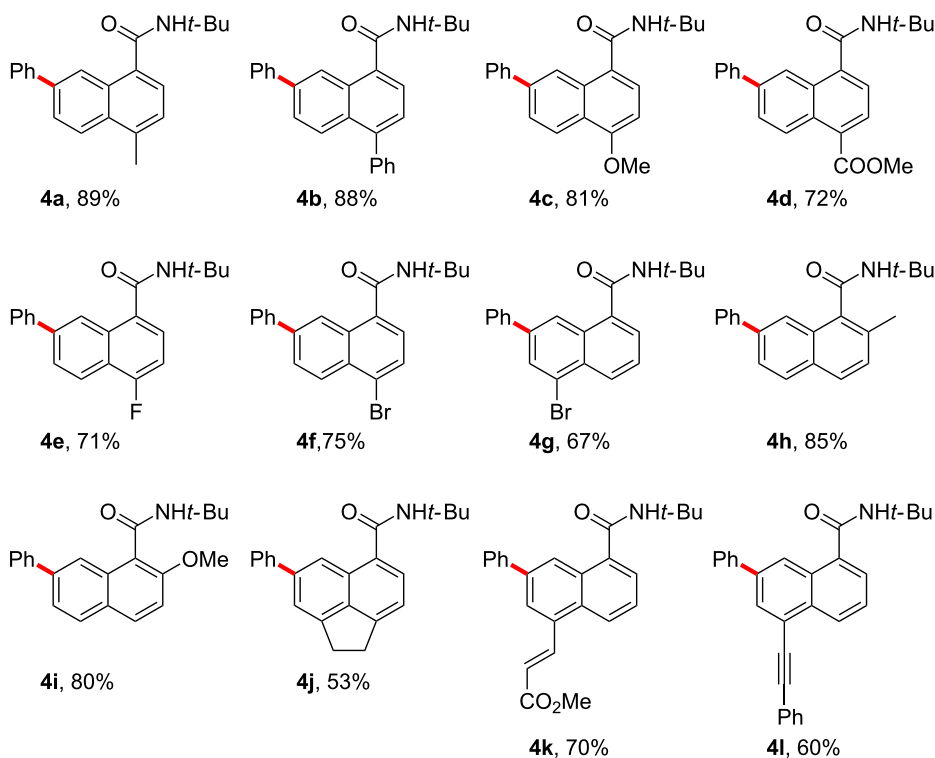
Scheme 2: Scope of aryliodonium salts. Reaction conditions: **1a** (0.2 mmol), **2** (0.3 mmol) in DCE (1 mL) at 70 °C under N_2 for 24 h. Isolated yield. ^a60 °C. ^b80 °C. ^c50 °C.

Cu(III) and aryl group added at the C8- and C7-positions of the naphthalene ring, respectively. Finally, the breakdown of the C8–Cu bond delivers Cu(I), meantime, the OTf anion takes away the proton from the C7-position, affording the desired product **3** or **4**.

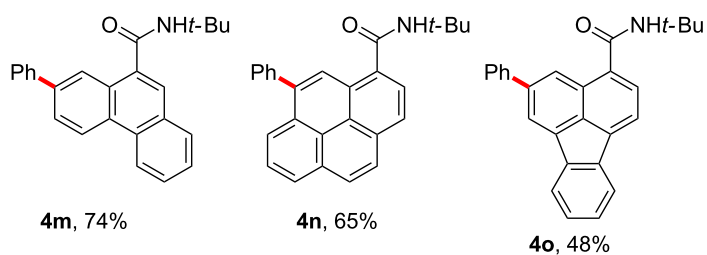
Subsequently, the photophysical properties of the arylation products **4k**, **4n** and **4o** were investigated (Figure 1). Their absorption bands cover from 300 nm to 400 nm, which corresponds to π – π^* electron transition (Figure 1a and Table S2, Supporting Information File 1). The measurement of emission



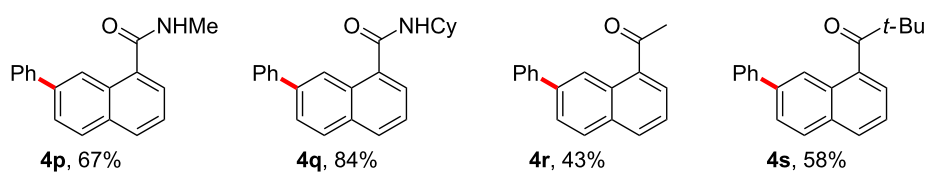
substituted naphthalenes



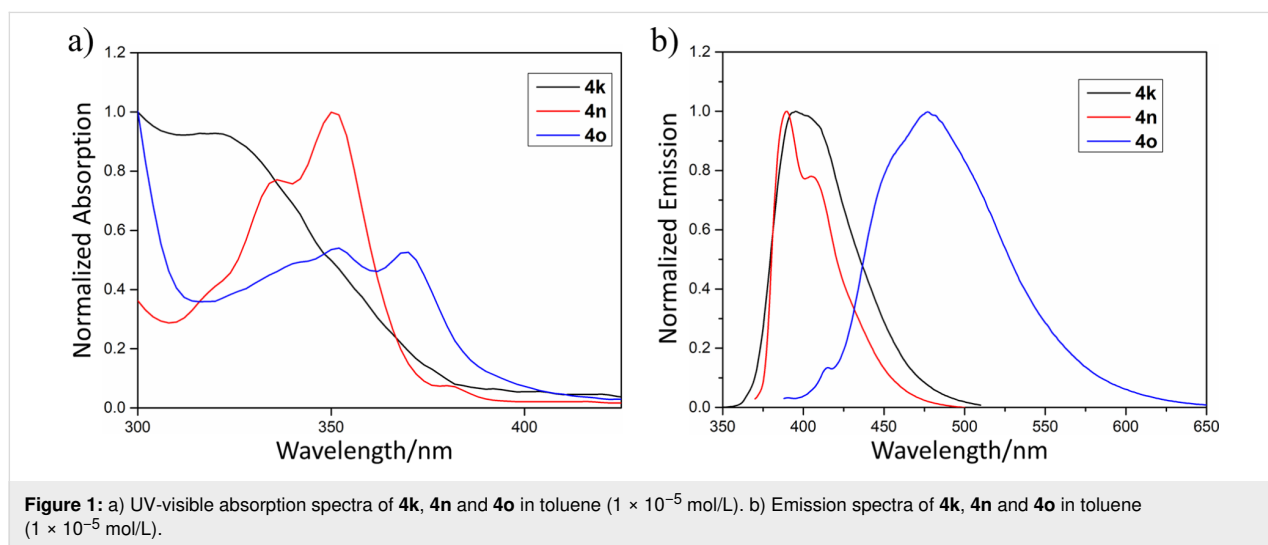
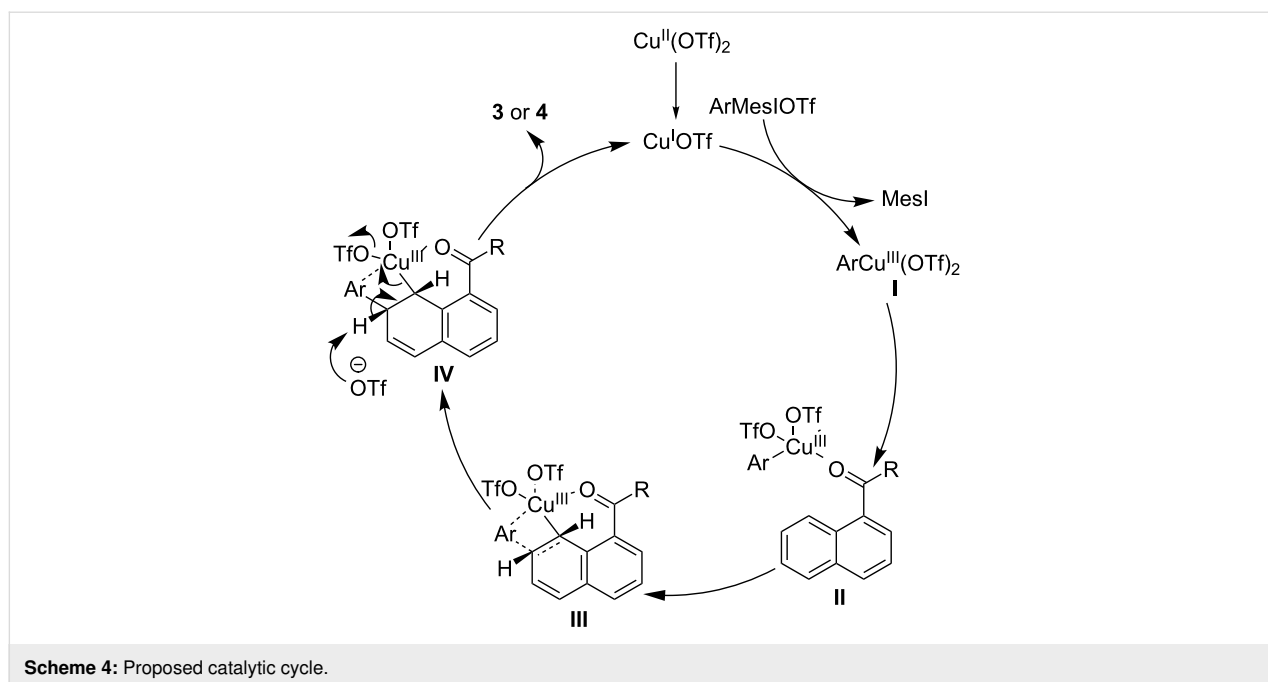
other PAH substrates



other directing groups



Scheme 3: Scope of PAHs. Reaction conditions: **1** (0.2 mmol), **2a** (0.3 mmol) in DCE (1 mL) at 70 °C under N_2 for 24 h. Isolated yield. DCE = 1,2-dichloroethane.



spectra demonstrates that **4k** and **4n** emit violet fluorescence with emission maxima at 395 nm and 390 nm, respectively, while **4o** exhibits a sky-blue emission with an emission maximum at 477 nm (Figure 1b and Table S2, Supporting Information File 1).

Conclusion

In summary, we have developed a highly efficient strategy to accomplish the direct C7–H arylation of 1-naphthamides by the usage of Cu(II) as a catalyst and arylidonium salts as arylating reagents, which features mild reaction conditions, excellent functional group tolerance, and moreover, does not need to use precious metal catalysts. This protocol is also compatible with

other PAH substrates including phenanthrene-9-carboxamide, pyrene-1-carboxamide and fluoranthene-3-carboxamide, which provide an opportunity for the development of diverse organic photoelectrical materials.

Supporting Information

Supporting Information File 1

Detailed experimental procedures, characterization data and copies of ^1H and ^{13}C NMR spectra of products.

[<https://www.beilstein-journals.org/bjoc/content/supplementary/1860-5397-16-49-S1.pdf>]

Acknowledgements

We thank the Comprehensive Training Platform Specialized Laboratory, College of Chemistry, Sichuan University.

Funding

We thank the National Natural Science Foundation of China (Nos. 21871193, 21772133, and 21672154) for financial support.

ORCID® iDs

Jingbo Lan - <https://orcid.org/0000-0001-5937-0987>

Jingsong You - <https://orcid.org/0000-0002-0493-2388>

Preprint

A non-peer-reviewed version of this article has been previously published as a preprint doi:10.3762/bxiv.2020.11.v1

References

- Wang, C.; Dong, H.; Hu, W.; Liu, Y.; Zhu, D. *Chem. Rev.* **2012**, *112*, 2208–2267. doi:10.1021/cr100380z
- Sun, Z.; Ye, Q.; Chi, C.; Wu, J. *Chem. Soc. Rev.* **2012**, *41*, 7857–7889. doi:10.1039/c2cs35211g
- Figueira-Duarte, T. M.; Müllen, K. *Chem. Rev.* **2011**, *111*, 7260–7314. doi:10.1021/cr100428a
- Wu, J.; Pisula, W.; Müllen, K. *Chem. Rev.* **2007**, *107*, 718–747. doi:10.1021/cr068010r
- Anthony, J. E. *Chem. Rev.* **2006**, *106*, 5028–5048. doi:10.1021/cr050966z
- Jiang, W.; Li, Y.; Wang, Z. *Chem. Soc. Rev.* **2013**, *42*, 6113–6127. doi:10.1039/c3cs60108k
- Stille, J. K. *Angew. Chem., Int. Ed. Engl.* **1986**, *25*, 508–524. doi:10.1002/anie.198605081
- Miyaura, N.; Suzuki, A. *Chem. Rev.* **1995**, *95*, 2457–2483. doi:10.1021/cr00039a007
- Li, Y.; Gao, J.; Di Motta, S.; Negri, F.; Wang, Z. *J. Am. Chem. Soc.* **2010**, *132*, 4208–4213. doi:10.1021/ja100276x
- Zeng, W.; Gopalakrishna, T. Y.; Phan, H.; Tanaka, T.; Herng, T. S.; Ding, J.; Osuka, A.; Wu, J. *J. Am. Chem. Soc.* **2018**, *140*, 14054–14058. doi:10.1021/jacs.8b09075
- Hindenberg, P.; Busch, M.; Paul, A.; Bernhardt, M.; Gemessy, P.; Rominger, F.; Romero-Nieto, C. *Angew. Chem., Int. Ed.* **2018**, *57*, 15157–15161. doi:10.1002/anie.201809754
- Dewar, M. J. S.; Grisdale, P. J. *J. Am. Chem. Soc.* **1962**, *84*, 3541–3546. doi:10.1021/ja00877a024
- Yang, Y.; Lan, J.; You, J. *Chem. Rev.* **2017**, *117*, 8787–8863. doi:10.1021/acs.chemrev.6b00567
- Alberico, D.; Scott, M. E.; Lautens, M. *Chem. Rev.* **2007**, *107*, 174–238. doi:10.1021/cr0509760
- McGlacken, G. P.; Bateman, L. M. *Chem. Soc. Rev.* **2009**, *38*, 2447–2464. doi:10.1039/b805701j
- Ackermann, L.; Vicente, R.; Kapdi, A. R. *Angew. Chem., Int. Ed.* **2009**, *48*, 9792–9826. doi:10.1002/anie.200902996
- Daugulis, O.; Do, H.-Q.; Shabashov, D. *Acc. Chem. Res.* **2009**, *42*, 1074–1086. doi:10.1021/ar9000058
- Daugulis, O.; Zaitsev, V. G. *Angew. Chem., Int. Ed.* **2005**, *44*, 4046–4048. doi:10.1002/anie.200500589
- Biafora, A.; Krause, T.; Hackenberger, D.; Belitz, F.; Gooßen, L. J. *Angew. Chem., Int. Ed.* **2016**, *55*, 14752–14755. doi:10.1002/anie.201607270
- Shi, Y.; Zhang, L.; Lan, J.; Zhang, M.; Zhou, F.; Wei, W.; You, J. *Angew. Chem., Int. Ed.* **2018**, *57*, 9108–9112. doi:10.1002/anie.201804528
- Tan, G.; You, Q.; Lan, J.; You, J. *Angew. Chem., Int. Ed.* **2018**, *57*, 6309–6313. doi:10.1002/anie.201802539
- Huang, L.; Weix, D. J. *Org. Lett.* **2016**, *18*, 5432–5435. doi:10.1021/acs.orglett.6b02862
- Yang, S.; Cheng, R.; Zhang, M.; Bin, Z.; You, J. *ACS Catal.* **2019**, *9*, 6188–6193. doi:10.1021/acscatal.9b01426
- Moon, S.; Nishii, Y.; Miura, M. *Org. Lett.* **2019**, *21*, 233–236. doi:10.1021/acs.orglett.8b03675
- Li, S.; Deng, G.-J.; Yin, F.; Li, C.-J.; Gong, H. *Org. Chem. Front.* **2017**, *4*, 417–420. doi:10.1039/c6qo00663a
- Zhang, M.; Luo, A.; Shi, Y.; Su, R.; Yang, Y.; You, J. *ACS Catal.* **2019**, *9*, 11802–11807. doi:10.1021/acscatal.9b04352
- Zhao, D.; Wang, W.; Yang, F.; Lan, J.; Yang, L.; Gao, G.; You, J. *Angew. Chem., Int. Ed.* **2009**, *48*, 3296–3300. doi:10.1002/anie.200900413
- Wu, J.; Cheng, Y.; Lan, J.; Wu, D.; Qian, S.; Yan, L.; He, Z.; Li, X.; Wang, K.; Zou, B.; You, J. *J. Am. Chem. Soc.* **2016**, *138*, 12803–12812. doi:10.1021/jacs.6b03890
- Zhang, L.; Wang, Y.; Shi, Y.; Wu, Y.; Lan, J.; Ma, W.; You, J. *ACS Catal.* **2019**, *9*, 5358–5364. doi:10.1021/acscatal.9b00925
- Phipps, R. J.; Gaunt, M. J. *Science* **2009**, *323*, 1593–1597. doi:10.1126/science.1169975
- Chen, B.; Hou, X.-L.; Li, Y.-X.; Wu, Y.-D. *J. Am. Chem. Soc.* **2011**, *133*, 7668–7671. doi:10.1021/ja201425e
- Yang, Y.; Li, R.; Zhao, Y.; Zhao, D.; Shi, Z. *J. Am. Chem. Soc.* **2016**, *138*, 8734–8737. doi:10.1021/jacs.6b05777

License and Terms

This is an Open Access article under the terms of the Creative Commons Attribution License (<http://creativecommons.org/licenses/by/4.0>). Please note that the reuse, redistribution and reproduction in particular requires that the authors and source are credited.

The license is subject to the *Beilstein Journal of Organic Chemistry* terms and conditions: (<https://www.beilstein-journals.org/bjoc>)

The definitive version of this article is the electronic one which can be found at: [doi:10.3762/bjoc.16.49](https://doi.org/10.3762/bjoc.16.49)



Efficient synthesis of 3,6,13,16-tetrasubstituted-tetrabenzo[*a,d,j,m*]coronenes by selective C–H/C–O arylations of anthraquinone derivatives

Seiya Terai, Yuki Sato, Takuya Kochi and Fumitoshi Kakiuchi*

Full Research Paper

Open Access

Address:

Department of Chemistry, Faculty of Science and Technology, Keio University, 3-14-1 Hiyoshi, Kohoku-ku, Yokohama, Kanagawa 223-8522, Japan

Email:

Fumitoshi Kakiuchi* - kakiuchi@chem.keio.ac.jp

* Corresponding author

Keywords:

C–H arylation; C–O arylation; oxidative cyclization; polycyclic aromatic hydrocarbons; ruthenium catalyst

Beilstein J. Org. Chem. **2020**, *16*, 544–550.

doi:10.3762/bjoc.16.51

Received: 31 January 2020

Accepted: 16 March 2020

Published: 31 March 2020

This article is part of the thematic issue "C–H functionalization for materials science".

Guest Editor: K. Itami

© 2020 Terai et al.; licensee Beilstein-Institut.

License and terms: see end of document.

Abstract

An efficient synthesis of tetrabenzo[*a,d,j,m*]coronene derivatives having alkyl and alkoxy substituents at the 3, 6, 13, and 16-positions was achieved based on the ruthenium-catalyzed coupling reactions of anthraquinone derivatives with arylboronates via C–H and C–O bond cleavage. The reaction sequence involving the arylation, carbonyl methylenation, and oxidative cyclization effectively provided various tetrabenzo[*a,d,j,m*]coronenes in short steps from readily available starting materials. Tetrabenzo[*a,d,j,m*]coronenes possessing two different types of substituents were obtained selectively by sequential chemoselective C–O arylation and C–H arylation. The ¹H NMR spectra of the tetrabenzo[*a,d,j,m*]coronene product indicated its self-assembling behavior in CDCl₃.

Introduction

Polycyclic aromatic hydrocarbons (PAHs) and their derivatives have attracted much attention from researchers due to their high potential as organic optoelectronic materials [1–3] and great efforts have been devoted to the development of their efficient synthetic methods [4]. One of the important steps in most of the PAH syntheses is the construction of carbon–carbon bonds between aryl groups to form biaryl frameworks. Traditionally, transition-metal-catalyzed cross-coupling reactions of aryl halides or pseudohalides with arylmetal reagents have been employed for the connection of two aryl units [5–9].

However, in search of more efficient synthetic routes, C–H arylation reactions have been increasingly utilized in recent years for the rapid expansion of the aromatic frameworks [10–15].

We have been working on the efficient syntheses of PAH derivatives based on the ruthenium-catalyzed C–H/C–O arylation reactions developed in our group [16–33]. In the presence of ruthenium carbonyl phosphine complexes, the reaction of aromatic ketones possessing C–H bonds or C–OR (R = alkyl) bonds

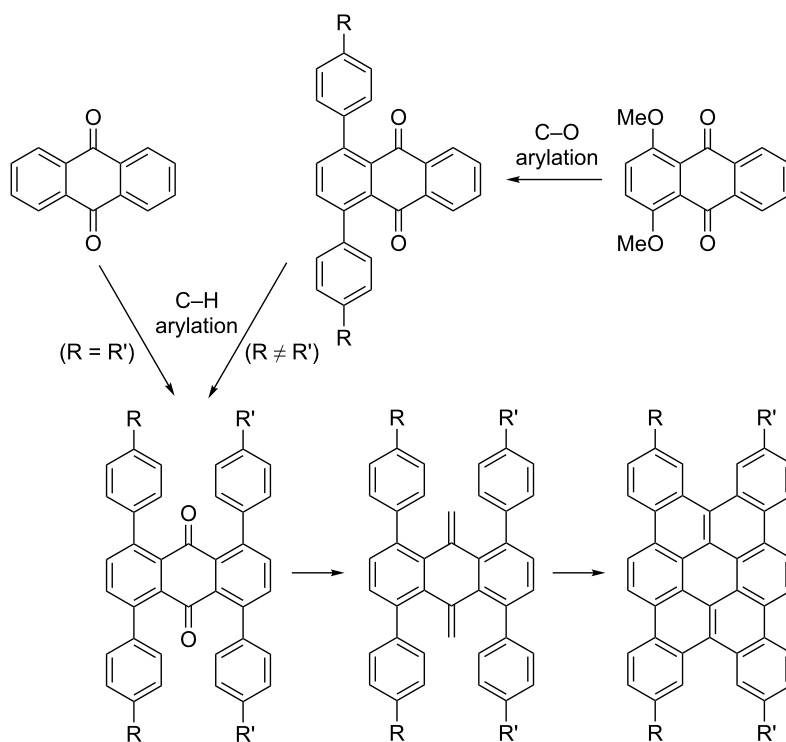
with arylboronates provided C–H or C–O arylation products [21–33]. Anthraquinone was chosen as a convenient template for the PAH syntheses, because various anthraquinone derivatives possessing zero to four oxygen substituents at the *ortho*-positions are readily available and the regioselective arylation at the positions of either C–H or C–O bonds provided a variety of multiarylated anthraquinone derivatives [16–20]. Using this method, we have synthesized various π -extended aromatic compounds such as multiarylated acenes [16,18,20], dibenzo[*h,rst*]pentaphenes and dibenzo[*fg,qr*]pentacenes [19].

In the course of our reaction development, it was found that an introduction of two different aryl groups at the *ortho*-positions can be achieved by chemoselective C–O arylation of aromatic ketones possessing both C–H and C–O bonds and subsequent C–H arylation. We envisioned that the application of this strategy to the anthraquinone template would provide its derivatives possessing two different types of aryl groups in a designed manner and lead to the preparation of tetrabenzo[*a,d,j,m*]coronenes having two different types of substituents (Scheme 1). While 1,4,5,8-tetraarylanthraquinones prepared by the ruthenium-catalyzed C–H arylation of anthraquinone with a *para*-substituted arylboronate may be converted to 3,6,13,16-tetrasubstituted tetrabenzo[*a,d,j,m*]coronenes via carbonyl methylenation and oxidative cyclization, the two-step sequential C–O and C–H arylation of 1,4-

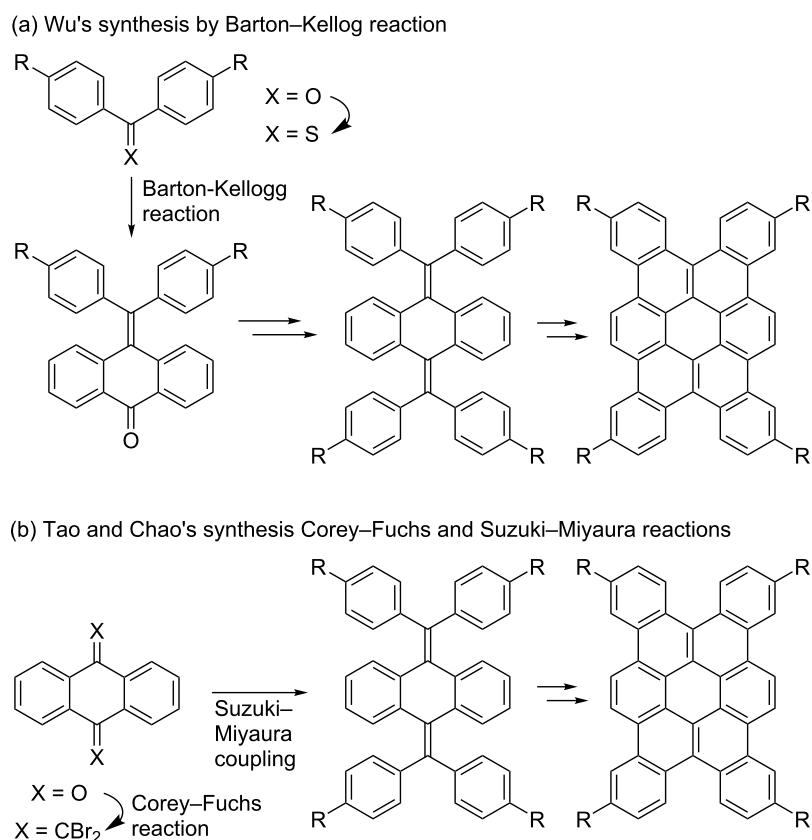
dimethoxyanthraquinone followed by subsequent methylenation/cyclization would provide tetrabenzo[*a,d,j,m*]coronenes having two different types of substituents.

Coronene derivatives such as hexabenzocoronenes and ovalenes have been extensively studied because of their optoelectronic and self-assembling properties [34–44]. Various synthetic methods have been developed for coronene derivatives in general [34–37], however, only a few strategies have been reported for the syntheses of tetrabenzo[*a,d,j,m*]coronenes [43,44]. Wu and co-workers reported the synthesis of 2,7,12,17-tetrasubstituted tetrabenzo[*a,d,j,m*]coronenes by using the Barton–Kellogg reaction, followed by dehydrogenative photocyclization, and FeCl₃-mediated oxidative cyclization (Scheme 2a) [43]. Tao, Chao, and co-workers succeeded in the preparation of similar tetrasubstituted tetrabenzocoronenes by a Corey–Fuchs reaction, followed by a Suzuki–Miyaura cross-coupling, and a two-step dehydrogenative cyclization using DDQ and FeCl₃ (Scheme 2b) [44]. However, 3,6,13,16-tetrasubstituted tetrabenzo[*a,d,j,m*]coronenes have not been reported using these reported methods.

Here, we describe a convenient method for the synthesis of 3,6,13,16-tetrasubstituted tetrabenzo[*a,d,j,m*]coronenes based on a ruthenium-catalyzed C–O/C–H multiarylation of anthraquinone and its derivatives.



Scheme 1: Projected synthetic routes for 3,6,13,16-tetrasubstituted tetrabenzo[*a,d,j,m*]coronenes.

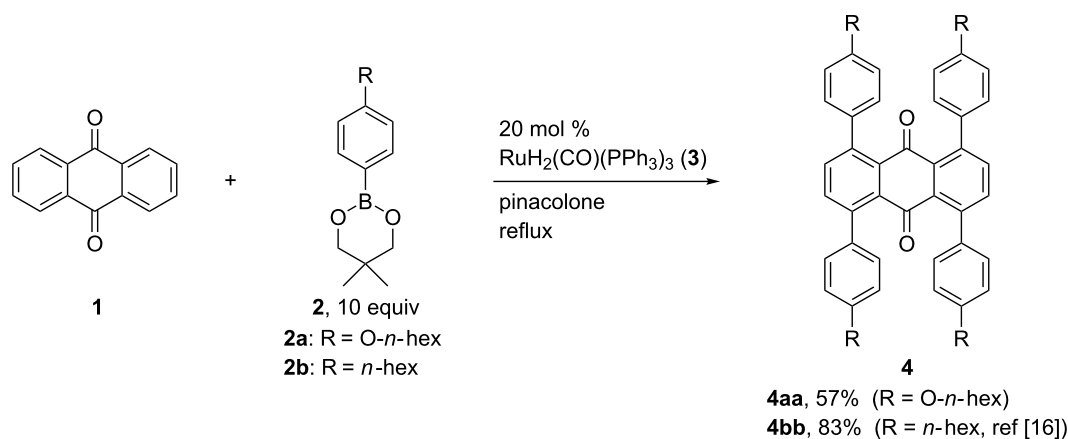


Scheme 2: Reported syntheses of 2,7,12,17-tetrasubstituted tetrabenzo[*a,d,j,m*]coronenes.

Results and Discussion

Our efforts toward the synthesis of tetrabenzo[*a,d,j,m*]coronenes started with the preparation of tetraarylanthraquinones. Previously, we reported the synthesis of anthraquinone derivatives possessing four aryl groups at the 1, 4, 5, and 8-positions through a $\text{RuH}_2(\text{CO})(\text{PPh}_3)_3$ -catalyzed C–H arylation of anthraquinone (**1**) with arylboronates **2** [16]. Using this method,

we examined the synthesis of a tetraarylanthraquinone possessing four hexyloxy groups. When the reaction of **1** with 4-hexyloxyphenylboronate **2a** was carried out in the presence of 20 mol % of $\text{RuH}_2(\text{CO})(\text{PPh}_3)_3$ (**3**) in refluxing pinacolone, the corresponding tetraarylation product **4aa** was obtained in 57% yield (Scheme 3). Tetrakis(4-hexylphenyl)anthraquinone (**4bb**), the synthesis of which has been described in the above-



Scheme 3: C–H tetraarylation of anthraquinone (**1**).

mentioned publication [16], was also prepared using 4-hexylphenylboronate (**2b**) accordingly and used for further transformations. The reaction of **1** with **2b** was also attempted using 10 mol % of **3**, however, it only gave mono-, di- and triarylation products, and the tetraarylation product **4bb** was not detected.

Tetraarylanthraquinones containing two different aryl groups were also prepared via the above-mentioned chemoselective C–O arylation and subsequent C–H arylation. The chemoselective C–O diarylation of 1,4-dimethoxyanthraquinone to form 1,4-diarylanthraquinones has been previously reported by our group [19], and 1,4-bis(4-hexyloxyphenyl)anthraquinone (**5a**) and 1,4-bis(4-hexylphenyl)anthraquinone (**5b**) were prepared accordingly. When the reaction of **5a** with 4-methylphenylboronate **2c** was conducted in the presence of 40 mol % of **3** in refluxing pinacolone, the *ortho*-C–H diarylation occurred giving the 1,4-bis(4-hexyloxyphenyl)-5,8-bis(4-methylphenyl)anthraquinone (**4ac**) in 91% yield. The C–H diarylation of **5b** with **2a** also proceeded smoothly to provide the corresponding tetraarylanthraquinone **4ba** in 94% yield (Scheme 4).

Next, the conversion of tetraarylanthraquinones **4** to tetrabenzo[*a,d,j,m*]coronenes was investigated. After examining various carbonyl methylenation methods, we found that the dimethylenation products **6** can be obtained in high yields through methylation of the carbonyl groups, followed by dehy-

dration. Thus, the reaction of **4aa** with methyllithium and subsequent treatment of the crude diol with NaH₂PO₂·H₂O and NaI in refluxing acetic acid gave the corresponding dimethylenation product **6aa** in 96% yield (Table 1, entry 1). The oxidative cyclization of **6aa** by treatment with 12 equiv of FeCl₃ at 35 °C for 0.5 h provided the desired tetrabenzo[*a,d,j,m*]corronene derivative **7aa** in 37% yield. This method was also applicable to the conversion of tetrakis(4-hexylphenyl)anthraquinone **4bb** as well as the tetraarylanthraquinones containing two different aryl groups, **4ac** and **4ba**, leading to the corresponding tetrabenzo[*a,d,j,m*]corronene derivatives, **7bb**, **7ac**, and **7ba**, respectively (Table 1, entries 2–4).

Next, the effect of the substituents in compounds **7** on their optical properties was studied by UV–vis spectroscopy (Figure 1). The UV–vis spectra of **7aa**, **7bb**, and **7ba** were measured in chloroform, and the normalized UV–vis spectra are shown in Figure 1. These compounds showed similar peak patterns between 300 and 500 nm, and the π – π^* transitions (p-band) for **7aa**, **7bb**, and **7ba** were observed at 426 nm [11]. The peaks corresponding to n – π^* transitions (α -band) were observed at 456–469 nm and were red-shifted with growing intensity as the number of hexyloxy groups increases.

The self-assembling property of tetrabenzo[*a,d,j,m*]coronene **7aa** was also examined (Figure 2), as Wu and co-workers have studied the self-assembling property of the tetra-

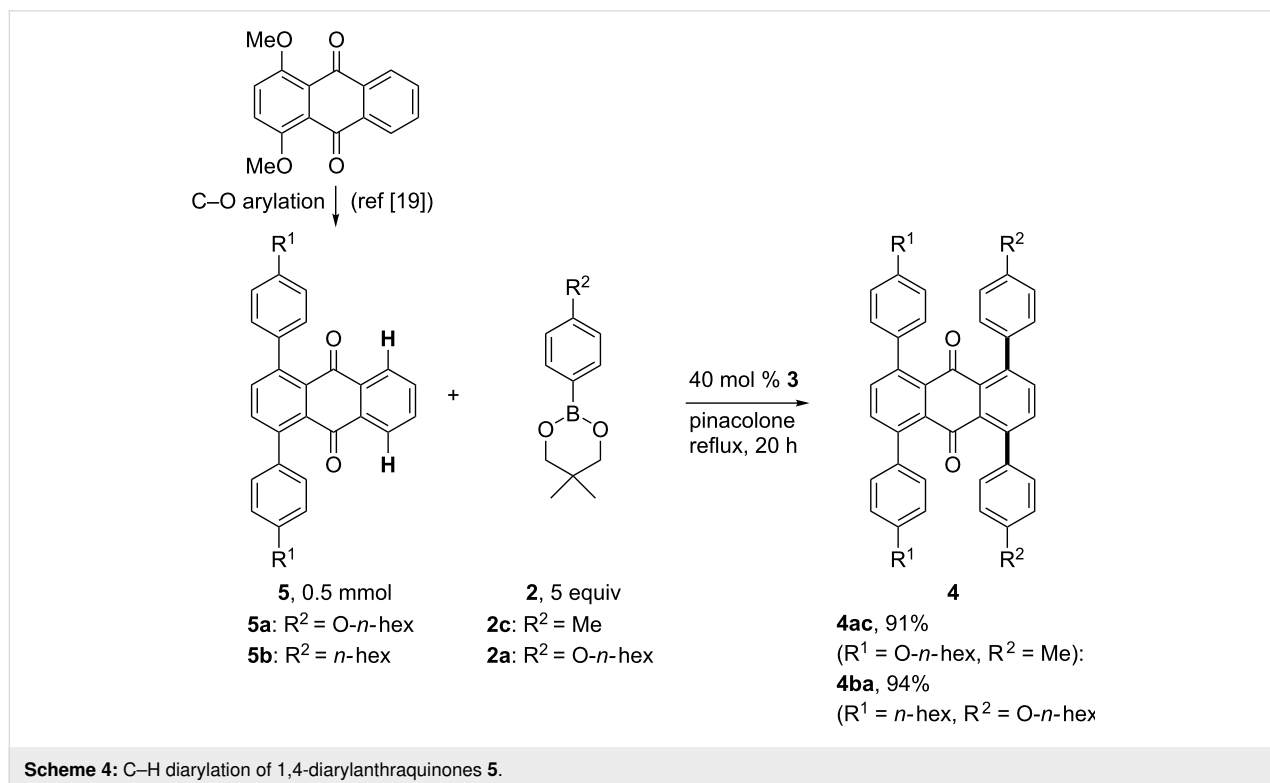
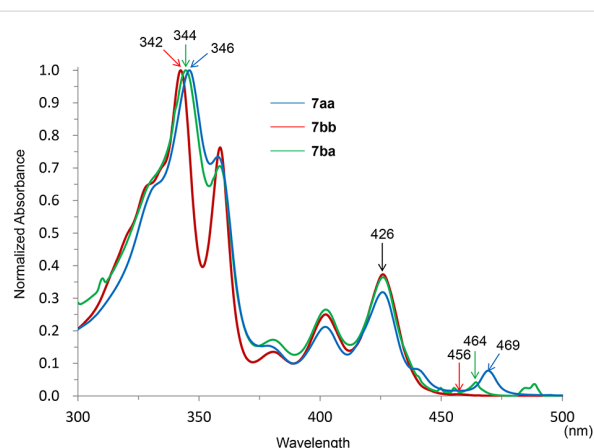


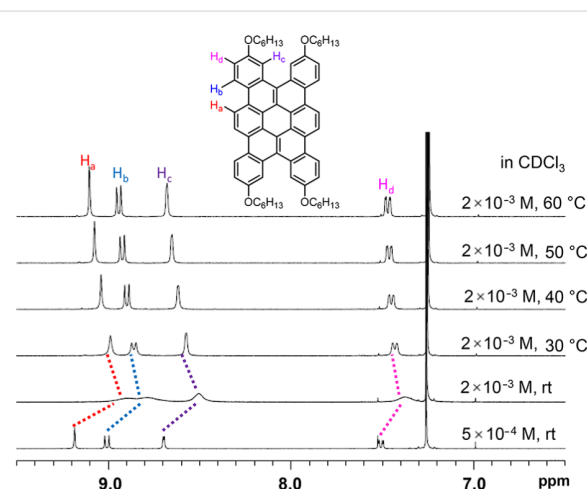
Table 1: Synthesis of 3,6,13,16-tetrasubstituted tetrabenzo[*a,d,j,m*]coronenes.

entry	R ¹	R ²	yield of 6 (%) ^a	yield of 7 (%) ^b
1	<i>n</i> -hexO	<i>n</i> -hexO	6aa : 96	7aa : 37
2	<i>n</i> -hex	<i>n</i> -hex	6bb : 85	7bb : 73
3	<i>n</i> -hexO	Me	6ac : 78	7ac : 48
4	<i>n</i> -hex	<i>n</i> -hexO	6ba : 85	7ba : 48

^aReaction conditions: 1) **4** (0.2 mmol), MeLi (2 mmol), THF (10 mL), –78 °C to rt, 2 h; 2) NaH₂PO₂·H₂O (2 mmol), NaI (2 mmol), AcOH (6 mL), reflux, 2 h; ^breaction conditions: **6** (0.02 mmol), FeCl₃ (0.24 mmol), MeNO₂ (1 mL), CH₂Cl₂ (5 mL), gentle N₂ bubbling, 35 °C, 0.5 h.

**Figure 1:** Normalized UV-vis absorption spectra of **7aa**, **7bb**, and **7ba**.

benzo[*a,d,j,m*]coronene derivative possessing *n*-octyl groups at the 2, 7, 12, and 17-positions by ¹H NMR spectroscopy and suggested its intermolecular π – π interaction in solution [10]. When the ¹H NMR spectrum of **7aa** was measured at 2×10^{-3} M at rt, a considerable broadening of the signals in the aromatic region was observed. By increasing the temperature from rt to 60 °C, all signals in the aromatic region became sharper and low-field shifted. The dilution of the solution to 5×10^{-4} M at rt also led to a downfield shift and sharpening of the signals. These observations suggest that **7aa** assembles by intermolecular π – π interaction in CDCl₃ as was seen by Wu and co-workers for their compound possessing substituents at different positions.

**Figure 2:** Effects of the concentration and the temperature on the ¹H NMR spectra of **7aa**.

Conclusion

The synthesis of a new class of tetrabenzo[*a,d,j,m*]coronene derivatives having alkyl and alkoxy-substituents at the 3, 6, 13, and 16-positions was achieved based on a ruthenium-catalyzed coupling reaction of anthraquinone derivatives with aryl-boronates via a C–H or/and C–O bond cleavage. The reaction sequence involving the arylation, carbonyl methylenation, and oxidative cyclization effectively provided various 3,6,13,16-tetrasubstituted tetrabenzo[*a,d,j,m*]coronenes in short steps from readily available starting materials. The tetrabenzo[*a,d,j,m*]coronenes possessing two different types of sub-

stituents were obtained selectively by sequential chemoselective C–O and C–H arylations. The strategy developed in this study should be useful for the synthesis of PAH derivatives with multiple substituents having different properties.

Supporting Information

Supporting Information File 1

General experimental procedures, characterization data and NMR spectra of new compounds.

[<https://www.beilstein-journals.org/bjoc/content/supplementary/1860-5397-16-51-S1.pdf>]

Funding

This work was supported, in part, by a Grant-in-Aid for Scientific Research on Innovative Areas 2707 “Middle molecule strategy” from the Ministry of Education, Culture, Sports, Science and Technology, Japan and by the Research Program of “Five-star Alliance” in “NJRC Mater. & Dev.”. T.K. is grateful for financial support provided by JSPS KAKENHI Grant Number JP18H04271 (Precisely Designed Catalysts with Customized Scaffolding).

ORCID® IDs

Fumitoshi Kakiuchi - <https://orcid.org/0000-0003-2605-4675>

References

- Grimsdale, A. C.; Leok Chan, K.; Martin, R. E.; Jokisz, P. G.; Holmes, A. B. *Chem. Rev.* **2009**, *109*, 897–1091. doi:10.1021/cr000013v
- Feng, F.; Liu, L.; Wang, S. *Nat. Protoc.* **2010**, *5*, 1255–1264. doi:10.1038/nprot.2010.79
- Wang, C.; Dong, H.; Hu, W.; Liu, Y.; Zhu, D. *Chem. Rev.* **2012**, *112*, 2208–2267. doi:10.1021/cr100380z
- Narita, A.; Wang, X.-Y.; Feng, X.; Müllen, K. *Chem. Soc. Rev.* **2015**, *44*, 6616–6643. doi:10.1039/c5cs00183h
- Miyaura, N., Ed. *Cross-Coupling Reactions: A Practical Guide*; Top. Curr. Chem., Vol. 2019; 2002. doi:10.1007/3-540-45313-x
- Martin, R.; Buchwald, S. L. *Acc. Chem. Res.* **2008**, *41*, 1461–1473. doi:10.1021/ar800036s
- Nishihara, Y., Ed. *Applied Cross-Coupling Reactions*; Springer: Heidelberg, Germany, 2013. doi:10.1007/978-3-642-32368-3
- de Meijere, A.; Bräse, S.; Oestreich, M., Eds. *Metal-Catalyzed Cross-Coupling Reactions and More*; Wiley-VCH: Weinheim, Germany, 2014. doi:10.1002/9783527655588
- Tobisu, M.; Chatani, N. *Acc. Chem. Res.* **2015**, *48*, 1717–1726. doi:10.1021/acs.accounts.5b00051
- Hussain, I.; Singh, T. *Adv. Synth. Catal.* **2014**, *356*, 1661–1696. doi:10.1002/adsc.201400178
- Kuninobu, Y.; Sueki, S. *Synthesis* **2015**, *47*, 3823–3845. doi:10.1055/s-0035-1560346
- Segawa, Y.; Maekawa, T.; Itami, K. *Angew. Chem., Int. Ed.* **2015**, *54*, 66–81. doi:10.1002/anie.201403729
- Sharma, U.; Modak, A.; Maity, S.; Maji, A.; Maiti, D. Direct arylation via C–H activation. In *New Trends in Cross-Coupling: Theory and Applications*; Colacot, T. J., Ed.; RSC Publishing: Cambridge, UK, 2015; pp 551–609. doi:10.1039/9781782620259-00551
- Zha, G.-F.; Qin, H.-L.; Kantchev, E. A. B. *RSC Adv.* **2016**, *6*, 30875–30885. doi:10.1039/c6ra02742c
- Hagui, W.; Doucet, H.; Soulé, J.-F. *Chem* **2019**, *5*, 2006–2078. doi:10.1016/j.chempr.2019.06.005
- Kitazawa, K.; Kochi, T.; Sato, M.; Kakiuchi, F. *Org. Lett.* **2009**, *11*, 1951–1954. doi:10.1021/ol900393x
- Kitazawa, K.; Kochi, T.; Nitani, M.; Ie, Y.; Aso, Y.; Kakiuchi, F. *Chem. Lett.* **2011**, *40*, 300–302. doi:10.1246/cl.2011.300
- Matsumura, D.; Kitazawa, K.; Terai, S.; Kochi, T.; Ie, Y.; Nitani, M.; Aso, Y.; Kakiuchi, F. *Org. Lett.* **2012**, *14*, 3882–3885. doi:10.1021/ol301608m
- Suzuki, Y.; Yamada, K.; Watanabe, K.; Kochi, T.; Ie, Y.; Aso, Y.; Kakiuchi, F. *Org. Lett.* **2017**, *19*, 3791–3794. doi:10.1021/acs.orglett.7b01666
- Izumoto, A.; Kondo, H.; Kochi, T.; Kakiuchi, F. *Synlett* **2017**, *28*, 2609–2613. doi:10.1055/s-0036-1590937
- Kakiuchi, F.; Kan, S.; Igi, K.; Chatani, N.; Murai, S. *J. Am. Chem. Soc.* **2003**, *125*, 1698–1699. doi:10.1021/ja029273f
- Kakiuchi, F.; Matsuura, Y.; Kan, S.; Chatani, N. *J. Am. Chem. Soc.* **2005**, *127*, 5936–5945. doi:10.1021/ja043334n
- Kitazawa, K.; Kotani, M.; Kochi, T.; Langeloth, M.; Kakiuchi, F. *J. Organomet. Chem.* **2010**, *695*, 1163–1167. doi:10.1016/j.jorganchem.2010.01.022
- Hiroshima, S.; Matsumura, D.; Kochi, T.; Kakiuchi, F. *Org. Lett.* **2010**, *12*, 5318–5321. doi:10.1021/ol102325f
- Ogiwara, Y.; Miyake, M.; Kochi, T.; Kakiuchi, F. *Organometallics* **2017**, *36*, 159–164. doi:10.1021/acs.organomet.6b00540
- Koseki, Y.; Kitazawa, K.; Miyake, M.; Kochi, T.; Kakiuchi, F. *J. Org. Chem.* **2017**, *82*, 6503–6510. doi:10.1021/acs.joc.6b02623
- Suzuki, I.; Kondo, H.; Kochi, T.; Kakiuchi, F. *J. Org. Chem.* **2019**, *84*, 12975–12982. doi:10.1021/acs.joc.9b01756
- Kakiuchi, F.; Usui, M.; Ueno, S.; Chatani, N.; Murai, S. *J. Am. Chem. Soc.* **2004**, *126*, 2706–2707. doi:10.1021/ja0393170
- Ueno, S.; Mizushima, E.; Chatani, N.; Kakiuchi, F. *J. Am. Chem. Soc.* **2006**, *128*, 16516–16517. doi:10.1021/ja067612p
- Ogiwara, Y.; Kochi, T.; Kakiuchi, F. *Org. Lett.* **2011**, *13*, 3254–3257. doi:10.1021/ol2012007
- Kondo, H.; Akiba, N.; Kochi, T.; Kakiuchi, F. *Angew. Chem., Int. Ed.* **2015**, *54*, 9293–9297. doi:10.1002/anie.201503641
- Kondo, H.; Kochi, T.; Kakiuchi, F. *Org. Lett.* **2017**, *19*, 794–797. doi:10.1021/acs.orglett.6b03761
- Kondo, H.; Kochi, T.; Kakiuchi, F. *Chem. – Eur. J.* **2020**, *26*, 1737–1741. doi:10.1002/chem.201905157
- Feng, X.; Pisula, W.; Müllen, K. *Pure Appl. Chem.* **2009**, *81*, 2203–2224. doi:10.1351/pac-con-09-07-07
- Hopf, H. *Chem. Rec.* **2014**, *14*, 979–1000. doi:10.1002/tcr.201402056
- Zhang, Q.; Peng, H.; Zhang, G.; Lu, Q.; Chang, J.; Dong, Y.; Shi, X.; Wei, J. *J. Am. Chem. Soc.* **2014**, *136*, 5057–5064. doi:10.1021/ja413018f
- Hirose, T.; Miyazaki, Y.; Watabe, M.; Akimoto, S.; Tachikawa, T.; Kodama, K.; Yasutake, M. *Tetrahedron* **2015**, *71*, 4714–4721. doi:10.1016/j.tet.2015.05.071
- Witte, G.; Wöll, C. *J. Mater. Res.* **2004**, *19*, 1889–1916. doi:10.1557/jmr.2004.0251
- Wu, J.; Pisula, W.; Müllen, K. *Chem. Rev.* **2007**, *107*, 718–747. doi:10.1021/cr068010r

40. Ren, S.; Yan, C.; Vak, D.; Jones, D. J.; Holmes, A. B.; Wong, W. W. H. *Adv. Funct. Mater.* **2012**, *22*, 2015–2026. doi:10.1002/adfm.201102141
41. Wong, W. W. H.; Subbiah, J.; Puniredd, S. R.; Purushothaman, B.; Pisula, W.; Kirby, N.; Müllen, K.; Jones, D. J.; Holmes, A. B. *J. Mater. Chem.* **2012**, *22*, 21131–21137. doi:10.1039/c2jm34394k
42. Dumszlaff, T.; Yang, B.; Maghsoumi, A.; Velpula, G.; Mali, K. S.; Castiglioni, C.; De Feyter, S.; Tommasini, M.; Narita, A.; Feng, X.; Müllen, K. *J. Am. Chem. Soc.* **2016**, *138*, 4726–4729. doi:10.1021/jacs.6b01976
43. Zhang, X.; Jiang, X.; Zhang, K.; Mao, L.; Luo, J.; Chi, C.; Chan, H. S. O.; Wu, J. *J. Org. Chem.* **2010**, *75*, 8069–8077. doi:10.1021/jo101701k
44. Pola, S.; Kuo, C.-H.; Peng, W.-T.; Islam, M. M.; Chao, I.; Tao, Y.-T. *Chem. Mater.* **2012**, *24*, 2566–2571. doi:10.1021/cm301190c

License and Terms

This is an Open Access article under the terms of the Creative Commons Attribution License (<http://creativecommons.org/licenses/by/4.0>). Please note that the reuse, redistribution and reproduction in particular requires that the authors and source are credited.

The license is subject to the *Beilstein Journal of Organic Chemistry* terms and conditions: (<https://www.beilstein-journals.org/bjoc>)

The definitive version of this article is the electronic one which can be found at:
[doi:10.3762/bjoc.16.51](https://doi.org/10.3762/bjoc.16.51)



Regioselectively α - and β -alkynylated BODIPY dyes via gold(I)-catalyzed direct C–H functionalization and their photophysical properties

Takahide Shimada¹, Shigeki Mori², Masatoshi Ishida^{*1} and Hiroyuki Furuta^{*1}

Full Research Paper

[Open Access](#)

Address:

¹Department of Chemistry and Biochemistry, Graduate School of Engineering, and Center for Molecular Systems, Kyushu University, Fukuoka 819-0395, Japan and ²Advanced Research Support Center (ADRES), Ehime University, Matsuyama 790-8577, Japan

Email:

Masatoshi Ishida^{*} - ishida.masatoshi.686@m.kyushu-u.ac.jp;
Hiroyuki Furuta^{*} - hfuruta@cstf.kyushu-u.ac.jp

^{*} Corresponding author

Keywords:

alkynylation; BODIPY; direct C–H functionalization; gold(I)

Beilstein J. Org. Chem. **2020**, *16*, 587–595.

doi:10.3762/bjoc.16.53

Received: 01 February 2020

Accepted: 17 March 2020

Published: 01 April 2020

This article is part of the thematic issue "C–H functionalization for materials science".

Guest Editor: K. Itami

© 2020 Shimada et al.; licensee Beilstein-Institut.

License and terms: see end of document.

Abstract

A series of α - and β -ethynyl-substituted BODIPY derivatives (**3a**, **4a**, **5a**, **5b**, **6a**, **6b**) were synthesized by gold(I)-catalyzed direct C–H alkynylation reactions of dipyrromethane and BODIPY, respectively, with ethynylbenziodoxolone (EBX) in a regioselective manner. Depending on the position of the ethynyl substituent in the BODIPY skeleton, the photophysical properties of the resulting α - and β -substituted BODIPYs are notably altered. The lowest S_0 – S_1 transition absorbance and fluorescence bands are both bathochromically shifted as the number of substituents increases, while the emission quantum yields of the β -ethynylated derivatives are significantly lower than those of α -ethynylated ones. The current method should be useful for fine-tuning of the photophysical properties of BODIPY dyes as well as for constructing BODIPY-based building cores for functional π -materials.

Introduction

Boron-dipyrromethene (BODIPY, **1**) and its derivatives are representative families of fluorophores that have been widely used in applications for bioimaging [1–6], photodynamic therapy [7–12], photocatalysis [13–16], optics [17–20], and so forth. The structure of BODIPY derivatives is composed of a dipyrromethene (an oxidized form of dipyrromethane **2**) and a coordinated difluoroboron moiety [21]. The rigid π -conjugated scaffold of BODIPYs demonstrates fascinating optical features such as intense and narrow S_0 – S_1 absorption and emission bands in

the visible-to-near-infrared region, a high fluorescence quantum yield, and good photostability. For the applications mentioned above, various BODIPY dyes functionalized at the *meso*-, α -, and β -pyrrolic positions have been extensively developed to tune the optoelectronic properties [21]. Therefore, the development of more efficient and shorter step synthetic methods for the BODIPY derivatives, such as direct C–H functionalizations (e.g., arylation [22–28], annulation [29], olefination [30], styrylation [31], and borylation [32]), has been in

great demand recently rather than the conventional multistep synthesis with nucleophilic substitution/cross-coupling via halogenation of BODIPYs [33] or from the activated precursors [34] via unstable pyrrolic intermediates. In particular, halogenation (e.g., bromination) of BODIPY derivatives often affords a mixture of multiply halogenated products, which is tedious to separate by column chromatography.

The introduction of one or more alkynyl groups into the BODIPY skeleton indeed produces useful building blocks for functional π -materials. For example, ethynyl-tethered BODIPY derivatives serve as a substrate in the copper-catalyzed azide–alkyne cycloaddition (CuAAC) reaction, which is known

as “click” reaction, allowing for a biological tissue labelling [35,36]. In addition, ethynyl-substituted BODIPYs yield unique π -conjugated BODIPY-based macrocycles by Glaser-coupling reactions [37]. Conventionally, an alkylation of the BODIPY core has been achieved by palladium-catalyzed Sonogashira cross-coupling with halogenated BODIPYs (Figure 1b) [35,37]. However, due to the coexistence of multiple C–H bonds, a regioselective direct C–H alkylation of the BODIPY core has not yet been achieved.

Inspired by the works of Waser and co-workers showing the gold(I)-catalyzed C–H electrophilic alkylation of various heterocycles (e.g., pyrroles, indoles, etc.) with ethynylbenz-

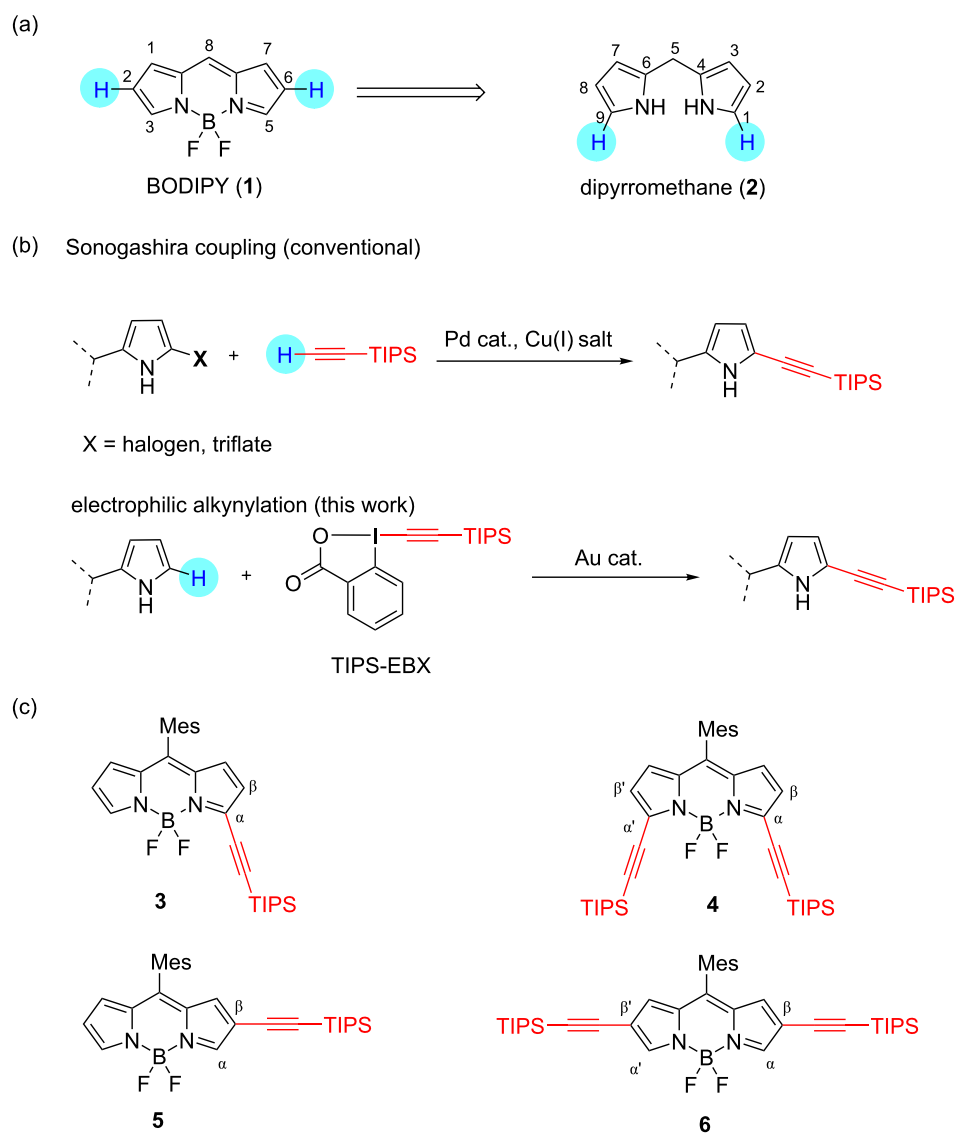


Figure 1: (a) Chemical structures of BODIPY (1) and dipyrromethane (2). (b) C–C bond forming alkynylations of pyrrole and its derivatives by Sonogashira coupling and electrophilic alkylation. (c) Peripheral alkynylated BODIPY derivatives (3–6) prepared in this work. TIPS: triisopropylsilyl group; Mes: 2,4,6-trimethylphenyl group.

iodoxolone (EBX) as an activated ethynyl synthon [38–42], we investigated the synthesis of ethynyl-substituted BODIPY derivatives **3–6** by gold(I)-catalyzed direct C–H functionalization (Figure 1c). By taking advantage of the reactivity of β -(2 and 6)-positions of BODIPY (**1**), which are susceptible to electrophilic reactions, β,β' -diethynyl-substituted BODIPYs **5** and **6** were prepared regioselectively, through the C–H alkylation of **1** without any directing groups. In addition, the corresponding dipyrromethane **2**, which is a precursor of BODIPY, was first transformed into the alkynylated form under catalytic conditions, and subsequent oxidation followed by boron complexation to afford α -monoethynyl and α,α' -diethynyl-substituted BODIPYs **3** and **4**, respectively. The resulting ethynylated BODIPY isomers demonstrated site-dependent photophysical properties.

Results and Discussion

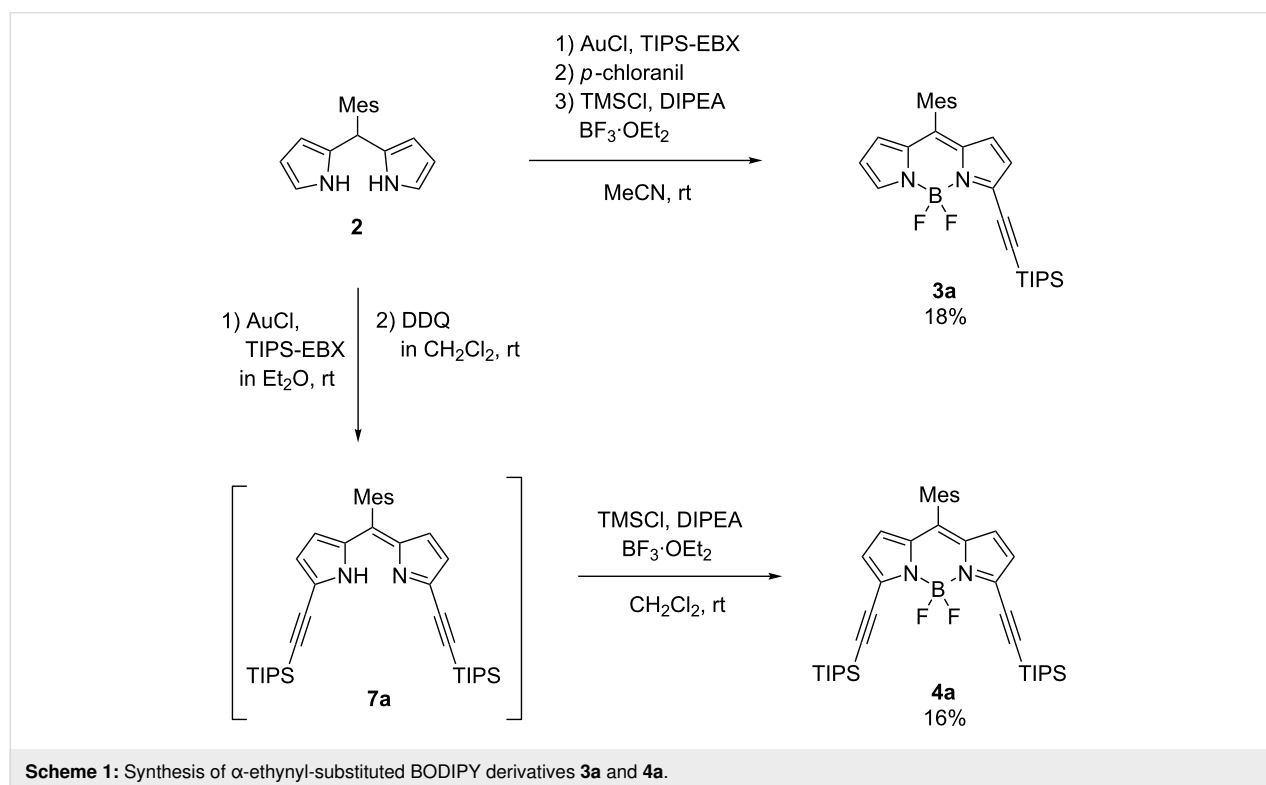
Synthesis and characterization

To prepare the α,α' -diethynyl BODIPY **4a**, 5-mesityldipyrromethane **2** was used as the substrate for the gold(I) catalyzed reaction (Scheme 1). Mixing five mol % of gold(I) chloride and two equivalents of TIPS-EBX with a diethyl ether solution of **2** under ambient conditions yielded a mixture of ethynyl-substituted dipyrromethanes as judged by mass spectrometry. The product mixture was treated with 2,3-dichloro-5,6-dicyano-1,4-benzoquinone (DDQ) to give the α,α' -diethynyl-substituted dipyrin **7a**. Subsequent boron complexation in the presence of

trimethylsilyl chloride (TMSCl) as a fluoride scavenger afforded **4a** in 16% yield over three steps. Separately, α -ethynyl-monosubstituted dipyrin **3a**, was obtained via a one-pot reaction in 18% yield (in three steps from **2**).

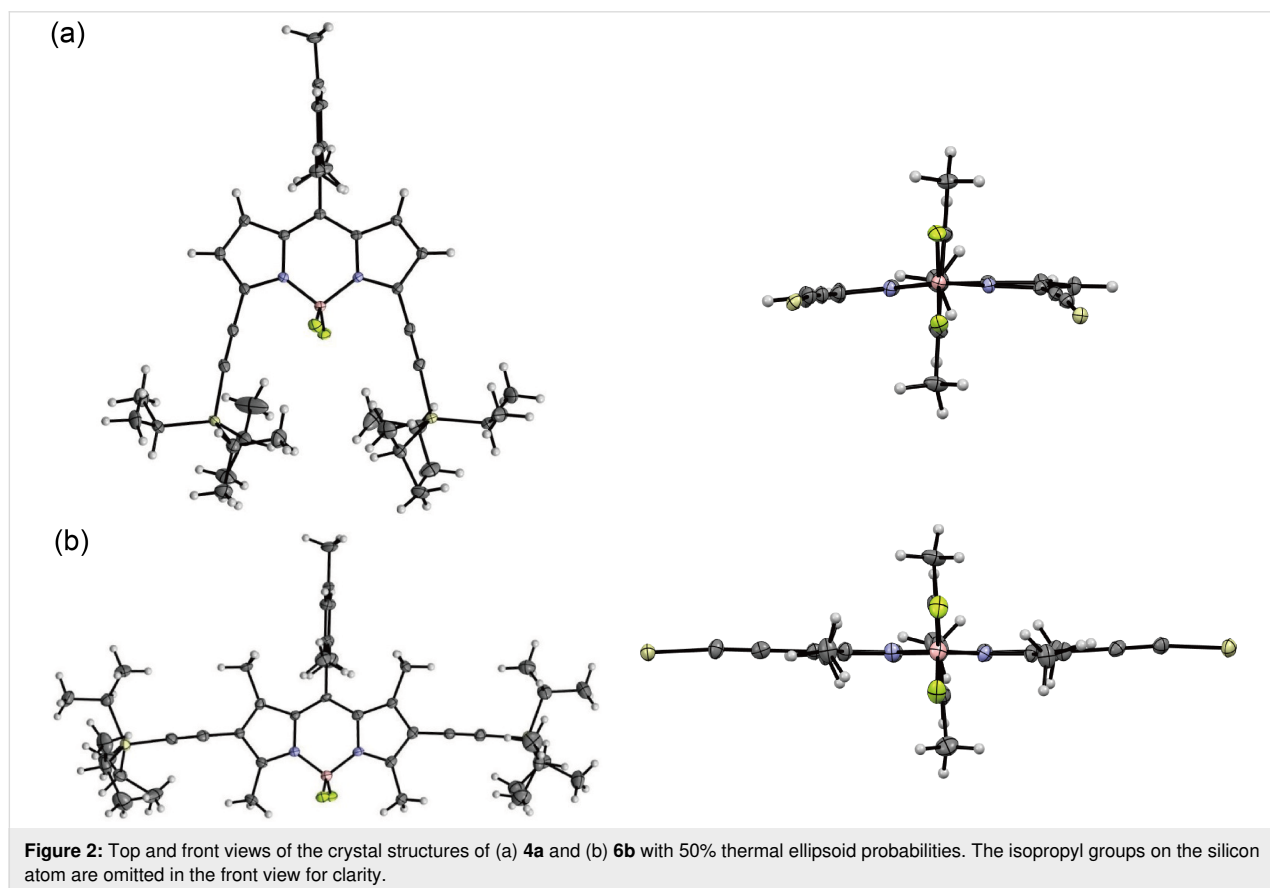
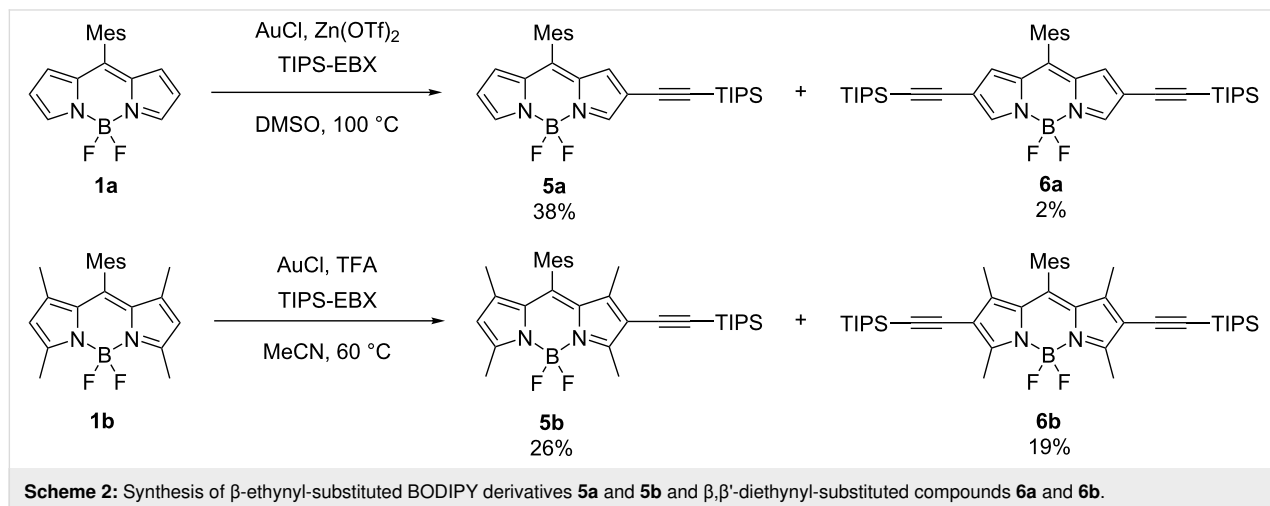
On the other hand, the β,β' -diethynyl-substituted BODIPY derivatives **5a** and **6a**, were synthesized by a similar gold-catalyzed reaction of unsubstituted BODIPY **1a** in 38% and 2% yields, respectively, in the presence of zinc(II) triflate as an activator of TIPS-EBX at 100 °C [41]. In contrast to the reaction of dipyrromethane **2**, the double C–H activation at the 2,6-positions of **1a** required harsh conditions (Table S1, Supporting Information File 1). The representative procedure of the reaction with EBX/gold(I) catalyst at room temperature gave only traces of **5a** with a large amount of unreacted starting material remaining. The addition of acid in expectation of the activation of TIPS-EBX was effective in promoting the gold–alkyne interactions [40,41]. After the investigation of various reaction conditions, such as gold catalysts (e.g., gold(I) cyanide), solvents (e.g., CH_2Cl_2 , THF, MeCN, DMF), additives (e.g., TFA, $\text{Sc}(\text{OTf})_3$), and temperature, the reaction conditions as mentioned earlier were chosen for the synthesis of **5a** and **6a** (Table S1, Supporting Information File 1).

Because of the electron-deficient nature of BODIPY, the reactivity of the 2,6-positions is intrinsically low toward electrophiles, which hampers the β -selective functionalization. We,



therefore, tested the corresponding reaction using tetramethyl-substituted BODIPY **1b** that is expected to have an enhanced electron density of the BODIPY core compared with **1a** (Scheme 2). Under milder conditions, the yield of the β,β' -diethynylated product **6b** was indeed improved to be 19% (from 2% of **6a**). These results indicate that electron-rich substrates facilitate the direct electrophilic alkynylation of the BODIPY core.

The structures of the series of TIPS-ethynyl-substituted BODIPY derivatives **3–6** were characterized by ^1H and ^{19}F NMR spectroscopy, high-resolution mass spectrometry, and X-ray crystallographic analysis. The solid-state structures of the diethynyl-substituted BODIPYs were unambiguously elucidated by X-ray diffraction analysis (**3a** and **6b**; Figure 2 and Table S2 in Supporting Information File 1). The BODIPY cores of **3a** and **6b** are almost planar with smaller mean-plane deviations



(defined by the 12 atoms of the tricyclic ring system) of 0.075 and 0.025 Å, respectively. The *meso*-mesityl groups are oriented perpendicularly to the BODIPY plane for both derivatives, indicating the rigid interlocked structures of **3a** and **6b** by the bulky *o*-methyl groups. In particular, the β -methyl substituents of **6b** are sterically hindered by the neighbouring *meso*-aryl ring. The regioselective 2,6-diethynylation of **6a** through the above alkynylation was also confirmed by its preliminary X-ray structure (Figure S20b, Supporting Information File 1).

The ^1H NMR spectra of the BODIPY derivatives in CDCl_3 reflect the characteristic structural features. The proton signals assignable to the α -pyrrolic CHs appeared in the lowest field region (δ ca. 8.00 ppm), and the β -CH resonances are in the range of 6.5 to 6.7 ppm (Figure 3). The disappearance of the α -pyrrole proton signals of **4a** is notable. In the case of **3a**, only a singlet signal appeared at 7.95 ppm for the α -pyrrole CH. In contrast, **6a** revealed two singlet signals at 7.99 and 6.70 ppm, assignable to the α - and β -pyrrole CHs, respectively. The ^1H NMR spectrum of the mono-substituted compound **5a** represents an unsymmetrical resonance pattern similar to that of **3a** with two α -CH signals at 7.97 and 7.96 ppm. The proposed structures of all BODIPY compounds were elucidated based on

the comparative NMR analysis and mass spectrometry (see Supporting Information File 1).

Optical properties

The α - and β -ethynyl-substituted BODIPYs exhibit large bathochromic shifts in the absorption and fluorescence spectra relative to the unsubstituted **1a** with extended π -conjugation (Figure 4 and Figure 5). The molar absorption coefficients (ϵ) of the S_0 – S_1 bands of the α -ethynyl-substituted BODIPYs are substantially enhanced as the number of substituted groups increases (Figure 4a). Along with the absorption spectral profiles of **3a** and **4a**, sharp emission bands emerge with mirror structures (Figure 5a). The fluorescence quantum yields of **3a** and **4a** remain high ($\Phi_f = 0.95$ and 0.56, respectively) and are comparable to that of **1a** (Table 1). The smaller Stokes shift values of $\approx 178\text{ cm}^{-1}$ and longer emission lifetimes of $\approx 7.83\text{ ns}$ indicate the rigid scaffolds of α,α -disubstituted **4a** in the excited state.

In the case of β -substituted BODIPYs, the S_0 – S_1 absorption bands of **5a** and **6a** are significantly broadened with the full width at half maximum (fwhm) of 1827 and 1438 cm^{-1} , respectively, compared to those of the α -substituted compounds **3a** and **4a** (625 and 508 cm^{-1} , respectively, Figure 4a). According-

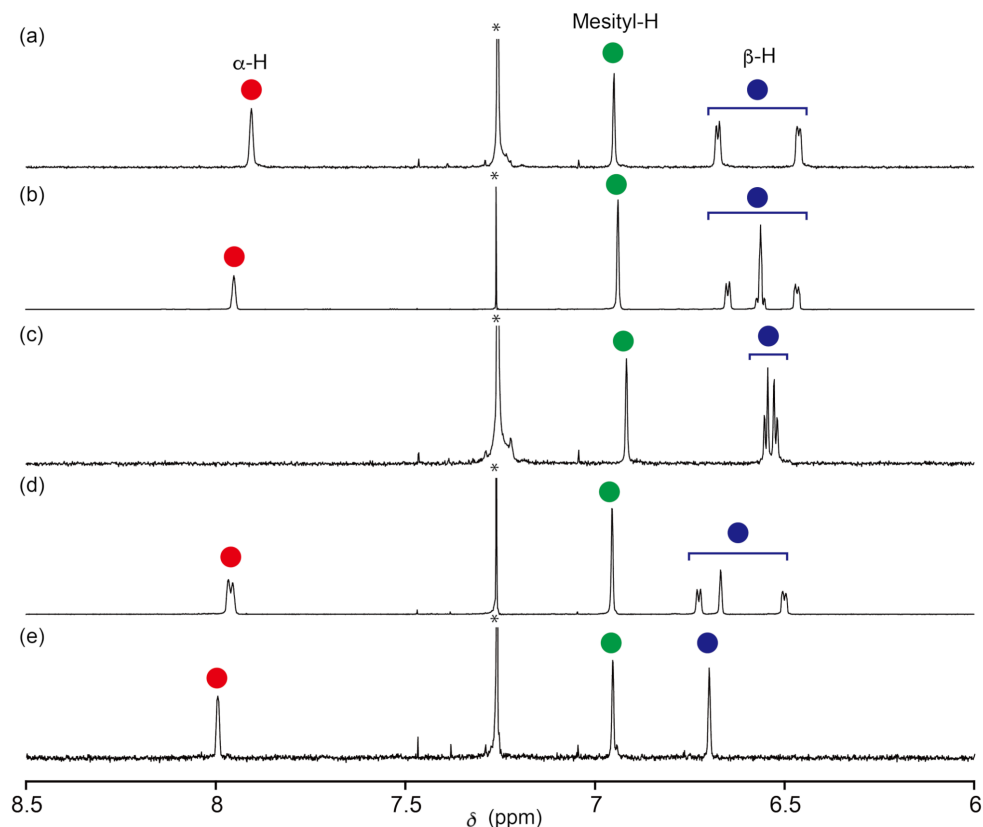


Figure 3: Partial ^1H NMR spectra of (a) **1a**, (b) **3a**, (c) **4a**, (d) **5a**, and (e) **6a** recorded in CDCl_3 at 298 K. Asterisks indicate the residual solvent peak.

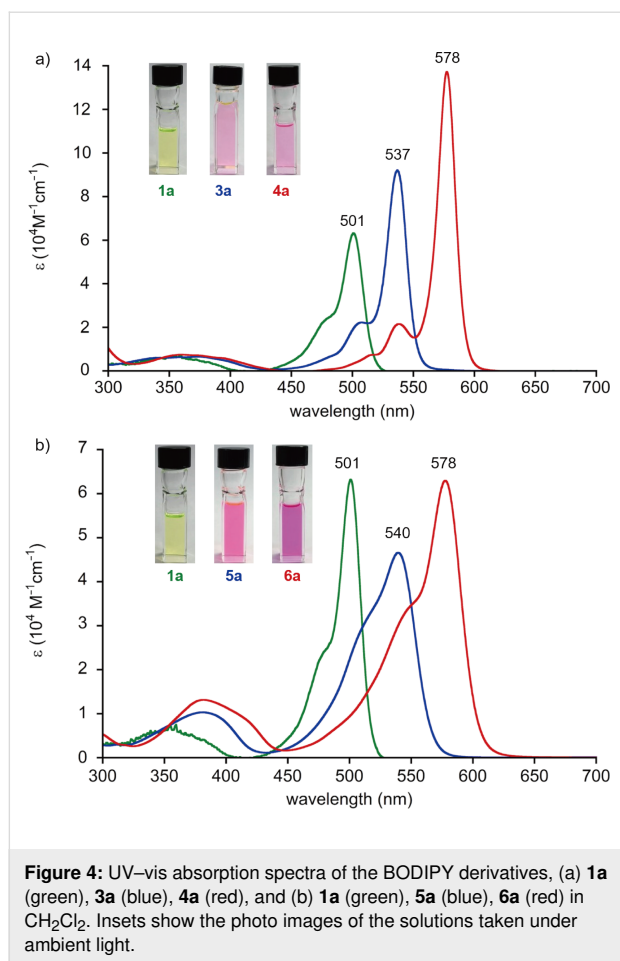


Figure 4: UV-vis absorption spectra of the BODIPY derivatives, (a) **1a** (green), **3a** (blue), **4a** (red), and (b) **1a** (green), **5a** (blue), **6a** (red) in CH_2Cl_2 . Insets show the photo images of the solutions taken under ambient light.

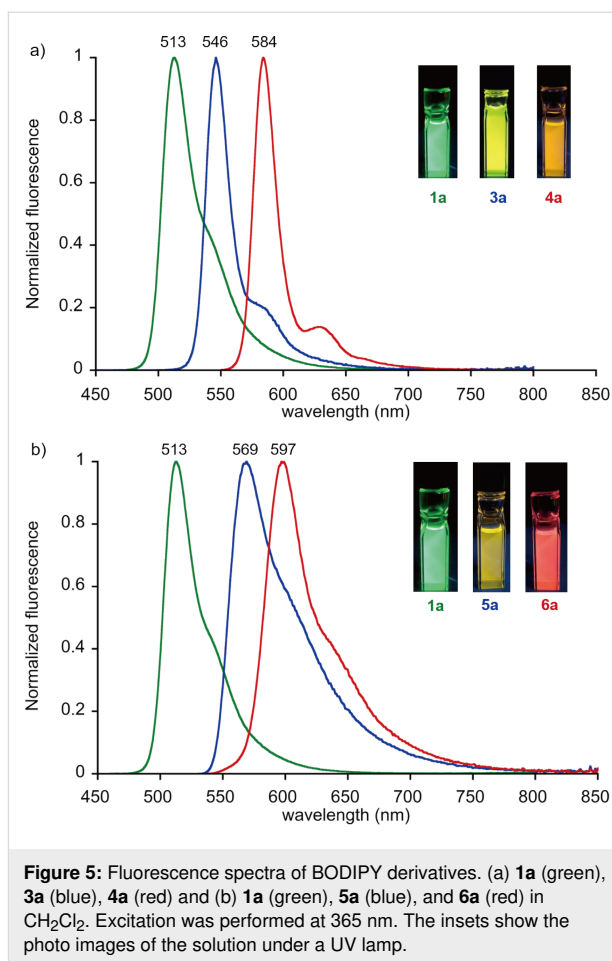


Figure 5: Fluorescence spectra of BODIPY derivatives. (a) **1a** (green), **3a** (blue), **4a** (red) and (b) **1a** (green), **5a** (blue), **6a** (red) in CH_2Cl_2 . Excitation was performed at 365 nm. The insets show the photo images of the solution under a UV lamp.

ly, the relatively broad emission bands were observed with lowered quantum yields, Φ_f of 0.25 and 0.16, respectively (Figure 5b and Table 1). The larger Stokes shift and shorter emission lifetime suggest a rapid decay of the excited species after structural relaxation (vide infra, Table 1). Also, inter-system crossing to the triplet state can be another pathway to

understand the lower emission quantum yield of the BODIPYs. However, reactive singlet oxygen species ($^1\text{O}_2$) was not observed under the aerobic conditions probed by the near-infrared photoluminescence at 1270 nm. The above spectral features were likewise shown with the β -ethylene-substituted BODIPYs [32].

Table 1: Spectral properties of BODIPYs in CH_2Cl_2 .

	λ_{max} (nm)	$\epsilon_{\text{max}}^{\text{a}}$ ($\text{M}^{-1} \text{ cm}^{-1}$)	$\lambda_{\text{em}}^{\text{b}}$ (nm)	Stokes shift (cm^{-1})	Φ_f^{c}	τ_f^{d} (ns)
1a	501	6.3×10^4	513	467	0.86	6.60
3a	537	9.2×10^4	546	307	0.95	5.81
4a	578	1.4×10^5	584	178	0.56	7.83
5a	540	4.0×10^4	569	944	0.25	5.70
6a	578	6.3×10^4	597	551	0.16	5.52
1b	502	8.8×10^4	510	312	0.96	5.35
5b	529	7.8×10^4	547	622	0.86	5.59
6b	558	9.7×10^4	574	500	0.77	4.97

^aAbsorption coefficients of the $\text{S}_0\text{--S}_1$ bands in CH_2Cl_2 . The reference values are taken from the literature [32,43]. ^bEmission maxima at wavelength.

^cEmission quantum yield determined by integrating sphere. ^dEmission lifetime probed at the maxima of the bands.

Similarly, the bathochromic shifts of the absorption and fluorescence bands for the tetramethyl-substituted derivatives **5b** and **6b** were observed in CH₂Cl₂ solution (Figure S21, Supporting Information File 1). However, due to the rigid structure of the highly substituted BODIPY cores, higher emission quantum yields of 0.86 and 0.77 were estimated, respectively (Table 1).

Electrochemical properties

Cyclic voltammetry and differential pulse voltammetry of the BODIPY derivatives **3a–6a** were performed in dichloromethane solutions containing 0.1 M tetra-*n*-butylammonium hexafluorophosphate (TBAPF₆) as a supporting electrolyte (Figure S23, Supporting Information File 1). All the derivatives exhibited reversible one-electron reduction waves and the irreversible oxidation ones, except for **4a**. Upon installing the TIPS-ethynyl substituents into the BODIPY core, the reduction potentials are significantly shifted in the anodic direction rather than the extent of the shifts in the oxidation potentials [30]. The electron-deficient effect of the substituents is pronounced for the doubly substituted derivatives **4a** and **6a**. Consequently, the electrochemical energy gaps of **3a–6a** are estimated to be 2.30, 2.14, 2.35, and 2.21 V, respectively, which is consistent with the calculated HOMO–LUMO energy gaps (vide infra, Figure S24, Supporting Information File 1).

Theoretical calculations

To gain insight into the substitution effect on the electronic properties of the BODIPY derivatives, density functional theory (DFT) calculations were performed at the B3LYP/6-31G(d) level of theory. The *a*₂-symmetry of the HOMOs and *b*₂-symmetry of the LUMOs of each, the α - and β -ethynyl-substituted BODIPYs are almost identical to those of the unsubstituted compound **1a** (Figure S24, Supporting Information File 1). The HOMO energies of the α -ethynyl-substituted derivatives **3a** and **4a**, are destabilized with broken degeneracy upon increasing the number of ethynyl substituents. On the other hand, the corresponding energies of the β -substituted derivatives **5a** and **6a** are not drastically altered because of a nodal plane near the 1,7-positions in the HOMO and smaller MO coefficients at the 2,6-positions than those at the 3,5-positions. Rather, a stabilization of the LUMO energies is found in **5a** and **6a** even though the MO hybridization of the BODIPY core with π -orbitals of ethynyl moieties is less affected. The mesomeric effect on the ethynyl substituents at the β -position of the BODIPY core is thus different from the α -substituted ones.

Furthermore, to understand the excited-state properties (e.g., Stokes shifts) of the substituted BODIPYs, the S₁-state geometries for **4a** and **6a** were obtained by the time-dependent (TD) DFT methods. As a result, the excited-state structure of **6a** exhibits a remarkably bent distortion of the core with a plane

angle of 16.1°, whereas the structure of **4a** remains coplanar (Figure S25, Supporting Information File 1). The corresponding energy gap between the HOMO and LUMO of **6a** is significantly decreased with the geometry relaxation at the S₁ state compared to that of the S₀-state structure, which could be the origin of the large Stokes shift for **6a**. Therefore, in comparison with the α -substituted compounds **3a** and **4a**, the less emissive character of the β -ethynyl-substituted derivatives **5a** and **6a** agreed with the fact that the photoexcited dynamics of β -substituted BODIPYs intend to the rapid decay with structural relaxation.

Conclusion

In summary, we have synthesized novel regioselectively alkynylated BODIPY derivatives via a gold(I)-catalyzed direct C–H functionalization with TIPS-EBX reagents. This atom-economical method for the late-stage alkynylation of BODIPY dyes could be an alternate approach for functionalized fluorescent dyes without the need of preparing unstable halogenated pyrrole precursors. The resulting α - and β -ethynyl-substituted BODIPYs displayed distinct substitution-site-dependent spectral features, for instance, the extent of the bathochromic shifts of the absorption and fluorescence, variable Stokes shift and the emission quantum yields. The TIPS-protected ethynyl groups of these BODIPY dyes can be applied as substrates for the “click” CuAAC reaction toward novel functional fluorescent materials.

Supporting Information

Supporting Information File 1

Experimental methods including detailed synthetic procedures, compound characterization data, and DFT calculations.

[<https://www.beilstein-journals.org/bjoc/content/supplementary/1860-5397-16-53-S1.pdf>]

Supporting Information File 2

Crystallographic information file of compound **3a**.

[<https://www.beilstein-journals.org/bjoc/content/supplementary/1860-5397-16-53-S2.cif>]

Supporting Information File 3

Crystallographic information file of compound **6b**.

[<https://www.beilstein-journals.org/bjoc/content/supplementary/1860-5397-16-53-S3.cif>]

Acknowledgements

We thank Dr. T. Ono at Kyushu University for the help of absolute photoluminescence quantum yield measurements.

Funding

The present work was supported by JSPS KAKENHI Grant Numbers (JP19H04586 and JP19K05439). Funding from the Tokuyama Research Foundation is gratefully acknowledged.

ORCID® IDs

Shigeki Mori - <https://orcid.org/0000-0001-6731-2357>

Masatoshi Ishida - <https://orcid.org/0000-0002-1117-2188>

Hirofumi Furuta - <https://orcid.org/0000-0002-3881-8807>

References

- Ni, Y.; Wu, J. *Org. Biomol. Chem.* **2014**, *12*, 3774–3791. doi:10.1039/c3ob42554a
- Tao, J.; Sun, D.; Sun, L.; Li, Z.; Fu, B.; Liu, J.; Zhang, L.; Wang, S.; Fang, Y.; Xu, H. *Dyes Pigm.* **2019**, *168*, 166–174. doi:10.1016/j.dyepig.2019.04.054
- Kim, T.-I.; Park, S.; Choi, Y.; Kim, Y. *Chem. – Asian J.* **2011**, *6*, 1358–1361. doi:10.1002/asia.201100025
- Liu, P.; Jing, X.; Yu, F.; Lv, C.; Chen, L. *Analyst* **2015**, *140*, 4576–4583. doi:10.1039/c5an00759c
- Sharker, S. M.; Jeong, C. J.; Kim, S. M.; Lee, J.-E.; Jeong, J. H.; In, I.; Lee, H.; Park, S. Y. *Chem. – Asian J.* **2014**, *9*, 2921–2927. doi:10.1002/asia.201402399
- Gao, M.; Wang, R.; Yu, F.; Chen, L. *Biomaterials* **2018**, *160*, 1–14. doi:10.1016/j.biomaterials.2018.01.011
- Gorbe, M.; Costero, A. M.; Sancenón, F.; Martínez-Mañez, R.; Ballesteros-Cillero, R.; Ochando, L. E.; Chulvi, K.; Gotor, R.; Gil, S. *Dyes Pigm.* **2019**, *160*, 198–207. doi:10.1016/j.dyepig.2018.08.007
- Kamkaew, A.; Lim, S. H.; Lee, H. B.; Kiew, L. V.; Chung, L. Y.; Burgess, K. *Chem. Soc. Rev.* **2013**, *42*, 77–88. doi:10.1039/c2cs35216h
- Yogo, T.; Urano, Y.; Ishitsuka, Y.; Maniwa, F.; Nagano, T. *J. Am. Chem. Soc.* **2005**, *127*, 12162–12163. doi:10.1021/ja0528533
- Auwah, S. G.; You, Y. *RSC Adv.* **2012**, *2*, 11169–11183. doi:10.1039/c2ra21404k
- Huang, L.; Li, Z.; Zhao, Y.; Zhang, Y.; Wu, S.; Zhao, J.; Han, G. *J. Am. Chem. Soc.* **2016**, *138*, 14586–14591. doi:10.1021/jacs.6b05390
- Turan, I. S.; Yildiz, D.; Turksoy, A.; Gunaydin, G.; Akkaya, E. U. *Angew. Chem., Int. Ed.* **2016**, *55*, 2875–2878. doi:10.1002/anie.201511345
- Suryani, O.; Higashino, Y.; Sato, H.; Kubo, Y. *ACS Appl. Energy Mater.* **2019**, *2*, 448–458. doi:10.1021/acsaem.8b01474
- Bandyopadhyay, S.; Anil, A. G.; James, A.; Patra, A. *ACS Appl. Mater. Interfaces* **2016**, *8*, 27669–27678. doi:10.1021/acsaami.6b08331
- Li, W.; Xie, Z.; Jing, X. *Catal. Commun.* **2011**, *16*, 94–97. doi:10.1016/j.catcom.2011.09.007
- Luo, G.-G.; Fang, K.; Wu, J.-H.; Mo, J. *Chem. Commun.* **2015**, *51*, 12361–12364. doi:10.1039/c5cc03897a
- Zhang, C.; Zhao, J.; Wu, S.; Wang, Z.; Wu, W.; Ma, J.; Guo, S.; Huang, L. *J. Am. Chem. Soc.* **2013**, *135*, 10566–10578. doi:10.1021/ja405170j
- Wu, W.; Zhao, J.; Sun, J.; Guo, S. *J. Org. Chem.* **2012**, *77*, 5305–5312. doi:10.1021/jo300613g
- Sun, J.; Zhong, F.; Yi, X.; Zhao, J. *Inorg. Chem.* **2013**, *52*, 6299–6310. doi:10.1021/ic302210b
- Liu, Q.; Yin, B.; Yang, T.; Yang, Y.; Shen, Z.; Yao, P.; Li, F. *J. Am. Chem. Soc.* **2013**, *135*, 5029–5037. doi:10.1021/ja3104268
- Loudet, A.; Burgess, K. *Chem. Rev.* **2007**, *107*, 4891–4932. doi:10.1021/cr078381n
- Verbelen, B.; Leen, V.; Wang, L.; Boens, N.; Dehaen, W. *Chem. Commun.* **2012**, *48*, 9129–9131. doi:10.1039/c2cc34549h
- Ren, W.; Xiang, H.; Peng, C.; Musha, Z.; Chen, J.; Li, X.; Huang, R.; Hu, Y. *RSC Adv.* **2018**, *8*, 5542–5549. doi:10.1039/c7ra13070h
- Zhang, M.; Hao, E.; Zhou, J.; Yu, C.; Bai, G.; Wang, F.; Jiao, L. *Org. Biomol. Chem.* **2012**, *10*, 2139–2145. doi:10.1039/c2ob06689k
- Verbelen, B.; Boodts, S.; Hofkens, J.; Boens, N.; Dehaen, W. *Angew. Chem., Int. Ed.* **2015**, *54*, 4612–4616. doi:10.1002/anie.201410853
- Luo, L.; Wu, D.; Li, W.; Zhang, S.; Ma, Y.; Yan, S.; You, J. *Org. Lett.* **2014**, *16*, 6080–6083. doi:10.1021/ol502883x
- Zhou, X.; Wu, Q.; Yu, Y.; Yu, C.; Hao, E.; Wei, Y.; Mu, X.; Jiao, L. *Org. Lett.* **2016**, *18*, 736–739. doi:10.1021/acs.orglett.5b03706
- Wang, D.; Cheng, C.; Wu, Q.; Wang, J.; Kang, Z.; Guo, X.; Wu, H.; Hao, E.; Jiao, L. *Org. Lett.* **2019**, *21*, 5121–5125. doi:10.1021/acs.orglett.9b01722
- Yang, X.; Jiang, L.; Yang, M.; Zhang, H.; Lan, J.; Zhou, F.; Chen, X.; Wu, D.; You, J. *J. Org. Chem.* **2018**, *83*, 9538–9546. doi:10.1021/acs.joc.8b01239
- Wang, J.; Li, Y.; Gong, Q.; Wang, H.; Hao, E.; Lo, P.-C.; Jiao, L. *J. Org. Chem.* **2019**, *84*, 5078–5090. doi:10.1021/acs.joc.9b00020
- Wang, J.; Wu, Q.; Gong, Q.; Cheng, K.; Liu, Q.; Yu, C.; Hao, E.; Jiao, L. *Adv. Synth. Catal.* **2019**, *361*, 769–777. doi:10.1002/adsc.201801338
- Chen, J.; Mizumura, M.; Shinokubo, H.; Osuka, A. *Chem. – Eur. J.* **2009**, *15*, 5942–5949. doi:10.1002/chem.200802541
- Feng, Z.; Jiao, L.; Feng, Y.; Yu, C.; Chen, N.; Wei, Y.; Mu, X.; Hao, E. *J. Org. Chem.* **2016**, *81*, 6281–6291. doi:10.1021/acs.joc.6b00858
- Kowada, T.; Yamaguchi, S.; Fujinaga, H.; Ohe, K. *Tetrahedron* **2011**, *67*, 3105–3110. doi:10.1016/j.tet.2011.02.073
- Wirtz, M.; Grüter, A.; Rebmann, P.; Dier, T.; Volmer, D. A.; Huch, V.; Jung, G. *Chem. Commun.* **2014**, *50*, 12694–12697. doi:10.1039/c4cc05288a
- Albrecht, M.; Lippach, A.; Exner, M. P.; Jerbi, J.; Springborg, M.; Budisa, N.; Wenz, G. *Org. Biomol. Chem.* **2015**, *13*, 6728–6736. doi:10.1039/c5ob00505a
- Sakida, T.; Yamaguchi, S.; Shinokubo, H. *Angew. Chem., Int. Ed.* **2011**, *50*, 2280–2283. doi:10.1002/anie.201006314
- Brand, J. P.; Charpentier, J.; Waser, J. *Angew. Chem., Int. Ed.* **2009**, *48*, 9346–9349. doi:10.1002/anie.200905419
- Brand, J. P.; Waser, J. *Org. Lett.* **2012**, *14*, 744–747. doi:10.1021/ol203289v
- Brand, J. P.; Waser, J. *Angew. Chem., Int. Ed.* **2010**, *49*, 7304–7307. doi:10.1002/anie.201003179
- Li, Y.; Waser, J. *Beilstein J. Org. Chem.* **2013**, *9*, 1763–1767. doi:10.3762/bjoc.9.204
- Li, Y.; Hari, D. P.; Vita, M. V.; Waser, J. *Angew. Chem., Int. Ed.* **2016**, *55*, 4436–4454. doi:10.1002/anie.201509073
- Nepomnyashchii, A. B.; Bröring, M.; Ahrens, J.; Bard, A. J. *J. Am. Chem. Soc.* **2011**, *133*, 8633–8645. doi:10.1021/ja2010219

License and Terms

This is an Open Access article under the terms of the Creative Commons Attribution License (<http://creativecommons.org/licenses/by/4.0>). Please note that the reuse, redistribution and reproduction in particular requires that the authors and source are credited.

The license is subject to the *Beilstein Journal of Organic Chemistry* terms and conditions: (<https://www.beilstein-journals.org/bjoc>)

The definitive version of this article is the electronic one which can be found at:
[doi:10.3762/bjoc.16.53](https://doi.org/10.3762/bjoc.16.53)



Direct borylation of terrylene and quaterrylene

Haruka Kano, Keiji Uehara, Kyohei Matsuo, Hironobu Hayashi, Hiroko Yamada* and Naoki Aratani*

Letter

[Open Access](#)

Address:
Division of Materials Science, Nara Institute of Science and Technology (NAIST), 8916-5 Takayama-cho, Ikoma 630-0192, Japan

Email:
Hiroko Yamada* - hyamada@ms.naist.jp; Naoki Aratani* - aratani@ms.naist.jp

* Corresponding author

Keywords:
borylation; π -conjugation; oligorylene; single crystal X-ray structure; solubility

Beilstein J. Org. Chem. **2020**, *16*, 621–627.
doi:10.3762/bjoc.16.58

Received: 04 February 2020

Accepted: 13 March 2020

Published: 06 April 2020

This article is part of the thematic issue "C–H functionalization for materials science".

Guest Editor: K. Itami

© 2020 Kano et al.; licensee Beilstein-Institut.
License and terms: see end of document.

Abstract

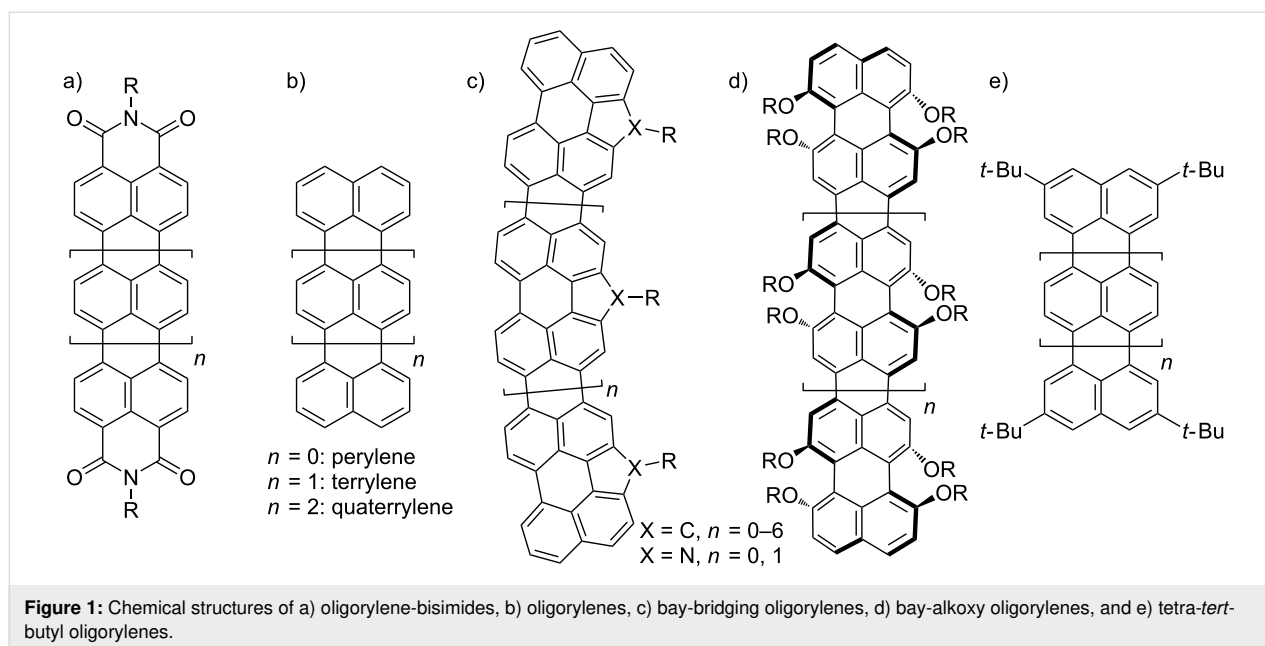
The preparation of large rylene often needs the use of solubilizing groups along the rylene backbone, and all the substituents of the terrylenes and quaterrylenes were introduced before creating the rylene skeleton. In this work, we successfully synthesized 2,5,10,13-tetrakis(4,4,5,5-tetramethyl-1,3,2-dioxaborolan-2-yl)terrylene (**TB4**) by using an iridium-catalyzed direct borylation of C–H bonds in terrylene in 56% yield. The product is soluble in common organic solvents and could be purified without column chromatography. Single crystal X-ray diffraction analysis revealed that the terrylene core is not disturbed by the substituents and is perfectly flat. The photophysical properties of **TB4** are also unchanged by the substituents because the carbon atoms at 2,5,10,13-positions have less coefficients on its HOMO and LUMO, estimated by theoretical calculations. Finally, the same borylation reaction was applied for quaterrylene, resulting in the formation of soluble tetra-borylated quaterrylene despite a low yield. The post modification of rylene enables us to prepare their borylated products as versatile units after creating the rylene skeletons.

Introduction

Compared with fruitful researches of oligorylene-bisimides for organic devices and single molecular spectroscopy [1–6], genuine oligorylenes have been sporadically investigated mainly because of their synthetic difficulty and low solubility (Figure 1) [7]. To be applied to electronic or photovoltaic components, the scalable synthesis of pure soluble compounds is essential. Recently, facile preparation methods of terrylene [8] and quaterrylene [9] were reported, after 50 years from the first reports, respectively [10,11]. Friedel–Crafts ring condensation reaction of 3-(1-naphthyl)perylene with AlCl_3 reproducibly pro-

vided a pure terrylene [8]. Scholl reaction using a superacid catalyst in combination with 2,3-dichloro-5,6-dicyano-1,4-benzoquinone (DDQ) as oxidant provides a scalable preparation of quaterrylene [9], but unfortunately the low solubility prevents ^1H NMR characterization. Larger oligorylenes have not been synthesized without the use of solubilizing groups along the rylene backbone.

For instance, bay-bridging perylenes with long alkyl chains [12–15] and bay-alkoxy-substitution [16–18] enable us to prepare



longer rylene (Figure 1c and 1d). However, tying the bay regions with carbon or nitrogen atoms causes bowing of the oligorylene backbone without disrupting the planarity of the aromatic backbone to give a flat banana-shaped molecule [15]. On the other hand, the bay-alkoxy-substitution is estimated to twist the core, which changes the original characteristics of rylene but eventually helps to enhance the solubility of the macromolecules [7]. In order to avoid such deformation of the molecular skeleton, the solubilizing groups should be attained at the terminal positions. In this regard, the tetra-*tert*-butyl series of rylene made it possible to study their intrinsic physical properties as a function of molecular length (Figure 1e) [19,20], while the low solubility of *tert*-butylpentarylene indicates that even such bulky group had reached its limit to interrupt π -stacking. The synthesis of higher oligorylenes would require more robust solubilizing groups.

All the substituents of the terrylenes and quaterrylene were installed before creating the rylene skeleton and no derivatives have been produced by the post modification probably because their low solubility hampers such strategy. Therefore, the substituents on the rylene skeleton have been quite limited because they must suffer the harsh conditions of the rylene skeleton preparation.

Basic reactivity of rylene with electrophiles is predicted from perylene in which the most reactive sites are the 3,4,9,10-positions [21]. On the other hand, the regioselectivity of the iridium (Ir)-catalyzed direct C–H borylation [22–25] gives 2,5,8,11-tetraborylated perylene [26]. The regioselectivity of the perylene borylation is determined by the steric factors rather than by

the electron distribution in the arene and this regioselectivity complements that of electrophilic substitutions [26].

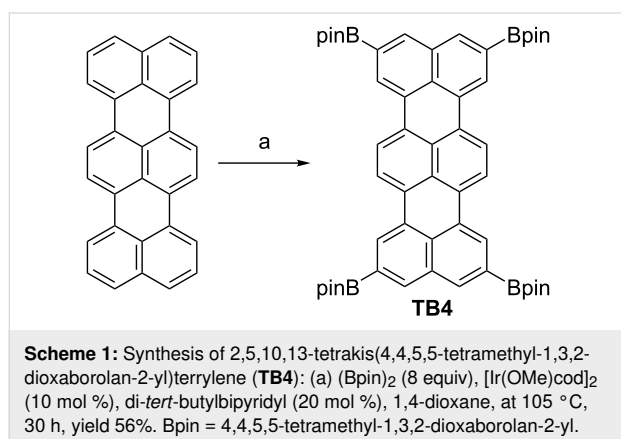
In light of the above, we plan to perform the Ir-catalyzed direct borylation of C–H bonds in terrylene because 1) the regioselectivity of the reaction is unique and should be remarkably high, thus terrylene will be borylated at the 2, 5, 10, and 13 positions, which don't deform the rylene cores, 2) the product obtained is soluble in common organic solvents so that the separation and characterization would be readily performed, and 3) the resultant pure soluble terrylene derivative as a versatile unit can be functionalized by using conventional metal-catalyzed coupling reactions.

Results and Discussion

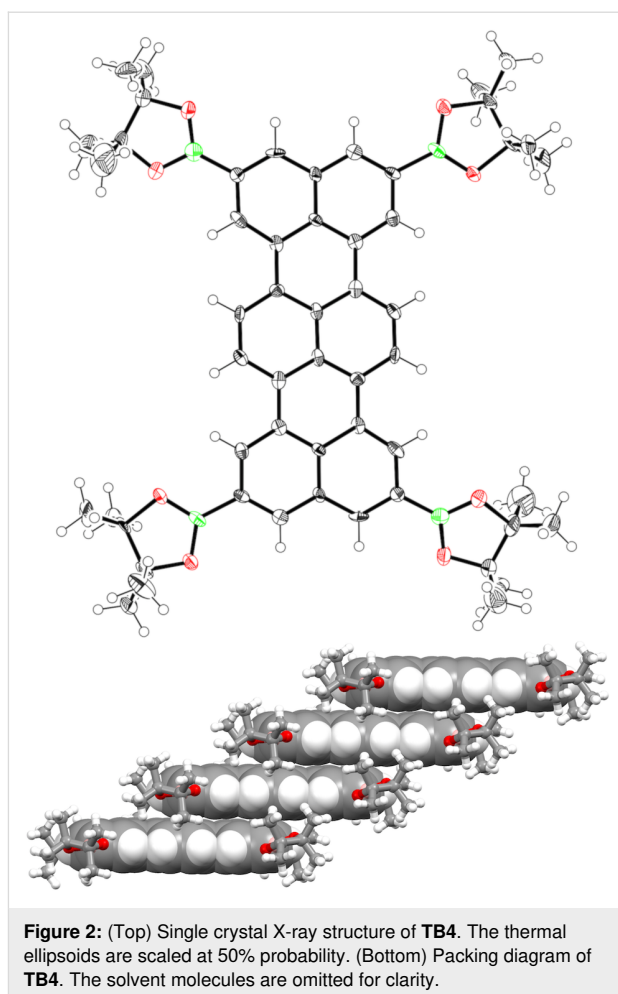
According to the literature [8], terrylene was prepared from a 3-(1-naphthyl)perylene by using 8 equivalents of AlCl_3 in chlorobenzene at 80 °C for 4 h. The crude product was purified by Soxhlet extraction followed by recrystallization from toluene. After these simple manipulations, the pure terrylene was isolated. Note that the terrylene is slightly soluble in halogenated solvents, hence a ^1H NMR spectrum in CDCl_3 at room temperature can be measured.

The reaction of terrylene (0.16 mmol), bis(pinacolato)diboron (8 equiv), $[\text{Ir}(\text{OMe})\text{cod}]_2$ (10 mol %) and di-*tert*-butylbipyridyl (20 mol %) in 1,4-dioxane (5 mL) under Ar at 105 °C for 30 h gave a deep orange solution (Scheme 1). Matrix assisted laser desorption/ionization (MALDI) mass spectrometry of the reaction mixture detected a single parent ion peak at $m/z = 880.4687$ (calcd for $\text{C}_{54}\text{H}_{60}\text{B}_4\text{O}_8 = 880.4660$ $[\text{M}]^+$), making us expect its

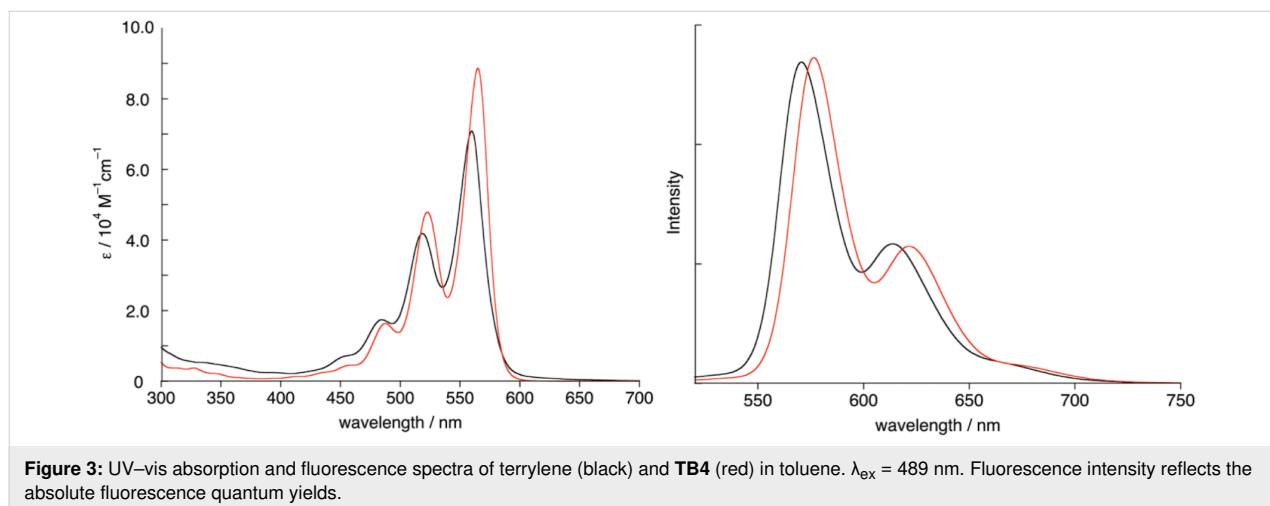
selective tetra-substitution with high yield. To isolate a pure product, the solvent was removed, then the reaction mixture was passed through a silica pad with CH_2Cl_2 , followed by reprecipitation from MeOH. The yield of 2,5,10,13-tetrakis(4,4,5,5-tetramethyl-1,3,2-dioxaborolan-2-yl)terrylene (**TB4**) was 56%. Since insoluble materials and polar byproducts can be removed by short silica gel and the formation of tri-, bis- and mono-substituted compounds is negligible, **TB4** can be purified without column chromatography.



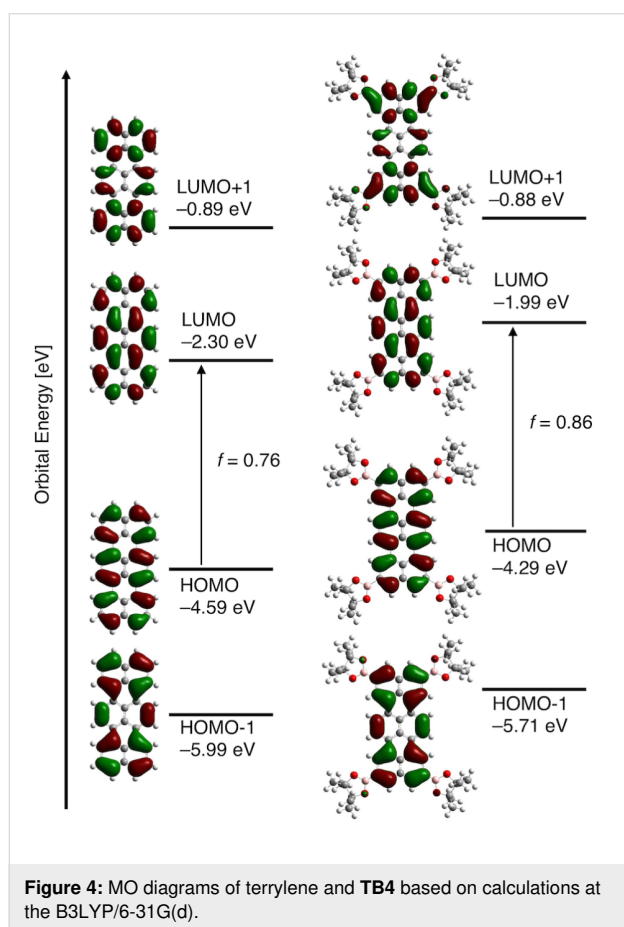
The ^1H NMR spectrum of **TB4** in CDCl_3 exhibited a highly symmetric D_{2h} signal pattern that consists of three singlet peaks at 8.58, 8.37 and 8.23 ppm due to aromatic protons. The structure of **TB4** was unambiguously revealed by single crystal X-ray diffraction analysis (Figure 2). The crystals suitable for X-ray diffraction were obtained by vapor diffusion of hexane into a solution of **TB4** in CH_2Cl_2 . The terrylene core is perfectly planar and forms a face-to-face stacking columnar structure with an interplanar distance of 3.40 Å along the *a* axis. The BO_2 units are slightly tilted from the aromatic plane (6.7 and 20.3°).



TB4 in toluene absorbs UV–vis light with an absorption maximum at 566 nm, and emits fluorescence at 576 nm with a quantum yield of $\Phi_F = 0.86$ at 298 K (Figure 3). Both peaks are slightly red-shifted relative to those of intact terrylene ($\lambda_{\text{abs}} = 560$ nm and $\lambda_{\text{em}} = 571$ nm with $\Phi_F = 0.82$ in toluene).

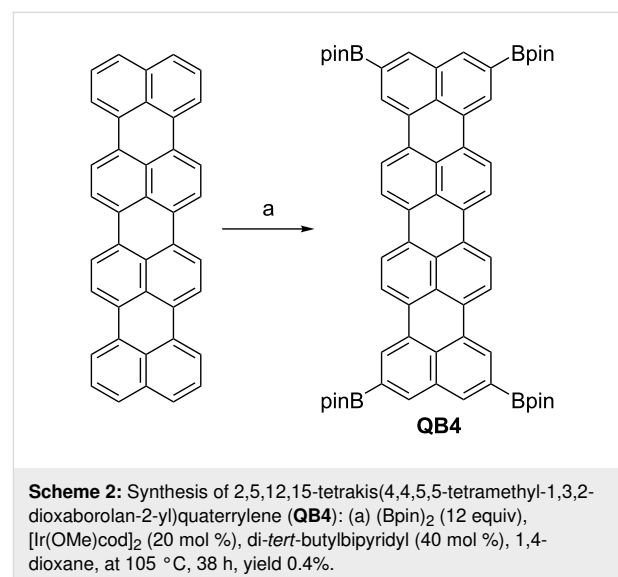


We employed density functional theory (DFT) and time-dependent (TD)-DFT calculations, both of them at the B3LYP/6-31G(d) level and with Gaussian 09, to make these electronic features understandable (Figure 4) [27]. The HOMO, HOMO–1, LUMO, and LUMO+1 for terrylene are nondegenerate and the coefficient distribution in these four frontier MOs seem to be delocalized over the whole aromatic core. The highest band of terrylene at 553 nm is mainly caused by transition from HOMO (–4.59 eV) to LUMO (–2.30 eV) (oscillator strength, $f = 0.76$). Although the frontier MOs for **TB4** are overall destabilized due to the smaller electronegativity of boron, the impact of substituents to the HOMO and LUMO distributions is negligible because of the existence of node at 2,5,10,13-positions. The longest band of **TB4** at 563 nm comprises the transition from equally destabilized HOMO (–4.29 eV) to LUMO (–1.99 eV) (oscillator strength, $f = 0.86$). The transition energies and oscillator strengths simulated by TD-DFT calculations showed a good agreement with the observed absorption spectra.



Taking the successful result of the terrylene borylation, next we tried to perform the same reaction to quaterrylene (Scheme 2). The quaterrylene was prepared by the oxidative condensation

reaction of perylene with TfOH and DDQ [9]. However, the crude product was not completely purified by Soxhlet extraction and by crystallization in our hands. The borylation reaction of hardly soluble crude quaterrylene gave a deep green suspension. MALDI mass spectrometry of the reaction mixture detected an ion peak at $m/z = 1004.5018$ (calcd for $C_{64}H_{64}B_4O_8 = 1004.5003$ [M]⁺), indicating that the mixture contains tetrasubstituted quaterrylene. To isolate the product, the combination of silica gel column chromatography and gel permeation chromatography techniques, followed by reprecipitation from MeOH gave a 2,5,12,15-tetrakis(4,4,5,5-tetramethyl-1,3,2-dioxaborolan-2-yl)quaterrylene (**QB4**) in 0.4% yield. The poor solubility of starting material prevented a smooth reaction.



It is difficult to observe accurate characteristics of quaterrylene in solution owing to its remarkable insolubility. The much improved solubility of **QB4** enables ¹H NMR measurement in CDCl₃, which exhibits a highly symmetric D_{2h} signal pattern that consists of two singlet peaks at 8.63 and 8.25 ppm, and two doublet peaks at 8.44 and 8.32 ppm for aromatic protons.

The UV–visible absorption spectrum of **QB4** in toluene is shown in Figure 5. Compared with *tert*-butylquaterrylene in dioxane [19], a slightly red-shifted absorption peak at 668 nm is observed. Interestingly, **QB4** emits only weak fluorescence as was described for tetra-*tert*-butylquaterrylene [20].

The coefficient distribution of four frontier MOs of quaterrylenes basically exhibits the same symmetric pattern with terrylenes (Figure 6). The longest band of **QB4** at 676 nm comprises the transition from high energy level of HOMO (–4.13 eV) to LUMO (–2.26 eV) (oscillator strength, $f = 1.41$).

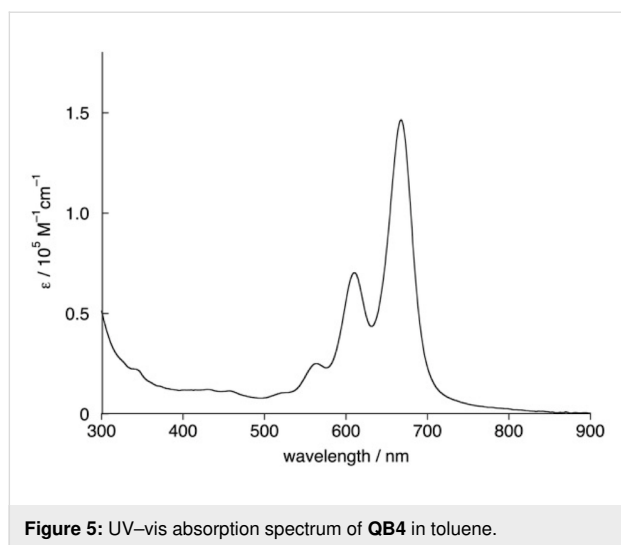


Figure 5: UV-vis absorption spectrum of QB4 in toluene.

The simulated absorption showed a good agreement with the observed spectra.

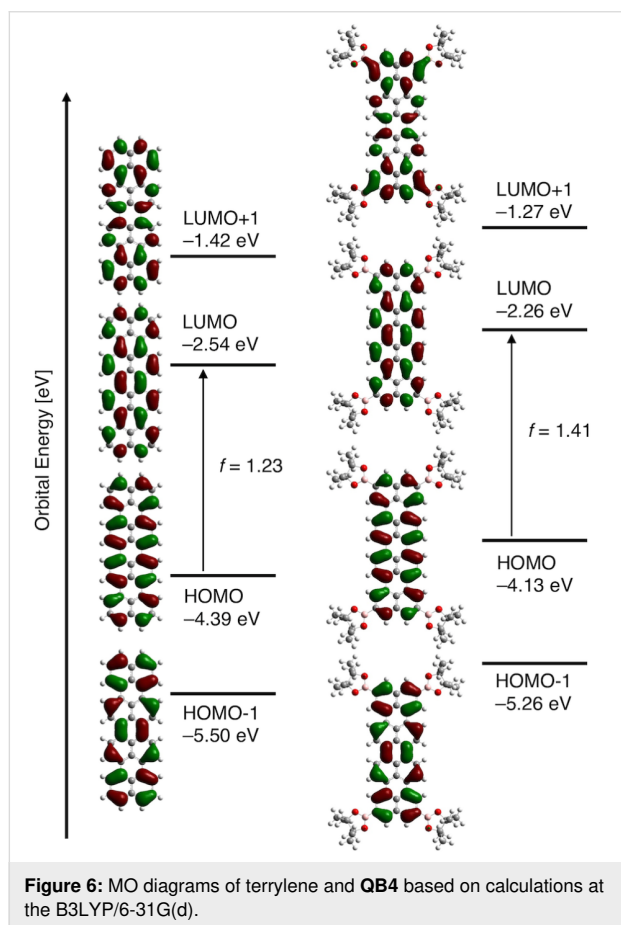
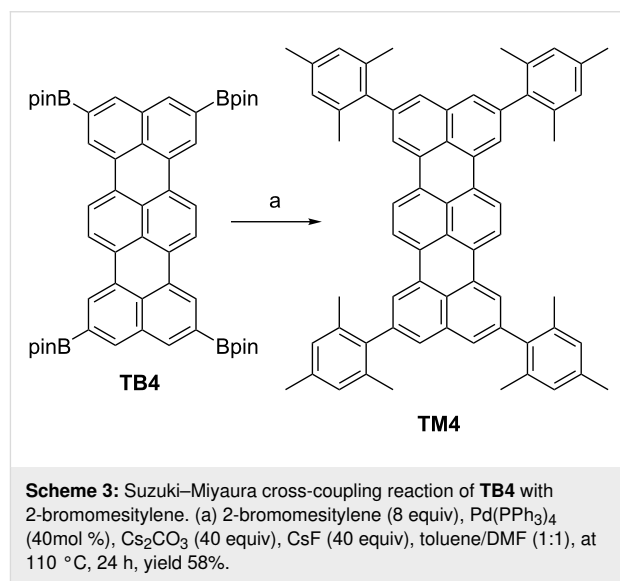


Figure 6: MO diagrams of terrylene and QB4 based on calculations at the B3LYP/6-31G(d).

The calculated HOMO levels of -4.29 eV for **TB4** and -4.13 eV for **QB4** are pretty high among electron-rich compounds. Thus we tested the stability of **TB4** and **QB4** under air

by means of UV-vis absorption spectroscopy. Surprisingly almost no spectral changes for both compounds were observed after 12 h, probably because the most reactive sites are protected by the steric hindrance of Bpin moieties.

Finally, to demonstrate the utility of the borylated oligorylenes, the Suzuki–Miyaura cross-coupling reaction of **TB4** under the standard conditions was performed (Scheme 3). Coupling of **TB4** and 2-bromomesitylene with $\text{Pd}(\text{PPh}_3)_4$, Cs_2CO_3 and CsF in a mixture of toluene/DMF furnished 2,5,10,13-tetramesityl-terrylene (**TM4**) in 58% yield. **TM4** was successfully isolated through a silica gel pad and by reprecipitation. The structure of **TM4** was characterized by mass spectrometry and ^1H and ^{13}C NMR spectroscopy. High-resolution MALDI mass spectrometry detected the parent ion peak at $m/z = 848.4377$ (calcd. for $\text{C}_{66}\text{H}_{56} = 848.4377 [\text{M}]^+$). The ^1H NMR spectrum of **TM4** in CDCl_3 reveals only a single set of signals that consists of four singlet peaks for aromatic protons at 8.21, 8.02, 7.44, and 7.03 ppm.



Conclusion

In this work, we synthesized soluble terrylene and quaterylene derivatives by using an Ir-catalyzed borylation reaction. Our results provide a highly potential route to various functional oligorylene derivatives. In fact, **TB4** could be transformed into the tetraarylterrylene **TM4** in good yield by the conventional cross-coupling reaction. **TB4** exhibits face-to-face interaction in the crystals, resulting in the 1D columnar structure as a whole, which is expected to have higher carrier mobility. Recently, oligo-*perinaphthalenes*, namely oligorylenes, are of great interest as good model compounds of armchair graphene nanoribbons (AGNRs), since AGNRs with a width of $N = 3p + 2$ are predicted to be metallic with a small bandgap

[28–30], and the narrowest AGNR is polyrylene (5-AGNR, $p = 1$) [31,32]. Many potential applications await techniques to prepare large scale quantities of functionalized oligorylenes. We believe that our approach opens fruitful oligorylene researches that find many uses in organic devices.

Experimental

^1H NMR (500 MHz) and ^{13}C NMR (126 MHz) spectra were recorded with a JEOL JNM-ECX500 spectrometer at 20 °C by using tetramethylsilane as an internal standard. High-resolution mass spectra (HRMS) were measured with the matrix-assisted laser desorption/ionization-time-of-flight (MALDI-TOF) method on a JEOL SpiralTOF/JMS-S3000 spectrometer. X-ray crystallographic data were recorded at 103 K with a BRUKER-APEXII X-ray diffractometer using Mo K α radiation equipped with a large area CCD detector. UV–vis absorption spectra were measured with a JASCO UV/Vis/NIR spectrophotometer V-570, and fluorescence spectra were measured with a JASCO PL spectrofluorometer FP-6600. Fluorescence quantum yields were measured on a HAMAMATSU Absolute PL Quantum Yield Measurement System C9920-02G. TLC and gravity column chromatography were performed on Art. 5554 (Merck KGaA) plates and silica gel 60N (Kanto Chemical), respectively. All solvents and chemicals were of reagent-grade quality, obtained commercially, and used without further purification. Terrylene and quaterylene were prepared according to the literature [8,9]. For spectral measurements, spectral-grade toluene was purchased from Nacalai Tesque.

Synthesis of TB4. [Ir(OMe)(cod)]₂ (10.6 mg, 16 μmol), di-*tert*-butylbipyridyl (8.6 mg, 32 μmol), terrylene (60 mg, 0.16 mmol) and (Bpin)₂ (325 mg, 1.3 mmol) were added to a flask and dissolved in 1,4-dioxane (5 mL) under Ar. After bubbled with Ar for 10 min, the mixture was heated at 105 °C for 30 h and concentrated. Extracted with CH₂Cl₂ and washed with H₂O, dried over Na₂SO₄ and concentrated. The residue was dissolved with CH₂Cl₂ and passed through a pad of silica gel and reprecipitated with MeOH to afford **TB4** (78 mg, 56%). ^1H NMR (500 MHz, CDCl₃) δ 8.58 (s, 4H), 8.37 (s, 4H), 8.23 (s, 4H), 1.44 (s, 48H) ppm; ^{13}C NMR (126 MHz, CDCl₃) δ 136.60, 133.49, 131.50, 130.71, 130.53, 129.88, 127.02, 126.04, 121.61, 84.61, 25.28 ppm; HRMS (Spiral MALDI) m/z : [M]⁺ calcd for C₅₄H₆₀B₄O₈, 880.4686; found, 880.4687; UV–vis (toluene): λ_{max} (ϵ [10⁴ M^{−1} cm^{−1}]) = 489 (1.5), 524 (4.1) and 566 (7.2) nm; fluorescence (toluene): λ_{max} (λ_{ex} = 489 nm) = 576 and 622 nm.

Crystallographic data have been deposited with Cambridge Crystallographic Data Centre: Deposition number CCDC-1981465. Copies of the data can be obtained free of charge via <http://www.ccdc.cam.ac.uk/conts/retrieving.html>.

Synthesis of QB4. [Ir(OMe)(cod)]₂ (26.5 mg, 0.04 mmol), di-*tert*-butylbipyridyl (21.5 mg, 0.08 mmol), quaterylene (100 mg, 0.20 mmol) and (Bpin)₂ (609 mg, 2.4 mmol) was added to a flask and dissolved in 1,4-dioxane (2 mL) under Ar. After bubbled with Ar for 10 min, the mixture was heated at 105 °C for 38 h and concentrated. Extracted with CH₂Cl₂ and washed with H₂O, dried over Na₂SO₄ and concentrated. The residue was dissolved with CH₂Cl₂ and passed through a pad of silica gel. The combination of silica gel column chromatography and gel permeation column chromatography, followed by reprecipitation with MeOH afforded **QB4** (0.7 mg, 0.4%). ^1H NMR (500 MHz, CDCl₃) δ 8.63 (s, 4H), 8.44 (d, J = 8.5 Hz, 4H), 8.32 (d, J = 8.5 Hz, 4H), 8.25 (s, 4H), 1.44 (s, 48H) ppm; HRMS (Spiral MALDI) m/z : [M]⁺ calcd for C₆₄H₆₄B₄O₈, 1004.5003; found, 1004.5018; UV–vis (toluene): λ_{max} = 565, 610 and 668 nm.

Synthesis of TM4. TB4 (8.8 mg, 0.01 mmol), 2-bromomesitylene (7.2 μL , 0.08 mmol), Pd(PPh₃)₄ (4.6 mg, 4 μmol), Cs₂CO₃ (130 mg, 0.4 mmol) and CsF (61 mg, 0.4 mmol) were added to a flask. The atmosphere was exchanged by applying vacuum and backfilling with Ar (this process was conducted three times). Toluene (0.3 mL) and DMF (0.3 mL) were added to the flask and the resulting mixture was stirred at 110 °C for 24 h. Upon cooling to room temperature, the mixture was extracted with Et₂O, washed with H₂O, and evaporated. The residue was dissolved with CH₂Cl₂ and passed through a pad of silica gel, followed by reprecipitation with MeOH to afford **TM4** (4.9 mg, 58%). ^1H NMR (500 MHz, CDCl₃) δ 8.21 (s, 4H), 8.02 (s, 4H), 7.44 (s, 4H), 7.03 (s, 4H), 2.38 (s, 12H), 2.16 (s, 24H) ppm; ^{13}C NMR (126 MHz, CDCl₃) δ 139.83, 138.83, 137.13, 136.34, 135.49, 131.51, 130.83, 129.90, 128.35, 127.90, 126.22, 122.10, 121.59, 21.26, 21.15 ppm; HRMS (Spiral MALDI) m/z : [M]⁺ calcd for C₆₆H₅₆, 848.4377; found, 848.4377; UV–vis (toluene): λ_{max} (ϵ [10⁴ M^{−1} cm^{−1}]) = 493 (1.8), 528 (4.9) and 572 (8.6) nm; fluorescence (toluene): λ_{max} (λ_{ex} = 489 nm) = 583, 629 and 682 nm.

Supporting Information

Supporting Information File 1

Crystallographic information file (cif) for the **TB4** crystal.
[<https://www.beilstein-journals.org/bjoc/content/supplementary/1860-5397-16-58-S1.cif>]

Supporting Information File 2

^1H and ^{13}C NMR as well as MS spectra for newly synthesized compounds.
[<https://www.beilstein-journals.org/bjoc/content/supplementary/1860-5397-16-58-S2.pdf>]

Acknowledgements

We thank Ms Yoshiko Nishikawa (NAIST) for MS measurements.

Funding

This work was supported by the Japan Society for the Promotion of Science (JSPS) KAKENHI Grant Nos. JP18K14190 (H.H.), JP17H03042, JP19K22112 (N.A.) and CREST JST (no. JPMJCR15F1) (H.Y.).

ORCID® iDs

Hironobu Hayashi - <https://orcid.org/0000-0002-7872-3052>

Hiroko Yamada - <https://orcid.org/0000-0002-2138-5902>

Naoki Aratani - <https://orcid.org/0000-0002-3181-6526>

References

- Lee, S. K.; Zu, Y.; Herrmann, A.; Geerts, Y.; Müllen, K.; Bard, A. J. *J. Am. Chem. Soc.* **1999**, *121*, 3513–3520. doi:10.1021/ja984188m
- Langhals, H.; Christian, S.; Hofer, A. *J. Org. Chem.* **2013**, *78*, 9883–9891. doi:10.1021/jo401597u
- Langhals, H.; Zgela, D.; Lüling, R. *J. Org. Chem.* **2015**, *80*, 12146–12150. doi:10.1021/acs.joc.5b02092
- Liu, C.; Zhang, S.; Li, J.; Wei, J.; Müllen, K.; Yin, M. *Angew. Chem., Int. Ed.* **2019**, *58*, 1638–1642. doi:10.1002/anie.201810541
- Yuan, Z.; Lee, S.-L.; Chen, L.; Li, C.; Mali, K. S.; De Feyter, S.; Müllen, K. *Chem. – Eur. J.* **2013**, *19*, 11842–11846. doi:10.1002/chem.201302086
- Tam-Chang, S.-W.; Seo, W.; Iverson, I. K.; Casey, S. M. *Angew. Chem., Int. Ed.* **2003**, *42*, 897–900. doi:10.1002/anie.200390236
- Markiewicz, J. T.; Wudl, F. *ACS Appl. Mater. Interfaces* **2015**, *7*, 28063–28085. doi:10.1021/acsami.5b02243
- Avlasevich, Y.; Kohl, C.; Müllen, K. *J. Mater. Chem.* **2006**, *16*, 1053–1057. doi:10.1039/b516264e
- Thamatam, R.; Skraba, S. L.; Johnson, R. P. *Chem. Commun.* **2013**, *49*, 9122–9124. doi:10.1039/c3cc46270f
- Clar, E.; Kelly, W.; Laird, R. M. *Monatsh. Chem.* **1956**, *87*, 391–398. doi:10.1007/bf00902634
- Ott, R.; Zeschko, E.; Zinke, A. *Monatsh. Chem.* **1963**, *94*, 51–62. doi:10.1007/bf00900219
- Li, Y.; Gao, J.; Di Motta, S.; Negri, F.; Wang, Z. *J. Am. Chem. Soc.* **2010**, *132*, 4208–4213. doi:10.1021/ja100276x
- Qi, Q.; Burrezo, P. M.; Phan, H.; Herng, T. S.; Gopalakrishna, T. Y.; Zeng, W.; Ding, J.; Casado, J.; Wu, J. *Chem. – Eur. J.* **2017**, *23*, 7595–7606. doi:10.1002/chem.201701102
- Zeng, W.; Hong, Y.; Medina Rivero, S.; Kim, J.; Zafra, J. L.; Phan, H.; Gopalakrishna, T. Y.; Herng, T. S.; Ding, J.; Casado, J.; Kim, D.; Wu, J. *Chem. – Eur. J.* **2018**, *24*, 4944–4951. doi:10.1002/chem.201706041
- Zeng, W.; Phan, H.; Herng, T. S.; Gopalakrishna, T. Y.; Aratani, N.; Zeng, Z.; Yamada, H.; Ding, J.; Wu, J. *Chem* **2017**, *2*, 81–92. doi:10.1016/j.chempr.2016.12.001
- Geerts, Y.; Quante, H.; Platz, H.; Mahr, R.; Hopmeier, M.; Böhm, A.; Müllen, K. *J. Mater. Chem.* **1998**, *8*, 2357–2369. doi:10.1039/a804337j
- Former, C.; Becker, S.; Grimsdale, A. C.; Müllen, K. *Macromolecules* **2002**, *35*, 1576–1582. doi:10.1021/ma011724d
- Miletić, T.; Fermi, A.; Papadakis, I.; Orfanos, I.; Karampitsos, N.; Avramopoulos, A.; Demetri, N.; De Leo, F.; Pope, S. J. A.; Papadopoulos, M. G.; Couris, S.; Bonifazi, D. *Helv. Chim. Acta* **2017**, *100*, e1700192. doi:10.1002/hlca.201700192
- Bohnen, A.; Koch, K.-H.; Lüttke, W.; Müllen, K. *Angew. Chem., Int. Ed. Engl.* **1990**, *29*, 525–527. doi:10.1002/anie.199005251
- Koch, K.-H.; Müllen, K. *Chem. Ber.* **1991**, *124*, 2091–2100. doi:10.1002/cber.19911240935
- Matsumoto, A.; Suzuki, M.; Hayashi, H.; Kuzuhara, D.; Yuasa, J.; Kawai, T.; Aratani, N.; Yamada, H. *Chem. – Eur. J.* **2016**, *22*, 14462–14466. doi:10.1002/chem.201602188
- Ishiyama, T.; Miyaura, N. *J. Organomet. Chem.* **2003**, *680*, 3–11. doi:10.1016/s0022-328x(03)00176-1
- Cho, J.-Y.; Tse, M. K.; Holmes, D.; Maleczka, R. E., Jr.; Smith, M. R., III. *Science* **2002**, *295*, 305–308. doi:10.1126/science.1067074
- Ishiyama, T.; Takagi, J.; Ishida, K.; Miyaura, N.; Anastasi, N. R.; Hartwig, J. F. *J. Am. Chem. Soc.* **2002**, *124*, 390–391. doi:10.1021/ja0173019
- Ishiyama, T.; Takagi, J.; Hartwig, J. F.; Miyaura, N. *Angew. Chem., Int. Ed.* **2002**, *41*, 3056. doi:10.1002/1521-3773(20020816)41:16<3056::aid-anie3056>3.0.co;2-#
- Coventry, D. N.; Batsanov, A. S.; Goeta, A. E.; Howard, J. A. K.; Marder, T. B.; Perutz, R. N. *Chem. Commun.* **2005**, 2172–2174. doi:10.1039/b501778e
- Gaussian 09*, Revision B.01; Gaussian, Inc.: Wallingford, CT, 2010.
- Nakada, K.; Fujita, M.; Dresselhaus, G.; Dresselhaus, M. S. *Phys. Rev. B* **1996**, *54*, 17954–17961. doi:10.1103/physrevb.54.17954
- Son, Y.-W.; Cohen, M. L.; Louie, S. G. *Phys. Rev. Lett.* **2006**, *97*, 216803. doi:10.1103/physrevlett.97.216803
- Yang, L.; Park, C.-H.; Son, Y.-W.; Cohen, M. L.; Louie, S. G. *Phys. Rev. Lett.* **2007**, *99*, 186801. doi:10.1103/physrevlett.99.186801
- Zhang, H.; Lin, H.; Sun, K.; Chen, L.; Zagranyski, Y.; Aghdassi, N.; Duhm, S.; Li, Q.; Zhong, D.; Li, Y.; Müllen, K.; Fuchs, H.; Chi, L. *J. Am. Chem. Soc.* **2015**, *137*, 4022–4025. doi:10.1021/ja511995r
- Cai, Z.; She, L.; He, Y.; Wu, L.; Cai, L.; Zhong, D. *Macromol. Chem. Phys.* **2017**, *218*, 1700155. doi:10.1002/macp.201700155

License and Terms

This is an Open Access article under the terms of the Creative Commons Attribution License (<http://creativecommons.org/licenses/by/4.0>). Please note that the reuse, redistribution and reproduction in particular requires that the authors and source are credited.

The license is subject to the *Beilstein Journal of Organic Chemistry* terms and conditions: (<https://www.beilstein-journals.org/bjoc>)

The definitive version of this article is the electronic one which can be found at:
[doi:10.3762/bjoc.16.58](https://doi.org/10.3762/bjoc.16.58)



Synthesis of C₇₀-fragment buckybowls bearing alkoxy substituents

Yumi Yakiyama, Shota Hishikawa and Hidehiro Sakurai*

Full Research Paper

Open Access

Address:

Division of Applied Chemistry, Graduate School of Engineering,
Osaka University, 2-1 Yamadaoka, Suita, Osaka 565-0871, Japan

Email:

Hidehiro Sakurai* - hsakurai@chem.eng.osaka-u.ac.jp

* Corresponding author

Keywords:

buckybowl; C₇₀; rearrangement through C–H bond activation

Beilstein J. Org. Chem. **2020**, *16*, 681–690.

doi:10.3762/bjoc.16.66

Received: 12 February 2020

Accepted: 02 April 2020

Published: 15 April 2020

This article is part of the thematic issue "C–H functionalization for materials science".

Guest Editor: K. Itami

© 2020 Yakiyama et al.; licensee Beilstein-Institut.

License and terms: see end of document.

Abstract

Buckybowls bearing a C₇₀ fragment having two alkoxy groups were synthesized and their structural and optical properties were investigated by single crystal X-ray analysis and UV–vis spectroscopy. In the synthesis of dioxole derivative **5b**, the regioisomer **5c** was also produced. The yield of **5c** was increased by increasing the reaction temperature, indicating that the rearrangement might involve the equilibrium between the Pd(IV) intermediates through C–H bond activation.

Introduction

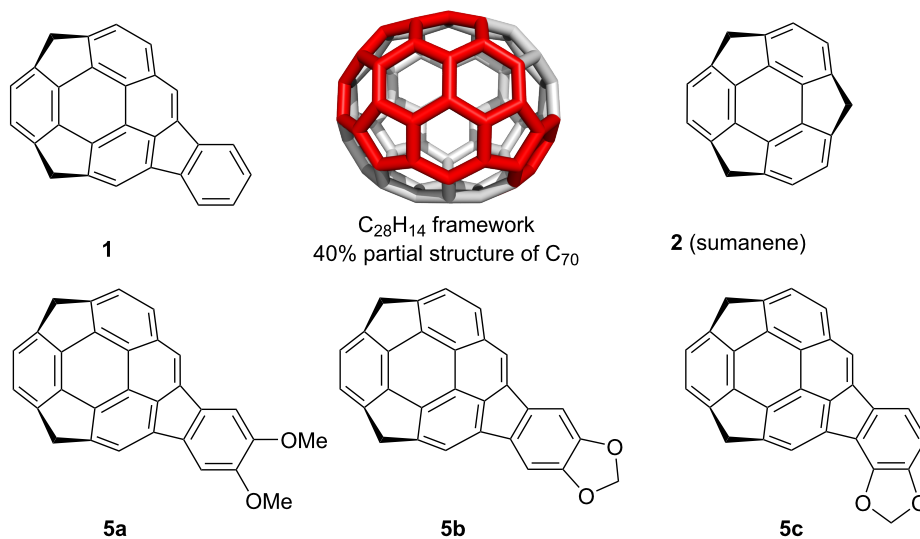
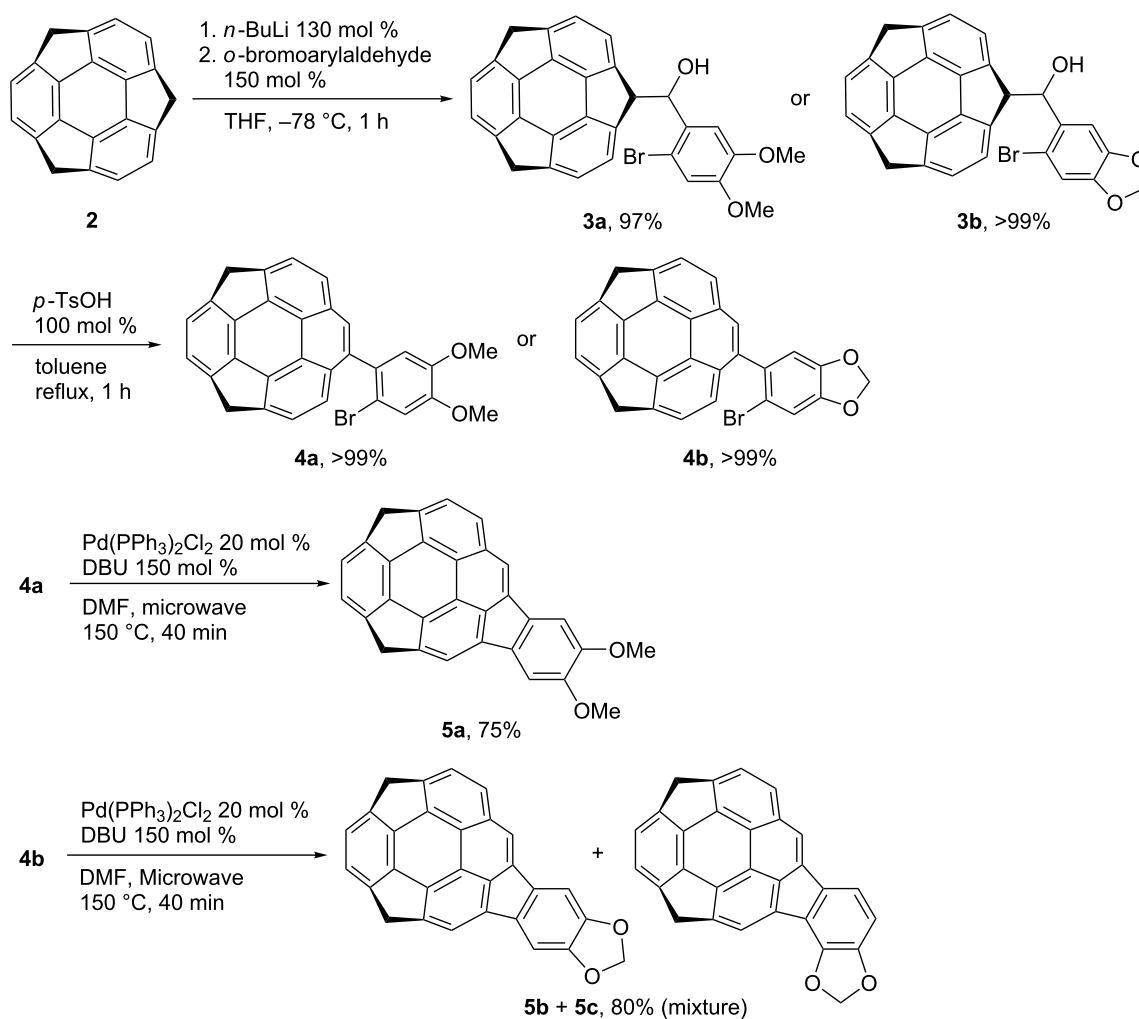
The study of buckybowls, the bowl-shaped π -conjugated aromatic hydrocarbons corresponding to the fragments of fullerenes, pioneered by the works on colannulene and sumanene, have been attracting great interests owing to their unique chemical and physical properties [1–8] and was extended to larger systems [9–17]. Among them, buckybowls having a C₇₀ fragment are expected to exhibit different properties from that with C₆₀ fragment because most of them consists of acene and/or pyrene units, which might give unique photochemical and electrochemical properties. Recently, we synthesized a buckybowl C₂₈H₁₄ **1**, which is corresponding to a 40% fragment of C₇₀, from C₆₀-fragment sumanene (**2**) in three steps via ring expansion by Wagner–Meerwein rearrangement, followed by Pd-catalyzed annulation (Figure 1) [18]. An UV–vis spectroscopy

study revealed that the electronic character of **1** rather resembled that of an indenopyrene moiety than that of benzopyrene. Our synthetic route allows to easily introduce substituents on the external aromatic ring of the indenopyrene using various types of *o*-bromo arylaldehydes. Related to our study on bucky-bowl-containing liquid crystals [19], we planned to introduce alkoxy groups on the **1** framework. Here, we report the synthesis and characterization of dimethoxy derivative **5a** and dioxole derivative **5b** together with an unexpected regioisomer **5c**.

Results and Discussion

Synthesis of dialkoxides **5a–c**

Dialkoxides **5a–c** were prepared according to the previous report on the synthesis of **1** (Scheme 1) [18,20]. The benzylic

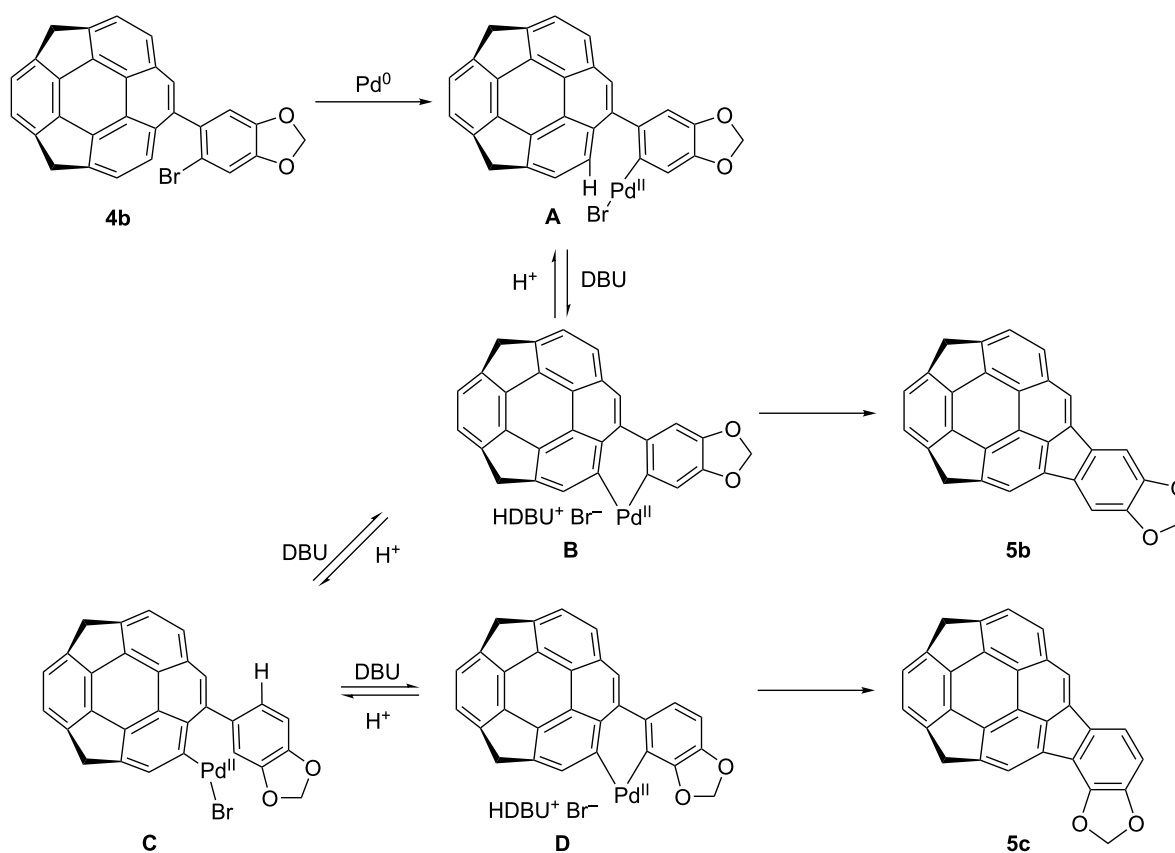
Figure 1: Structure of the target buckybowl **5a–c**.Scheme 1: Synthesis of dialkoxides **5a–c**.

carbanion generated by the addition of 130 mol % *n*-BuLi to **2** in THF at $-78\text{ }^{\circ}\text{C}$ was treated with 150 mol % of the corresponding arylaldehydes to afford **3a** and **3b** quantitatively. The Wagner–Meerwein rearrangement from **3a** and **3b** to **4a** and **4b** by 100 mol % of *p*-TsOH in toluene under reflux conditions also occurred quantitatively. The final cyclization of **4a** was carried out using 20 mol % of $\text{Pd}(\text{PPh}_3)_2\text{Cl}_2$ and 150 mol % DBU in DMF at $150\text{ }^{\circ}\text{C}$ under microwave irradiation conditions to afford the desired dimethoxy derivative **5a** in 75% yield. In contrast, when the reaction of **4b** was performed, not only the desired product **5b** but also the unexpected regioisomer **5c** was obtained. The temperature dependency of the product ratio between **5b** and **5c** was investigated and the results are shown in Table 1. The cyclization did not proceed under $140\text{ }^{\circ}\text{C}$, and at $140\text{ }^{\circ}\text{C}$ the total yield is low (41% after 40 min microwave irradiation) but the ratio of **5b** was the highest (**5b/5c** = 10:1). The reaction efficiency was high at $150\text{ }^{\circ}\text{C}$ to reach 80% total yield, and the ratio of **5b/5c** was 10:3. By increasing the temperature, the ratio of **5c** was increased although the total yield was decreased. It should be noted that the conversion between **5b** and **5c** under the same conditions was not observed.

Table 1: The change of **5b/5c** ratio in the product mixture at various temperatures.

reaction temp. ($^{\circ}\text{C}$)	yield (%)	5b/5c
140	41	10/1
150	80	10/3
160	67	10/4
170	77	10/5
180	50	10/7

The above results strongly suggested the existence of an equilibrium between the intermediates corresponding to products **5b** and **5c**. A possible mechanism is shown in Scheme 2 [21–25]. After the oxidative addition of **4b** to Pd^0 to generate intermediate **A**, the neutral palladium(II) intermediate **B** is formed. Two competitive processes, the reductive elimination from **B** to give the product **5b**, and the 1,5-palladium migration from **A** to **C** through **B**, might exist, and from **C**, after the bond rotation, the intermediate **D** would form to afford the isomer **5c**. The selectivity of these two processes are dependent on the temperature as shown in Table 1. It is assumed that the ring-rotation process, which generated the regioisomer did not occurred in case of **4a**



Scheme 2: Proposed mechanism of the formation of **5b** and **5c**.

because of two larger methoxy groups than the methylenedioxy group.

Crystal structures of **5a–c**

Single crystals of **5a–c** were successfully obtained by vapour diffusion method using CHCl_3 /hexane conditions. Figure 2 shows the crystal structure of **5a**. The crystal was obtained as a racemic compound containing a pair of two enantiomers defined by bowl chirality [26], as a result of the rapid bowl inversion under the crystallization conditions. **5a** formed a columnar structure with alternative stack in convex-to-concave manner along the *b* axis with the overlap of the half part of the bowl structure (Figure 2b). All the columns along the *a* axis possessed the same stacking direction, while the neighboring columns along the *c* axis were in opposite directions (Figure 2c). Although the relatively low diffraction data quality prohibited the detailed discussion about the interaction distances, both π – π ($\text{C9}\cdots\text{C14}$, $\text{C5}\cdots\text{C10}$) and $\text{CH}\cdots\pi$ ($\text{C11}\cdots\text{C11}$) interactions were confirmed within the column. These columns were further connected with the neighboring columns which possessed the same stacking direction (along the *a* axis) by $\text{CH}\cdots\pi$ interactions ($\text{C16}\cdots\text{C23}$, $\text{C16}\cdots\text{C19}$, $\text{C29}\cdots\text{C3}$, $\text{C29}\cdots\text{C15}$), while connected to the columns with opposite stacking direction via $\text{CH}\cdots\text{O}$ type weak hydrogen bonds ($\text{C13}\cdots\text{O1}$) along the *c* axis (Figure 2c).

5b also gave the mixture of the two enantiomers, however, they were disordered with 50% site occupancy (Figure 2a). The POAV (π -orbital axis vector) pyramidalization angle ϕ [27], which is often used for quantifying the curvature of curved π -conjugated materials (Figure 3a) showed 6.5° at C1 as the minimum value, and 7.6° at C3, which is surrounded by two

hexagonal rings and one pentagonal ring, as the maximum value, while the none-substituted **1** shows 6.2° and 7.6° , respectively (Table 2) [18]. Bowl depths, defined by the length of the perpendicular lines (Figure 3b, double-headed arrow) from its peripheral carbons to the bottom hexagonal ring's plane (Figure 3c, red coloured part) in **5b** were 0.80 – 0.84 Å from the peripheral benzylic carbons and 0.80 – 0.89 Å from the peripheral aromatic carbons, respectively, while 0.74 – 0.79 Å and 0.79 – 0.99 Å in **1**, respectively (Table 2) [18]. As observed in the crystal of **5a**, **5b** formed convex-to-concave type stacking columns along the *c* axis while the stacking mode was eclipsed manner, in which molecular skeletons were completely overlapped (Figure 4b,c). The stacking directions of the columns were alternatively changed along the *b* axis. Unlike **5a**, the stacking columns in **5b** were exclusively stabilized by $\text{CH}\cdots\pi$ interactions ($\text{C6}\cdots\text{C6}$: 3.77 Å, $\text{C9}\cdots\text{C9}$: 3.77 Å, $\text{C16}\cdots\text{C17}$: 3.51 Å) (Figure 4b). These columns were further connected to

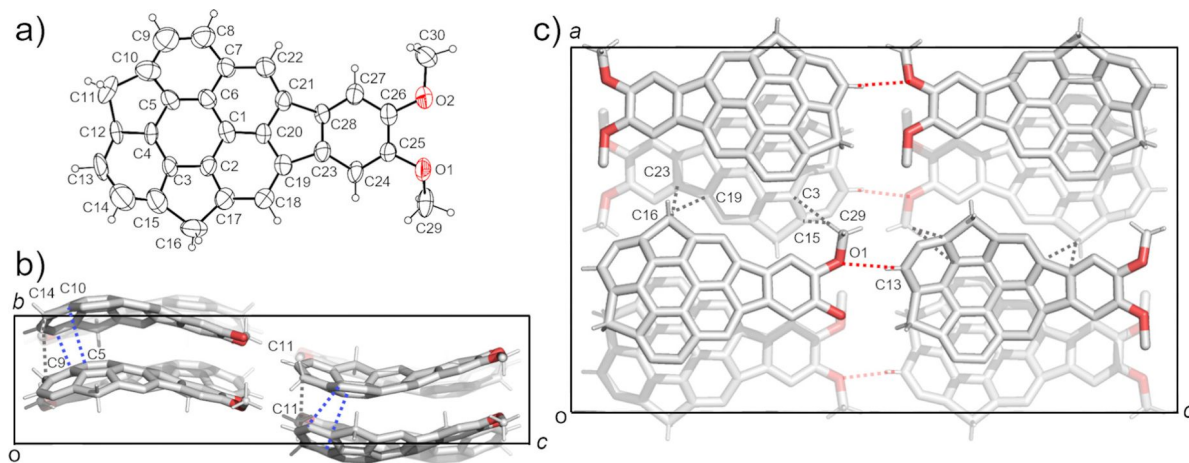
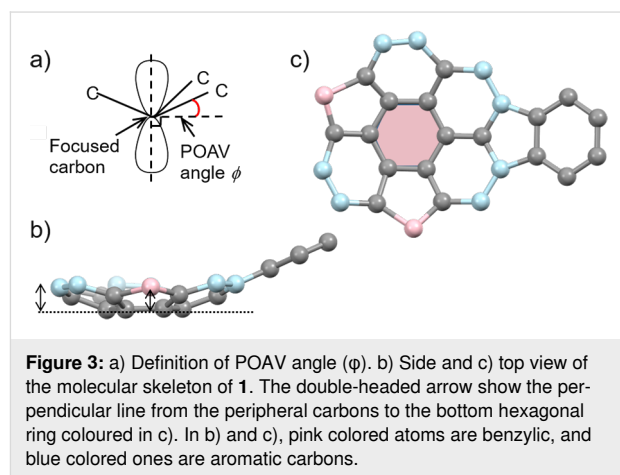


Figure 2: Crystal structure of **5a**. a) ORTEP drawing of the crystallographically independent unit with thermal ellipsoid at 50% probability b) Packing structure viewed from the *a* axis and c) from the *b* axis. The dotted lines indicate: blue: π – π , grey: $\text{CH}\cdots\pi$, red: $\text{CH}\cdots\text{O}$ interactions. In b) and c), hydrogen atoms which are not engaged in any interactions are omitted for clarity.

Table 2: Experimental POAV angles and bowl depths of **5b** at the specific focused carbons.

molecule		POAV angle $\varphi/^\circ$				bowl depth/ \AA				
						benzylic		aromatic		
5b	C1	6.5	C3b	7.6	C6	0.84	C6	0.81	C9	0.80
	C2	6.7	C4	7.3	C9	0.80	C7A	0.89	C11	0.89
	C3a	6.7					C8B	0.88	C12	0.84

^aCalculated using $\angle\text{C4-C3-C8A}$, $\angle\text{C8A-C3-C2}$, $\angle\text{C2-C3-C4}$; ^bcalculated using $\angle\text{C4-C3-C7B}$, $\angle\text{C7B-C3-C2}$, $\angle\text{C2-C3-C4}$.

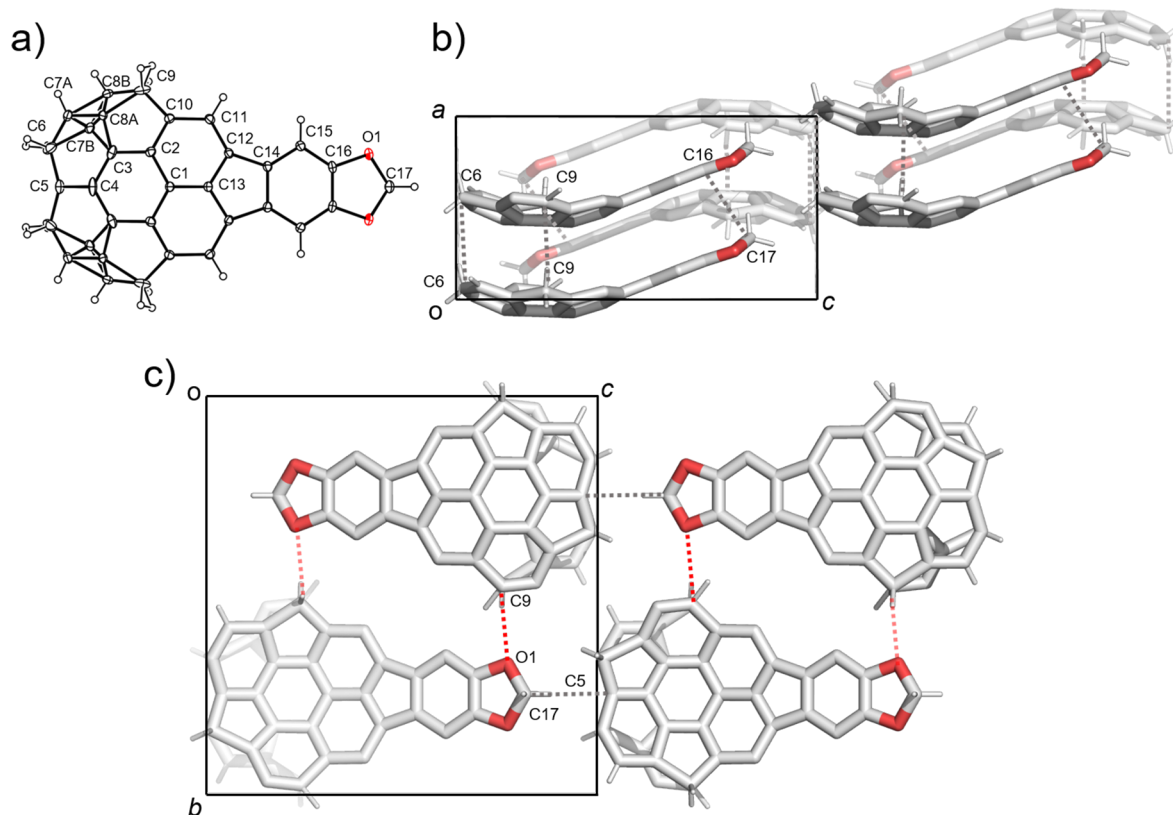


Figure 4: Crystal structure of **5b**. a) ORTEP drawing of the crystallographically independent unit with thermal ellipsoid at 50% probability. b) Packing structure viewed from the *b* axis and c) from the *a* axis. The dotted lines indicate; grey: CH... π , red: CH...O interactions. In b) and c), hydrogen atoms which are not engaged in any interactions and the contribution of the one enantiomer are omitted for clarity.

the neighboring columns by CH...O type hydrogen bonds (C9...O1: 3.32 \AA) along the *b* axis and CH... π interactions (C17...C5: 3.60 \AA) along the *c* axis (Figure 4c).

In the crystal structure of **5c**, two crystallographically independent units were observed (Figure 5a). **5c** also contained both of the enantiomers and formed a columnar structure along the *b* axis with the slipped stack manner, which was composed of only one side of the enantiomer (Figure 5b,c). The columns with the same stacking direction were arranged along the *a* axis,

while an alternative stacking direction was observed along the *c* axis. Although relatively low diffraction data quality prohibited the detailed discussion about the interaction distances, the stabilization of the 1-dimensional stacking column of **5c** by both π - π (C5...C44, C27...C54, C14...C44, C12...C43) and CH... π (C11...C42, C42...C9) was clearly observed (Figure 4b c). As found in the other two, the stacking columns in **5c** crystal were also further connected each other by both CH... π interaction (C58...C38, C37...C50) and CH...O type hydrogen bonds (C37...O1, C11...O2, C40...O4) (Figure 5c).

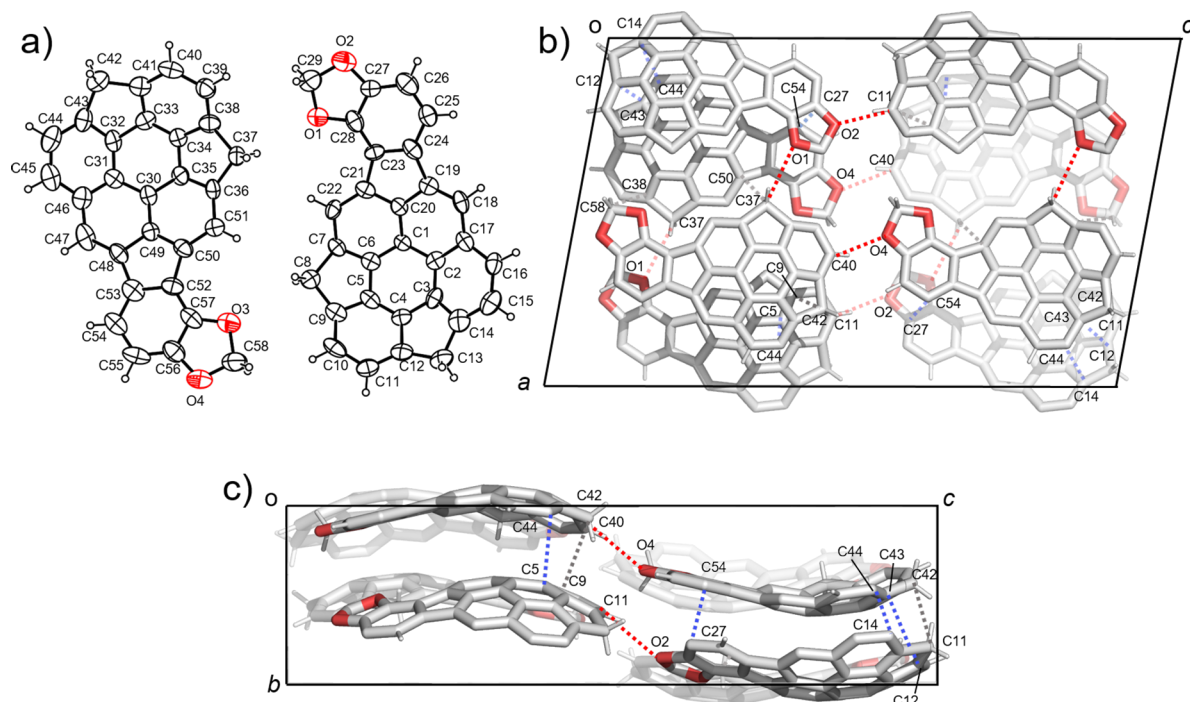


Figure 5: Crystal structure of **5c**. a) ORTEP drawing of the crystallographically independent unit with thermal ellipsoid at 50% probability b) Packing structure viewed from the *b* axis and c) from the *a* axis. The dotted lines indicate; blue: π - π , grey: $\text{CH}\cdots\pi$, red: $\text{CH}\cdots\text{O}$ interactions. In b) and c), hydrogen atoms which are not engaged in any interactions are omitted for clarity.

Photophysical properties of the dialkoxides were investigated by UV-vis and emission spectroscopies (Figure 6). UV-vis spectra of **5a** and **5b** well reflected the electric property of **1**,

showing two strong bands observed at around 280–300 nm and 330–350 nm, and a broad one at around 350–480 nm, which was attributable to the indenopyrene moiety of **1** (Figure 6a)

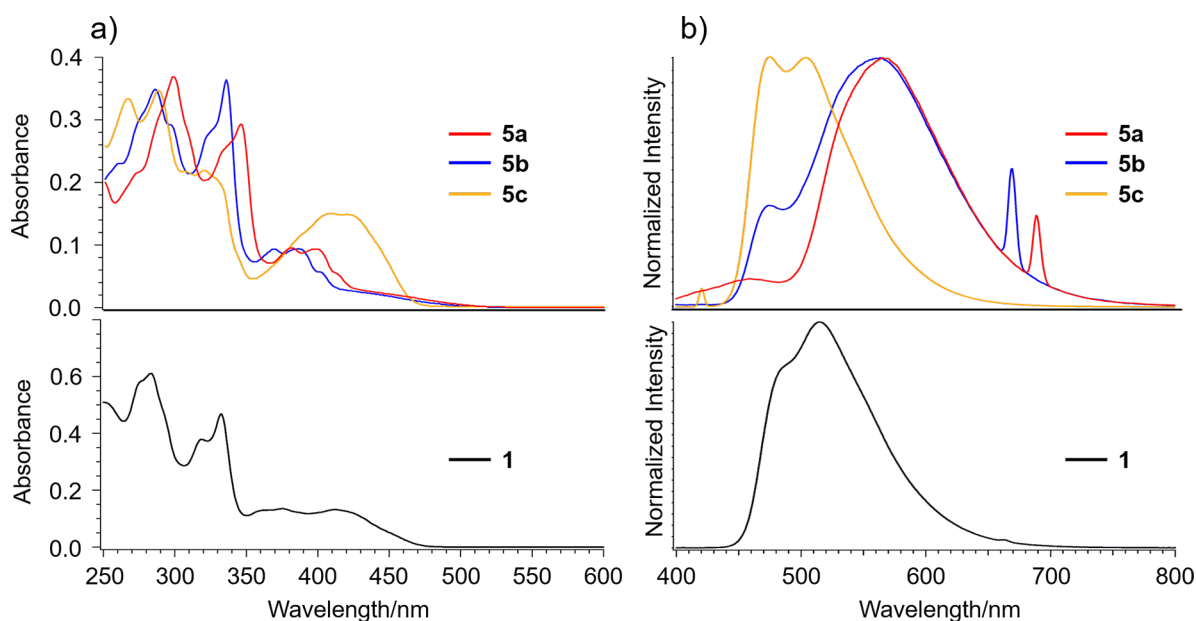


Figure 6: a) UV-vis spectra and b) emission spectra of **1** and dialkoxides **5a–c**. For all the spectra, the concentration was 1×10^{-5} M in CH_2Cl_2 . Excitation wavelength: 332 nm for **1**; 345 nm for **5a**; 335 nm for **5b**; 319 nm for **5c**.

[18]. Meanwhile, **5a** and **5b** showed emission bands at 564 nm and 566 nm, respectively, which were red shifted around 50 nm from that of **1**, clearly indicating the effect of the introduction of dialkoxides (Figure 6b). In contrast, **5c** exhibited different features in both UV–vis and emission spectra from the other two. In the UV–vis spectrum of **5c**, the splitted sharp absorptions at 266 and 287 nm and a broad band at 320 nm together with a relatively strong broad band at 409 nm are visible. The emission spectrum of **5c** was similar to that of **1** rather than those of **5a** and **5b**. These differences indicate the substitution position of the dialkoxides significantly affected the electric nature of the molecules even though **5a–c** possess the same molecular skeleton of **1**.

Conclusion

As described above, we succeeded in synthesizing three different alkoxy-substituted C₇₀-fragment buckybowls **5a–c**. In particular, **5c** was not an intended molecule, but was formed unexpectedly through the rearrangement through the Pd-catalyzed C–H bond activation reaction. The X-ray crystal structure analysis of **5a–c** clearly revealed their nature in the solid state to form a 1-dimensional columnar structure stabilised by π – π and/or CH $\cdots\pi$ interactions with full or partial overlap of the molecular skeleton as seen in the crystal structure of **1**, however, each packing fashion is different depending on the substituent. UV–vis and emission spectra of **5a–c** well showed the effect of the introduction of the dialkoxides onto the skeleton of **1**, in which the substitution position also contributed to their electric properties. These results give us a lot of suggestions for further investigations to design buckybowl-containing liquid crystals [19].

Experimental

General

All experiments with moisture- and air-sensitive compounds were performed in anhydrous solvents under nitrogen atmosphere in flame-dried glassware. All reagents were purchased from commercial sources and used without further purification unless otherwise noted. The microwave experiment was carried out with a Biotage Initiator Eight EXP. UV–vis absorption spectra were recorded on a JASCO V-670 spectrometer and a SHIMADZU UV-1800 spectrometer. Fluorescence spectra were recorded on a JASCO FP-6500 spectrometer. Melting points were determined on a Stanford Research Systems MPA 100 or a Yanako MP-500P apparatus and were uncorrected. Infrared (IR) spectra were recorded on a JASCO FT IR-4100 spectrometer using dispersed KBr pellets. ¹H and ¹³C NMR spectra were measured at 23 °C on a JEOL RESONANCE JNM-ECZ400S spectrometer at 400 MHz and 100 MHz, respectively. CDCl₃ was used as a solvent and the residual solvent peaks were used as an internal standard (¹H NMR: CDCl₃ 7.26 ppm; ¹³C NMR:

CDCl₃ 77.00 ppm). High-resolution fast atom bombardment (FAB) mass spectra were measured on a JEOL JMS-700 spectrometer. TLC analysis was performed using Merck silica gel 60 F₂₅₄, and the preparative TLC (PTLC) purification was conducted using Wakogel B-5F PTLC plates. Elemental analyses were measured on a J-Science Micro corder JM10 at the Analysis Center at Osaka University.

General experimental procedure for the addition reaction

In a similar manner as described in [18], to a solution of **2** (0.20 mmol) in dry THF (20 mL) was added dropwise *n*-BuLi in hexane solution (0.26 mmol) at –78 °C. After stirring for 10 min, to the reaction mixture was added arylaldehyde (0.30 mmol) at –78 °C. The mixture was stirred for 1 h, warmed up to room temperature and quenched by sat. NH₄Cl_{aq}. The resulting mixture was extracted with CH₂Cl₂. The extract was washed with brine, dried over anhydrous Na₂SO₄, filtered and concentrated under reduced pressure. The mixture was purified by PTLC (ethyl acetate/hexane = 3:2 for **3a**, ethyl acetate/hexane = 1:4 for **3b**) to afford **3**.

General experimental procedure for the rearrangement reaction

In a similar manner as described in [18], to the mixture of **3** (0.19 mmol) and *p*-toluenesulfonic acid (0.19 mmol) was added a dry toluene (20 mL). The mixture was refluxed with stirring for 1 h. After the addition of sat. NaHCO_{3aq}, the mixture was extracted with CH₂Cl₂. The extract was washed with brine, dried over anhydrous Na₂SO₄, filtered and concentrated under reduced pressure. The mixture was purified by PTLC (CH₂Cl₂/hexane = 4:1 for **4a**, CH₂Cl₂/hexane = 3:2 for **4b**) to afford **4**.

Preparation of dialkoxides by intramolecular coupling reaction

In a similar manner as described in [18], in a glove box to the microwave vial was added **4** (0.030 mmol), Pd(PPh₃)₂Cl₂ (6.0 μmol), and degassed DMF (3 mL) and prior sealing the vial DBU (6.7 μL, 0.045 mmol) and the mixture was stirred for 40 min at 150 °C using microwave. After the addition of ethyl acetate/hexane, the mixture was washed with water (3 times) and brine (3 times), dried over anhydrous Na₂SO₄, filtered and concentrated under reduced pressure. The mixture was purified by PTLC (only CH₂Cl₂ for **5a**, CH₂Cl₂/hexane = 1:3 for **5b** and **5c**) to afford both **5** as yellow solid.

Characterization data

3a: yellow solid; yield: 97% (98.3 mg (0.19 mmol) from 52.8 mg (0.20 mmol) of **2**). mp 133 °C; IR (KBr) ν : 3438, 3003, 2922, 2841, 1502, 1398, 1257, 1213, 1159, 1032, 798 cm^{–1}; ¹H NMR (CDCl₃) δ (ppm) 7.29 (s, 1H), 7.08 (s, 2H), 7.05 (s,

1H), 7.04 (d, $J = 8.0$ Hz, 1H), 7.00 (d, $J = 8.0$ Hz, 1H), 6.81 (d, $J = 7.6$ Hz, 1H), 6.68 (d, $J = 7.6$ Hz, 1H), 5.92 (dd, $J = 5.6$, 3.2 Hz, 1H), 4.67 (d, $J = 19.4$ Hz, 2H), 4.00 (d, $J = 5.6$ Hz, 1H), 3.90 (s, 3H), 3.86 (s, 3H), 3.39 (dd, $J = 19.4$, 4.8 Hz, 2H), 2.76 (d, $J = 3.6$ Hz, 1H); ^{13}C NMR (CDCl_3) δ (ppm) 150.00, 149.87, 148.97, 148.91, 148.86, 148.82, 148.76, 148.74, 148.64, 148.46, 147.91, 147.30, 133.58, 125.81, 124.18, 123.54, 123.46, 123.38, 115.10, 112.33, 111.05, 74.39, 61.75, 56.26, 41.85, 41.84; FAB MS m/z : [M^+] calcd for $\text{C}_{30}\text{H}_{21}\text{BrO}_3$, 508.0674; found, 508.0665.

3b: yellow solid; yield: >99% (148 mg (0.30 mmol) from 79.2 mg (0.30 mmol) of **2**). mp 133 °C; IR (KBr) ν : 3546, 3041, 3014, 2889, 1502, 1475, 1398, 1236, 1038, 931, 795 cm^{-1} ; ^1H NMR (CDCl_3) δ (ppm) 7.31 (s, 1H), 7.11 (s, 2H), 7.07 (s, 1H), 7.06 (d, $J = 7.6$ Hz, 1H), 7.05 (d, $J = 7.6$ Hz, 1H), 6.82 (d, $J = 7.6$ Hz, 1H), 6.79 (d, $J = 7.6$ Hz, 1H), 6.07 (d, $J = 1.6$ Hz, 1H), 6.04 (d, $J = 1.6$ Hz, 1H), 5.91 (dd, $J = 6.4$, 3.6 Hz, 1H), 4.70 (d, $J = 17.6$ Hz, 2H), 4.00 (d, $J = 6.4$ Hz, 1H), 3.41 (d, $J = 19.6$ Hz, 2H), 2.74 (d, $J = 3.6$ Hz, 1H); ^{13}C NMR (CDCl_3) δ (ppm) 149.94, 149.89, 148.86, 148.77, 148.73, 148.72, 148.62, 147.86, 147.79, 147.57, 147.40, 135.04, 125.71, 124.18, 123.45, 123.41, 113.00, 112.51, 108.37, 101.92, 74.54, 61.71, 41.82; FAB MS m/z : [M^+] calcd for $\text{C}_{29}\text{H}_{17}\text{BrO}_3$, 492.0361; found, 492.0364.

4a: yellow solid; yield: >99% (98.5 mg (0.19 mmol) from 98.3 mg (0.19 mmol) of **3a**). mp 186 °C; IR (KBr) ν : 3018, 2929, 2897, 2839, 1601, 1498, 1437, 1375, 1327, 1244, 1209, 1167, 1020, 791 cm^{-1} ; ^1H NMR (CDCl_3) δ (ppm) 7.92 (d, $J = 4.0$ Hz, 2H), 7.85 (d, $J = 8.0$ Hz, 1H), 7.83 (s, 1H), 7.54 (s, 2H), 7.53 (d, $J = 8.0$ Hz, 1H), 7.25 (d, $J = 4.0$ Hz, 1H), 7.02 (s, 1H), 4.35–4.52 (m, 4H), 4.00 (s, 3H), 3.86 (s, 3H); ^{13}C NMR (CDCl_3) δ (ppm) 149.21, 148.40, 143.94, 143.89, 143.74, 141.20, 141.11, 140.62, 140.46, 139.13, 133.43, 130.55, 130.33, 127.58, 125.81, 125.58, 124.39, 124.20, 124.11, 124.02, 123.23, 115.68, 114.67, 114.31, 56.45, 56.26, 42.14, 42.03; FAB MS m/z : [M^+] calcd for $\text{C}_{30}\text{H}_{19}\text{BrO}_2$, 490.0568; found, 490.0569.

4b: yellow solid; yield: >99% (86.0 mg (0.17 mmol) from 81.6 mg (0.17 mmol) of **3b**). mp 124 °C; IR (KBr) ν : 3026, 2897, 1469, 1383, 1223, 1043, 930, 796 cm^{-1} ; ^1H NMR (CDCl_3) δ (ppm) 7.88 (s, 2H), 7.86 (d, $J = 8.0$ Hz, 1H), 7.82 (s, 1H), 7.59 (d, $J = 8.0$ Hz, 1H), 7.49 (s, 2H), 7.31 (s, 1H), 7.03 (s, 1H), 6.12 (s, 1H), 6.11 (s, 1H), 4.46 (d, $J = 20.2$ Hz, 2H), 4.28 (d, $J = 20.2$ Hz, 2H); ^{13}C NMR (CDCl_3) δ (ppm) 148.17, 147.48, 143.91, 143.87, 143.73, 141.14, 141.10, 141.04, 141.01, 140.56, 140.37, 139.07, 134.48, 130.49, 130.22, 127.62, 125.75, 125.54, 124.33, 124.14, 124.06, 123.97, 123.06, 114.94, 113.04, 111.85, 102.10, 53.61, 42.10, 41.99; FAB MS m/z : [M^+] calcd for $\text{C}_{29}\text{H}_{15}\text{BrO}_2$, 474.0255; found, 474.0258.

5a: yellow solid; yield: 75% (4.9 mg (11.9 μmol) from 7.8 mg (15.9 μmol) of **4a**). mp 281 °C (dec.); IR (KBr) ν : 2929, 2889, 2831, 1606, 1473, 1392, 1290, 1205, 1163, 1053, 858, 783 cm^{-1} ; ^1H NMR (CDCl_3) δ (ppm) 8.16 (s, 1H), 7.98 (s, 1H), 7.93 (d, $J = 8.0$ Hz, 1H), 7.81 (d, $J = 8.0$ Hz, 1H), 7.57 (s, 1H), 7.47 (s, 1H), 7.39 (d, $J = 7.6$ Hz, 1H), 7.34 (d, $J = 7.6$ Hz, 1H), 4.36 (s, 2H), 4.29 (s, 2H), 4.06 (s, 6H); ^{13}C NMR (CDCl_3) δ (ppm) 149.65, 148.38, 148.32, 147.55, 146.49, 146.01, 144.38, 143.85, 142.90, 138.02, 135.45, 135.32, 134.48, 132.17, 127.44, 127.06, 126.66, 124.92, 124.15, 122.85, 120.67, 118.06, 106.01, 104.79, 56.41, 42.77, 41.67; anal. calcd for $\text{C}_{30}\text{H}_{18}\text{O}_2(\text{H}_2\text{O})_{0.5}$: C, 85.90%; H, 4.57%; found: C, 85.75%; H, 4.92%.

5b: yellow solid; yield: 80% (6.3 mg (16.0 μmol) from 7.9 mg (20.0 μmol) of **4b**). mp 270 °C (dec.); IR (KBr) ν : 3041, 3006, 2920, 2887, 1460, 1390, 1286, 1159, 1038, 943, 850, 785 cm^{-1} ; ^1H NMR (CDCl_3) δ (ppm) 8.12 (s, 1H), 7.93 (s, 1H), 7.92 (d, $J = 8.0$ Hz, 1H), 7.80 (d, $J = 8.0$ Hz, 1H), 7.48 (s, 1H), 7.39 (s, 1H), 7.38 (d, $J = 7.2$ Hz, 1H), 7.33 (d, $J = 7.2$ Hz, 1H), 6.07 (s, 2H), 4.34 (s, 2H), 4.28 (s, 2H); ^{13}C NMR (CDCl_3) δ (ppm) 148.32, 148.14, 146.93, 146.53, 146.13, 144.39, 144.34, 143.94, 142.86, 137.59, 136.96, 135.21, 135.01, 134.36, 133.59, 127.39, 127.17, 126.55, 124.94, 124.15, 122.87, 120.94, 118.16, 103.56, 102.51, 101.60, 42.75, 41.66; anal. calcd for $\text{C}_{29}\text{H}_{14}\text{O}_2(\text{H}_2\text{O})_{0.4}$: C, 86.73%; H, 3.71%; found: C, 86.74%; H, 3.55%.

5c: yellow solid; yield: 80% (as 10:3 mixture with **5b** (reaction temp. 150 °C)). mp 267 °C (dec.); IR (KBr) ν : 2877, 1647, 1469, 1429, 1236, 1097, 1047, 933, 802 cm^{-1} ; ^1H NMR (CDCl_3) δ (ppm) 8.14 (s, 1H), 8.09 (s, 1H), 7.91 (d, $J = 8.0$ Hz, 1H), 7.81 (d, $J = 8.0$ Hz, 1H), 7.54 (d, $J = 8.0$ Hz, 1H), 7.40 (d, $J = 8.0$ Hz, 1H), 7.36 (d, $J = 8.0$ Hz, 1H), 6.82 (d, $J = 8.0$ Hz, 1H), 6.17 (s, 2H), 4.36 (s, 2H), 4.29 (s, 2H); ^{13}C NMR (CDCl_3) δ (ppm) 148.56, 148.06, 146.54, 146.49, 145.77, 144.46, 144.15, 144.05, 142.86, 142.32, 139.70, 137.81, 135.70, 134.69, 134.47, 131.71, 127.37, 126.88, 126.61, 124.96, 124.13, 123.19, 120.68, 120.60, 115.81, 105.84, 101.66, 42.74, 41.70; anal. calcd for $\text{C}_{29}\text{H}_{14}\text{O}_2(\text{H}_2\text{O})_{0.4}$: C, 86.73%; H, 3.71%; found: C, 86.58%; H, 3.50%.

Single crystal X-ray analysis

The diffraction data for **5a** and **5c** were collected on a Rigaku FR-E Superbright rotating-anode X-ray source with a Mo-target ($\lambda = 0.71073$ Å) equipped with a Rigaku RAXIS VII imaging plate as the detector at 150 K in house. The diffraction images processing and absorption correction were performed by using RIGAKU RAPID AUTO [28].

The diffraction data for **5b** was recorded on an ADSC Q210 CCD area detector with a synchrotron radiation ($\lambda = 0.70000$ Å)

at 2D beamline in Pohang Accelerator Laboratory (PAL). The diffraction images were processed by using HKL3000 [29]. Absorption correction was performed with the program PLATON.

All the structures were solved by direct methods (SHELXT-2014, 2015 [30] (for **5a**, **5b**) or XS [31] (for **5c**)) and refined by full-matrix least squares calculations on F^2 (SHELXL-2015) [32] using the Olex2 program package [33].

5a: C₃₀H₁₈O₂, orthorhombic, space group *pbca* (No. 61), $a = 17.382(4)$ Å, $b = 7.290(2)$ Å, $c = 28.978(6)$ Å, $V = 3672(1)$ Å³, $\rho_{\text{calcd}} = 1.485$ g/cm³, $Z = 8$, 925 unique reflections out of 4205 with $I > 2\sigma(I)$, 291 parameters, $3.65^\circ < \theta < 15.71^\circ$, $R_1 = 0.1319$, $wR_2 = 0.2925$, GOF = 0.903.

5b: C_{14.5}H₇O, monoclinic, space group *P2₁/m* (No. 11), $a = 3.7712(7)$ Å, $b = 15.097(3)$ Å, $c = 14.845(3)$ Å, $\beta = 113.312(3)^\circ$, $V = 845.1(3)$ Å³, $\rho_{\text{calcd}} = 1.550$ g/cm³, $Z = 4$, 2296 unique reflections out of 2458 with $I > 2\sigma(I)$, 166 parameters, $1.92^\circ < \theta < 30.03^\circ$, $R_1 = 0.0718$, $wR_2 = 0.2346$, GOF = 1.153.

5c: C₂₉H₁₄O₂, monoclinic, space group *P2₁/c* (No. 14), $a = 17.274(4)$ Å, $b = 7.441(2)$ Å, $c = 27.913(6)$ Å, $\beta = 90.85(3)^\circ$, $V = 3526(1)$ Å³, $\rho_{\text{calcd}} = 1.486$ g/cm³, $Z = 4$, 2351 unique reflections out of 7995 with $I > 2\sigma(I)$, 253 parameters, $3.03^\circ < \theta < 27.37^\circ$, $R_1 = 0.1217$, $wR_2 = 0.1498$, GOF = 1.000.

CCDC 1981719 (**5a**), 1981720 (**5b**) and 1981721 (**5c**) contain the crystallographic data for this paper. These data can be obtained free of charge from The Cambridge Crystallographic Data Centre (<https://www.ccdc.cam.ac.uk/>).

Supporting Information

Supporting Information File 1

CIF files of compounds **5a–c**.

[<https://www.beilstein-journals.org/bjoc/content/supplementary/1860-5397-16-66-S1.zip>]

Supporting Information File 2

¹H and ¹³C NMR data of **3a**, **3b**, **4a**, **4b** and **5a–c**, simulated UV–vis spectra of **5a**, **5b** and **5c**.

[<https://www.beilstein-journals.org/bjoc/content/supplementary/1860-5397-16-66-S2.pdf>]

Funding

This work was supported by a Grant-in-Aid for Scientific Research on Innovative Area “ π Space Figuration” from MEXT

(No. JP26102002), and JSPS KAKENHI (19H00912). The X-ray diffraction study of **5b** with synchrotron radiation was performed at the Pohang Accelerator Laboratory (Beamline 2D) supported by POSTECH.

ORCID® iDs

Yumi Yakiyama - <https://orcid.org/0000-0003-4278-2015>

Hidehiro Sakurai - <https://orcid.org/0000-0001-5783-4151>

Preprint

A non-peer-reviewed version of this article has been previously published as a preprint doi:10.3762/bxiv.2020.18.v1

References

- Wu, Y.-T.; Siegel, J. S. *Chem. Rev.* **2006**, *106*, 4843–4867. doi:10.1021/cr050554q
- Tsefrikas, V. M.; Scott, L. T. *Chem. Rev.* **2006**, *106*, 4868–4884. doi:10.1021/cr050553y
- Amaya, T.; Hirao, T. *Chem. Commun.* **2011**, *47*, 10524–10535. doi:10.1039/c1cc12532j
- Sygula, A. *Eur. J. Org. Chem.* **2011**, 1611–1625. doi:10.1002/ejoc.201001585
- Higashibayashi, S.; Sakurai, H. *Chem. Lett.* **2011**, *40*, 122–128. doi:10.1246/cl.2011.122
- Schmidt, B. M.; Lentz, D. *Chem. Lett.* **2014**, *43*, 171–177. doi:10.1246/cl.130984
- Saito, M.; Shinokubo, H.; Sakurai, H. *Mater. Chem. Front.* **2018**, *2*, 635–661. doi:10.1039/c7qm00593h
- Nestoros, E.; Stuparu, M. C. *Chem. Commun.* **2018**, *54*, 6503–6519. doi:10.1039/c8cc02179a
- Scott, L. T. *Angew. Chem., Int. Ed.* **2004**, *43*, 4994–5007. doi:10.1002/anie.200400661
- Jackson, E. A.; Steinberg, B. D.; Bancu, M.; Wakamiya, A.; Scott, L. T. *J. Am. Chem. Soc.* **2007**, *129*, 484–485. doi:10.1021/ja067487h
- Amaya, T.; Nakata, T.; Hirao, T. *J. Am. Chem. Soc.* **2009**, *131*, 10810–10811. doi:10.1021/ja9031693
- Wu, T.-C.; Hsin, H.-J.; Kuo, M.-Y.; Li, C.-H.; Wu, Y.-T. *J. Am. Chem. Soc.* **2011**, *133*, 16319–16321. doi:10.1021/ja2067725
- Wu, T.-C.; Chen, M.-K.; Lee, Y.-W.; Kuo, M.-Y.; Wu, Y.-T. *Angew. Chem., Int. Ed.* **2013**, *52*, 1289–1293. doi:10.1002/anie.201208200
- Chen, M.-K.; Hsin, H.-J.; Wu, T.-C.; Kang, B.-Y.; Lee, Y.-W.; Kuo, M.-Y.; Wu, Y.-T. *Chem. – Eur. J.* **2014**, *20*, 598–608. doi:10.1002/chem.201303357
- Amaya, T.; Ito, T.; Hirao, T. *Angew. Chem., Int. Ed.* **2015**, *54*, 5483–5487. doi:10.1002/anie.201500548
- Liu, J.; Osella, S.; Ma, J.; Berger, R.; Beljonne, D.; Schollmeyer, D.; Feng, X.; Müllen, K. *J. Am. Chem. Soc.* **2016**, *138*, 8364–8367. doi:10.1021/jacs.6b04426
- Tian, X.; Roch, L. M.; Baldrige, K. K.; Siegel, J. S. *Eur. J. Org. Chem.* **2017**, 2801–2805. doi:10.1002/ejoc.201700606
- Hishikawa, S.; Okabe, Y.; Tsuruoka, R.; Higashibayashi, S.; Ohtsu, H.; Kawano, M.; Yakiyama, Y.; Sakurai, H. *Chem. Lett.* **2017**, *46*, 1556–1559. doi:10.1246/cl.170612
- Shoji, Y.; Kajitani, T.; Ishiwari, F.; Ding, Q.; Sato, H.; Anetai, H.; Akutagawa, T.; Sakurai, H.; Fukushima, T. *Chem. Sci.* **2017**, *8*, 8405–8410. doi:10.1039/c7sc03860g

20. Bavin, P. M. G. *Can. J. Chem.* **1959**, *37*, 2023–2030.
doi:10.1139/v59-294
21. Mota, A. J.; Dedieu, A.; Bour, C.; Suffert, J. *J. Am. Chem. Soc.* **2005**, *127*, 7171–7182. doi:10.1021/ja050453+
22. Mota, A. J.; Dedieu, A. *Organometallics* **2006**, *25*, 3130–3142.
doi:10.1021/om060128a
23. Mota, A. J.; Dedieu, A. *J. Org. Chem.* **2007**, *72*, 9669–9678.
doi:10.1021/jo701701s
24. Misawa, N.; Tsuda, T.; Shintani, R.; Yamashita, K.; Nozaki, K.
Chem. – Asian J. **2018**, *13*, 2566–2572. doi:10.1002/asia.201800603
25. The authors acknowledge the referee for the suggestion about the reaction mechanism.
26. Kanagaraj, K.; Lin, K.; Wu, W.; Gao, G.; Zhong, Z.; Su, D.; Yang, C.
Symmetry **2017**, *9*, 174. doi:10.3390/sym9090174
27. Haddon, R. C. *J. Am. Chem. Soc.* **1987**, *109*, 1676–1685.
doi:10.1021/ja00240a013
28. *RAPID-AUTO*; Rigaku Corporation: Tokyo, Japan, 2001.
29. Minor, W.; Cymborowski, M.; Otwinowski, Z.; Chruszcz, M.
Acta Crystallogr., Sect. D: Biol. Crystallogr. **2006**, *62*, 859–866.
doi:10.1107/s0907444906019949
30. Sheldrick, G. M. *Acta Crystallogr., Sect. A: Found. Adv.* **2015**, *71*, 3–8.
doi:10.1107/s2053273314026370
31. *SHELXTL*; Bruker AXS Inc.: Madison, Wisconsin, USA, 2012.
32. Sheldrick, G. M. *Acta Crystallogr., Sect. C: Struct. Chem.* **2015**, *71*, 3–8. doi:10.1107/s2053229614024218
33. Dolomanov, O. V.; Bourhis, L. J.; Gildea, R. J.; Howard, J. A. K.; Puschmann, H. *J. Appl. Crystallogr.* **2009**, *42*, 339–341.
doi:10.1107/s0021889808042726

License and Terms

This is an Open Access article under the terms of the Creative Commons Attribution License (<http://creativecommons.org/licenses/by/4.0>). Please note that the reuse, redistribution and reproduction in particular requires that the authors and source are credited.

The license is subject to the *Beilstein Journal of Organic Chemistry* terms and conditions: (<https://www.beilstein-journals.org/bjoc>)

The definitive version of this article is the electronic one which can be found at:
[doi:10.3762/bjoc.16.66](https://doi.org/10.3762/bjoc.16.66)



One-pot synthesis of dicyclopenta-fused peropyrene via a fourfold alkyne annulation

Ji Ma¹, Yubin Fu¹, Junzhi Liu^{*2} and Xinliang Feng^{*1}

Letter

Open Access

Address:

¹Center for Advancing Electronics Dresden (cfaed) & Faculty of Chemistry and Food Chemistry, Technische Universität Dresden, 01062 Dresden, Germany and ²Department of Chemistry and State Key Laboratory of Synthetic Chemistry, The University of Hong Kong, Pokfulam Road, Hong Kong, China

Email:

Junzhi Liu^{*} - juliu@hku.hk; Xinliang Feng^{*} - xinliang.feng@tu-dresden.de

^{*} Corresponding author

Keywords:

alkyne annulation; cyclopenta-fused polycyclic aromatic hydrocarbons; nonplanarity; peropyrene; regioselectivity

Beilstein J. Org. Chem. **2020**, *16*, 791–797.

doi:10.3762/bjoc.16.72

Received: 19 February 2020

Accepted: 04 April 2020

Published: 20 April 2020

This article is part of the thematic issue "C–H functionalization for materials science".

Guest Editor: K. Itami

© 2020 Ma et al.; licensee Beilstein-Institut.

License and terms: see end of document.

Abstract

A novel dicyclopenta-fused peropyrene derivative **1** was synthesized via a palladium-catalyzed four-fold alkyne annulation of 1,3,6,8-tetrabromo-2,7-diphenylpyrene (**5**) with diphenylacetylene. The annulative π -extension reaction toward **1** involved a twofold [3 + 2] cyclopentannulation and subsequent twofold [4 + 2] benzannulation. The structure of **1** is unambiguously confirmed by X-ray crystallography; **1** adopted a twisted geometry due to the steric hindrance of the phenyl rings and the hydrogen substituents at the bay regions. Notably, compound **1** exhibits a narrow energy gap (1.78 eV) and a lower LUMO energy level than the parent peropyrene without the fusion of the five-membered rings. In addition, the effects of the *peri*-fused pentagons on the aromaticity and molecular orbitals of **1** were evaluated by theoretical calculations. This work presents an efficient method to develop π -extended aromatic hydrocarbons with cyclopenta moieties.

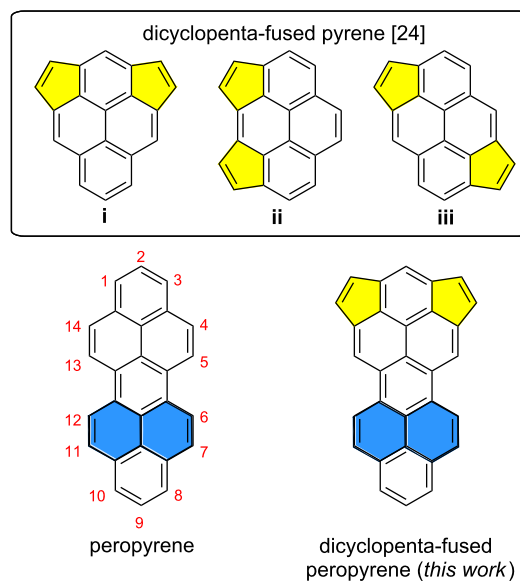
Introduction

Significant efforts have been recently devoted to the synthesis of nonalternant cyclopenta-fused polycyclic aromatic hydrocarbons (CP-PAHs), which represent the topological subunits of fullerenes and exhibit high chemical, physical and biological activities [1–10]. Thanks to development in organic synthetic methodology, CP-PAHs with peripheral pentagons could be realized [11–17]. Among them, the cyclopenta-fused pyrenes

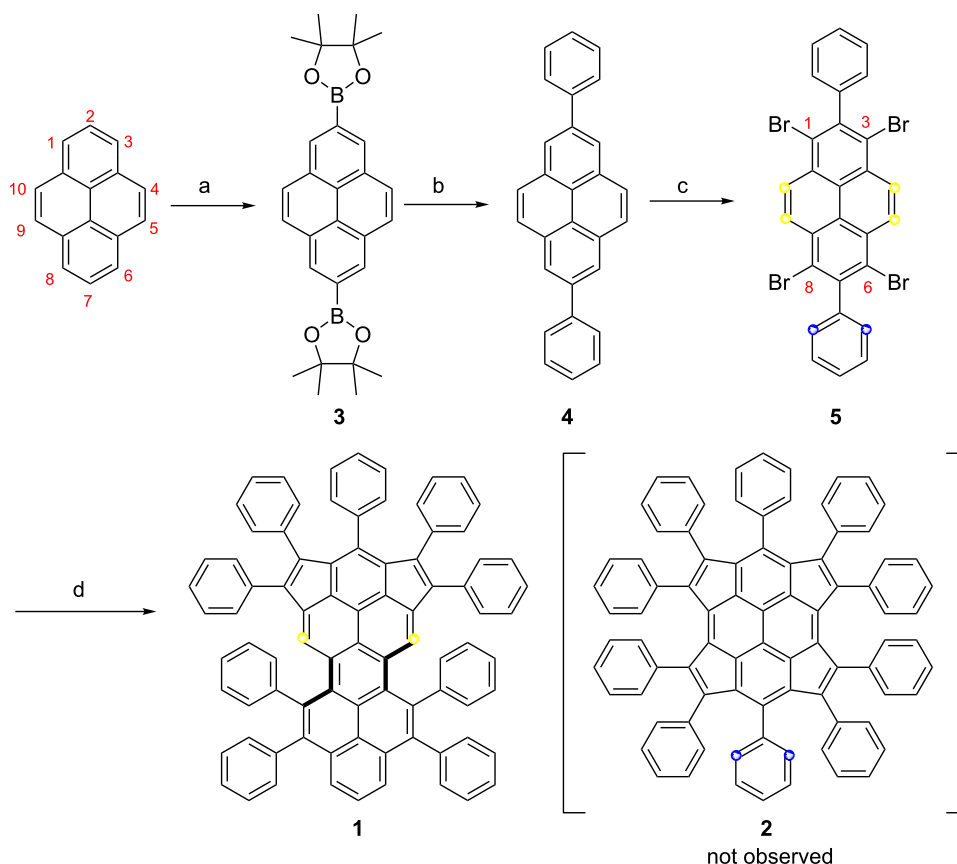
are an important class of CP-PAHs owing to their unique physical and photophysical properties, such as high electron affinities and anomalous fluorescence [17–20]. However, the reported synthetic methods towards the (di-)cyclopenta-fused pyrene congeners (**i–iii**, Scheme 1) have mainly been reliant on the flash vacuum pyrolysis of suitable precursors under harsh conditions ($T \geq 900$ °C), which resulted in relatively low yields

[21–24]. Palladium-catalyzed annulation has been recently proven as an efficient route to get access to aromatic hydrocarbons with *peri*-fused five-membered rings [25–27]. For instance, the dicyclopenta-fused pyrene derivatives **ii** and **iii** (Scheme 1) were successfully synthesized through palladium-catalyzed carbannulation of brominated pyrene with arylacetynes in good yield [28,29]. However, the larger CP-PAHs beyond the pyrene core, or its extended analogs [30] remain elusive. Peropyrene (Scheme 1), as the higher homolog of pyrene, has recently attracted attention because of its promising applications in optoelectronics, e.g., for singlet fission materials [31–33]. However, the synthesis of cyclopenta-fused aromatics based on peropyrene has never been achieved due to the lack of suitable synthetic protocols.

In this work, while aiming at the synthesis of the novel tetracyclopenta-fused pyrene derivative **2** through the quadruple annulation of 1,3,6,8-tetrabromo-2,7-diphenylpyrene (**5**) with 1,2-diphenylethyne, an unprecedented dicyclopenta-fused peropyrene congener **1** was obtained (Scheme 2). Interestingly, from the single-crystal analysis, compound **1** shows slight twisting of the



Scheme 1: Chemical structures of dicyclopenta-fused pyrene derivatives **i–iii**, peropyrene and the dicyclopenta-fused peropyrene reported in this work.



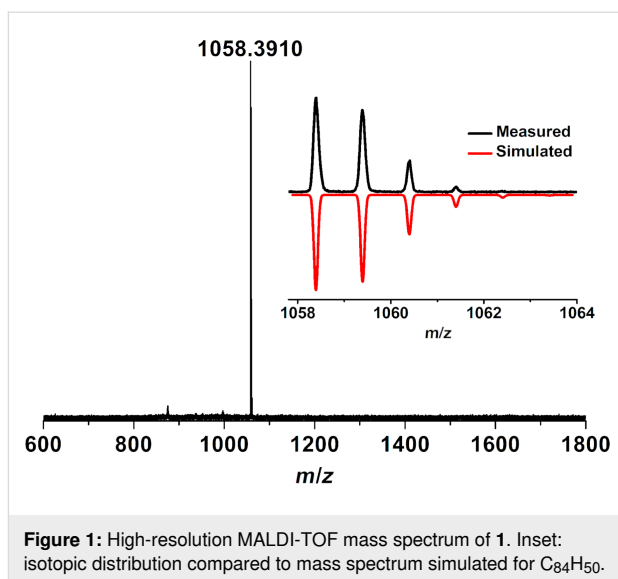
Scheme 2: Synthetic route towards compound **1**. a) B_2pin_2 , dtbpy, $[Ir(OMe)cod]_2$, cyclohexane, 70 °C, 20 h, 67%; b) $Pd(PPh_3)_4$, bromobenzene, Na_2CO_3 , toluene/EtOH/ H_2O , Aliquit 336, 90 °C, 48 h, 77%; c) Br_2 , nitrobenzene, 120 °C, 5 h, 86%; d) 1,2-diphenylethyne, $Pd_2(dba)_3$, $P(o-tol)_3$, KOAc, LiCl, DMF, 130 °C, microwave, 6 h, 5%.

peropyrene core with an overall end-to-end twist angle of 21.4° as a result of the steric repulsion at the bay positions. Compared to the parent peropyrene, the pentagon-annulated derivative **1** possesses a narrow optical energy gap (1.78 eV) and displays an efficient highest occupied molecular orbital (HOMO)–lowest unoccupied molecular orbital (LUMO) separation.

Results and Discussion

The synthesis of compound **1** is depicted in Scheme 2. Firstly, 2,7-bis(Bpin)pyrene (**3**) was prepared using an iridium-catalyzed borylation of pyrene (67% yield). Then, 2,7-diphenylpyrene (**4**) was obtained by Suzuki cross-coupling of **3** and bromobenzene in 77% yield. After that, the selective bromination of **4** with 4.4 equiv of bromine in nitrobenzene solution at 120°C afforded 1,3,6,8-tetrabromo-2,7-diphenylpyrene (**5**) in excellent yield (86%). Compared to insoluble 1,3,6,8-tetrabromopyrene [34], the diphenyl-substituted compound **5** exhibited excellent solubility in common organic solvents, such as dichloromethane, chloroform, tetrahydrofuran and toluene, allowing a full characterization by NMR analyses. Finally, the palladium-catalyzed cyclopentannulation of compound **5** with 1,2-diphenylethyne under microwave conditions using the catalyst system of $[\text{Pd}_2(\text{dba})_3]$ and $\text{P}(o\text{-tol})_3$ afforded a dark red solid in 5% yield after purification. The obtained product showed an intense peak at 1058.3910 during MALDI–TOF mass analysis (positive mode, dithranol as the matrix) that matched well with the expected molecular mass of m/z 1058.3913 (calcd for $\text{C}_{84}\text{H}_{50}$: $[\text{M}]^+$) for dicyclopenta-fused peropyrene **1**. Furthermore, the observed isotopic distribution was fully consistent with its simulated spectrum (Figure 1). Characterization of the resultant product by single crystal X-ray analysis unambiguously revealed the selective formation of **1** through twofold $[3 + 2]$ pentannulation and sequent twofold $[4 + 2]$ benzannulation, instead of the desired tetracyclopenta[*cd,fg,jk,mn*]pyrene (**2**). The selective formation of **1** could be rationalized by the steric hindrance of the phenyl rings after the twofold $[3 + 2]$ alkyne pentannulated intermediate (Scheme S2, Supporting Information File 1), and the sequent annulation was favorable for the formation of six-membered rings. Nevertheless, the existence of several rotamers of **1** derived from the restricted rotation of the peripheral phenyl ring substituents and its nonplanar geometry prevented the structure elucidation by proton NMR analysis [35].

Single crystals of **1** were obtained by slow evaporation from a carbon disulfide solution, allowing us to disclose the molecular structure by X-ray crystallography (Figure 2a). As shown in Figure 2a, the crystal structure of **1** clearly displayed a nonplanar conformation, resulting from steric repulsion between the phenyl groups and the hydrogen atoms at the bay po-



sitions. Interestingly, the splay angle of each bay position showed slight differences with a value of 17° and 21° , respectively. This contortion resulted in a molecular backbone with an overall end-to-end twist angle of 21.4° (Figure 2b), which is slightly larger than that of the reported 5,13-diphenylperopyrene derivative (18°) [32]. The twisted carbon skeleton of **1** makes it a chiral molecule with enantiomers (*P,P*) and (*M,M*) configuration in the packing mode through a face-to-face slip-stacking arrangement, with a minimum interplanar spacing of 6.84 \AA (Figure 2c). In addition, the C–C bond lengths in **1** are shown in Figure 2d. The short lengths of the black bold bonds ($1.368\text{--}1.392 \text{ \AA}$) in **1** suggested their double bond character ($\text{C}=\text{C}$ is typically 1.337 \AA). These results are in good agreement with the resonance structure of **1** that is assigned by Clar's aromatic sextet theory (Figure 2e). Interestingly, the long bond length of *a*, *b*, *c*, and *d* ($1.471\text{--}1.504 \text{ \AA}$) indicated that the double bonds on the five-membered rings have a small contribution to the overall aromatic delocalization of the carbon framework [26]. In order to evaluate the aromaticity of **1**, a nucleus-independent chemical shift (NICS) calculation was conducted. As shown in Figure 2d, the positive NICS(1) values of the five-membered rings A and C reveal the slightly anti-aromatic feature. The rings B, F and I appear to have more aromatic character, while the rings D, E, G and H become less aromatic, which is in accordance with the resonance structure of **1** as shown in Figure 2e.

The UV–vis absorption spectra of compounds **5** and **1** in DCM are compared in Figure 3a. The maximum absorption peak of **1** is significantly red-shifted compared to that of precursor **5**, which can be attributed to the extended conjugation of **1** after the annulation. Compound **1** shows a broad absorption band in the range of $449\text{--}690 \text{ nm}$ with the absorption maximum at

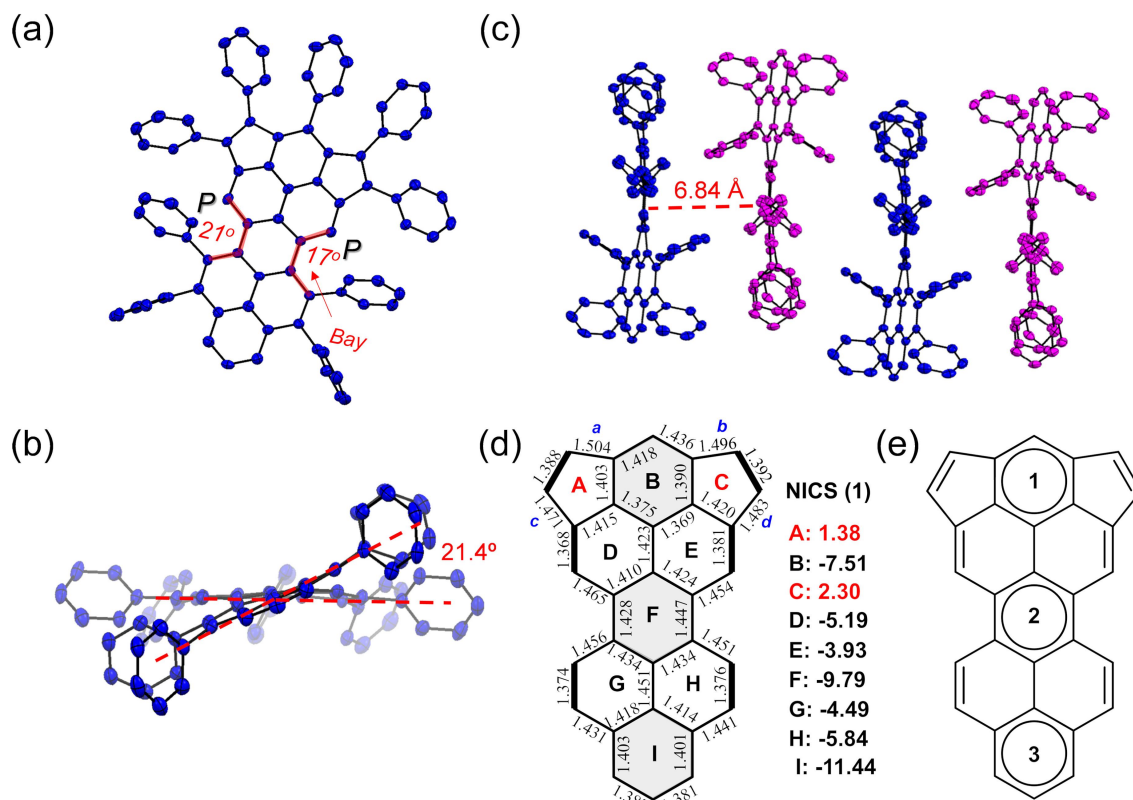


Figure 2: Single-crystal X-ray structure of 1. (a) Top view and (b) side view of the (P,P) isomer. (c) Crystal packing of the enantiomer pairs (P,P and M,M) of 1. Hydrogen atoms and solvent molecules are omitted for clarity. (d) Selected bond lengths (from the crystal structure) and calculated NICS(1) values of rings A–I in 1. (e) Clar valence structure representation of 1 with three benzeneoid rings.

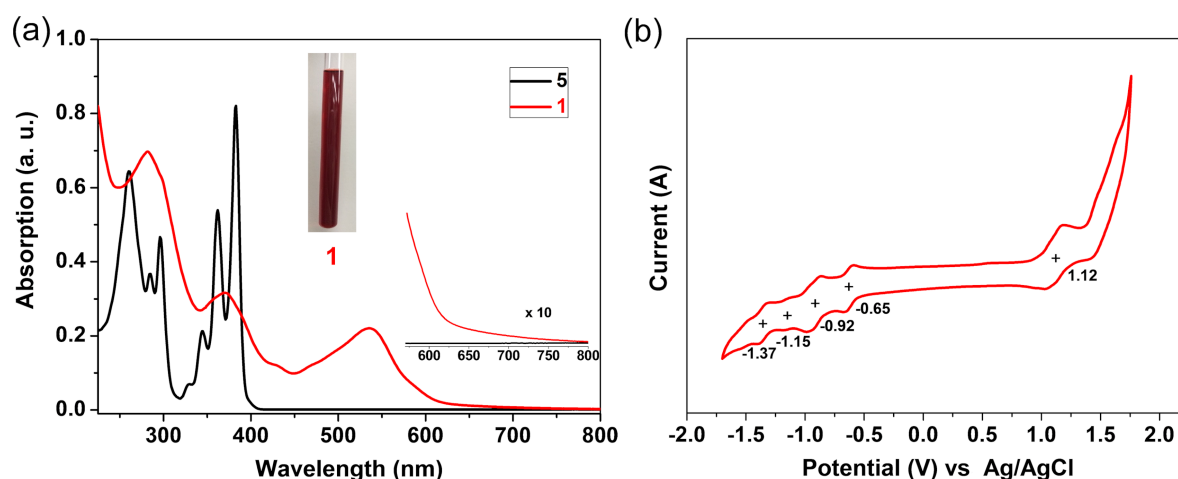


Figure 3: (a) UV-vis absorption spectra of precursor 5 and 1 in CH_2Cl_2 solution (10^{-5} M). Inset: photograph of a CH_2Cl_2 solution of 1. (b) Cyclic voltammogram of 1 (0.1 M $n\text{-Bu}_4\text{NPF}_6$ in DCM) at a scan rate of 50 mV s^{-1} .

537 nm, which also displays a large red-shift (70 nm) compared with the reported peropyrene derivative [32]. The optical energy gap of 1 is determined to be 1.78 eV from the onset of its UV-vis absorption spectrum. Similar to the cyclopenta-fused

pyrene derivatives [28,29], compound 1 does not show detectable fluorescence emission. Furthermore, the electrochemical properties of 1 was probed by cyclic voltammetry (CV) in DCM (Figure 3b). According to the CV analysis, com-

pound **1** exhibits one reversible oxidation wave with half-wave potentials ($E_{1/2}^{\text{ox}}$) at 1.12 V and four reduction waves with half-wave potentials ($E_{1/2}^{\text{red}}$) at –0.65, –0.92, –1.15, and –1.37 V (vs Ag/AgCl). The HOMO/LUMO energy levels are estimated to be –5.37 / –3.80 eV, respectively, based on the onset potentials of the first oxidation/reduction waves. Accordingly, the corresponding electrochemical energy gap (E_g^{EC}) of **1** is derived to be 1.57 eV, which is slightly smaller than the optical energy gap (1.78 eV).

In order to gain a deeper insight into the effects of the fused 5-membered rings on the peropyrene core, the electronic structures and the frontier orbitals of the peropyrene derivative **6** without pentagons and of compound **1** are compared by DFT calculations at the B3LYP/6-311++G(d,p) level. As shown in Figure 4, the LUMO and HOMO of **6** are both delocalized over the aromatic core. In contrast to **6**, compound **1** presents a significant difference in the shape of its molecular orbitals. The LUMO of **1** is mainly localized on the core, whereas the

HOMO keeps a line of high electron density along the fused five-membered rings (rings A and C in Figure 2d) and the central six-membered ring B. The large difference between the LUMO and HOMO leads to an intramolecular charge transfer, resulting in broad absorption bands in the UV–vis spectrum (Figure 3a) [36]. In addition, the LUMO energy of **1** (–2.98 eV) is significantly lower than that of **6** (–2.38 eV), which is responsible for the narrower energy gap of **1** (2.24 eV).

Conclusion

In summary, we demonstrated the first synthesis and characterization of a dicyclopenta-fused peropyrene **1** starting from pyrene in four steps in which the twofold pentannulation and subsequent twofold benzannulation based on 1,3,6,8-tetrabromo-2,7-diphenylpyrene is the key step. The single crystal X-ray diffraction analysis revealed a twisted structure of **1** due to the steric hindrance at the bay positions. From the bond length analysis and DFT calculations, CP-PAH **1** consists of the aromatic peropyrene core with two slightly antiaromatic *peri*-

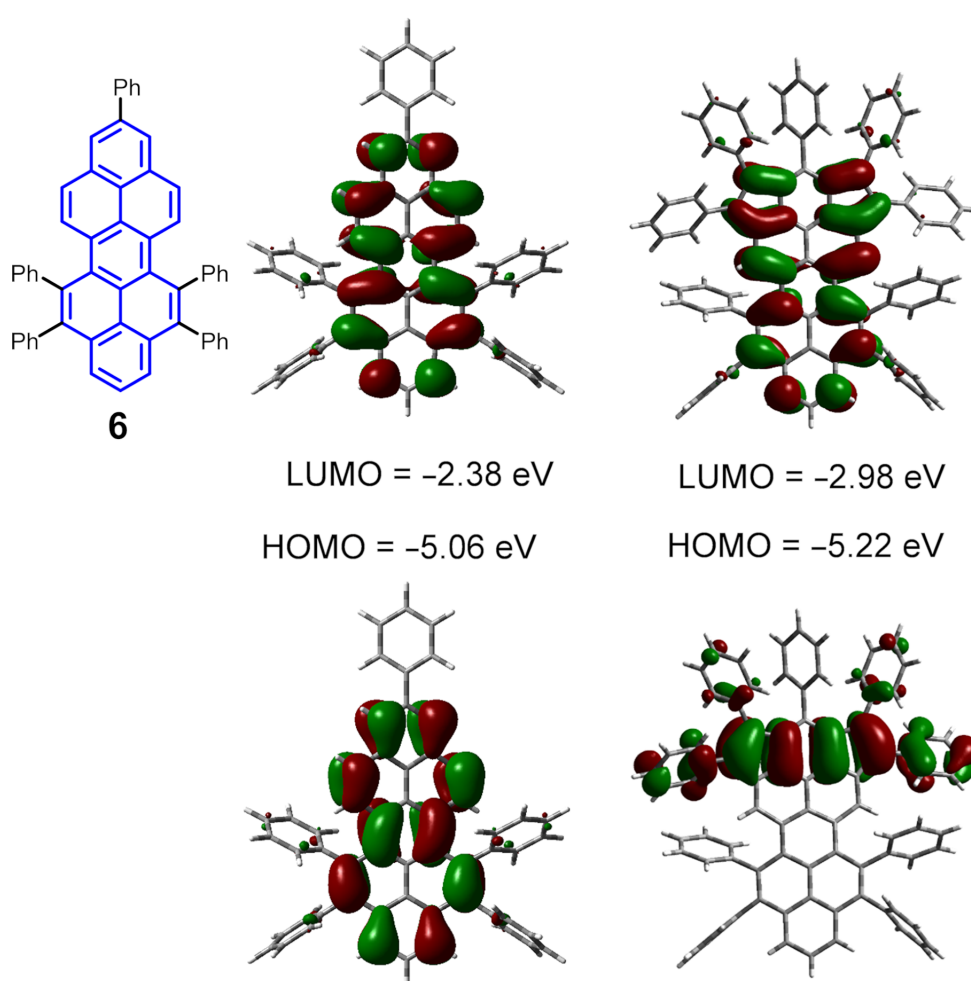


Figure 4: Molecular orbitals of peropyrene derivative **6** and the dicyclopenta-fused peropyrene **1**.

fused five-membered rings. In addition, dicyclopenta-fused peropyrene **1** possesses a decreased LUMO energy level compared to the parent peropyrene without five-membered rings, which is responsible for the resultant low energy gap (1.78 eV). This work report herein paves the way toward the synthesis of novel cyclopenta-fused PAHs in large π -systems.

Supporting Information

Supporting Information File 1

Experimental details, synthetic procedures, single crystal X-ray data for **1**, detailed theoretical calculations, and analytical data for the compounds.

[<https://www.beilstein-journals.org/bjoc/content/supplementary/1860-5397-16-72-S1.pdf>]

Acknowledgements

We thank Dr. Hartmut Komber (Leibniz-Institut für Polymerforschung Dresden e.V., Germany) for the high-temperature NMR measurement. We thank the Center for Information Services and High Performance Computing (ZIH) at TU Dresden for generous allocations of compute resources.

Funding

We thank the European Union's Horizon 2020 research and innovation program under grant agreement No 696656 (Graphene Flagship Core2), ERC Grant on T2DCP, the German Research Foundation (DFG) within the Cluster of Excellence "Center for Advancing Electronics Dresden (cfaed)" and EnhanceNano (No. 391979941) as well as the European Social Fund and the Federal State of Saxony (ESFProject "GRAPHD", TU Dresden) for financial support. J. Liu is grateful for the startup funding from The University of Hong Kong and the funding support from ITC to the SKL.

ORCID® iDs

Ji Ma - <https://orcid.org/0000-0003-4418-2339>

Yubin Fu - <https://orcid.org/0000-0002-2613-394X>

References

- Diederich, F.; Rubin, Y. *Angew. Chem., Int. Ed. Engl.* **1992**, *31*, 1101–1123. doi:10.1002/anie.199211013
- Plunkett, K. N. *Synlett* **2013**, *24*, 898–902. doi:10.1055/s-0032-1318434
- Trost, B. M.; Bright, G. M. *J. Am. Chem. Soc.* **1967**, *89*, 4244–4245. doi:10.1021/ja00992a064
- Wegner, H. A.; Scott, L. T.; de Meijere, A. *J. Org. Chem.* **2003**, *68*, 883–887. doi:10.1021/jo020367h
- Wegner, H. A.; Reisch, H.; Rauch, K.; Demeter, A.; Zachariasse, K. A.; de Meijere, A.; Scott, L. T. *J. Org. Chem.* **2006**, *71*, 9080–9087. doi:10.1021/jo0613939
- Chase, D. T.; Rose, B. D.; McClintock, S. P.; Zakharov, L. N.; Haley, M. M. *Angew. Chem., Int. Ed.* **2011**, *50*, 1127–1130. doi:10.1002/anie.201006312
- Ma, J.; Liu, J.; Baumgarten, M.; Fu, Y.; Tan, Y.-Z.; Schellhammer, K. S.; Ortmann, F.; Cuniberti, G.; Komber, H.; Berger, R.; Müllen, K.; Feng, X. *Angew. Chem., Int. Ed.* **2017**, *56*, 3280–3284. doi:10.1002/anie.201611689
- Naibi Lakshminarayana, A.; Chang, J.; Luo, J.; Zheng, B.; Huang, K.-W.; Chi, C. *Chem. Commun.* **2015**, *51*, 3604–3607. doi:10.1039/c4cc09812a
- Scott, L. T.; Jackson, E. A.; Zhang, Q.; Steinberg, B. D.; Bancu, M.; Li, B. *J. Am. Chem. Soc.* **2012**, *134*, 107–110. doi:10.1021/ja209461g
- Ma, J.; Zhang, K.; Schellhammer, K. S.; Fu, Y.; Komber, H.; Xu, C.; Popov, A. A.; Hennesdorf, F.; Weigand, J. J.; Zhou, S.; Pisula, W.; Ortmann, F.; Berger, R.; Liu, J.; Feng, X. *Chem. Sci.* **2019**, *10*, 4025–4031. doi:10.1039/c8sc05416a
- Koper, C.; Jenneskens, L. W.; Sarobe, M. *Tetrahedron Lett.* **2002**, *43*, 3833–3836. doi:10.1016/s0040-4039(02)00683-4
- Wood, J. D.; Jellison, J. L.; Finke, A. D.; Wang, L.; Plunkett, K. N. *J. Am. Chem. Soc.* **2012**, *134*, 15783–15789. doi:10.1021/ja304602t
- Xia, H.; Liu, D.; Xu, X.; Miao, Q. *Chem. Commun.* **2013**, *49*, 4301–4303. doi:10.1039/c2cc34992b
- Choi, Y.; Chatterjee, T.; Kim, J.; Kim, J. S.; Cho, E. J. *Org. Biomol. Chem.* **2016**, *14*, 6804–6810. doi:10.1039/c6ob01235c
- Bheemireddy, S. R.; Ubaldo, P. C.; Rose, P. W.; Finke, A. D.; Zhuang, J.; Wang, L.; Plunkett, K. N. *Angew. Chem., Int. Ed.* **2015**, *54*, 15762–15766. doi:10.1002/anie.201508650
- Dyker, G.; Merz, K.; Oppel, I. M.; Muth, E. *Synlett* **2007**, 0897–0900. doi:10.1055/s-2007-970785
- Havenith, R. W. A.; Jiao, H.; Jenneskens, L. W.; van Lenthe, J. H.; Sarobe, M.; Schleyer, P. v. R.; Kataoka, M.; Necula, A.; Scott, L. T. *J. Am. Chem. Soc.* **2002**, *124*, 2363–2370. doi:10.1021/ja011538n
- Steiner, E.; Fowler, P. W.; Jenneskens, L. W.; Havenith, R. W. A. *Eur. J. Org. Chem.* **2002**, 163–169. doi:10.1002/1099-0690(20021)2002:1<163::aid-ajoc163>3.0.co;2-3
- Gooijer, C.; Kozin, I.; Velthorst, N. H.; Sarobe, M.; Jenneskens, L. W.; Vlietstra, E. J. *Spectrochim. Acta, Part A* **1998**, *54*, 1443–1449. doi:10.1016/s1386-1425(98)00045-6
- Koper, C.; Sarobe, M.; Jenneskens, L. W. *Phys. Chem. Chem. Phys.* **2004**, *6*, 319–327. doi:10.1039/b312234d
- Otero-Lobato, M. J.; van Walree, C. A.; Havenith, R. W. A.; Jenneskens, L. W.; Fowler, P. W.; Steiner, E. *Tetrahedron* **2006**, *62*, 5510–5518. doi:10.1016/j.tet.2006.03.033
- Sarobe, M.; Jenneskens, L. W.; Kleij, A.; Petrousa, M. *Tetrahedron Lett.* **1997**, *38*, 7255–7258. doi:10.1016/s0040-4039(97)01685-7
- Sarobe, M.; Havenith, R. W. A.; Jenneskens, L. W. *Chem. Commun.* **1999**, 1021–1022. doi:10.1039/a901717h
- Scott, L. T.; Necula, A. *J. Org. Chem.* **1996**, *61*, 386–388. doi:10.1021/jo9516087
- Dang, H.; Garcia-Garibay, M. A. *J. Am. Chem. Soc.* **2001**, *123*, 355–356. doi:10.1021/ja002329q
- Dang, H.; Levitus, M.; Garcia-Garibay, M. A. *J. Am. Chem. Soc.* **2002**, *124*, 136–143. doi:10.1021/ja016189b
- Liu, E.-C.; Chen, M.-K.; Li, J.-Y.; Wu, Y.-T. *Chem. – Eur. J.* **2015**, *21*, 4755–4761. doi:10.1002/chem.201405763

28. Lütke Eversloh, C.; Avlasevich, Y.; Li, C.; Müllen, K. *Chem. – Eur. J.* **2011**, *17*, 12756–12762. doi:10.1002/chem.201101126
29. Bheemireddy, S. R.; Ubaldo, P. C.; Finke, A. D.; Wang, L.; Plunkett, K. N. *J. Mater. Chem. C* **2016**, *4*, 3963–3969. doi:10.1039/c5tc02305j
30. Yang, W.; Chalifoux, W. A. *Synlett* **2017**, *28*, 625–632. doi:10.1055/s-0036-1588688
31. Nichols, V. M.; Rodriguez, M. T.; Piland, G. B.; Tham, F.; Nesterov, V. N.; Youngblood, W. J.; Bardeen, C. J. *J. Phys. Chem. C* **2013**, *117*, 16802–16810. doi:10.1021/jp4051116
32. Yang, W.; Monteiro, J. H. S. K.; de Bettencourt-Dias, A.; Catalano, V. J.; Chalifoux, W. A. *Angew. Chem., Int. Ed.* **2016**, *55*, 10427–10430. doi:10.1002/anie.201604741
33. Yang, W.; Longhi, G.; Abbate, S.; Lucotti, A.; Tommasini, M.; Villani, C.; Catalano, V. J.; Lykhin, A. O.; Varganov, S. A.; Chalifoux, W. A. *J. Am. Chem. Soc.* **2017**, *139*, 13102–13109. doi:10.1021/jacs.7b06848
34. Venkataramana, G.; Sankararaman, S. *Eur. J. Org. Chem.* **2005**, 4162–4166. doi:10.1002/ejoc.200500222
35. Ackermann, M.; Freudenberger, J.; Jänsch, D.; Rominger, F.; Bunz, U. H. F.; Müllen, K. *Org. Lett.* **2018**, *20*, 3758–3761. doi:10.1021/acs.orglett.8b01334
36. Ganschow, M.; Koser, S.; Hodecker, M.; Rominger, F.; Freudenberger, J.; Dreuw, A.; Bunz, U. H. F. *Chem. – Eur. J.* **2018**, *24*, 13667–13675. doi:10.1002/chem.201802900

License and Terms

This is an Open Access article under the terms of the Creative Commons Attribution License (<http://creativecommons.org/licenses/by/4.0>). Please note that the reuse, redistribution and reproduction in particular requires that the authors and source are credited.

The license is subject to the *Beilstein Journal of Organic Chemistry* terms and conditions: (<https://www.beilstein-journals.org/bjoc>)

The definitive version of this article is the electronic one which can be found at:
doi:10.3762/bjoc.16.72



Bipyrrole boomerangs via Pd-mediated tandem cyclization–oxygenation. Controlling reaction selectivity and electronic properties

Liliia Moshniaha¹, Marika Żyła-Karwowska¹, Joanna Cybińska^{1,2}, Piotr J. Chmielewski¹, Ludovic Favereau³ and Marcin Stępień^{*1}

Full Research Paper

[Open Access](#)

Address:

¹Wydział Chemii, Uniwersytet Wrocławski, ul. F. Joliot-Curie 14, 50-383 Wrocław, Poland, ²PORT – Polski Ośrodek Rozwoju Technologii, ul. Stabłowicka 147, 54-066 Wrocław, Poland and ³Université Rennes, CNRS, ISCR (Institut des Sciences Chimiques de Rennes) UMR 6226, F-35000 Rennes, France

Email:

Marcin Stępień* - marcin.stepien@chem.uni.wroc.pl

* Corresponding author

Keywords:

donor–acceptor systems; double C–H bond activation; helicenes; pyrroles

Beilstein J. Org. Chem. **2020**, *16*, 895–903.

doi:10.3762/bjoc.16.81

Received: 11 February 2020

Accepted: 17 April 2020

Published: 04 May 2020

This article is part of the thematic issue "C–H functionalization for materials science".

Guest Editor: K. Itami

© 2020 Moshniaha et al.; licensee Beilstein-Institut.

License and terms: see end of document.

Abstract

Boomerang-shaped bipyrroles containing donor–acceptor units were obtained through a tandem palladium-mediated reaction consisting of a cyclization step, involving double C–H bond activation, and a double α -oxygenation. The latter reaction can be partly suppressed for the least reactive systems, providing access to α -unsubstituted boomerangs for the first time. These “ α -free” systems are highly efficient fluorophores, with emission quantum yields exceeding 80% in toluene. Preliminary measurements show that helicene-like boomerangs may be usable as circularly polarized luminescent materials.

Introduction

Nanographenes and other polycyclic aromatics as well as their heterocyclic analogues are typically obtained by tandem cyclodehydrogenations of oligoaryl precursors [1–3]. This general strategy is attractive because it does not require prefunctionalization of coupling sites and because it provides rapid access to complex π systems. Such cyclodehydrogenations can be performed using diverse oxidants [4], with FeCl₃

being particularly notable for its versatility, ease of use, and low price [5]. Nevertheless, the synthetic utility of oxidative couplings is often limited by several factors [6]. Consequently, incomplete ring fusion and various side reactions, e.g., chlorination [7], or unexpected rearrangements, are frequently observed [8]. The use of oxidative couplings is further limited for the synthesis of strained [9,10], electron-deficient, or sterically

congested aromatics [11–14]. Some of these limitations can be overcome by using prefunctionalized precursors [11], as exemplified by reductive Ullmann-type chemistry [15], catalytic direct arylations [11,14,16,17], photoinduced cyclodehydrochlorinations [18,19], or nucleophilic oxidative couplings [20], which may offer milder reaction conditions and superior regioselectivities, at the expense of atom and step economy [21]. The latter disadvantage may be obviated by transition-metal-mediated double C–H bond activation [22,23], which is functionally equivalent to conventional oxidative coupling reactions, and has become a powerful synthetic tool with a rapidly growing scope of use [24–26]. However, in the field of π -conjugated materials, this strategy has so far remained relatively unexplored [27].

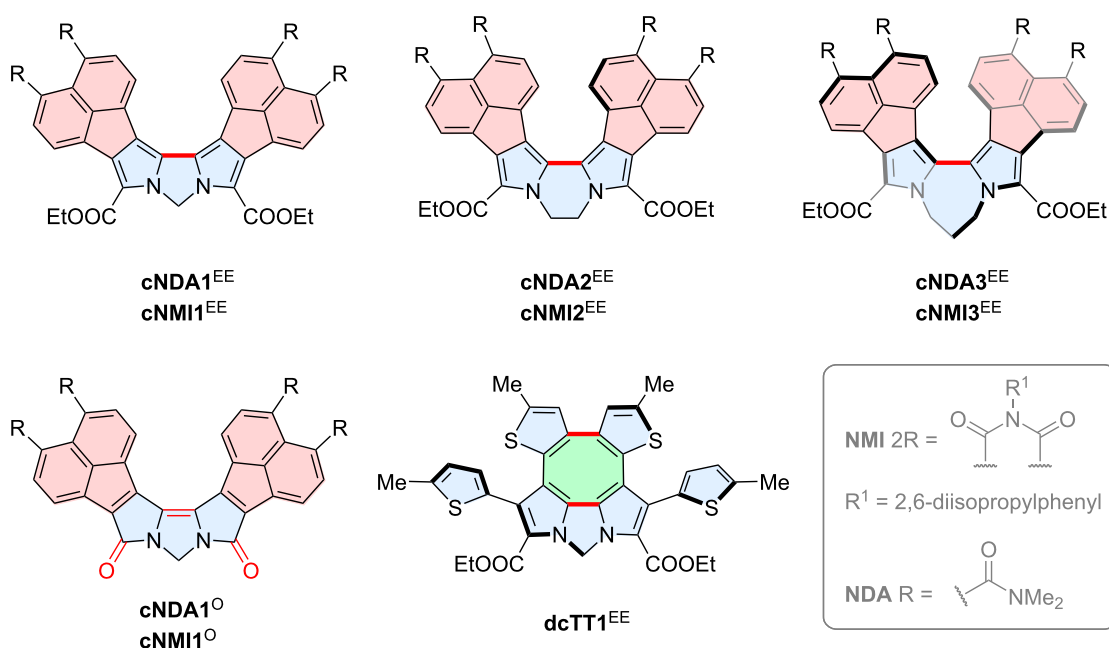
As a part of our ongoing research on π -extended electron-deficient oligopyrroles [13,28–31], we have recently reported that Pd(II)-mediated double C–H activation can be a useful tool for conversion of 1, n -dipyrrolylalkanes into boomerang-shaped N,N' -bridged α,α' -bipyrroles that are not accessible by means of conventional oxidative coupling methods (Scheme 1) [32]. Our approach is applicable to electron-deficient and sterically encumbered systems, notably those based on pyrrole derivatives fused with naphthalenediamide (NDA) and naphthalenemonoimide (NMI) moieties. The double C–H bond activation initially used palladium(II) acetate in acetic acid as the coupling system. The subsequent screening revealed, however, that a catalytic coupling could be also achieved in the presence of

silver(I) carbonate as the stoichiometric oxidant. The scope of such Pd(II)-induced couplings was further developed into tandem processes involving consecutive cyclization of substituents (**dcTT^{EE}**) and oxygenation of pyrrolic α -positions to form lactams **cNDA1^O** and **cNMI1^O**. The mechanism of those transformations was subsequently explored using NMR spectroscopy and DFT calculations [33]. In particular, the unprecedented double α -oxygenation of bipyrroles was shown to occur through stepwise acetoxylation, which we found to compete with α – α oligomerization. These new bipyrrole boomerangs exhibited enhanced fluorescence with Φ_{fl} values of up to 67%, while their bandgaps and chiroptical responses could be tuned by twisting the bipyrrole chromophore. The solvatochromism and apparent superradiance of these chromophores indicated a potential involvement of solvent-induced symmetry-breaking charge transfer in the excited state [34]. Here we report that the above Pd-mediated chemistry is capable of producing highly twisted dilactam boomerangs and provide first examples of α -free boomerang systems. These new derivatives are of interest as emitters for both polarized and unpolarized luminescence.

Results and Discussion

Synthesis

The starting 1, n -dipyrrolylalkane precursors (**Rn^H**, $n = 2$ or 3) were synthesized by reacting the appropriate pyrrolyl anions with either ethylene ditosylate or 1,3-dibromopropane (Scheme S1, Supporting Information File 1). In our initial coupling experiments, 1,2-dipyrrolylethanes (**NDA2^H**, **NMI2^H**) and 1,3-

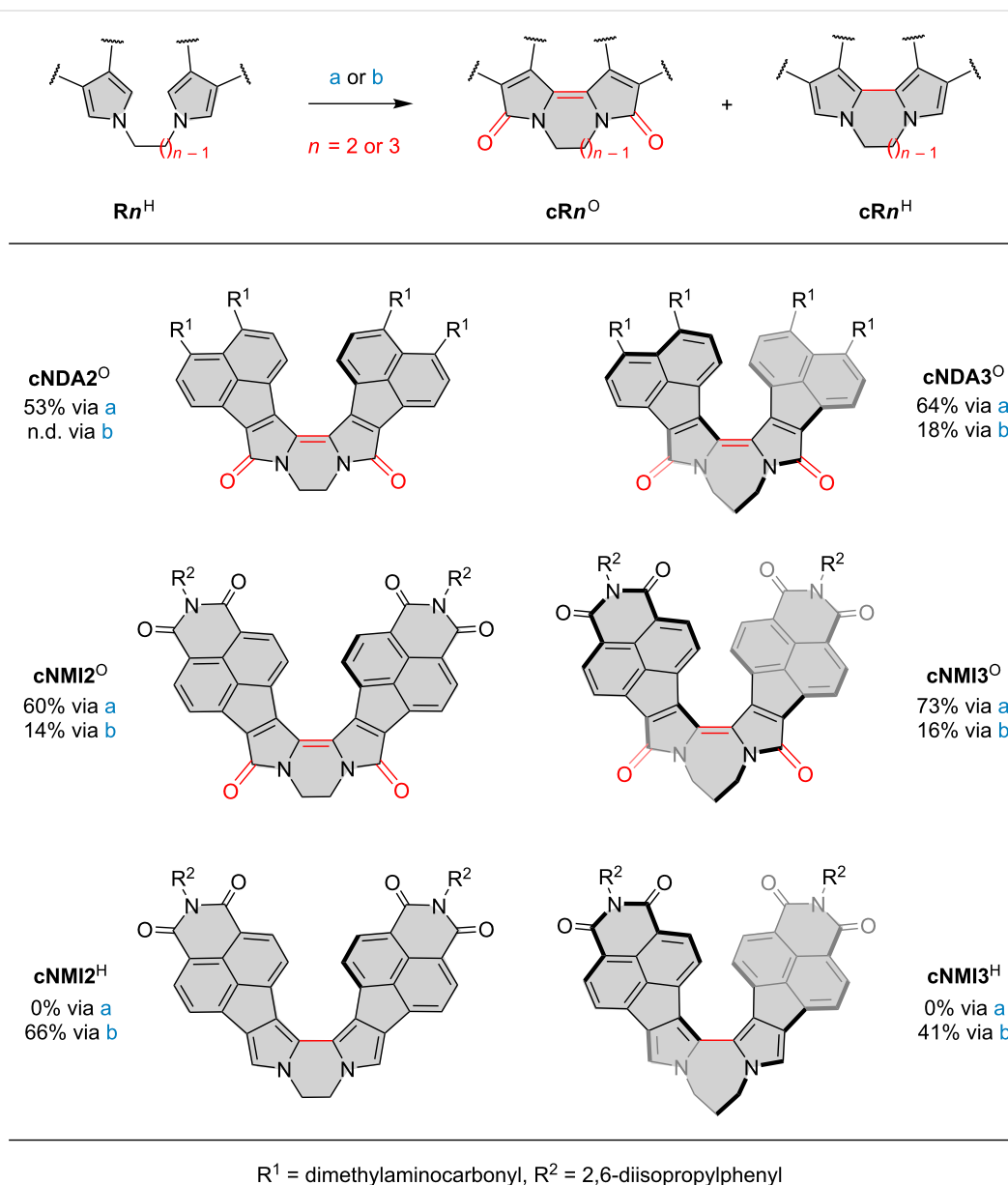


Scheme 1: The previously reported family of the boomerang bipyrroles obtained by Pd-induced double C–H bond activation [32].

dipyrrolylpropanes (**NDA3^H**, **NMI3^H**) were reacted with palladium(II) acetate in acetic acid to furnish the expected bipyrrole dilactams in 43–53% yields (Table 1, entries 1, 6, 11 and 17). Remarkably, it was found that **cNMI2^O** and **cNMI3^O** were obtained along with the intermediate α -unsubstituted boomerangs, **cNMI2^H** and **cNMI3^H**, respectively (Scheme 2). Analogous α -unsubstituted intermediates (**cNDA2^H** and **cNDA3^H**) were not isolated in reactions involving **NDA2^H** and **NDA3^H**. The latter behavior is consistent with the selectivity pattern observed previously for α -unsubstituted dipyrrolylmethanes **NDA1^H** and **NMI1^H**, for which we were only able to isolate the correspond-

ing dilactams **cNDA1^O** and **cNMI1^O**, respectively [32]. Transient formation of **cNDA1^H** could, however, be observed in situ for reactions involving **NDA1^H** [33].

Subsequent screening revealed that the yield of **cNMI2^H** and **cNMI3^H** could be increased when reactions were performed in more dilute solutions (Table 1, entries 14 and 20). Following our previous experimental and computational findings [32,33], we also checked whether the yields of dilactam products might be improved by increasing the concentration of acetate anions in the reaction mixture. Indeed, annulations of **NDAⁿ^H** and



Scheme 2: Synthesis and structures of α -free and α -oxygenated bipyrrole boomerangs. Reagents and conditions: (a) 30 mM in AcOH, 3 equiv Pd(OAc)₂, 6 equiv KOAc, 120 °C, 1 h; (b) 3 mM in AcOH, 3 equiv Pd(OAc)₂, 120 °C, 1 h. Isolated yields are given for each set of conditions. *M* enantiomers are depicted for **cNDA3^O**, **cNMI3^O**, **cNMI3^H**. n.d. = not determined.

Table 1: Screening of reaction conditions.^a

entry	reactant	c [mM] ^b	Pd(OAc) ₂ ^c	additive ^d	cRn ^O [%] ^e	cRn ^H [%] ^e
1	NDA2 ^H	30	3	none	46	0
2	NDA2 ^H	30	3	KOAc	53	0
3	NDA2 ^H	30	1	Ag ₂ CO ₃	34	0
4	NDA2 ^H	3	3	none	n.d. ^f	0
5	NDA2 ^H	3	3	KOAc	n.d. ^f	0
6	NDA3 ^H	30	3	none	43	0
7	NDA3 ^H	30	3	KOAc	64	0
8	NDA3 ^H	30	1	Ag ₂ CO ₃	37	0
9	NDA3 ^H	3	3	none	18	0
10	NDA3 ^H	3	3	KOAc	23	0
11	NMI2 ^H	30	3	none	52	6
12	NMI2 ^H	30	3	KOAc	60	0
13	NMI2 ^H	30	1	Ag ₂ CO ₃	43	14
14	NMI2 ^H	3	3	none	14	66
15	NMI2 ^H	3	3	KOAc	32	30
16	NMI2 ^H	3	0.1	Ag ₂ CO ₃	<10%	<10%
17	NMI3 ^H	30	3	none	56	9
18	NMI3 ^H	30	3	KOAc	73	0
19	NMI3 ^H	30	1	Ag ₂ CO ₃	34	6
20	NMI3 ^H	3	3	none	16	41
21	NMI3 ^H	3	3	KOAc	15	12
22	NMI3 ^H	3	0.1	Ag ₂ CO ₃	19	traces

^aConditions: acetic acid, 120 °C, 1 h; ^bconcentration of the starting dipyrrolylalkane (**Rn^H**); ^c[equiv] ^dKOAc (6 equiv), Ag₂CO₃ (2 equiv); ^eisolated yields; ^fn.d. = not determined. Only traces of **cNDA2^O** were present in the crude mixture.

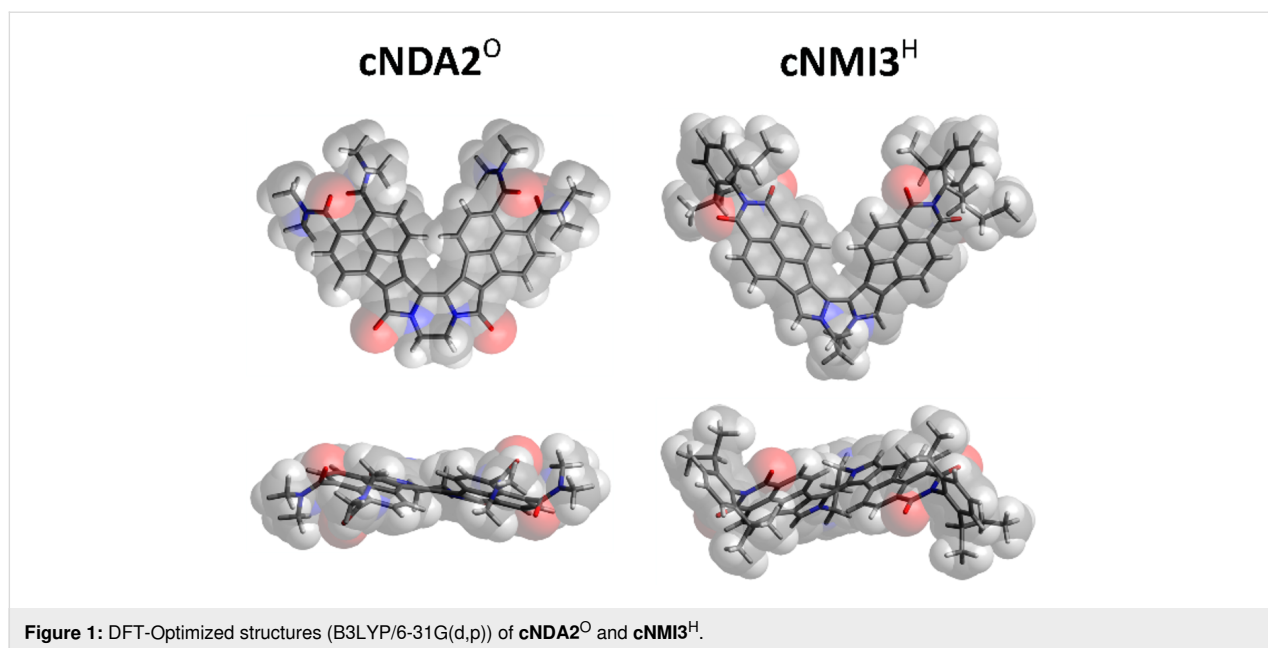
NMI^H carried out in the presence of 6 equiv of potassium acetate produced the corresponding dilactams in higher yields (53–73%) with complete conversion (Table 1, entries 2, 7, 12, and 18). Under these conditions, the **cNMI2^H** and **cNMI3^H** intermediates were not isolated. When the same reactions were, however, performed in higher dilution, the yields decreased and the **cNMI^O** to **cNMI^H** ratio was almost 1:1, showing the important role of the dipyrrolylalkane concentration in these transformations (Table 1, entries 15 and 21). Additional experiments carried out on **Rn^H** precursors revealed that the coupling and α -oxygenation can also be achieved with 1 equiv of Pd(OAc)₂ in the presence of 2 equiv of silver carbonate. Nevertheless, Ag₂CO₃ oxidation provided lower yields and the efficiency of this variant was dramatically diminished when the loading of palladium(II) acetate was decreased below 1 equiv (Table 1, entries 16 and 22).

Structure

The identity of the α -oxygenated products, **cRn^O**, was determined on the basis of high-resolution mass spectrometry and ¹H and ¹³C NMR data. In particular, the ¹H NMR spectrum of **cNMI2^O** revealed the absence of the pyrrolic α -H resonances, whereas the endocyclic CH₂ moiety yielded a pair of very broad

peaks at ca. 4.8–3.4 ppm. This splitting, which was also observed for **cNDA2^O**, is consistent with slow inversion of helicity occurring at the ethylene bridge. In the ¹H NMR spectrum of **cNMI2^H**, the linker CH₂ moiety and the 2,6-diisopropylphenyl (dipp) CH unit each produced a single broadened signal, indicating that the helix inversion occurs in the fast exchange regime. This apparently faster inversion in **cNMI2^H** than in the **cNMI2^O** and **cNDA2^O** lactams correlates with the higher bond order of the α - α linkage in the latter two systems. The chirality of **cNMI3^H** is reflected in its ¹H NMR spectrum, which shows diastereotopic differentiation of N-CH₂ protons of the bridge and the CH signals of the dipp substituents, consistent with a rigid C₂-symmetric structure. Analogous diastereotopic effects are observed for **cNDA3^O** and **cNMI3^O**. For **cNDA3^O**, the ¹H NMR spectrum is additionally complicated by the partially restricted rotation of the *N,N*-dimethylamide substituents in the NDA units. In conjunction with the helicity of the ring system, this restriction leads to effective diastereomerism.

The three-dimensional structures of all boomerangs were modeled using DFT calculations (Figure 1 and Supporting Information File 1). The length of the linker (*n*) in **cNDAⁿX** and



cNMIⁿ^X controls the in- and out-of-plane geometry of the chromophore. The observed changes can be expressed in terms of two parameters: α , the angle between the monopyrrole axis and the N–N vector, and θ , the torsion angle between the two monopyrrole axes (Supporting Information File 1, Table S1). In contrast to the previously reported **cR1^O** dilactams, which were nearly planar [32], systems with $n = 2$ and 3 are characterized by a twisting distortion, which produces helicene-like conformations. The distortion results from an increased splay angle α between the two pyrrolic subunits, which leads to a greater steric congestion and, consequently, to an increase of the θ twist.

Electronic properties

The absorption spectra of the **cNMI2^O** and **cNMI3^O** bipyrroles, recorded in dichloromethane, are red-shifted by respectively 74 and 86 nm relative to their **cNDAⁿ^O** congeners (Table 2, Figure 2, see also Supporting Information File 1 for more optical data). Within each lactam series, when the bridge length n is increased from 2 to 3, the lowest-energy band is shifted by ca. 17 nm to longer wavelengths. Pairs of lactam rings present in **cNMI2^O** and **cNMI3^O** form a quinoidal substructure, which produces a very significant bathochromic shift of their lowest-energy absorption bands (up to 176 nm in toluene) in comparison to the of α -unsubstituted analogues. Lactam bipyrroles **cNDAⁿ^O** and **cNMIⁿ^O** show noticeable solvatochromism which is stronger for $n = 2$ and is always negative. In contrast, the solvatochromism of α -free boomerangs is positive and even more pronounced. On going from toluene to acetonitrile, the onset of the lowest-energy band of **cNMI2^H** is shifted to longer wavelengths by 25 nm.

The **cNMI2^H** and **cNMI3^H** bipyrroles are very efficient fluorophores (Table 2), noticeably more emissive than the lactam analogues and the other previously reported boomerangs [32]. Highest fluorescence quantum yields were observed in toluene (83 and 80%, respectively). For comparison, the Φ_{fl} values for the lactams **cNMI2^O** and **cNMI3^O** are about 1%. Interestingly, the fluorescence of **cNMIⁿ^H** boomerang bipyrroles showed a stronger solvatochromic dependence than observed in their absorption spectra (Figure 2). In the more polar solvents, the emission profiles became significantly red shifted and broadened. At the same time, the fluorescence was only moderately quenched with increasing solvent polarity, and the quantum yields of 64 and 66% were recorded in acetonitrile for **cNMI2^H** and **cNMI3^H**, respectively.

To explore the chiral properties of the helically distorted boomerangs, the separation of enantiomers was attempted for all of them by means of chiral HPLC with CD detection, leading to enantioenriched samples of some boomerangs. The enantiomers of **cR2^O** were found to racemize very fast, thus it was not possible to separate them. The **cR3^X** systems, which contain a 7-membered ring, showed a remarkably diverse behavior. Enantiomers of **cNMI3^O** could not be separated, presumably because of very rapid racemization. The half-life time of **cNDA3^O** enantiomers (ca. 0.54 min) was too short to record their CD spectra, but was long enough for a kinetics study (Supporting Information File 1, Figures S8 and S9). Enantioenriched samples of **cNMI3^H** were configurationally most stable, showing no loss of their optical activity over the course of several hours in solution. Their CD spectra could be satisfactorily correlated with the TD-DFT data obtained for the

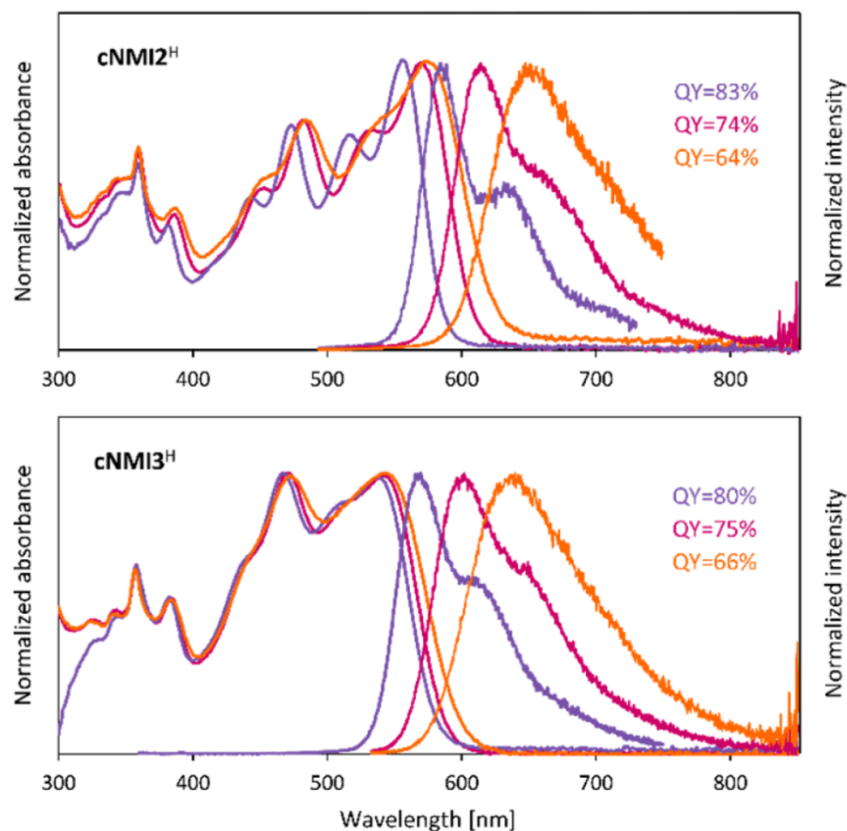


Figure 2: Absorption and emission spectra of **cNMI2^H** (top) and **cNMI3^H** (bottom) measured in toluene, dichloromethane and acetonitrile.

cNMI3^H enantiomers (Supporting Information File 1, Figures S5 and S22). Circularly polarized luminescence (CPL) measurements performed for enantioenriched samples of **cNMI3^H** revealed weak signals of opposite signs, with a maximum at ca. 570 nm consistent with the unpolarized luminescence of this system (Supporting Information File 1, Figure S6). The CPL signals rapidly decayed during the measurements, without any significant loss of the unpolarized emission intensity. This behavior, which precluded a quantitative analysis of the CPL properties, may be attributed to a photoinduced racemization process. The differences in configurational stability of boomerangs are reproduced by DFT calculations, which predict inversion barriers ΔG^\ddagger of 20.0 and 24.7 kcal/mol for models of **cNDA3^O** and **cNMI3^H**, respectively (Supporting Information File 1, Figures S31 and S32). The latter value is consistent with the observed greatest stability of **cNMI3^H**.

Frontier molecular orbitals of the boomerangs reveal features characteristic of donor–acceptor systems (Supporting Information File 1, Figures S25–S30). For dilactams, **cRn^O**, the HOMO orbital is primarily localized on the dilactam (bipyrrole) moiety, however, with some non-zero amplitudes on the NDA/NMI fragment, whereas the LUMO level encompasses the π system

more evenly. In the **cNMI_n^H** series ($n = 2, 3$), the HOMO and LUMO are formed by superposition of the corresponding MOs of the monomeric NMI pyrrole (Supporting Information File 1, Figures S23 and S24). However, the LUMO has observably lower amplitudes on the bipyrrole part of the molecule, whereas a more uniform coverage of the π system is seen for the HOMO orbital. The experimentally observed bandgap variations and absorption profiles (Table 2 and Table 3, Supporting Information File 1, Figures S1–S4, and S11–S16) were qualitatively reproduced in TD-DFT calculations performed for **cNDA2^O**, **cNDA3^O**, and **cNMI3^H** (Table 2 and Table 3, Supporting Information File 1, Tables S2–S4).

The redox properties of the new bipyrrole boomerangs were investigated by means of cyclic (CV) and differential pulse (DPV) voltammetry (Supporting Information File 1, Figures S11–S16). All systems showed at least two reversible one-electron reduction couples and up to two oxidation couples. The first oxidation was reversible for all systems studied except **cNMI2^H** and **cNDA3^O**. The second oxidations were chemically irreversible in all cases and typically produced new irreversible peaks upon the consecutive cathodic scans. In the previously reported **cNMI_n^{EE}** series ($n = 1, 2, 3$) it was also possible to

Table 2: Experimental and calculated^a properties of fused bipyrroles.

species	MO energies [eV] ^a			tol ^c	$\lambda_{\max}^{\text{abs}}$ [nm]		tol ^c	$\lambda_{\max}^{\text{em}}$ [nm] (QY)	
	HOMO	LUMO	HLG ^b		DCM ^d	MeCN ^e		DCM ^d	MeCN ^e
cNDA2 ^O	−5.47	−3.26	2.21	620	610	605	655 (0.07)	—	—
cNDA3 ^O	−5.34	−3.28	2.06	636	620	617	694 (0.25)	—	—
cNMI2 ^O	−5.95	−4.03	1.92	693	684	676	738 (0.01)	—	—
cNMI3 ^O	−5.88	−4.03	1.85	711	706	703	768 (0.01)	—	—
cNMI2 ^H	−5.50	−2.78	2.72	555	570	580	575 (0.83)	74 (0.61)	650 (0.64)
cNMI3 ^H	−5.56	−2.73	2.83	535	540	546	574 (0.80)	605 (0.75)	655 (0.66)

^aMolecular orbital energies, B3LYP/6-31G(d,p); ^bHOMO–LUMO gap; ^cin toluene; ^din dichloromethane; ^ein acetonitrile.

observe one reversible oxidation and four reductions, the first two being reversible [32]. The first oxidation potentials (E_{Ox1}) vary from 0.62 to 1.09 V, while the first reduction potentials (E_{Red1}) range from −1.54 to −0.60 V (Table 3). The boomerangs with unsubstituted pyrrole α -positions (**cNMI3**^H and **cNMI2**^H) are characterized by significantly lower oxidation and reduction potentials than the corresponding dilactam analogues. The electrochemical data obtained for **cNMI3**^O and **cNMI2**^O indicate a destabilization of their HOMOs by about 0.5 eV while relative stabilization of the LUMO approaches 1 eV with respect to **cNMI3**^H and **cNMI2**^H. This comparably stronger LUMO stabilization in the NMI lactam systems results in a considerable decrease of their electrochemical gap (ΔE , by ca. 0.5–0.7 V), relative to the α -free analogues. ΔE values for lactams **cRn**^O are relatively insensitive to the length of the alkylene linker n , in spite of the large changes of the inter-subunit torsion (θ , Supporting Information File 1, Table S1) caused by the increase of n . In line with the absorption spectroscopy data, the ΔE gap is reduced in the **cNMI**^O series by 0.25 to 0.36 V relative to the corresponding **cNDA**^O analogues. Interestingly, the difference between the first and second reduction potentials in the **cRn**^O dilactams is in the range of 0.25 to 0.33 V, indicat-

ing a strong coupling between the subunits. In comparison, this potential difference is much smaller in the α -free analogues **cNMI3**^H and **cNMI2**^H (ca. 0.1 V).

Conclusion

The present work shows that the tandem cyclization–oxygenation reaction is a general strategy for the synthesis of low-bandgap bipyrrole boomerangs and is applicable to targets with variable donor–acceptor character and increasing curvature of the bipyrrole linkage. The efficiency of the oxygenation step is dependent on a several of factors, i.e., Pd loading, concentration, and additives. The isolation of unoxxygenated products **cNMI2**^H and **cNMI3**^H emphasizes the role of acceptor units and decreased inter-pyrrole coupling in moderating the reactivity of α positions toward oxygenation. The latter systems are of interest because of their very high fluorescence quantum yields, the best so far recorded for this family of fluorophores. Our preliminary results indicate that bipyrrole boomerangs may be usable as CPL emitters, provided that their helicene-like twist is further stabilized against racemization. Efforts to achieve this goal are currently ongoing in our laboratory.

Table 3: Electrochemical data for the **cNDA**^O, **cNMI**^O and **cNMI**^H boomerangs derived from differential pulse voltammograms.^a

species	E_{Red4}	E_{Red3}	E_{Red2}	E_{Red1}	E_{Ox1}	E_{Ox2}	ΔE^b
cNDA1 ^{O c}	−2.52 ^d	−1.95 ^d	−1.36	−1.03	0.88 ^d	—	1.91
cNDA2 ^O	—	−1.82 ^d	−1.36	−1.07	0.98	1.08 ^d	2.05
cNDA3 ^O	—	—	−1.31	−1.03	0.89 ^d	1.01 ^d	1.92
cNMI1 ^{O c}	−1.84	−1.59	−0.83	−0.57	1.09 ^d	1.19 ^d	1.66
cNMI2 ^O	−1.90	−1.65	−0.85	−0.60	1.09	—	1.69
cNMI3 ^O	−1.97	−1.73	−0.86	−0.61	1.04	1.16 ^d	1.65
cNMI2 ^H	—	−2.46 ^d	−1.67	−1.59	0.62 ^d	0.76 ^d	2.21
cNMI3 ^H	—	−2.54	−1.80	−1.70	0.68	0.98 ^d	2.38

^aMeasurements were performed in dichloromethane solution using glassy carbon, platinum rod, and Ag/AgCl as working, auxiliary, and pseudoreference electrodes, respectively. All electrode potentials are in volt and are referenced with the ferrocene/ferrocenium couple as the internal standard.

^bElectrochemical HOMO–LUMO gap $\Delta E = E_{\text{Ox1}} - E_{\text{Red1}}$. ^cPreviously reported data [32]. ^dIrreversible.

Supporting Information

Supporting Information File 1

Synthetic, spectroscopic, and computational details.

[<https://www.beilstein-journals.org/bjoc/content/supplementary/1860-5397-16-81-S1.pdf>]

Supporting Information File 2

Cartesian coordinates.

[<https://www.beilstein-journals.org/bjoc/content/supplementary/1860-5397-16-81-S2.zip>]

Funding

Financial support from the National Science Center of Poland (UMO-2017/27/N/ST5/00613 L.M.) and the Foundation for Polish Science (TEAM POIR.04.04.00-00- 5BF1/17-00 M.S.) is gratefully acknowledged. L.F. acknowledges the Ministère de l'Éducation Nationale, de la Recherche et de la Technologie, the Centre National de la Recherche Scientifique (CNRS), and Rennes Metropole for financial support.

ORCID® iDs

Liliia Moshniaha - <https://orcid.org/0000-0001-9538-178X>
 Marika Żyła-Karwowska - <https://orcid.org/0000-0002-4709-9242>
 Piotr J. Chmielewski - <https://orcid.org/0000-0002-2548-6110>
 Ludovic Favereau - <https://orcid.org/0000-0001-7847-2911>
 Marcin Stępień - <https://orcid.org/0000-0002-4670-8093>

References

- Narita, A. Synthesis of Structurally Defined Nanographene Materials through Oxidative Cyclodehydrogenation. In *Synthetic Methods for Conjugated Polymers and Carbon Materials*; Leclerc, M.; Morin, J.-F., Eds.; Wiley-VCH: Weinheim, Germany, 2017; pp 183–228. doi:10.1002/9783527695959.ch6
- Stępień, M.; Gońka, E.; Żyła, M.; Sprutta, N. *Chem. Rev.* **2017**, *117*, 3479–3716. doi:10.1021/acs.chemrev.6b00076
- Wang, X.-Y.; Yao, X.; Narita, A.; Müllen, K. *Acc. Chem. Res.* **2019**, *52*, 2491–2505. doi:10.1021/acs.accounts.9b00322
- Grzybowski, M.; Sadowski, B.; Butenschön, H.; Gryko, D. T. *Angew. Chem., Int. Ed.* **2020**, *59*, 2998–3027. doi:10.1002/anie.201904934
- Sarhan, A. A. O.; Bolm, C. *Chem. Soc. Rev.* **2009**, *38*, 2730. doi:10.1039/b906026j
- Grzybowski, M.; Skonieczny, K.; Butenschön, H.; Gryko, D. T. *Angew. Chem., Int. Ed.* **2013**, *52*, 9900–9930. doi:10.1002/anie.201210238
- Simpson, C. D.; Brand, J. D.; Berresheim, A. J.; Przybilla, L.; Räder, H. J.; Müllen, K. *Chem. – Eur. J.* **2002**, *8*, 1424–1429. doi:10.1002/1521-3765(20020315)8:6<1424::aid-chem1424>3.0.co;2-z
- Ormsby, J. L.; Black, T. D.; Hilton, C. L.; Bharat; King, B. T. *Tetrahedron* **2008**, *64*, 11370–11378. doi:10.1016/j.tet.2008.09.105
- Golling, F. E.; Quernheim, M.; Wagner, M.; Nishiuchi, T.; Müllen, K. *Angew. Chem., Int. Ed.* **2014**, *53*, 1525–1528. doi:10.1002/anie.201309104
- Chen, F.; Tanaka, T.; Osuka, A. *Chem. Commun.* **2017**, *53*, 2705–2708. doi:10.1039/c7cc00329c
- Seifert, S.; Shoyama, K.; Schmidt, D.; Würthner, F. *Angew. Chem., Int. Ed.* **2016**, *55*, 6390–6395. doi:10.1002/anie.201601433
- Zhylytskaya, H.; Stępień, M. *Org. Chem. Front.* **2018**, *5*, 2395–2414. doi:10.1039/c8qo00423d
- Navakouski, M.; Zhylytskaya, H.; Chmielewski, P. J.; Lis, T.; Cybińska, J.; Stępień, M. *Angew. Chem., Int. Ed.* **2019**, *58*, 4929–4933. doi:10.1002/anie.201900175
- Shoyama, K.; Würthner, F. *J. Am. Chem. Soc.* **2019**, *141*, 13008–13012. doi:10.1021/jacs.9b06617
- Myśliwiec, D.; Stępień, M. *Angew. Chem., Int. Ed.* **2013**, *52*, 1713–1717. doi:10.1002/anie.201208547
- Feng, C.-N.; Hsieh, Y.-C.; Wu, Y.-T. *Chem. Rec.* **2015**, *15*, 266–279. doi:10.1002/tcr.201402066
- Matsuoka, W.; Ito, H.; Itami, K. *Angew. Chem., Int. Ed.* **2017**, *56*, 12224–12228. doi:10.1002/anie.201707486
- Daigle, M.; Picard-Lafond, A.; Soligo, E.; Morin, J.-F. *Angew. Chem., Int. Ed.* **2016**, *55*, 2042–2047. doi:10.1002/anie.201509130
- Morin, J.-F.; Daigle, M.; Desroches, M. Photochemical and Direct C–H Arylation Routes toward Carbon Nanomaterials. In *Synthetic Methods for Conjugated Polymers and Carbon Materials*; Leclerc, M.; Morin, J.-F., Eds.; Wiley-VCH: Weinheim, Germany, 2017; pp 229–253. doi:10.1002/9783527695959.ch7
- Ozaki, K.; Kawasumi, K.; Shibata, M.; Ito, H.; Itami, K. *Nat. Commun.* **2015**, *6*, 6251. doi:10.1038/ncomms7251
- Hassan, J.; Sévignon, M.; Gozzi, C.; Schulz, E.; Lemaire, M. *Chem. Rev.* **2002**, *102*, 1359–1470. doi:10.1021/cr000664r
- Åkermarck, B.; Ebersson, L.; Jonsson, E.; Pettersson, E. *J. Org. Chem.* **1975**, *40*, 1365–1367. doi:10.1021/jo00897a048
- Hellwinkel, D.; Kistenmacher, T. *Liebigs Ann. Chem.* **1989**, 945–949. doi:10.1002/jlac.198919890249
- Stuart, D. R.; Fagnou, K. *Science* **2007**, *316*, 1172–1175. doi:10.1126/science.1141956
- Yeung, C. S.; Dong, V. M. *Chem. Rev.* **2011**, *111*, 1215–1292. doi:10.1021/cr100280d
- Deng, Y.; Persson, A. K. Å.; Bäckvall, J.-E. *Chem. – Eur. J.* **2012**, *18*, 11498–11523. doi:10.1002/chem.201201494
- Rank, C. K.; Jones, A. W.; Wall, T.; Di Martino-Fumo, P.; Schröck, S.; Gerhards, M.; Patureau, F. W. *Chem. Commun.* **2019**, *55*, 13749–13752. doi:10.1039/c9cc05240b
- Zhylytskaya, H.; Cybińska, J.; Chmielewski, P.; Lis, T.; Stępień, M. *J. Am. Chem. Soc.* **2016**, *138*, 11390–11398. doi:10.1021/jacs.6b07826
- Żyła-Karwowska, M.; Zhylytskaya, H.; Cybińska, J.; Lis, T.; Chmielewski, P. J.; Stępień, M. *Angew. Chem., Int. Ed.* **2016**, *55*, 14658–14662. doi:10.1002/anie.201608400
- Moshniaha, L.; Żyła-Karwowska, M.; Chmielewski, P. J.; Lis, T.; Cybińska, J.; Gońka, E.; Oschwald, J.; Drewello, T.; Rivero, S. M.; Casado, J.; Stępień, M. *J. Am. Chem. Soc.* **2020**, *142*, 3626–3635. doi:10.1021/jacs.9b13942
- Navakouski, M.; Zhylytskaya, H.; Chmielewski, P. J.; Żyła-Karwowska, M.; Stępień, M. *J. Org. Chem.* **2020**, *85*, 187–194. doi:10.1021/acs.joc.9b02556

32. Żyła-Karwowska, M.; Moshniaha, L.; Hong, Y.; Zhylitskaya, H.; Cybińska, J.; Chmielewski, P. J.; Lis, T.; Kim, D.; Stępień, M. *Chem. – Eur. J.* **2018**, *24*, 7525–7530. doi:10.1002/chem.201801199
33. Żyła-Karwowska, M.; Moshniaha, L.; Zhylitskaya, H.; Stępień, M. *J. Org. Chem.* **2018**, *83*, 5199–5209. doi:10.1021/acs.joc.8b00630
34. Vauthey, E. *ChemPhysChem* **2012**, *13*, 2001–2011. doi:10.1002/cphc.201200106

License and Terms

This is an Open Access article under the terms of the Creative Commons Attribution License (<http://creativecommons.org/licenses/by/4.0>). Please note that the reuse, redistribution and reproduction in particular requires that the authors and source are credited.

The license is subject to the *Beilstein Journal of Organic Chemistry* terms and conditions: (<https://www.beilstein-journals.org/bjoc>)

The definitive version of this article is the electronic one which can be found at:
[doi:10.3762/bjoc.16.81](https://doi.org/10.3762/bjoc.16.81)



Synthesis and properties of tetrathiafulvalenes bearing 6-aryl-1,4-dithiafulvenes

Aya Yoshimura^{1,2}, Hitoshi Kimura¹, Kohei Kagawa¹, Mayuka Yoshioka¹, Toshiki Itou¹, Dhananjayan Vasu³, Takashi Shirahata^{1,2}, Hideki Yorimitsu³ and Yohji Misaki^{*1,2}

Full Research Paper

[Open Access](#)

Address:

¹Department of Materials Science and Biotechnology, Graduate School of Science and Engineering, Ehime University, 3 Bunkyo-cho, Matsuyama, Ehime 790-8577, Japan, ²Research Unit for Power Generation and Storage Materials, and Research Unit for Development of Organic Superconductors, Ehime University, 3 Bunkyo-cho, Matsuyama, Ehime 790-8577, Japan and ³Department of Chemistry, Graduate School of Science, Kyoto University, Sakyo-ku, Kyoto 606-8502, Japan

Email:

Yohji Misaki* - misaki.yohji.mx@ehime-u.ac.jp

* Corresponding author

Keywords:

cross-conjugated systems; electrochemical properties; extended π -conjugation; digital simulation analysis; tetrathiafulvalene

Beilstein J. Org. Chem. **2020**, *16*, 974–981.

doi:10.3762/bjoc.16.86

Received: 11 February 2020

Accepted: 04 April 2020

Published: 12 May 2020

This article is part of the thematic issue "C–H functionalization for materials science".

Guest Editor: K. Itami

© 2020 Yoshimura et al.; licensee Beilstein-Institut.

License and terms: see end of document.

Abstract

Novel multistage redox tetrathiafulvalenes (TTFs) bearing 6-aryl-1,4-dithiafulvene moieties were synthesized by palladium-catalyzed direct C–H arylation. In the presence of a catalytic amount of Pd(OAc)₂, P(*t*-Bu₃)-HBF₄, and an excess of Cs₂CO₃, the C–H arylation of TTF with several aryl bromides bearing 1,3-dithiol-2-ylidenes took place efficiently to produce the corresponding π -conjugated molecules. We also succeeded in the estimation of the oxidation potentials and number of electrons involved in each oxidation step of the obtained compounds by digital simulations.

Introduction

Tetrathiafulvalenes (TTFs) with extended π -conjugation have attracted attention as possible components of functional materials, such as molecular conductors, field-effect transistors (FETs), and positive electrode materials for rechargeable batteries because the TTF moiety has strong electron-donating properties attributed to the formation of stable aromatic 1,3-dithiol-2-ylidenes (1,3-dithiole rings) by one- and two-electron

oxidation [1–16]. Considerable efforts have been devoted to the development of peripherally benzene- or thiophene-substituted TTFs. As for peripherally benzene-functionalized TTFs, some synthetic approaches, crystal and electronic structures, electrochemical and optical properties, and the nature of radical ion complexes with DDQ or iodine were reported [17–24]. Peripherally thiophene-functionalized TTFs, as potential precursors to

conducting polymers, and organic metals were also prepared and characterized [25–29]. To design more tempting molecules, the attachment of 1,3-dithiole rings to aromatic rings appears very appealing since these allow to produce novel multistage redox systems. However, such molecules could formerly not be synthesized by conventional approaches. In 2011, a breakthrough synthesis of arylated TTF derivatives by a palladium-catalyzed direct C–H arylation was reported, and the structural and electrochemical properties of the products were clarified [30]. This motivated us to synthesize novel multistage redox-TTFs bearing 1,3-dithiole rings on aromatic rings, **1–3** (Figure 1). In addition, we focused on cross-conjugated systems with 1,3-dithiole rings, which are of interest as novel multistage redox systems as well as donor components for organic conductors [1,31–41]. The palladium-catalyzed C–H arylation might offer access to new cross-conjugated molecules bearing vinyl-extended TTF moieties (EBDTs), such as **4** (Figure 1), and the electrochemical properties of these representatives should be brought to light. Herein, we report the synthesis and electrochemical properties of tetrathiafulvalene derivatives **1–4**.

Results and Discussion

Synthesis

First, we tried to synthesize compounds **1** and **2** in one step from pristine TTF and **5**, respectively, through palladium-catalyzed C–H arylation (Table 1). When the aryl bromides **6a,b** were allowed to react with TTF under the conditions A, the products **1a,b** were produced in 46 and 48% yields, respectively (Table 1, entries 1 and 2). Attempted isolations of products **1c** and **1d** failed, despite complete conversions of TTF, because the polarities of the mono-, di-, and triarylated TTFs were extremely close to that of the tetraarylated TTF **1c** and the solubility of these compounds were low and almost beyond isolation for **1d** (Table 1, entries 3 and 4). The palladium-catalyzed C–H arylation of **5** with **6a,b** proceeded to give products **2a,b** in 75 and 86% yields, respectively (Table 1, entries 5 and 6). On the other hand, it was difficult to produce **3** in the same manner because 2-bromothiophenes **7** bearing a 1,3-dithiole ring at the 5-position were unstable, for example, **7a** decomposed at around 41–42 °C (Scheme 1a). Therefore, we achieved the synthesis of **3a** by Pd-catalyzed thienylation of TTF using acetal-protected **8**, followed by deprotection using PTSA·H₂O and

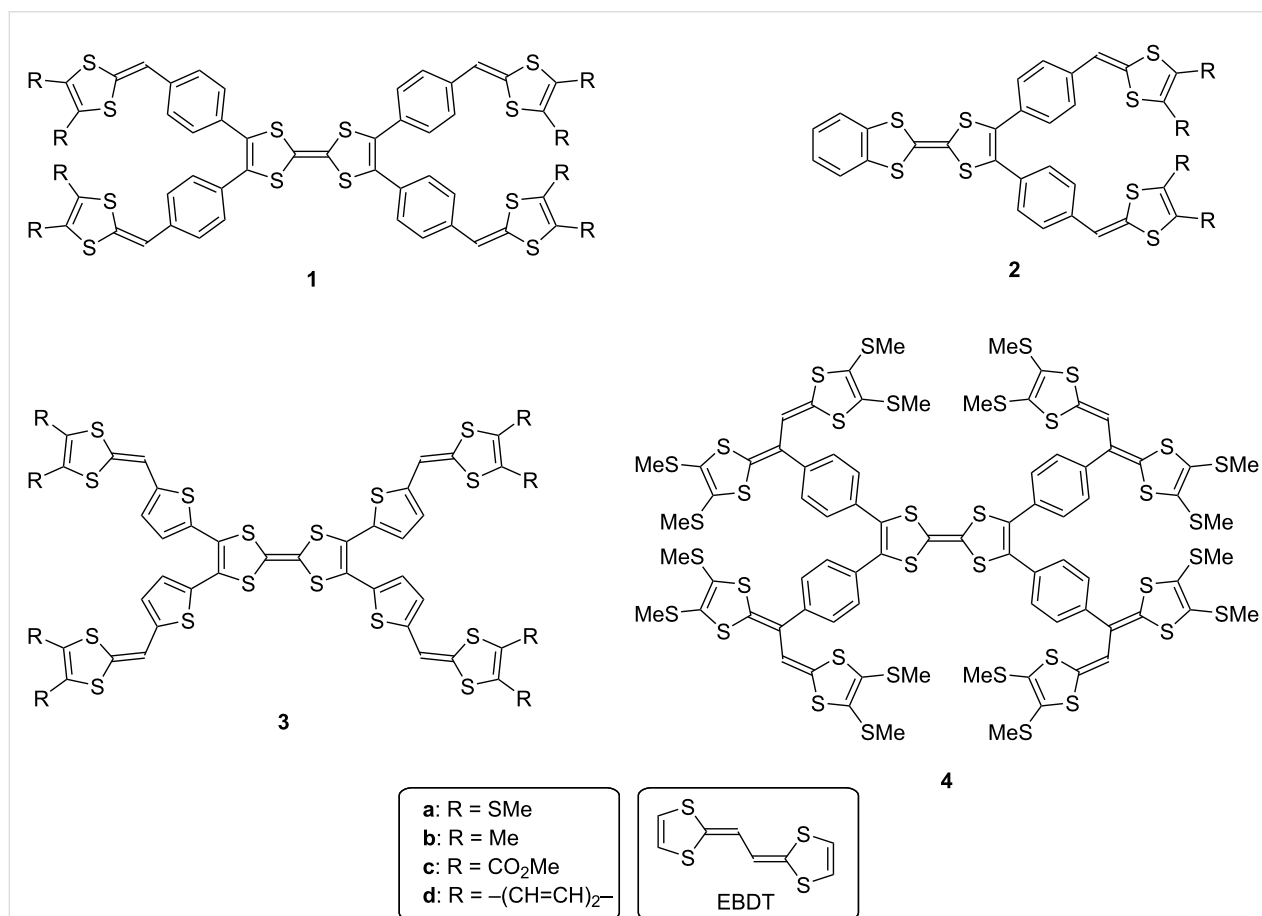
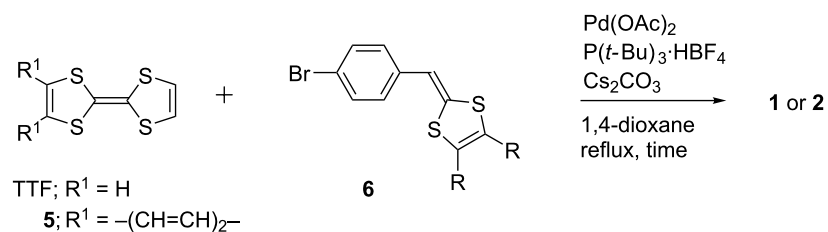


Figure 1: Target compounds.

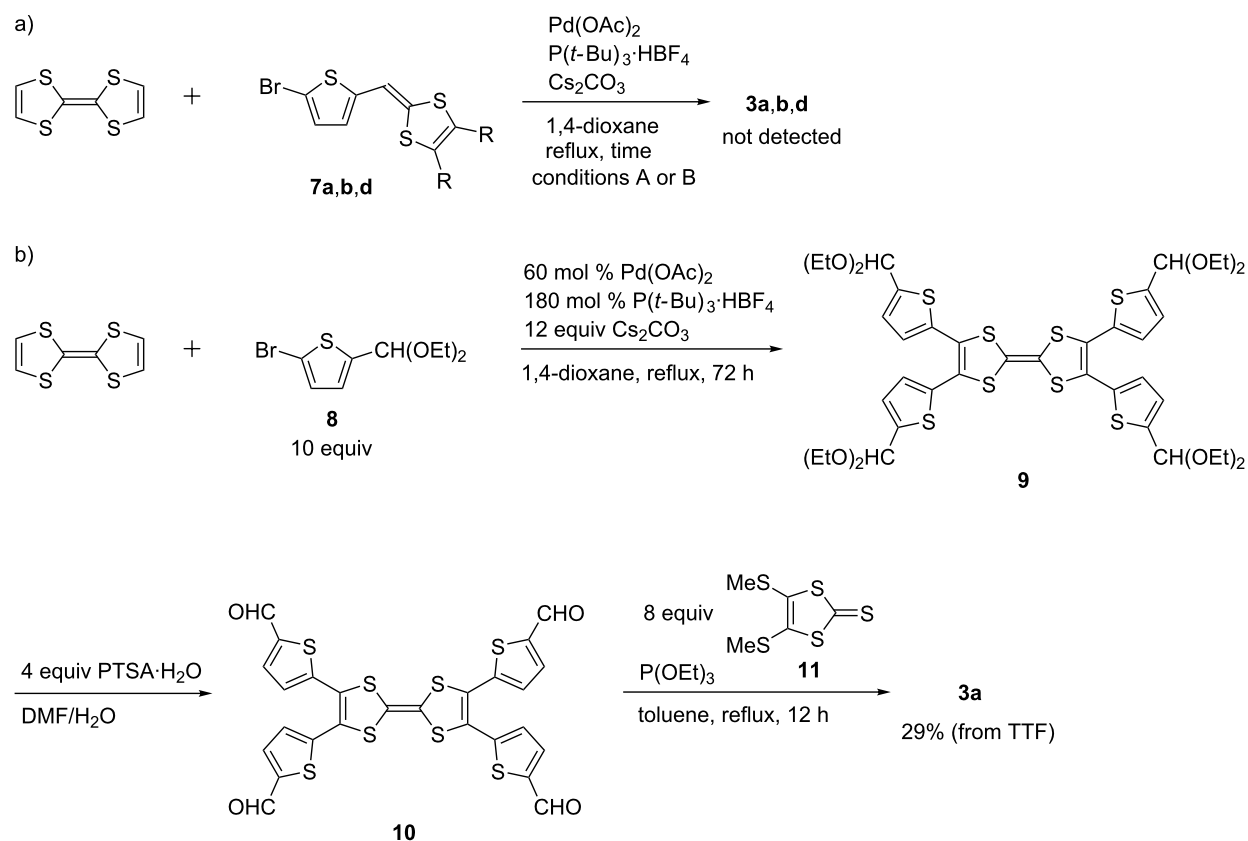
Table 1: Synthesis of compounds **1** and **2**.

conditions A: 30 mol % $\text{Pd}(\text{OAc})_2$, 90 mol % $\text{P}(\text{t-Bu})_3 \cdot \text{HBF}_4$, 6 equiv Cs_2CO_3 , 36 h

B: 60 mol % $\text{Pd}(\text{OAc})_2$, 180 mol % $\text{P}(\text{t-Bu})_3 \cdot \text{HBF}_4$, 12 equiv Cs_2CO_3 , 108 h

entry	TTF or 5	6 (equiv)	conditions	yield of 1 or 2 (%)
1	TTF	6a (5)	A	1a : 46
2	TTF	6b (5)	A	1b : 48
3	TTF	6c (5)	A or B	1c : 0 (mixture)
4	TTF	6d (5)	A or B	1d : 0 (mixture)
5	5	6a (2.5)	A ^a	2a : 75
6	5	6b (2.5)	A ^a	2b : 86

^aReaction time 24 h.

**Scheme 1:** Synthesis of compounds **3**.

P(OEt)₃-mediated cross coupling with **11** (Scheme 1b). The cross-conjugated molecule **4** was prepared in two procedures; one was the palladium-catalyzed C–H arylation of TTF with bromide **12** (Scheme 2a) and the other was the Vilsmeier–Haack reaction of **1a**, followed by triethyl phosphite-mediated cross coupling with **11** (Scheme 2b).

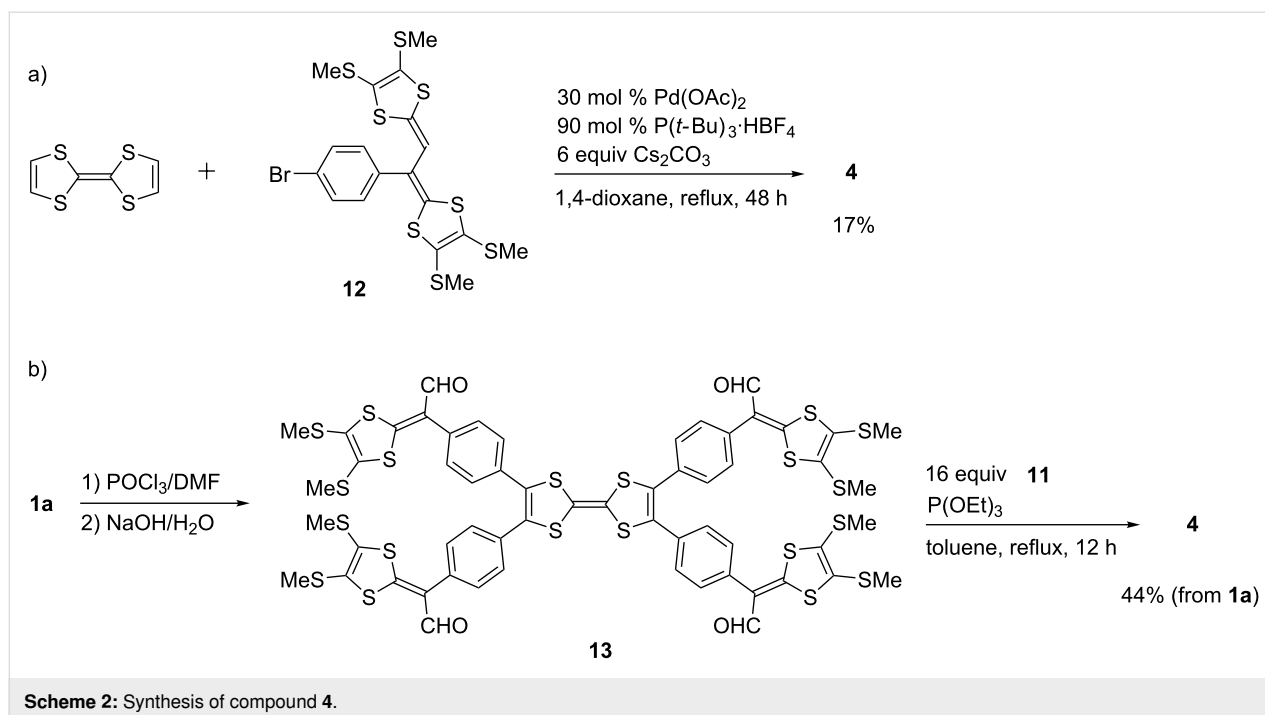
Theoretical calculations

The DFT calculations of compounds **1a**, **3a**, and **4** have been carried out by using the B3LYP/6-31G(d,p) method [42]. Figure 2 shows an optimized geometry of **1a**, and the 1,3-dithiole rings are labeled as A–E and A'–E'. This molecule adopted a nonplanar structure. The angle between the two 1,3-dithiole rings in the center (A–A') was 158.0°. The dihedral angles between A and B, A and B', A' and C, and A' and C' were 49.8°, 137.7°, 137.7°, and 49.9°, respectively. The HOMO, HOMO–1, and LUMO of **1a** are shown in Figure 3. The HOMO of **1a** was mainly located on the TTF moiety, whereas the HOMO–1 was located on the benzene ring and the outer 1,3-dithiole rings at the peripheral part of TTF. The LUMO of **1a** spread over the whole molecule except the outer 1,3-dithiole rings. The orbital energy of the HOMO of **1a** (–4.41 eV) was slightly higher than that of TTF (–4.57 eV). As such, the first oxidation of **1a** might occur at a lower potential than TTF [43].

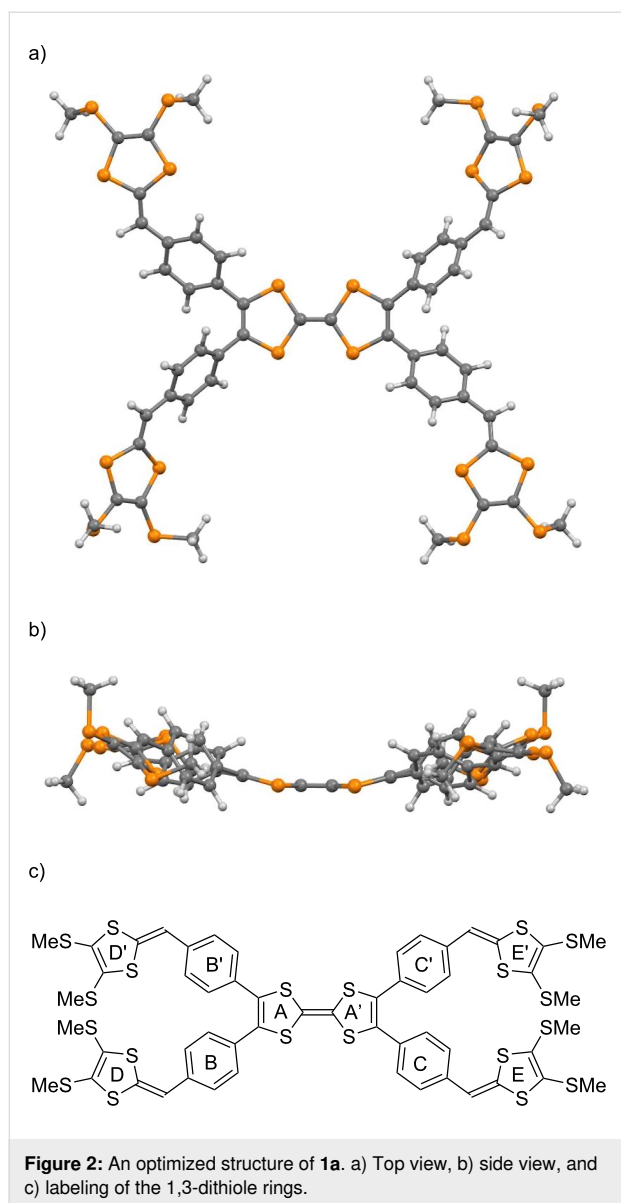
Cyclic voltammetry analysis

The redox behavior of **1–4** was investigated by cyclic voltammetry. The compounds **1a** and **1b** exhibited four and three pairs

of redox waves, respectively (around +0.03, +0.10, +0.17, and +0.42 V vs Fc/Fc⁺ for **1a** and –0.05, +0.10, and +0.46 V vs Fc/Fc⁺ for **1b**, Figure 4). The redox potentials of **1a,b** are summarized in Table 2 together with the related compound TTF. The redox waves observed at +0.42 V for **1a** and +0.46 V for **1b** were likely related to the second redox of the central TTF moiety because they were close to the *E*₂ of TTF (+0.37 V). The remaining redox processes observed at around +0.03, +0.10, and +0.17 V for **1a**, and –0.05 and +0.10 V for **1b** might have been derived from the first redox of the central TTF moiety and the redox of the four outer 1,3-dithiole rings. To elaborate the exact oxidation potentials and the number of electrons involved in each oxidation step, a digital simulation technique was applied [44]. As a result, the observed redox waves of **1a** matched the simulated waves (Table 2). It was indicated that the redox wave at +0.10 V was due to an overlap of the sequential two stages of the one- and two-electron transfer waves at +0.07 and +0.12 V, while the other waves corresponded to one-electron transfer processes. The simulation results of **1a** also showed that the redox wave simulated at +0.020 V might have been derived from the central TTF moiety because of the close ΔE values (+0.40 V for **1a** and +0.46 V for TTF). The same discussion was applied to **1b**. In addition, the potentials related to the outer 1,3-dithiole rings of **1a,b** were influenced by the substituents, that is, **1b** bearing electron-donating methyl groups had more negative redox potentials than **1a**. As a consequence, the one-electron redox process of the TTF moiety and the multi-electron redox processes of the outer 1,3-dithiole rings might have overlapped in **1b**.

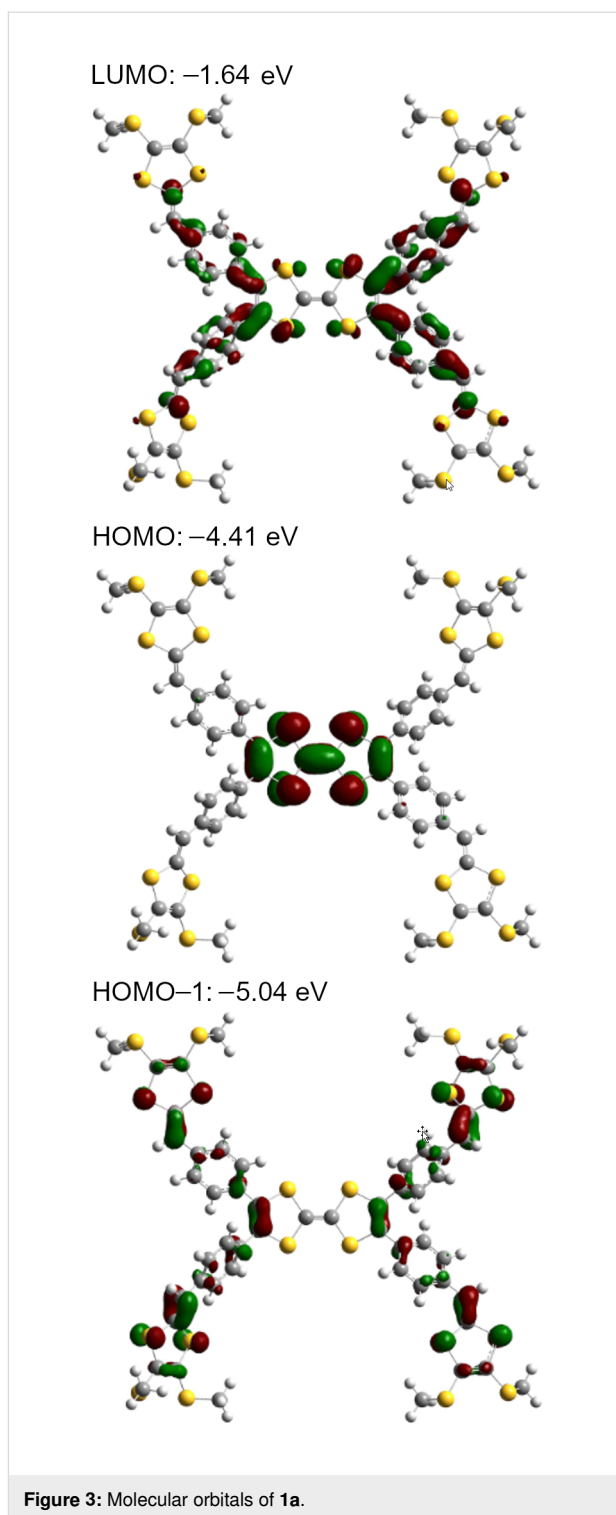


Scheme 2: Synthesis of compound **4**.



Compound **2a** exhibited three pairs of redox waves (-0.05 , $+0.09$, and $+0.49$ V vs Fc/Fc^+). The redox waves observed at -0.05 and $+0.49$ V were likely related to the TTF derivative (**5**) moiety, because they were close to the E_1 and E_2 of **5**, respectively (Table 2). The comparison of the peak currents of each wave indicated that the redox wave observed at $+0.09$ V involved a two-electron transfer, while the redox waves observed at -0.05 and $+0.49$ V corresponded to one-electron transfer processes (see the differential pulse voltammetry (DPV) in Supporting Information File 1, Figure S2). These results supported the above-mentioned oxidation potentials and the number of electrons involved in each oxidation step of **1a,b**.

Compound **4** exhibited three pairs of redox waves (around -0.09 , $+0.09$, and $+0.53$ V vs Fc/Fc^+). The redox potentials of **4**



and the simulation results are also summarized in Table 2, together with those of the related compounds TTF and **14** (see Figure 5). The redox process observed at $+0.53$ V was likely related to the second redox of the central TTF moiety because this was the closest to the value of the E_2 of TTF ($+0.37$ V) out of all potentials of the related compounds TTF and **14**. The

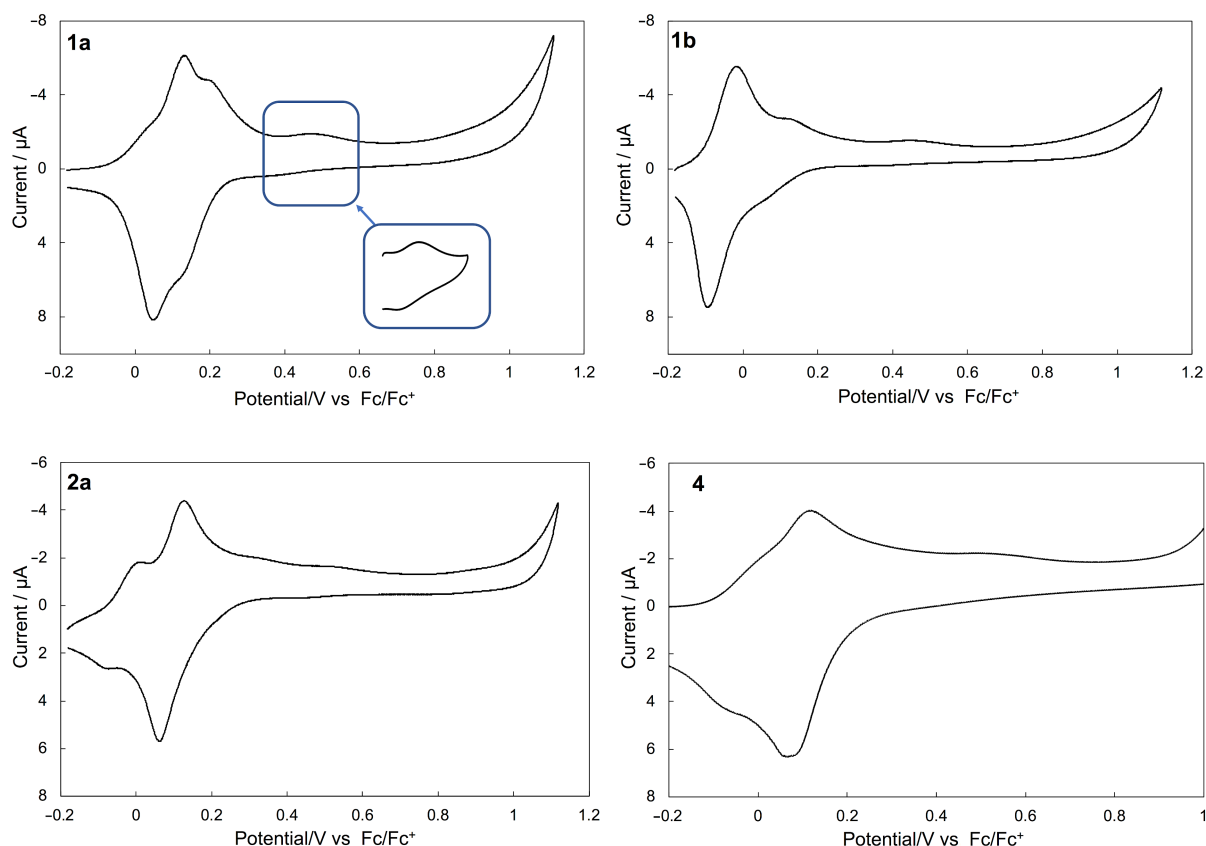


Figure 4: Cyclic voltammograms of **1a**, **1b**, **2a**, and **4** in PhCN/CS₂ 1:1 (v/v) solution.

Table 2: Redox potentials of **1**, **2a**, **4**, and related compounds^a.

compound	observed or simulated value	E_1	E_2	E_3	E_4	E_5	E_6	E_7	E_8	E_9	E_{10}
1a	observed	around +0.03 ^b	+0.10			+0.17	+0.42				
	simulated	+0.020	+0.070	+0.120		+0.200	+0.420				
1b	observed	−0.05				+0.10	+0.46 ^b				
2a	observed	−0.05	+0.09		+0.49						
4	observed	around −0.09			+0.09						+0.53 ^b
	simulated	−0.060	−0.030	+0.010	+0.047	+0.053	+0.098	+0.102	+0.110	+0.180	+0.500
TTF ^c	observed	−0.09	+0.37								
5^c	observed	−0.01	+0.42								
14^c	observed	−0.07	+0.09								

^aIn PhCN/CS₂ 1:1 (v/v) containing 0.1 M *n*-Bu₄NPF₆. ^bAnodic peak. ^cIn PhCN containing 0.1 M *n*-Bu₄NPF₆. All potentials were measured against an Ag/Ag⁺ reference electrode and converted to vs Fc/Fc⁺.

remaining redox processes observed at around −0.09 and +0.09 V might have been due to the first redox of the central TTF moiety, and the overall redox of the EBDT sites, respec-

tively. The observed potentials of **4** were generally consistent with the simulated ones. The results of a digital simulation also showed that the redox wave observed at around −0.09 V and

+0.09 V corresponded to three stages of one-electron transfer and six stages of one-electron transfer processes, respectively. In addition to the overlap of the first redox of the central TTF moiety and the redox of the EBDT sites, each redox potential of the succeeding eight-electron oxidations of the EBDT sites might have slightly shifted due to the non-equivalence of them. Also, the small ΔE value (0.16 V) of **14** caused the redox wave overlap. For these reasons, the first and second redox waves of **4** were broad compared to those of **1a** and **1b**.

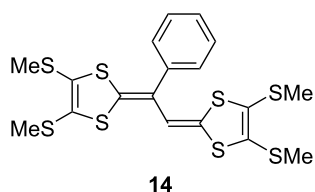


Figure 5: Related compound **14**.

The redox waves of **1a,b** and **4** derived from the second redox of the central TTF moiety (+0.42 V for **1a**, +0.46 V for **1b**, and +0.53 V for **4**) shifted to higher potentials than the second redox of TTF because of the instability of the hexacationic state of **1a,b**, and the decacationic state of **4** compared to the dicationic states of TTF caused by on-site Coulomb repulsion between positive charges in the central TTF moiety and the outer 1,3-dithiole rings. The same discussion could be applied to compounds **2a**. In addition, the observed peak currents of **1a** and **4** in the high potential region at +0.4 to +0.5 V were smaller than those of the simulated waves. This phenomenon might be understood by considering that electron transfer of this redox reaction was slow enough to become the rate-determining step because the crowded structure by which the TTF core is participating in this redox process is surrounded by extended aromatic rings bearing 1,3-dithiol rings.

Conclusion

We have synthesized novel multistage TTF derivatives **1–4** bearing 6-aryl-1,4-dithiafulvene moieties by palladium-catalyzed direct C–H arylation. The DFT calculations revealed the nonplanar structure of the compounds. Cyclic voltammograms of **1a** and **4** comprised four and three pairs of redox waves, respectively. As a result of the digital simulation of **1a**, it was shown that the redox wave observed at +0.10 V involved two stages of one- and two-electron transfer(s), while the other redox waves corresponded to one-electron transfer. The digital simulation of **4** showed 10 stages of one-electron transfer in total. In addition, the first and second redox waves of **4** were broad compared to those of **1** owing to the following three

reasons: a) overlap of the central TTF moiety and the redox of the EBDT sites, b) the succeeding eight-electron oxidations of the non-equivalent EBDT sites, and c) the small ΔE value (0.16 V) of the EBDT sites.

Supporting Information

Supporting Information File 1

Synthetic procedures, theoretical chemical and electrochemical details, and copies of NMR spectra. [https://www.beilstein-journals.org/bjoc/content/supplementary/1860-5397-16-86-S1.pdf]

Funding

This work was partially supported by a Grant-in-Aid for Scientific Research (JP15H03798), from the Ministry of Education, Culture, Sports, Science and Technology (MEXT). This work was also supported by a Grant-in-Aid for Research Promotion, Ehime University, to The Research Unit for Development of Organic Superconductors and to The Research Unit for Power Generation and Storage Materials.

ORCID® iDs

Aya Yoshimura - <https://orcid.org/0000-0001-9967-4598>
 Dhananjayan Vasu - <https://orcid.org/0000-0001-7597-3710>
 Takashi Shirahata - <https://orcid.org/0000-0003-0899-3767>
 Hideki Yorimitsu - <https://orcid.org/0000-0002-0153-1888>
 Yohji Misaki - <https://orcid.org/0000-0002-9079-8487>

Preprint

A non-peer-reviewed version of this article has been previously published as a preprint doi:10.3762/bxiv.2020.16.v1

References

- Yamada, J.; Sugimoto, T., Eds. *TTF Chemistry-Fundamental and Applications of Tetrathiafulvalene*; Kodansha-Springer: Tokyo, 2004.
- Canevet, D.; Sallé, M.; Zhang, G.; Zhang, D.; Zhu, D. *Chem. Commun.* **2009**, 2245–2269. doi:10.1039/b818607n
- Gorgues, A.; Hudhomme, P.; Sallé, M. *Chem. Rev.* **2004**, *104*, 5151–5184. doi:10.1021/cr0306485
- Segura, J. L.; Martín, N. *Angew. Chem., Int. Ed.* **2001**, *40*, 1372–1409. doi:10.1002/1521-3773(20010417)40:8<1372::aid-anie1372>3.0.co;2-i
- Iyoda, M.; Hasegawa, M.; Miyake, Y. *Chem. Rev.* **2004**, *104*, 5085–5114. doi:10.1021/cr030651o
- Hasegawa, M.; Iyoda, M. Tetrathiafulvalene: A Redox Unit for Functional Materials and a Building Block for Supramolecular Self-Assembly. In *Organic Redox Systems*; Nishinaga, T., Ed.; John Wiley & Sons: Hoboken, NJ, USA, 2015; pp 89–129. doi:10.1002/9781118858981.ch4
- Misaki, Y. *Sci. Technol. Adv. Mater.* **2009**, *10*, 024301. doi:10.1088/1468-6996/10/2/024301

8. Inatomi, Y.; Hojo, N.; Yamamoto, T.; Shimada, M.; Watanabe, S. Examination of Multi-Electron Reaction Type pi-Conjugated Organic Compounds as Cathode Active Material for Rechargeable Power Supply. In *ECS Meeting Abstracts, Volume MA2008-01, B1- Batteries General Session, Abstract #167*, 213th ECS meeting, Phoenix, Arizona, May 18–22, 2008; The Electrochemical Society, 2008. doi:10.1149/ma2008-01/5/167
9. Inatomi, Y.; Hojo, N.; Yamamoto, T.; Watanabe, S.-i.; Misaki, Y. *ChemPlusChem* **2012**, *77*, 973–976. doi:10.1002/cplu.201200197
10. Kato, M.; Ogi, D.; Yao, M.; Misaki, Y. *Chem. Lett.* **2013**, *42*, 1556–1558. doi:10.1246/cl.130841
11. Kato, M.; Senoo, K.-i.; Yao, M.; Misaki, Y. *J. Mater. Chem. A* **2014**, *2*, 6747–6754. doi:10.1039/c3ta14920j
12. Iwamoto, S.; Inatomi, Y.; Ogi, D.; Shibayama, S.; Murakami, Y.; Kato, M.; Takahashi, K.; Tanaka, K.; Hojo, N.; Misaki, Y. *Beilstein J. Org. Chem.* **2015**, *11*, 1136–1147. doi:10.3762/bjoc.11.128
13. Yamauchi, T.; Shibata, Y.; Aki, T.; Yoshimura, A.; Yao, M.; Misaki, Y. *Chem. Lett.* **2018**, *47*, 1176–1179. doi:10.1246/cl.180496
14. Ogi, D.; Fujita, Y.; Kato, M.; Yamauchi, T.; Shirahata, T.; Yao, M.; Misaki, Y. *Eur. J. Org. Chem.* **2019**, 2725–2728. doi:10.1002/ejoc.201801877
15. Yamauchi, T.; Kato, M.; Shirahata, T.; Yao, M.; Misaki, Y. *Chem. Lett.* **2019**, *48*, 1507–1510. doi:10.1246/cl.190703
16. Bryce, M. R. *J. Mater. Chem.* **2000**, *10*, 589–598. doi:10.1039/a908385e
17. Coffen, D. L.; Chambers, J. Q.; Williams, D. R.; Garrett, P. E.; Canfield, N. D. *J. Am. Chem. Soc.* **1971**, *93*, 2258–2268. doi:10.1021/ja00738a028
18. Ueno, Y.; Okawara, M. *Chem. Lett.* **1974**, *3*, 1135–1138. doi:10.1246/cl.1974.1135
19. Ueno, Y.; Nakayama, A.; Okawara, M. *J. Am. Chem. Soc.* **1976**, *98*, 7440–7441. doi:10.1021/ja00439a064
20. Yoneda, S.; Kawase, T.; Inaba, M.; Yoshida, Z.-i. *J. Org. Chem.* **1978**, *43*, 595–598. doi:10.1021/jo00398a015
21. Le Coustumer, G.; Mollier, Y. *J. Chem. Soc., Chem. Commun.* **1980**, 38–39. doi:10.1039/c39800000038
22. Babeau, A.; Tinh, N. H.; Gasparoux, H.; Polycarpe, C.; Torreilles, E.; Giral, L. *Mol. Cryst. Liq. Cryst.* **1982**, *72*, 171–176. doi:10.1080/0140658208084054
23. Starodub, V. A.; Baumer, V. N.; Guella, I. M.; Golovkina, I. F.; Alyoshin, V. G.; Nemoskalenko, V. V.; Senkiewicz, A. I. *Synth. Met.* **1983**, *5*, 101–111. doi:10.1016/0379-6779(83)90124-8
24. Tsujimoto, K.; Okeda, Y.; Ohashi, M. *J. Chem. Soc., Chem. Commun.* **1985**, 1803–1804. doi:10.1039/c39850001803
25. Charlton, A.; Underhill, A. E.; Williams, G.; Kalaji, M.; Murphy, P. J.; Hibbs, D. E.; Hursthouse, M. B.; Malik, K. M. A. *Chem. Commun.* **1996**, 2423–2424. doi:10.1039/cc9960002423
26. Charlton, A.; Underhill, A. E.; Williams, G.; Kalaji, M.; Murphy, P. J.; Malik, K. M. A.; Hursthouse, M. B. *J. Org. Chem.* **1997**, *62*, 3098–3102. doi:10.1021/jo962301q
27. Gompper, R.; Hock, J. *Synth. Met.* **1997**, *84*, 339–340. doi:10.1016/s0379-6779(97)80771-0
28. Zotti, G.; Zecchin, S.; Schiavon, G.; Berlin, A.; Huchet, L.; Roncali, J. *J. Electroanal. Chem.* **2001**, *504*, 64–70. doi:10.1016/s0022-0728(01)00429-6
29. Kakinuma, T.; Kojima, H.; Kawamoto, T.; Mori, T. *J. Mater. Chem. C* **2013**, *1*, 2900–2905. doi:10.1039/c3tc30089g
30. Mitamura, Y.; Yorimitsu, H.; Oshima, K.; Osuka, A. *Chem. Sci.* **2011**, *2*, 2017–2021. doi:10.1039/c1sc00372k
31. Gholami, M.; Tykwinski, R. R. *Chem. Rev.* **2006**, *106*, 4997–5027. doi:10.1021/cr0505573
32. Sugimoto, T.; Awaji, H.; Misaki, Y.; Yoshida, Z.-i.; Kai, Y.; Nakagawa, H.; Kasai, N. *J. Am. Chem. Soc.* **1985**, *107*, 5792–5793. doi:10.1021/ja00306a030
33. Sugimoto, T.; Misaki, Y.; Arai, Y.; Yamamoto, Y.; Yoshida, Z.-i.; Kai, Y.; Kasai, N. *J. Am. Chem. Soc.* **1988**, *110*, 628–629. doi:10.1021/ja00210a069
34. Misaki, Y.; Matsumura, Y.; Sugimoto, T.; Yoshida, Z.-i. *Tetrahedron Lett.* **1989**, *30*, 5289–5292. doi:10.1016/s0040-4039(01)93767-0
35. Amaresh, R. R.; Liu, D.; Konovalova, T.; Lakshmikantham, M. V.; Cava, M. P.; Kispert, L. D. *J. Org. Chem.* **2001**, *66*, 7757–7764. doi:10.1021/jo010663e
36. Rajagopal, D.; Lakshmikantham, M. V.; Cava, M. P. *Org. Lett.* **2002**, *4*, 2581–2583. doi:10.1021/ol026227b
37. Coffin, M. A.; Bryce, M. R.; Batsanov, A. S.; Howard, J. A. K. *J. Chem. Soc., Chem. Commun.* **1993**, 552–554. doi:10.1039/c39930000552
38. Bryce, M. R.; Coffin, M. A.; Skabara, P. J.; Moore, A. J.; Batsanov, A. S.; Howard, J. A. K. *Chem. – Eur. J.* **2000**, *6*, 1955–1962. doi:10.1002/1521-3765(20000602)6:11<1955::aid-chem1955>3.0.co;2-b
39. Hasegawa, M.; Fujioka, A.; Kubo, T.; Honda, T.; Miyamoto, H.; Misaki, Y. *Chem. Lett.* **2008**, *37*, 474–475. doi:10.1246/cl.2008.474
40. Horiuchi, H.; Misaki, Y. *Chem. Lett.* **2010**, *39*, 989–991. doi:10.1246/cl.2010.989
41. Nishiwaki, M.; Tezuka, M.; Shirahata, T.; Misaki, Y. *Chem. Lett.* **2011**, *40*, 467–469. doi:10.1246/cl.2011.467
42. *Gaussian 16*, Revision C.01; Gaussian, Inc.: Wallingford, CT, 2019.
43. The optimized geometries and energy levels of the LUMO, HOMO, and HOMO–1 of **3a** and **4** are shown in Supporting Information File 1, Figure S1.
44. *DigiElch 7 Prof software*; Elchsoft: Kleinromstedt, Germany.

License and Terms

This is an Open Access article under the terms of the Creative Commons Attribution License (<http://creativecommons.org/licenses/by/4.0>). Please note that the reuse, redistribution and reproduction in particular requires that the authors and source are credited.

The license is subject to the *Beilstein Journal of Organic Chemistry* terms and conditions: (<https://www.beilstein-journals.org/bjoc>)

The definitive version of this article is the electronic one which can be found at:
doi:10.3762/bjoc.16.86



Clickable azide-functionalized bromoarylaldehydes – synthesis and photophysical characterization

Dominik Göbel¹, Marius Friedrich^{1,2}, Enno Lork³ and Boris J. Nachtsheim^{*1}

Full Research Paper

Open Access

Address:

¹Institute for Organic and Analytical Chemistry, University of Bremen, Leobener Straße 7, 28359 Bremen, Germany, ²Department of Organic Chemistry, Technical University Kaiserslautern, Erwin-Schrödinger-Straße Geb.54, 67663 Kaiserslautern, Germany and ³Institute for Inorganic and Crystallographic Chemistry, University of Bremen, Leobener Straße NW2, 28359 Bremen, Germany

Email:

Boris J. Nachtsheim^{*} - nachtsheim@uni-bremen.de

^{*} Corresponding author

Keywords:

bromoarylaldehydes; click-chemistry; fluorenes; fluorescence; phosphorescence

Beilstein J. Org. Chem. **2020**, *16*, 1683–1692.

doi:10.3762/bjoc.16.139

Received: 11 May 2020

Accepted: 30 June 2020

Published: 14 July 2020

This article is part of the thematic issue "C–H functionalization for materials science".

Guest Editor: K. Itami

© 2020 Göbel et al.; licensee Beilstein-Institut.

License and terms: see end of document.

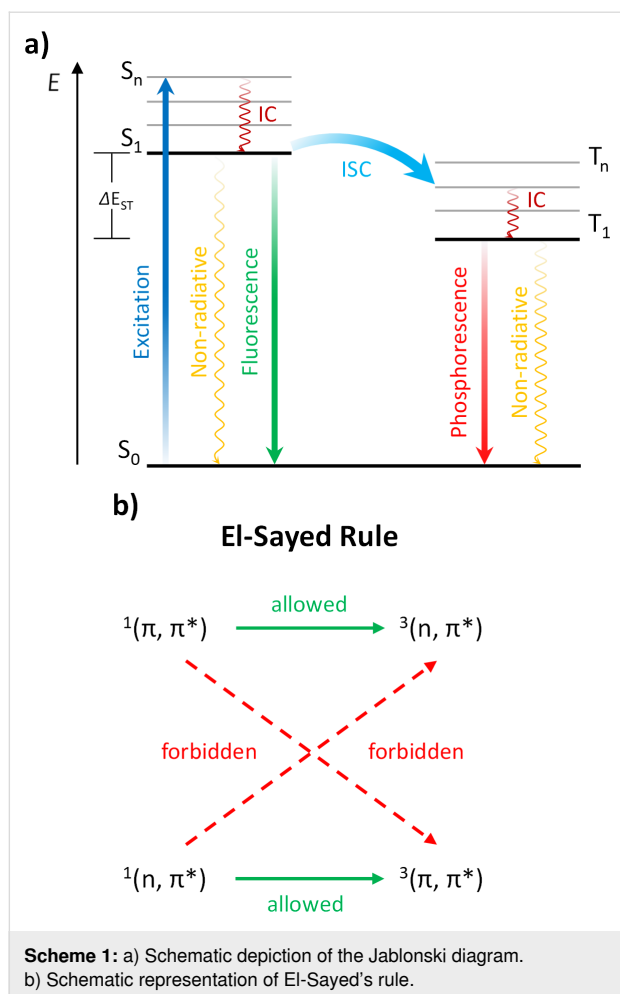
Abstract

Herein, we present a facile synthesis of three azide-functionalized fluorophores and their covalent attachment as triazoles in Huisgen-type cycloadditions with model alkynes. Besides two *ortho*- and *para*-bromo-substituted benzaldehydes, the azide functionalization of a fluorene-based structure will be presented. The copper(I)-catalyzed azide–alkyne cycloaddition (CuAAC) of the so-synthesized azide-functionalized bromocarbaldehydes with terminal alkynes, exhibiting different degrees of steric demand, was performed in high efficiency. Finally, we investigated the photophysical properties of the azide-functionalized arenes and their covalently linked triazole derivatives to gain deeper insight towards the effect of these covalent linkers on the emission behavior.

Introduction

Small organic luminophores exhibiting room-temperature phosphorescence (RTP) have attracted great attention due to promising applications in optoelectronic devices [1–8], biological imaging [9–12] and chemical sensing [13–15]. Referring to the Jablonski diagram (see Scheme 1a) [16,17], upon excitation from the singlet ground state (S_0) to higher singlet states (S_n), followed by internal conversion (IC), either non-radiative or radiative decay to S_0 can occur. While the latter decay (fluores-

cence) takes place without a change in the electron spin, phosphorescence is defined as the radiative transition from the lowest excited triplet state (T_1) to the singlet ground state (S_0) [18–21]. Triplet state excitons are generated by the spin-forbidden intersystem crossing (ISC) process from the first excited singlet state (S_1). Pursuant to the El-Sayed rule (see Scheme 1b) [22,23], ISC is spin allowed from $^1(n,\pi^*)$ to $^3(\pi,\pi^*)$ and from $^1(\pi,\pi^*)$ to $^3(n,\pi^*)$ excited states, while ISC is spin-



forbidden from $^1(n, \pi^*)$ to $^3(n, \pi^*)$ and from $^1(\pi, \pi^*)$ to $^3(\pi, \pi^*)$ excited states, owing to the poor orbital overlap, resulting in a decreased spin-orbit coupling.

Quenching processes of triplet states, induced by molecular motions, oxygen, or humidity, restrict the versatile application of such organic materials [24]. Thus, low temperatures [25–27] or inert conditions [28] are necessary to facilitate an afterglow emission.

Most phosphorescence studies are focused on metal complexes due to a strong heavy atom-induced spin-orbit coupling [29–33]. Considering the high price and the toxicity of many metal complexes, pure organic phosphors are highly desirable [16,17,34–37]. Two approaches are applied to achieve organic phosphors: (1) introduction of nonmetal heavy atoms, such as halogens (Br or I) or functionalities containing lone pairs, in particular carbonyl groups, nitrogen, sulfur, and phosphorus derivatives which facilitate the ISC process from S_1 to T_n and thus increase the spin-orbital coupling [38–47]. Also, decreasing the singlet–triplet splitting energy (ΔE_{ST}) caused by intramolecular

charge-transfer (ICT) interactions is an approved method [48,49]. (2) Significant reduction of non-radiative transitions can be achieved by the host–guest method [50–52] or by crystallization [53–57]. In difference to the liquid phase, the highly ordered packing and the restriction of molecular motions in the crystalline state favor a persistent luminescence.

The promotion of ISC processes through intermolecular halogen bonding to generate efficient RTP was initially investigated by Kim et al. [58]. They developed the minimalistic 2,5-dihexyloxy-4-bromobenzaldehyde (**1**) [59–63] which showed a weak fluorescence in solution, but exhibited a green phosphorescence with a quantum yield of $\Phi_P = 2.9\%$ in the crystalline state: this behavior was caused by intermolecular halogen bonds from the carbonyl-oxygen atom to an adjacent bromine atom (Figure 1a).

Despite multifarious examples of RTP in the crystalline state, purely organic compounds showing RTP in solution are rare [64–69]. Takeuchi et al. [28] reported a bromofluorencarbaldehyde **2** which shows blue fluorescence in chloroform at 298 K under air and green phosphorescence under argon with a phosphorescence quantum yield of $\Phi_P = 5.9\%$ (Figure 1b). This observation is reasoned by a strong (π, π^*) character of the T_2 state.

Although phosphorescent organic compounds are well investigated with respect to their photophysical properties in the crystalline state, in solution or physically embedded in polymer matrices, there is a significant lack of possibilities [61] for their targeted covalent attachment to higher structures. This is due to missing synthetic strategies to incorporate suitable linkable functionalities into those luminophores.

Our group is highly interested in the de novo synthesis of small organic luminophores and in this regard, we recently developed efficient methods for the synthesis of ESIPT-based luminophores [70–72]. Herein, we present the efficient functionalization of derivatives of the potent luminophores **1** and **2** with “clickable” azide functionalities to target the structures **3–5** and further investigated the influence of this functionalization, both in the unlinked azide state and the linked triazole state, on the emission properties of these compounds (Figure 1).

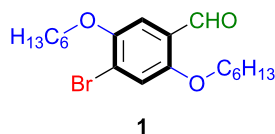
Results and Discussion

Syntheses *para*- and *ortho*-bromobenzaldehyde **3** and **4**

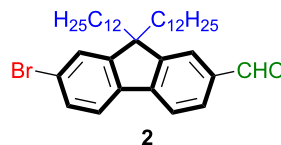
We initiated our synthetic investigations towards azide-functionalized *para*-bromobenzaldehyde **3** with a two-step sequence. Condensation with 2-amino-2-methylpropan-1-ol and oxidation

literature examples:

a) Kim et al. [58]



b) Takeuchi et al. [28]



this work:

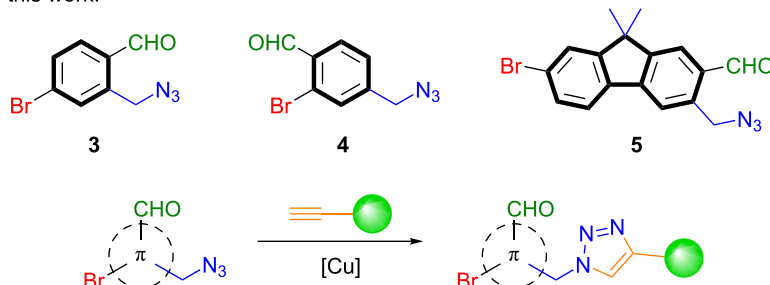
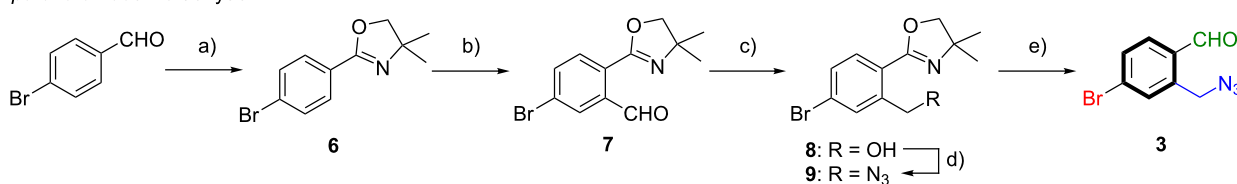
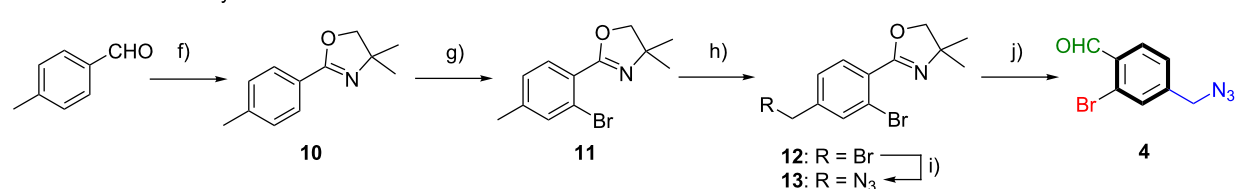


Figure 1: Top: literature examples of organic compounds showing RTP in the crystalline state (a) and in solution (b). Bottom: azide-linked derivatives presented in this work.

with NBS yielded oxazoline **6** in a good yield. Directed *ortho*-metalation utilizing $\text{TMPMgCl}\cdot\text{LiCl}$ under mild conditions and subsequent smooth formylation with DMF afforded benzaldehyde **7** (see Scheme 2). Due to rapid decomposition of **7** under ambient and acidic conditions, rapid aqueous work-up was conducted, followed by reduction with NaBH_4 , yielding the corresponding primary alcohol **8** in 81% yield over two steps. The transformation to azide **9** was accomplished by deprotonation

using 1,8-diazabicyclo[5.4.0]undec-7-ene (DBU) and reaction with diphenylphosphoryl azide (DPPA) in excellent yield. Finally, the oxazoline group, which acted as directing and protecting group, was removed in a three-step sequence of *N*-methylation, reduction of the in situ formed iminium ion and acidic hydrolysis. This afforded the azide-functionalized *para*-bromobenzaldehyde **3** in 78% yield and an overall yield of 56% (starting from 4-bromobenzaldehyde).

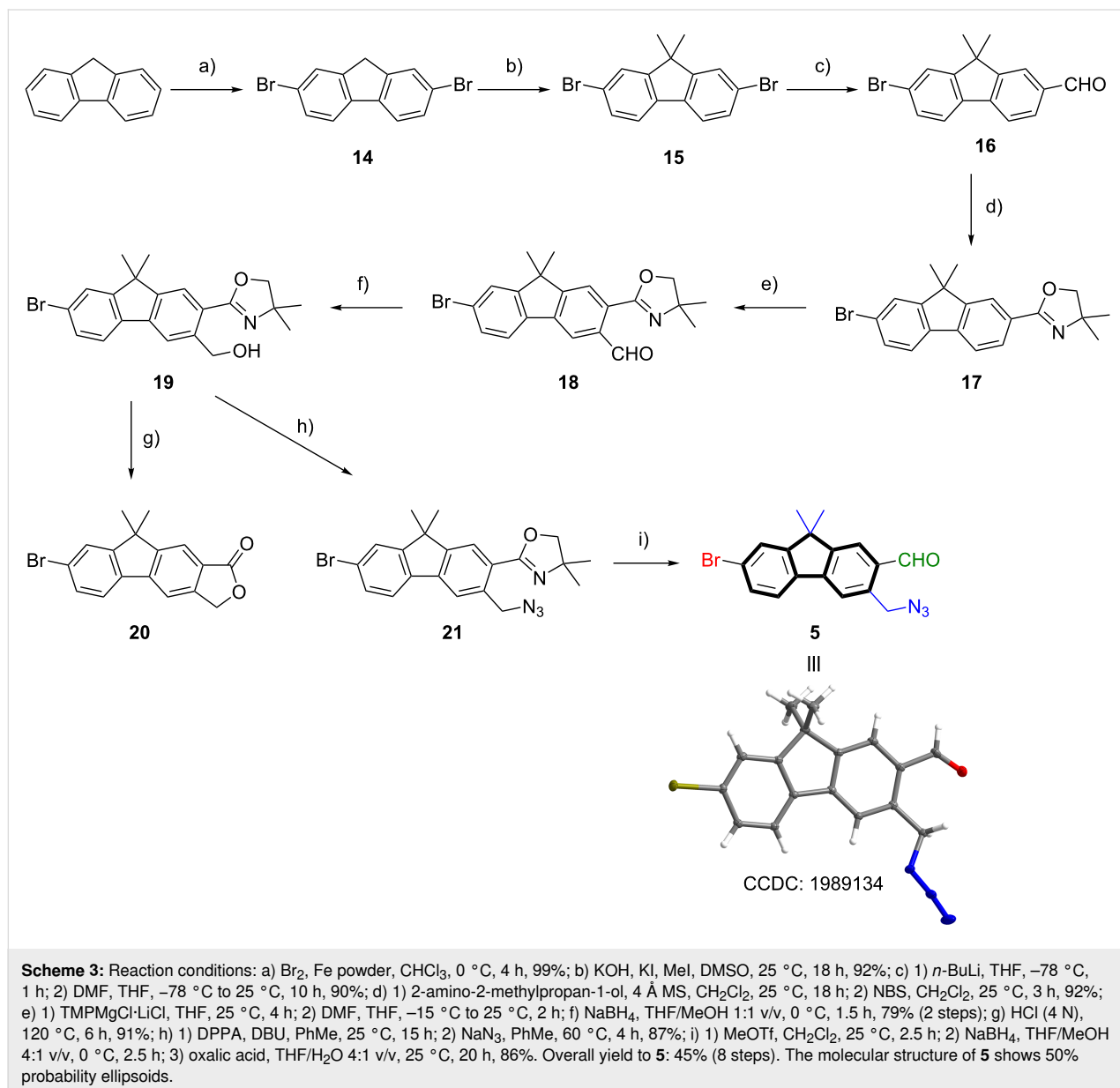
para-bromobenzaldehyde:*ortho*-bromobenzaldehyde:

Scheme 2: Reaction conditions for *para*-bromobenzaldehyde **3**: a) 1) 2-amino-2-methylpropan-1-ol, 4 Å MS, CH_2Cl_2 , 25 °C, 18 h; 2) NBS, CH_2Cl_2 , 25 °C, 5 h, 91%; b) 1) $\text{TMPMgCl}\cdot\text{LiCl}$, THF, 25 °C, 4 h; 2) DMF, THF, 0 °C to 25 °C, 1.5 h; c) NaBH_4 , THF/MeOH 1:1 v/v, 0 °C, 1 h, 81% (2 steps); d) DPPA, DBU, PhMe, 25 °C, 18 h, 98%; e) 1) MeOTf, CH_2Cl_2 , 25 °C, 2.5 h; 2) NaBH_4 , THF/MeOH 4:1 v/v, 0 °C, 2.5 h; 3) oxalic acid, THF/ H_2O 4:1 v/v, 25 °C, 20 h, 78%. Overall yield from 4-bromobenzaldehyde to **3**: 56% (5 steps). Reaction conditions for *ortho*-bromobenzaldehyde **4**: f) 1) 2-amino-2-methylpropan-1-ol, 4 Å MS, CH_2Cl_2 , 25 °C, 18 h; 2) NBS, CH_2Cl_2 , 25 °C, 4 h, 98%; g) 1) $\text{TMPMgCl}\cdot\text{LiCl}$, THF, 25 °C, 4 h; 2) $(\text{CBrCl}_2)_2$, THF, 0 °C to 25 °C, 10 h, 76%; h) NBS, AIBN, CCl_4 , 100 °C, 7 h, 66%; i) NaN_3 , DMF, 25 °C, 4 h, 99%; j) 1) MeOTf, CH_2Cl_2 , 25 °C, 2.5 h; 2) NaBH_4 , THF/MeOH 4:1 v/v, 0 °C, 2.5 h; 3) oxalic acid, THF/ H_2O 4:1 v/v, 25 °C, 20 h, 85%. Overall yield from 4-methylbenzaldehyde to **4**: 41% (5 steps).

Azide-functionalized *ortho*-bromobenzaldehyde **4** was prepared by a similar route as aldehyde **3**. Initially, oxazoline formation from 4-methylbenzaldehyde yielded 2-aryloxazoline **10** in almost quantitative yield. The introduction of the *ortho*-bromine substituent was again accomplished by metalation using $\text{TMPMgCl}\cdot\text{LiCl}$ and subsequent reaction with 1,2-dibromotetrachloroethane to afford **11** in 76% yield. A second bromination at the benzylic position provided the dibrominated derivative **12** in 66% yield. The substitution reaction of benzyl bromide with sodium azide delivered the primary azide **13** in quantitative yield. Again, the final back-conversion of the oxazoline group to the corresponding aldehyde afforded azide-functionalized *ortho*-bromobenzaldehyde **4** in 85% yield and an overall yield of 41% (starting from 4-methylbenzaldehyde).

Bromofluorenecarbaldehyde **5**

The synthetic route to azide-functionalized 7-bromofluorene-2-carbaldehyde **5** started from unfunctionalized fluorene. Double bromination to **14**, followed by double methylation of the methylene bridge to **15** and a lithiation/formylation sequence afforded 7-bromofluorene-2-carbaldehyde **16** in excellent yield over three steps. Conversion to the 2-aryloxazoline **17** was accomplished in 92% yield using the same method as described for the synthesis of **6** and **10**. *ortho*-Metalation with $\text{TMPMgCl}\cdot\text{LiCl}$ [70] and conversion of the magnesiated species with DMF to carbaldehyde **18** was followed by reduction with NaBH_4 to give the primary alcohol **19**. In contrast to benzaldehyde **7**, carbaldehyde **18** showed no decomposition at ambient temperature. While acidic hydrolysis of **19** provided exocyclic

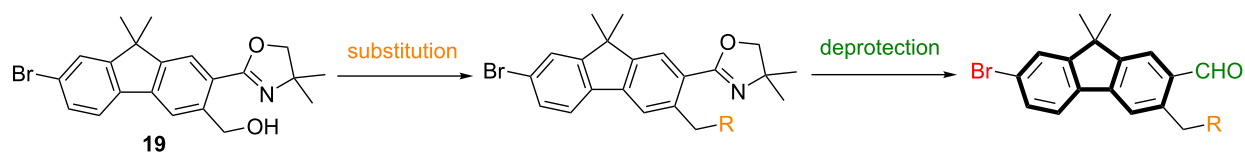


γ -lactone **20**, the substitution reaction with DPPA/ NaN_3 yielded the primary azide in 87% yield. In accordance to previous deprotection reactions, fluorene **21** was converted by means of a three-step sequence to the desired azide-functionalized 7-bromofluorene-2-carbaldehyde **5** in 86% yield and an overall yield of 45% (starting from fluorene). The molecular structure of **5** could be verified by X-ray diffraction (XRD, see Scheme 3).

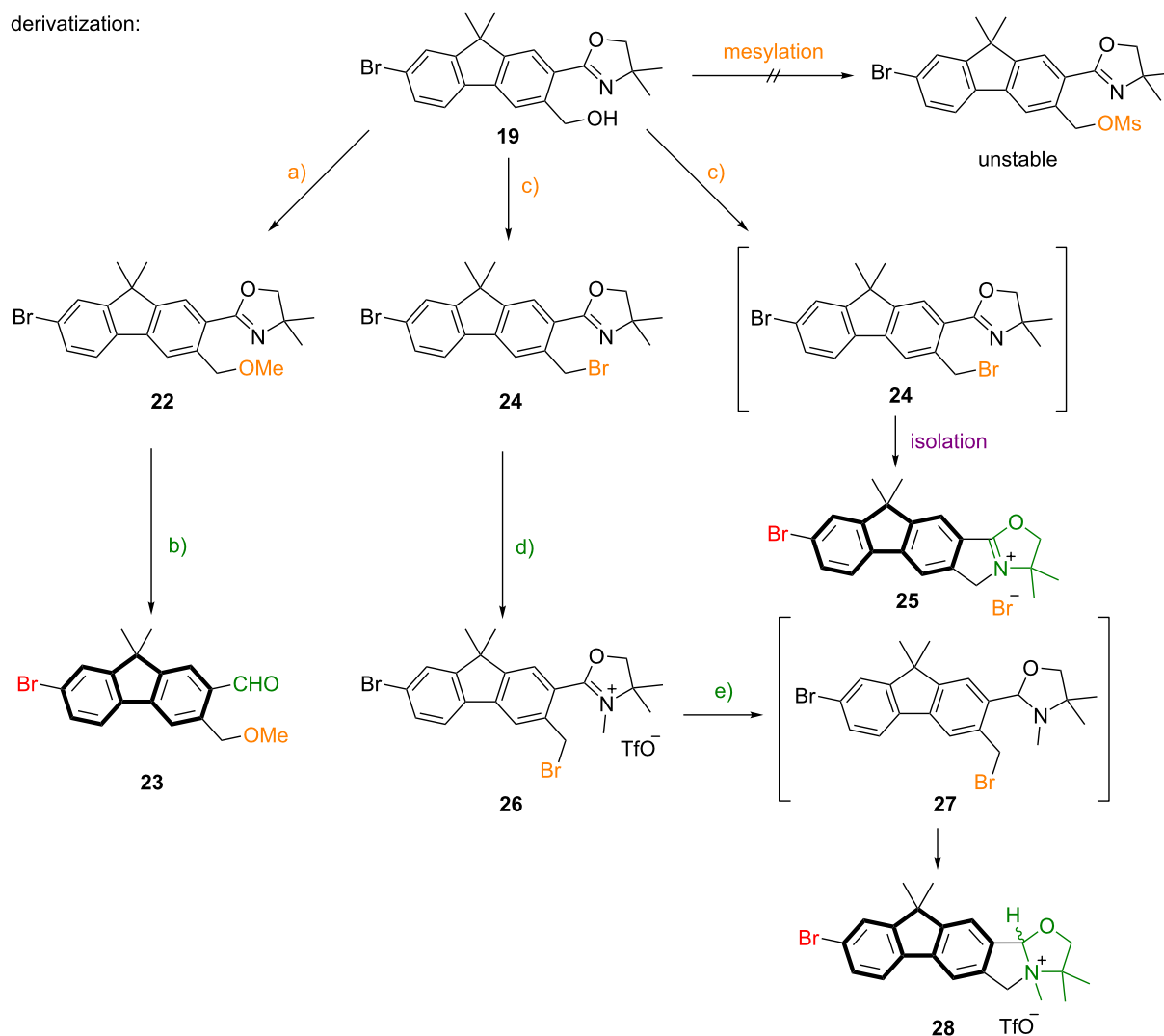
Derivatization of fluorenyl methanol **19**

To gain deeper insights into the emission behavior of fluorenes bearing different functional groups in the side chains, fluorenyl-methanol **19** was subjected to derivatization reactions (see Scheme 4). Deprotonation and subsequent methylation afforded methoxy derivative **22**, which was then converted into the methoxy-functionalized 7-bromofluorene-2-carbaldehyde **23** in 75% yield. Implementation of potent leaving groups in the side

general approach:



derivatization:



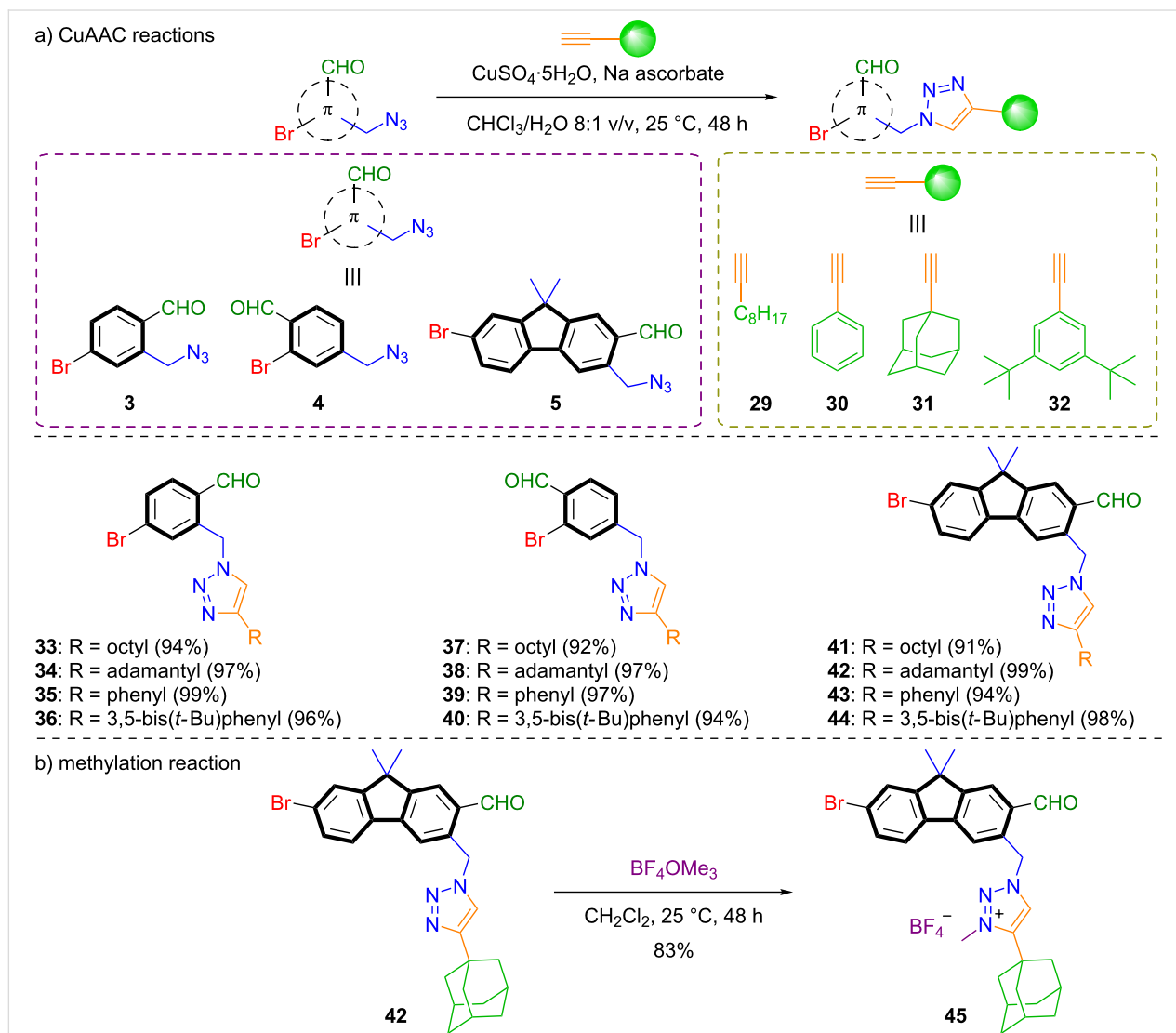
Scheme 4: Reaction conditions: a) 1) NaH , THF, $0\text{ }^{\circ}\text{C}$, 30 min; 2) MeI , THF, $0\text{ }^{\circ}\text{C}$ to $25\text{ }^{\circ}\text{C}$, 2 h, 99%; b) 1) MeOTf , CH_2Cl_2 , $25\text{ }^{\circ}\text{C}$, 3 h; 2) NaBH_4 , THF/ MeOH 4:1 v/v, $0\text{ }^{\circ}\text{C}$, 3 h; 3) oxalic acid, THF/ H_2O 4:1 v/v, $25\text{ }^{\circ}\text{C}$, 24 h, 75%. Overall yield from fluorene to **23**: 44% (8 steps). c) CBr_4 , PPh_3 , CH_2Cl_2 , $0\text{ }^{\circ}\text{C}$ to $25\text{ }^{\circ}\text{C}$, 2 h, 95%; or NBS , PPh_3 , CH_2Cl_2 , $0\text{ }^{\circ}\text{C}$ to $25\text{ }^{\circ}\text{C}$, 2 h, 91%; or PBr_3 , CH_2Cl_2 , $0\text{ }^{\circ}\text{C}$ to $25\text{ }^{\circ}\text{C}$, 2 h, 92%; d) MeOTf , CH_2Cl_2 , $25\text{ }^{\circ}\text{C}$, 3 h; e) NaBH_4 , THF/ MeOH 4:1 v/v, $0\text{ }^{\circ}\text{C}$, 3 h. Overall yield from **24** to **28**: 56% (2 steps).

chain as complement linkable functionalities via S_N -reaction was initiated by mesylation. Unfortunately, the mesylated fluorene showed such a high reactivity that rapid decomposition occurred. However, bromination was conducted by various substitution methods delivering benzyl bromide **24**, which upon isolation cyclized to iminium bromide **25** in high yield. To suppress this unexpected cyclization, careful fine-adjustment of the work-up conditions were made. Here, upon complete formation of **24**, rapid filtration of the reaction mixture through a plug of neutral alumina, solvent evaporation and quick conversion in the next step was successfully applied. Deprotection to the carbaldehyde was performed using the well applied three-step methylation/reduction/hydrolysis sequence. Methylation of the oxazoline nitrogen afforded iminium salt **26**, which was

reduced to oxazolidine **27**. Again, similar to **25**, cyclization took place and ammonium triflate **28** was isolated in 56% yield (starting from **24**). In contrast to the cyclization of oxazoline **24**, oxazolidine **27** cyclized already during the reaction, caused by the increased basicity of the ring nitrogen.

CuAAC reactions of bromocarbaldehydes

We further investigated the reactivity of azide-functionalized bromocarbaldehydes **3**, **4**, and **5** in copper(I)-catalyzed azide–alkyne cycloaddition reactions (CuAAC). For this, we treated the azide-functionalized luminophores with alkynes exhibiting different degrees of steric demand, including 1-decyne (**29**), phenylacetylene (**30**), 1-ethynyladamantane (**31**) and 1,3-di-*tert*-butyl-5-ethynylbenzene (**32**, see Scheme 5). All tri-



Scheme 5: a) CuAAC reactions of azide-functionalized bromocarbaldehydes **3**, **4** and **5** with terminal alkynes to triazoles **33–44**. General reaction conditions for CuAAC reactions: Azide (1.00 equiv), terminal alkyne (1.05 equiv), $\text{CuSO}_4 \cdot 5\text{H}_2\text{O}$ (0.1 equiv), sodium ascorbate (0.50 equiv), CHCl_3 (0.1 M) and water (12.5 mM) at 25 °C for 48 h. b) Methylation reaction of adamantyl-substituted triazole **42** with Meerwein's salt (trimethyloxonium tetrafluoroborate).

azoles **33–44**, based on the bromocarbaldehydes **3**, **4**, and **5** were successfully isolated in excellent yields of >90%. As a further model functionalization, the sterically demanding adamantyl substituted triazole **42** was subjected to a methylation reaction with Meerwein's salt (trimethyloxonium tetrafluoroborate) to deliver the *N*-methylated triazole **45** in 83% yield.

Photophysical properties

Finally, we examined the photophysical properties of both the azides and the triazoles. UV–vis absorption measurements of *para*-bromobenzaldehyde **3** and *ortho*-bromobenzaldehyde **4** as well as the corresponding triazoles **33–40** were conducted in chloroform. Intense absorption bands below 270 nm were observed, which could be attributed to typical π – π^* transitions derived from the single-benzene core. In addition, unstructured absorption bands above 290 nm were observed, while *ortho*-derivatives exhibited more broadened bands than the *para*-derivatives (see Figure 2a and Figures S1–S11 in Supporting Information File 1). The emission spectra for *para*-bromocarbaldehyde **3** and adamantyltriazole **34** in the solid-state show maxima at 440 nm (for compound **3**) and 416 nm (for compound **34**) (see Figure 2b). Additionally, fluorescence lifetimes (τ) of **3** and **34** were determined by time correlated single photon counting (TCSPC), indicating low lifetimes of 2.21 ns (for compound **3**) and 3.23 ns (for compound **34**) for lower populated species (see Figure S6, Supporting Information File 1). Quantum yields (Φ) of both derivatives are below 1% in the solid-state. In chloroform, no luminescence was detected for the *para* derivatives. All *ortho* derivatives exhibited luminescence neither in solution nor in the solid-state [73].

These observations for the *para*- and *ortho*-bromobenzaldehydes indicate that the phosphorescence is quenched in these systems, yielding only a weak fluorescence. This may be owing to the azide moiety, either as a functional group or as part of the triazole heterocycle. Similar observations were already made for luminescent materials [74,75].

Fluorene derivatives were subjected to photophysical measurements as well. UV–vis absorption spectra of bromofluorencarbaldehydes **5** and **16** show intense absorption bands at 331 and 330 nm. Furthermore, adamantyltriazole **42** and the corresponding tetrafluoroborate salt **45** exhibit similar absorption properties, while the methylated species **45** shows a comparable slightly red-shifted absorption band (see Figure 3a and Figures S12–S14 in Supporting Information File 1). Emission measurements of carbaldehydes **5** and **16** revealed that the solid-state emission bands are more blue-shifted than the emission bands in solution (see Figure 3b). Similar observations were made for adamantyltriazole **42** and tetrafluoroborate salt **45** with maxima at 510 nm and 540 nm (see Figure 3c). However, TCSPC demonstrated that solely fluorescence was observed in all physical states for all investigated compounds with a maximum lifetime τ of 11.6 ns for methylated triazole **45** in chloroform (see Figure 3d). Quantum yields Φ were determined to be <1% for all structures. Further fluorene derivatives – methoxymethyl carbaldehyde **23**, iminium bromide **25** and ammonium triflate **28** – exhibit intense absorption maxima around 320 nm (see Figure S13, Supporting Information File 1). For compounds **25** and **28**, the emission maxima in the solid-state were red-shifted compared to the emission bands in chloroform solution (see Figures S31 and S33, Supporting Information File 1). Alde-

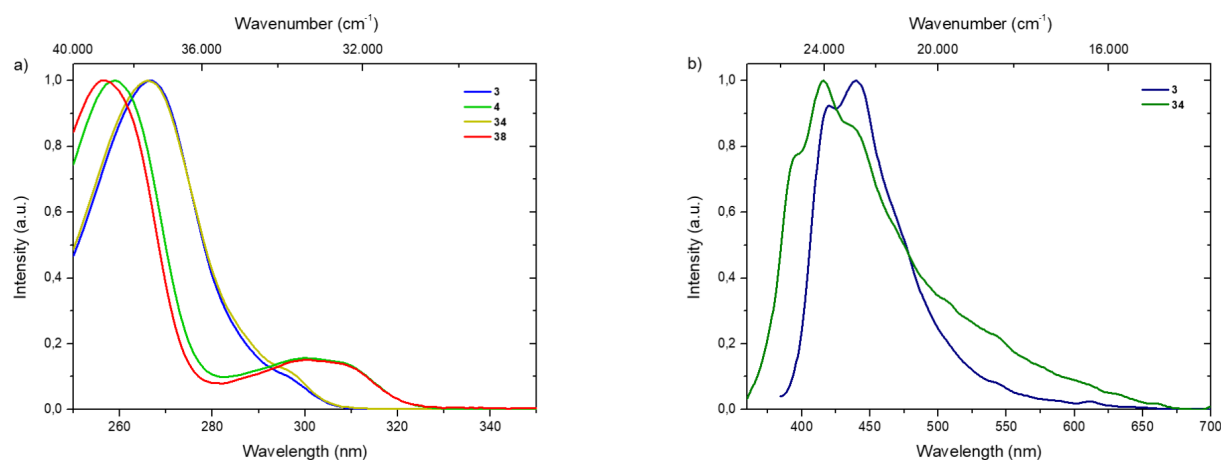


Figure 2: a) Normalized UV–vis absorption spectra of **3** (blue line), **34** (olive line), **4** (green line) and **38** (red line) in CHCl_3 ($c = 10^{-5} \text{ mol}\cdot\text{L}^{-1}$). b) Normalized emission spectra of **3** (navy line), **34** (green line) in the solid-state.

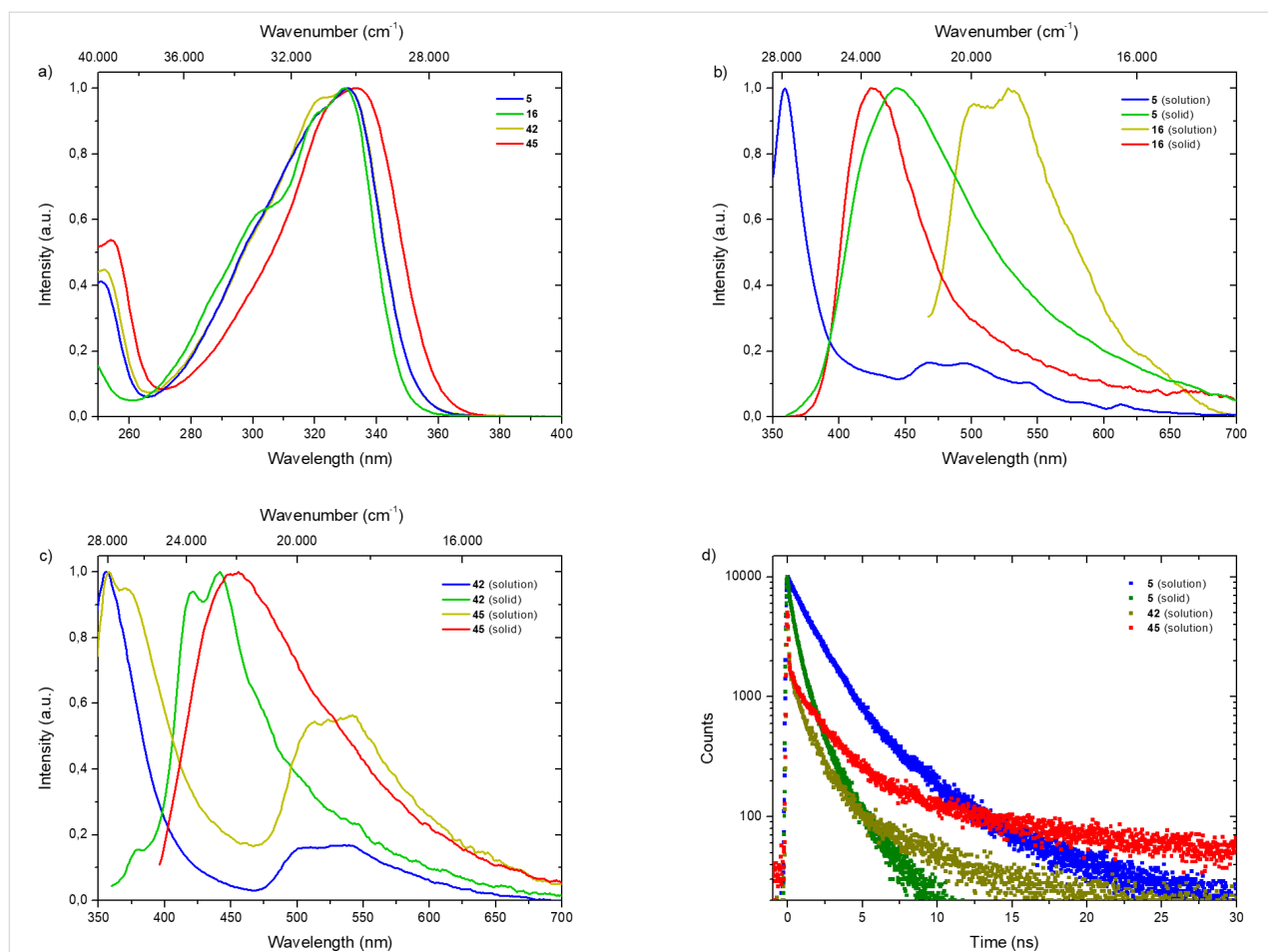


Figure 3: a) Normalized UV-vis absorption spectra of **5** (blue line), **16** (green line), **42** (olive line) and **45** (red line) in CHCl₃. b) Normalized emission spectra of **5** (in solution, blue line and in the solid-state, green line) and **16** (in solution, olive line and in the solid-state, red line). c) Normalized emission spectra of **42** (in solution, blue line and in the solid-state, green line) and **45** (in solution, olive line and in the solid-state, red line). d) Time resolved emission decay curves of **5** (in solution, blue dots and in the solid-state, green dots), **42** (in solution, olive dots) and **45** (in solution, red dots) at 25 °C. In all diluted measurements ($c = 10^{-5} \text{ mol}\cdot\text{L}^{-1}$) CHCl₃ was used as solvent and solutions were sparged with argon for 30 minutes.

hyde **23** exhibits a deep violet emission maximum at 360 nm in chloroform solution and no emission in the solid-state (see Figure S30, Supporting Information File 1). Lifetimes τ were defined up to 8.66 ns for iminium bromide **25**, with quantum yields Φ below 1% (see Figure S32, Supporting Information File 1). The absence of any long living triplet species in all fluorene derivatives in solution as well as in the solid-state again indicates undesirable quenching events, induced by the azide functionalities, similar to *para*- and *ortho*-bromobenzaldehydes.

Conclusion

In summary, azide-functionalized *ortho*- and *para*-bromobenzaldehydes and fluorene derivatives were successfully synthesized. The azide bearing arenes were efficiently linked with even sterically highly demanding alkynes in CuAAC. Initial photophysical investigations of azide-functionalized bromocarbaldehydes and fluorenes revealed that the azide moiety and the triazole heterocycle efficiently quench phosphorescent transi-

tions. Efforts of installing other functional groups suitable for covalent connections or modifications of the alkyl bridge between the arene and the azide are underway in our laboratories.

Supporting Information

Supporting Information File 1

Detailed experimental procedures, characterization data, photophysical properties, and copies of NMR spectra.

[<https://www.beilstein-journals.org/bjoc/content/supplementary/1860-5397-16-139-S1.pdf>]

Acknowledgements

We thank Prof. Dr. Nadja-C. Bigall, Dr. Dirk Dorfs and Pascal Rusch (all from Leibniz University Hannover) for supporting the photophysical measurements.

ORCID® iDs

Marius Friedrich - <https://orcid.org/0000-0002-7309-5288>Enno Lork - <https://orcid.org/0000-0002-0582-9913>Boris J. Nachtsheim - <https://orcid.org/0000-0002-3759-2770>

Preprint

A non-peer-reviewed version of this article has been previously published as a preprint <https://doi.org/10.26434/chemrxiv.12238967.v1>

References

- Kabe, R.; Notsuka, N.; Yoshida, K.; Adachi, C. *Adv. Mater. (Weinheim, Ger.)* **2016**, *28*, 655–660. doi:10.1002/adma.201504321
- Tao, Y.; Yang, C.; Qin, J. *Chem. Soc. Rev.* **2011**, *40*, 2943–2970. doi:10.1039/c0cs00160k
- Goushi, K.; Yoshida, K.; Sato, K.; Adachi, C. *Nat. Photonics* **2012**, *6*, 253–258. doi:10.1038/nphoton.2012.31
- Zhang, Q.; Li, B.; Huang, S.; Nomura, H.; Tanaka, H.; Adachi, C. *Nat. Photonics* **2014**, *8*, 326–332. doi:10.1038/nphoton.2014.12
- Chaudhuri, D.; Wettach, H.; van Schooten, K. J.; Liu, S.; Sigmund, E.; Höger, S.; Lupton, J. M. *Angew. Chem., Int. Ed.* **2010**, *49*, 7714–7717. doi:10.1002/anie.201003291
- Chaudhuri, D.; Sigmund, E.; Meyer, A.; Röck, L.; Klemm, P.; Lautenschlager, S.; Schmid, A.; Yost, S. R.; Van Voorhis, T.; Bange, S.; Höger, S.; Lupton, J. M. *Angew. Chem., Int. Ed.* **2013**, *52*, 13449–13452. doi:10.1002/anie.201307601
- Murawski, C.; Leo, K.; Gather, M. C. *Adv. Mater. (Weinheim, Ger.)* **2013**, *25*, 6801–6827. doi:10.1002/adma.201301603
- Baldo, M. A.; O'Brien, D. F.; You, Y.; Shoustikov, A.; Sibley, S.; Thompson, M. E.; Forrest, S. R. *Nature* **1998**, *395*, 151–154. doi:10.1038/25954
- Gao, R.; Mei, X.; Yan, D.; Liang, R.; Wei, M. *Nat. Commun.* **2018**, *9*, 2798. doi:10.1038/s41467-018-05223-3
- Miao, Q.; Xie, C.; Zhen, X.; Lyu, Y.; Duan, H.; Liu, X.; Jokerst, J. V.; Pu, K. *Nat. Biotechnol.* **2017**, *35*, 1102–1110. doi:10.1038/nbt.3987
- Zhen, X.; Tao, Y.; An, Z.; Chen, P.; Xu, C.; Chen, R.; Huang, W.; Pu, K. *Adv. Mater. (Weinheim, Ger.)* **2017**, *29*, 1606665. doi:10.1002/adma.201606665
- Zhang, G.; Palmer, G. M.; Dewhurst, M. W.; Fraser, C. L. *Nat. Mater.* **2009**, *8*, 747–751. doi:10.1038/nmat2509
- DeRosa, C. A.; Seaman, S. A.; Mathew, A. S.; Gorick, C. M.; Fan, Z.; Demas, J. N.; Peirce, S. M.; Fraser, C. L. *ACS Sens.* **2016**, *1*, 1366–1373. doi:10.1021/acssensors.6b00533
- Lehner, P.; Staudinger, C.; Borisov, S. M.; Klimant, I. *Nat. Commun.* **2014**, *5*, 4460. doi:10.1038/ncomms5460
- Kwon, M. S.; Lee, D.; Seo, S.; Jung, J.; Kim, J. *Angew. Chem., Int. Ed.* **2014**, *53*, 11177–11181. doi:10.1002/anie.201404490
- Xiao, L.; Fu, H. *Chem. – Eur. J.* **2019**, *25*, 714–723. doi:10.1002/chem.201802819
- Jia, W.; Wang, Q.; Shi, H.; An, Z.; Huang, W. *Chem. – Eur. J.* **2020**, *26*, 4437–4448. doi:10.1002/chem.201904500
- Kasha, M. *Chem. Rev.* **1947**, *41*, 401–419. doi:10.1021/cr60129a015
- Lewis, G. N.; Calvin, M. J. *Am. Chem. Soc.* **1945**, *67*, 1232–1233. doi:10.1021/ja01223a513
- Lewis, G. N.; Kasha, M. J. *Am. Chem. Soc.* **1944**, *66*, 2100–2116. doi:10.1021/ja01240a030
- Lewis, G. N.; Lipkin, D.; Magel, T. T. *J. Am. Chem. Soc.* **1941**, *63*, 3005–3018. doi:10.1021/ja01856a043
- Lower, S. K.; El-Sayed, M. A. *Chem. Rev.* **1966**, *66*, 199–241. doi:10.1021/cr60240a004
- El-Sayed, M. A. *J. Chem. Phys.* **1963**, *38*, 2834–2838. doi:10.1063/1.1733610
- Hirata, S. *Adv. Opt. Mater.* **2017**, *5*, 1700116. doi:10.1002/adom.201700116
- Menning, S.; Krämer, M.; Coombs, B. A.; Rominger, F.; Beeby, A.; Dreuw, A.; Bunz, U. H. F. *J. Am. Chem. Soc.* **2013**, *135*, 2160–2163. doi:10.1021/ja400416r
- Yuan, W. Z.; Shen, X. Y.; Zhao, H.; Lam, J. W. Y.; Tang, L.; Lu, P.; Wang, C.; Liu, Y.; Wang, Z.; Zheng, Q.; Sun, J. Z.; Ma, Y.; Tang, B. Z. *J. Phys. Chem. C* **2010**, *114*, 6090–6099. doi:10.1021/jp909388y
- Zhang, G.; Chen, J.; Payne, S. J.; Kooi, S. E.; Demas, J. N.; Fraser, C. L. *J. Am. Chem. Soc.* **2007**, *129*, 8942–8943. doi:10.1021/ja0720255
- Xu, J.; Takai, A.; Kobayashi, Y.; Takeuchi, M. *Chem. Commun.* **2013**, *49*, 8447–8449. doi:10.1039/c3cc44809f
- Schulze, M.; Steffen, A.; Würthner, F. *Angew. Chem., Int. Ed.* **2015**, *54*, 1570–1573. doi:10.1002/anie.201410437
- Hirata, S.; Totani, K.; Yamashita, T.; Adachi, C.; Vacha, M. *Nat. Mater.* **2014**, *13*, 938–946. doi:10.1038/nmat4081
- Pan, Z.; Lu, Y.-Y.; Liu, F. *Nat. Mater.* **2012**, *11*, 58–63. doi:10.1038/nmat3173
- Tong, B.; Mei, Q.; Wang, S.; Fang, Y.; Meng, Y.; Wang, B. *J. Mater. Chem.* **2008**, *18*, 1636–1639. doi:10.1039/b800977e
- Liu, Z. W.; Guan, M.; Bian, Z. Q.; Nie, D. B.; Gong, Z. L.; Li, Z. B.; Huang, C. H. *Adv. Funct. Mater.* **2006**, *16*, 1441–1448. doi:10.1002/adfm.200600099
- Zhao, J.; Chen, K.; Hou, Y.; Che, Y.; Liu, L.; Jia, D. *Org. Biomol. Chem.* **2018**, *16*, 3692–3701. doi:10.1039/c8ob00421h
- Forni, A.; Lucenti, E.; Botta, C.; Cariatì, E. *J. Mater. Chem. C* **2018**, *6*, 4603–4626. doi:10.1039/c8tc01007b
- Baroncini, M.; Bergamini, G.; Ceroni, P. *Chem. Commun.* **2017**, *53*, 2081–2093. doi:10.1039/c6cc09288h
- Mukherjee, S.; Thilagar, P. *Chem. Commun.* **2015**, *51*, 10988–11003. doi:10.1039/c5cc03114a
- Shi, H.; Song, L.; Ma, H.; Sun, C.; Huang, K.; Lv, A.; Ye, W.; Wang, H.; Cai, S.; Yao, W.; Zhang, Y.; Zheng, R.; An, Z.; Huang, W. *J. Phys. Chem. Lett.* **2019**, *10*, 595–600. doi:10.1021/acs.jpclett.8b03712
- Li, J.-A.; Zhou, J.; Mao, Z.; Xie, Z.; Yang, Z.; Xu, B.; Liu, C.; Chen, X.; Ren, D.; Pan, H.; Shi, G.; Zhang, Y.; Chi, Z. *Angew. Chem., Int. Ed.* **2018**, *57*, 6449–6453. doi:10.1002/anie.201800762
- Xiong, Y.; Zhao, Z.; Zhao, W.; Ma, H.; Peng, Q.; He, Z.; Zhang, X.; Chen, Y.; He, X.; Lam, J. W. Y.; Tang, B. Z. *Angew. Chem., Int. Ed.* **2018**, *57*, 7997–8001. doi:10.1002/anie.201800834
- Gu, L.; Shi, H.; Miao, C.; Wu, Q.; Cheng, Z.; Cai, S.; Gu, M.; Ma, C.; Yao, W.; Gao, Y.; An, Z.; Huang, W. *J. Mater. Chem. C* **2018**, *6*, 226–233. doi:10.1039/c7tc04452f
- Cai, S.; Shi, H.; Zhang, Z.; Wang, X.; Ma, H.; Gan, N.; Wu, Q.; Cheng, Z.; Ling, K.; Gu, M.; Ma, C.; Gu, L.; An, Z.; Huang, W. *Angew. Chem., Int. Ed.* **2018**, *57*, 4005–4009. doi:10.1002/anie.201800697
- Cai, S.; Shi, H.; Tian, D.; Ma, H.; Cheng, Z.; Wu, Q.; Gu, M.; Huang, L.; An, Z.; Peng, Q.; Huang, W. *Adv. Funct. Mater.* **2018**, *28*, 1705045. doi:10.1002/adfm.201705045
- Cai, S.; Shi, H.; Li, J.; Gu, L.; Ni, Y.; Cheng, Z.; Wang, S.; Xiong, W.-w.; Li, L.; An, Z.; Huang, W. *Adv. Mater. (Weinheim, Ger.)* **2017**, *29*, 1701244. doi:10.1002/adma.201701244

45. Yang, Z.; Mao, Z.; Zhang, X.; Ou, D.; Mu, Y.; Zhang, Y.; Zhao, C.; Liu, S.; Chi, Z.; Xu, J.; Wu, Y.-C.; Lu, P.-Y.; Lien, A.; Bryce, M. R. *Angew. Chem., Int. Ed.* **2016**, *55*, 2181–2185. doi:10.1002/anie.201509224
46. Gong, Y.; Chen, G.; Peng, Q.; Yuan, W. Z.; Xie, Y.; Li, S.; Zhang, Y.; Tang, B. Z. *Adv. Mater. (Weinheim, Ger.)* **2015**, *27*, 6195–6201. doi:10.1002/adma.201502442
47. An, Z.; Zheng, C.; Tao, Y.; Chen, R.; Shi, H.; Chen, T.; Wang, Z.; Li, H.; Deng, R.; Liu, X.; Huang, W. *Nat. Mater.* **2015**, *14*, 685–690. doi:10.1038/nmat4259
48. Yu, Z.; Wu, Y.; Peng, Q.; Sun, C.; Chen, J.; Yao, J.; Fu, H. *Chem. – Eur. J.* **2016**, *22*, 4717–4722. doi:10.1002/chem.201600300
49. Chen, X.; Xu, C.; Wang, T.; Zhou, C.; Du, J.; Wang, Z.; Xu, H.; Xie, T.; Bi, G.; Jiang, J.; Zhang, X.; Demas, J. N.; Trindle, C. O.; Luo, Y.; Zhang, G. *Angew. Chem., Int. Ed.* **2016**, *55*, 9872–9876. doi:10.1002/anie.201601252
50. Lin, Z.; Kabe, R.; Nishimura, N.; Jinnai, K.; Adachi, C. *Adv. Mater. (Weinheim, Ger.)* **2018**, *30*, 1803713. doi:10.1002/adma.201803713
51. Li, D.; Lu, F.; Wang, J.; Hu, W.; Cao, X.-M.; Ma, X.; Tian, H. *J. Am. Chem. Soc.* **2018**, *140*, 1916–1923. doi:10.1021/jacs.7b12800
52. Kabe, R.; Adachi, C. *Nature* **2017**, *550*, 384–387. doi:10.1038/nature24010
53. Gan, N.; Wang, X.; Ma, H.; Lv, A.; Wang, H.; Wang, Q.; Gu, M.; Cai, S.; Zhang, Y.; Fu, L.; Zhang, M.; Dong, C.; Yao, W.; Shi, H.; An, Z.; Huang, W. *Angew. Chem., Int. Ed.* **2019**, *58*, 14140–14145. doi:10.1002/anie.201907572
54. Yang, J.; Ren, Z.; Chen, B.; Fang, M.; Zhao, Z.; Tang, B. Z.; Peng, Q.; Li, Z. *J. Mater. Chem. C* **2017**, *5*, 9242–9246. doi:10.1039/c7tc03656f
55. Shimizu, M.; Shigitani, R.; Nakatani, M.; Kuwabara, K.; Miyake, Y.; Tajima, K.; Sakai, H.; Hasobe, T. *J. Phys. Chem. C* **2016**, *120*, 11631–11639. doi:10.1021/acs.jpcc.6b03276
56. Xie, Y.; Ge, Y.; Peng, Q.; Li, C.; Li, Q.; Li, Z. *Adv. Mater. (Weinheim, Ger.)* **2017**, *29*, 1606829. doi:10.1002/adma.201606829
57. Bergamini, G.; Fermi, A.; Botta, C.; Giovanella, U.; Di Motta, S.; Negri, F.; Peresutti, R.; Gingras, M.; Ceroni, P. *J. Mater. Chem. C* **2013**, *1*, 2717–2724. doi:10.1039/c3tc00878a
58. Bolton, O.; Lee, K.; Kim, H.-J.; Lin, K. Y.; Kim, J. *Nat. Chem.* **2011**, *3*, 205–210. doi:10.1038/nchem.984
59. Yu, Y.; Kwon, M. S.; Jung, J.; Zeng, Y.; Kim, M.; Chung, K.; Gierschner, J.; Youk, J. H.; Borisov, S. M.; Kim, J. *Angew. Chem., Int. Ed.* **2017**, *56*, 16207–16211. doi:10.1002/anie.201708606
60. Kwon, M. S.; Jordahl, J. H.; Phillips, A. W.; Chung, K.; Lee, S.; Gierschner, J.; Lahann, J.; Kim, J. *Chem. Sci.* **2016**, *7*, 2359–2363. doi:10.1039/c5sc03986j
61. Kwon, M. S.; Yu, Y.; Coburn, C.; Phillips, A. W.; Chung, K.; Shanker, A.; Jung, J.; Kim, G.; Pipe, K.; Forrest, S. R.; Youk, J. H.; Gierschner, J.; Kim, J. *Nat. Commun.* **2015**, *6*, 8947. doi:10.1038/ncomms9947
62. Lee, D.; Jung, J.; Bilby, D.; Kwon, M. S.; Yun, J.; Kim, J. *ACS Appl. Mater. Interfaces* **2015**, *7*, 2993–2997. doi:10.1021/am5087165
63. Bolton, O.; Lee, D.; Jung, J.; Kim, J. *Chem. Mater.* **2014**, *26*, 6644–6649. doi:10.1021/cm503678r
64. Goudappagouda; Manthanath, A.; Wakchaure, V. C.; Ranjeesh, K. C.; Das, T.; Vanka, K.; Nakanishi, T.; Babu, S. S. *Angew. Chem., Int. Ed.* **2019**, *58*, 2284–2288. doi:10.1002/anie.201811834
65. Kuila, S.; Rao, K. V.; Garain, S.; Samanta, P. K.; Das, S.; Pati, S. K.; Eswaramoorthy, M.; George, S. J. *Angew. Chem., Int. Ed.* **2018**, *57*, 17115–17119. doi:10.1002/anie.201810823
66. Yu, Z.; Wu, Y.; Xiao, L.; Chen, J.; Liao, Q.; Yao, J.; Fu, H. *J. Am. Chem. Soc.* **2017**, *139*, 6376–6381. doi:10.1021/jacs.7b01574
67. Huang, C.-H.; Wu, P.-J.; Chung, K.-Y.; Chen, Y.-A.; Li, E. Y.; Chou, P.-T. *Phys. Chem. Chem. Phys.* **2017**, *19*, 8896–8901. doi:10.1039/c7cp00074j
68. Ventura, B.; Bertocco, A.; Braga, D.; Catalano, L.; d'Agostino, S.; Grepioni, F.; Taddei, P. *J. Phys. Chem. C* **2014**, *118*, 18646–18658. doi:10.1021/jp5049309
69. Koch, M.; Perumal, K.; Blacque, O.; Garg, J. A.; Saiganesh, R.; Kabilan, S.; Balasubramanian, K. K.; Venkatesan, K. *Angew. Chem., Int. Ed.* **2014**, *53*, 6378–6382. doi:10.1002/anie.201402199
70. Göbel, D.; Clamor, N.; Nachtsheim, B. J. *Org. Biomol. Chem.* **2018**, *16*, 4071–4075. doi:10.1039/c8ob01072b
71. Göbel, D.; Clamor, N.; Lork, E.; Nachtsheim, B. J. *Org. Lett.* **2019**, *21*, 5373–5377. doi:10.1021/acs.orglett.9b01350
72. Göbel, D.; Duvinage, D.; Stauch, T.; Nachtsheim, B. J. *J. Mater. Chem. C* **2020**. doi:10.1039/d0tc00776e
73. Sarkar, S.; Hendrickson, H. P.; Lee, D.; DeVine, F.; Jung, J.; Geva, E.; Kim, J.; Dunietz, B. D. *J. Phys. Chem. C* **2017**, *121*, 3771–3777. doi:10.1021/acs.jpcc.6b12027
74. Xie, S.; Proietti, G.; Ramström, O.; Yan, M. *J. Org. Chem.* **2019**, *84*, 14520–14528. doi:10.1021/acs.joc.9b02050
75. Lord, S. J.; Lee, H.-I. D.; Samuel, R.; Weber, R.; Liu, N.; Conley, N. R.; Thompson, M. A.; Twieg, R. J.; Moerner, W. E. *J. Phys. Chem. B* **2010**, *114*, 14157–14167. doi:10.1021/jp907080r

License and Terms

This is an Open Access article under the terms of the Creative Commons Attribution License (<http://creativecommons.org/licenses/by/4.0>). Please note that the reuse, redistribution and reproduction in particular requires that the authors and source are credited.

The license is subject to the *Beilstein Journal of Organic Chemistry* terms and conditions: (<https://www.beilstein-journals.org/bjoc>)

The definitive version of this article is the electronic one which can be found at: [doi:10.3762/bjoc.16.139](https://doi.org/10.3762/bjoc.16.139)